Synthesis, characterisation and testing of Au/SBA-15 catalysts for elimination of volatile organic compounds by complete oxidation at low temperatures

Emmanuel Okechukwu Iro

A thesis submitted in partial fulfilment of the requirements of Teesside University for the degree of Doctor of Philosophy

September 2017

Abstract

Optimised SBA-15 mesoporous silica with high surface area (794 m^2/g) and very thick pore wall (~ 5.0 nm), which maintained its structural and hydrothermal stability in steam, up to 800 °C was successfully synthesised and used as support material for synthesis of Au/SBA-15 catalysts. Gold nano-particles of different sizes were anchored on SBA-15 using cationic gold precursor ($Au(en_2)Cl_3$), post or one pot functionalisation of SBA-15 with MPTMS, APTMS or phosphine ligand before gold loading via $HAuCl_4$ gold precursor. Characterisation of the catalysts were done using the following techniques: Scanning Electron Microscopy (SEM), Energy Dispersive X-ray spectroscopy (EDX), Transmission Electron Microscopy (TEM), X-Ray Diffraction spectroscopy (XRD), Fourier – Transform Infrared Spectroscopy (FT-IR), Nitrogen Physisorption and Hiden Analytical CATLAB system. Characterisation results confirmed that gold particle size, dispersion of gold on SBA-15 and the oxidation state of gold had significant influence on the catalytic activity of Au/SBA-15 catalysts. The most active and stable Au/SBA-15 catalyst (Au-0.6Mdp/SBA-15), prepared by one pot synthesis of SBA-15 with MPTMS before gold loading, had high surface area of 726 m^2/g, with the smallest gold particle size of 1.3 nm, well dispersed on SBA-15 support. Hydrogen reduced Au/SBA-15 catalysts were more active than their as-synthesised forms in complete oxidation of non-chlorinated VOCs, with the most active Au/SBA-15 catalyst (Au-0.6Mdp/SBA-15) attaining 100 % acetone conversion at 250 °C and 11% propane conversion at and 300 °C. The as-synthesised form of Au-0.6Mdp/SBA-15 catalyst attained 100 % acetone conversion at 280 °C and 1.8 % propane conversion at 300 °C. The reduced Au-0.6Mdp/SBA-15 catalyst was also more active than the as-synthesised form in complete oxidation of aromatic and olefin VOC mixture (BTEXB of 820 ppm). For chlorinated VOCs using dichloromethane (DCM) as model compound, only the as-synthesised form of Au/SBA-15 catalyst was active, attaining 100 % DCM conversion at 305 °C. The reduced form of Au/SBA-15 catalyst was inactive, probably

due to instant poisoning from strong attachment of chlorides with metallic gold. A novel coating technique (fine spray of catalyst, colloidal silica and methyl cellulose slurry on heated reactor at 150°C), which drastically reduced the amount of catalyst required for VOC oxidation was developed to introduce only 2.5 mg of Au-0.6Mdp/SBA-15 catalyst in the channels of a micro-reactor. Higher conversion of propane (VOC model compound) was achieved with the catalytic micro-reactor. The use of the micro-reactor has the potential to reduce the amount of expensive catalyst used and attain higher VOC conversions at lower temperatures, which could boost the commercial viability of this noble catalytic device for elimination of indoor VOCs.

Glossary of terms and acronyms

1. **Absorption**: the process by which atoms, molecules or ions enter a bulk phase (liquid, gas, solid)
2. **Adsorption:** the adhesion of molecules of gas, liquid or dissolved solids to a surface
3. **Boiling Point**: the temperature at which the vapour pressure of a liquid equals the external pressure surrounding the liquid, causing the liquid to change to vapour.
4. **Catalyst**: a substance that speeds up a chemical reaction, but is not consumed by the reaction, hence can be recovered afterwards.
5. **Chemical Reactor:** a vessel, tube, pipe or any other container within which a chemical reaction is made to take place.
6. **Characterisation**: analytical techniques or methods used to identify, isolate, probe and measure materials structure and properties.
7. **Coating**: covering applied to the surface of an object
8. **Condensation:** change in the state of matter from the gas phase to the liquid phase
9. **Condensation reaction**: a chemical reaction in which two molecules or moieties, usually functional groups, combine to form a large molecule, together with the loss of some molecules.
10. **Desorption**: the process whereby a substance is released from or through a surface
11. **Exothermic reaction**: a chemical reaction that releases energy by light or heat. It is the opposite of an endothermic reaction.
12. **Functionalisation:** a process of changing the surface chemistry of a material by adding new functions, features, capabilities or properties to the material.
13. **Hydrolysis**: a reaction involving the breaking of a bond in a molecule using water.
14. **Hydrophobicity**: property of a substance (non-polar molecules) to repel water.

15. **Heat transfer**: exchange of thermal energy and heat between physical systems. The transfer of heat is normally from a higher temperature object to a lower temperature object.
16. **Mass transfer:** describes the transport of mass from one point to another.
17. **Micro-reactor**: or micro-structured reactor, or micro-channel reactor is a device in which chemical reaction takes place in narrow confinement typically less than 100 μm
18. **Polymerisation**: a process of reacting monomer molecules together in a chemical reaction to form polymer chains
19. **Rate of reaction:** the speed at which a chemical reaction proceeds. It is often expressed in terms of either the concentration (amount per unit volume) of product formed in a unit time or the concentration of a reactant consumed in a unit time.
20. **Synthesis:** a type of reaction in which multiple reactants combine to form a single product.
21. **Vapour pressure:** or equilibrium vapour pressure is the pressure exerted by a vapour in thermodynamic equilibrium with its condensed phases (solid or liquid) at a given temperature in a closed system. The equilibrium vapour pressure is an indication of a liquid's evaporation rate.
22. **(a):** unit cell parameter
23. **Au-0.6Adp/SBA-15 catalyst**: Prepared by one-pot synthesis of SBA-15 with APTMS before loading with $HAuCl_4$ gold precursor
24. **Au-A0.8/SBA-15 catalyst:** Prepared by post functionalisation of SBA-15 with APTMS before loading with $HAuCl_4$
25. **Au-en/SBA-15 catalyst**: Prepared by loading cationic gold precursor: $Au(en)_2Cl_3$ (en=ethylenediamine) on SBA-15

26. **Au-M0.8/SBA-15 catalyst**: Prepared by post functionalisation of SBA-15 with MPTMS before loading with $HaACl_4$
27. **Au-0.6Mdp/SBA-15 catalyst**: Prepared by one-pot synthesis of SBA-15 with MPTMS before loading with $HAuCl_4$ gold precursor
28. **APTMS:** 3-aminopropyl-trimethoxy-silane
29. **a.u**: arbitrary unit
30. **BET**: Brunauer – Emmett –Teller
31. **BJH**: Barrett – Joyner – Halenda
32. **BTEXB**: a gas mixture of benzene, toluene, ethylbenzene, xylene and 1,3-butadiene
33. **DCM:** Dichloromethane
34. **EDX:** Energy Dispersive X-ray spectroscopy
35. **EPR**: Electron Paramagnetic Resonance
36. **FT-IR**: Fourier – Transform Infrared Spectroscopy
37. **GHSV**: Gas Hourly Space Velocity
38. **IUPAC**: International Union of Pure and Applied Chemistry
39. **MPTMS**: 3-mercaptopropyl-trimethoxy-silane
40. **SEM:** Scanning Electron Microscopy
41. **SEM:** Secondary Electron Multiplier detectors
42. **SSR:** Steady state reaction
43. **TEM:** Transmission Electron Microscopy
44. **TPR**: Temperature Programmed Reduction
45. **TPRx**: Temperature Programmed Reaction
46. **VOCs**: Volatile Organic compounds
47. **XPS**: X-ray Photoelectron Spectroscopy
48. **XRD**: X-Ray Diffraction spectroscopy

Declaration

The report and results contained in this thesis are my original work, except where otherwise stated and has not been submitted for another degree anywhere else.

I certify that the statement above is correct

Emmanuel Okechukwu Iro

Dedication

To my loving wife, Kenechi, whose endurance, dedicated partnership and prayers were catalysts behind the success of my humble effort. To my sweet daughters, Zoey and Zita, I love you with all my heart.

Acknowledgements

My deepest gratitude first goes to my Director of Studies, Professor Maria Olea, who from her wealth of research expertise and experience laid a solid foundation for my research. Her unwavering enthusiasm, mentoring and dedicated commitment was a daily motivation for me to excel.

My appreciation also goes to my supervisors, Professor Simon Hodgson and Professor Meez Islam for all their support. I specially thank all laboratory staff and fellow research colleagues at Teesside University. I wish to acknowledge and thank Professor Takehiko Sasaki of The University of Tokyo, Japan, Professor Bill Henderson, University of Waikato, New Zealand and Pramodh Chirra from Lucite International, UK for their kind assistance with TEM, Phosphine-SBA-15 functionalisation and N_2 adsorption – desorption measurements respectively.

Finally, I am indebted to my loving parents, Chief Gabriel and Lolo Mary Iro (KSJ), my parents-in-law, Chief Elder Rufus and Pastor (Mrs) Mercy Okeke, my siblings, brothers and sister-in-law, Chief and Lolo Jude and Adaure Njoku, Barrister Chris and Mrs Laeticia Wogu, Major Stephen and Mrs Nancy Okoi, Engr. Tony and Mrs Joy Iro and Miss Fortune Iro. My brothers and sisters-in-law, Barrister Ugo and Mrs Iulia Okeke, Miss Nkiru, Miss Ijeoma and Mr. Joshua Okeke and all my extended family and friends too many to mention, I am truly grateful for all your support, encouragements and prayers throughout the course of my study, may the good Lord bless you all in no small measure.

List of Tables:

List of figures:

Table of Contents

CHAPTER 1. Introduction

1.1. Background

Gold's fascinating qualities such as its lustrous yellow colour, tarnish resistance in normal conditions, excellent conduction of electricity and its extreme malleability makes it highly sort after by many. In chemistry however, especially in the field of catalysis, gold was ignored as it was considered inactive due to its chemical inertness [1]. However, a major revolution took place from the mid-1980s led by the pioneering work of Haruta who reported that gold supported on metal oxides when reduced to small nano-particles between 1 – 5 nm in sizes suddenly became very active. Haruta demonstrated this in complete catalytic oxidation of carbon monoxide to carbon dioxide, with the gold catalysts still active even at – 77 ºC. This exceptional and unprecedented fit has not been attained by any noble or transition metal oxide catalyst for oxidation of carbon monoxide at such a low temperature. Haruta's discovery generated a great deal of interest among scientists and prompted a wide scale research into the development and application of gold based catalysts to a wide variety of chemical reactions, among which is the complete oxidation of volatile organic compounds at low temperatures [2-4].

The specific reasons for the high catalytic activity of supported gold nanoparticle is still a subject of debate, however from a wide range of literature available from 1987 till present, it is mostly accepted that the catalytic activity of gold based catalysts is highly influenced by [2, 5-9] :

I. Size of gold particles on the support
II. Shape of the gold particles
III. Dispersion of gold on the support
IV. Gold – support interface interactions

V. The oxidation state(s) of gold

VI. Catalyst synthesis methods

VII. Nature of catalyst support

Available literature so far show that it is quite challenging to synthesis stable gold nano-particles on most supports. This is because gold nano-particles have a high area to volume ratio which easily causes them to stick together (agglomeration). Gold agglomeration is the main cause of deactivation in gold based catalysts [10]. As a consequence, gold nano-particles are extremely unstable [10]. In comparison to other mesoporous silicas, SBA-15 is most appropriate as support material for gold nano-particles since its thicker pore walls are known to effectively confine metal nano-particles within its pores, which are usually 5 – 8 nm in diameter [11]. Unfortunately, gold nano-particles are mobile on silica surfaces and easily aggregate due to weak interaction between gold and silica [12]. The main aim of this research project is to develop cost effective synthetic methods which could re-engineer the surface of SBA-15 to form strong interaction with gold, thereby generating very small and stable gold nano-particles, well dispersed on SBA-15 high surface area. An attempt was also made to improve on the structural and hydrothermal stability of SBA-15 as catalyst support for gold oxidation catalysts, to retain their high surface area after gold impregnation and chemical reaction. An appropriate coating method was developed to introduce small amount of the Au/SBA-15 catalyst to a high surface area micro-reactor device. This innovative idea is aimed at reducing the amount of expensive catalyst used, in addition to taking advantage of the high heat transfer offered by microreactor system to boost high catalytic activity at low temperatures for complete oxidation of volatile organic compounds.

Volatile organic compounds (VOCs) are organic compounds such as alkanes, olefins, alcohols, ketones, aldehydes, esters, aromatic and halogenated hydrocarbons with high vapour pressures due to their low boiling points at room temperature which causes them to

vaporise easily into atmospheric environment [13, 14]. Emission of VOCs to the atmosphere have harmful consequences on the environment, and are also linked to both acute and chronic diseases in humans [15, 16]. Complete catalytic oxidation of VOCs at low temperatures is quite promising for elimination of VOCs, especially at very low concentrations in part per billion (ppb) levels typical in indoor air, however, it is extremely difficult to achieve. In fact, most catalysts require heating up to at least 150 °C for any significant catalytic oxidation to occur [17-19], making catalytic oxidation technology expensive, especially for indoor air clean-up technology. There is therefore the need to synthesise low temperature VOC oxidation catalysts with high catalytic activity and reaction stability.

1.2. Catalytic oxidation of volatile organic compounds at low temperatures

Catalysts used for complete oxidation of VOCs are classified into three main groups: noble metal based catalysts, transition metal oxide catalysts and alloy catalysts [20]. Although noble metal catalysts are expensive, they are still largely preferred because they show lower light off temperatures in complete oxidation of hydrocarbons [18, 21-25].

Complete oxidation of VOCs on catalyst surfaces can involve species on the catalyst surface and in the gas phase. Three main reaction mechanisms generally used to explain the adsorption and desorption of gaseous reactants and product species include: (1) Langmuir-Hinshelwood mechanism; (2) Mars-van Krevelen mechanism and (3) Eley- Rideal mechanism.

Langmuir – Hinshelwood mechanism (Figure 1) require adsorption of reactant species (e.g. VOC + O_2) on catalytically active surface, followed by reaction, and desorption of products.

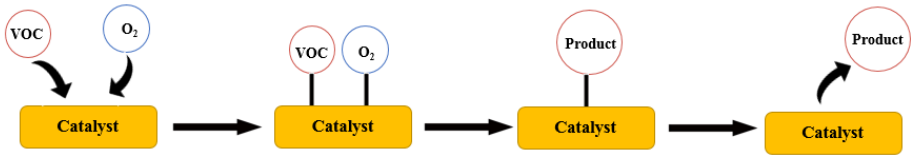

Figure 1. Langmuir-Hinshelwood mechanism illustrated

Mars-van Krevelen mechanism (Figure 2) requires a redox process in which oxygen is consumed from the catalyst surface by reaction with the VOC, and then is replenished by oxygen from the gas phase.

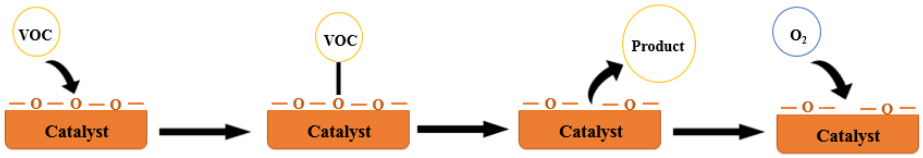

Figure 2. Mars-van Krevelen mechanism illustrated

Eley-Rideal mechanism (Figure 3) is similar to the Mars-van Krevelen mechanism, except that the products are formed from adsorbed oxygen and VOC in the gas phase

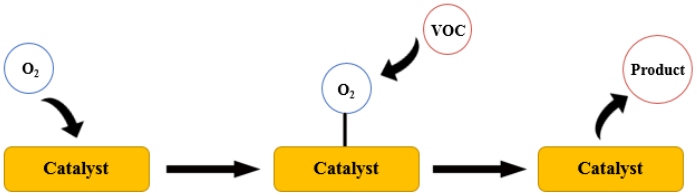

Figure 3. Eley-Rideal mechanism illustrated

The validity of each mechanism strongly depends on the properties of the catalyst (active metal and the support), as well as the nature of the VOCs [26]. For example, for reducible metal or metal oxide catalysts, the Mars-van Krevelen mechanism is usually important [27].

1.3. Noble metal based catalysts

Noble metal based catalysts - Pt, Pd, Ag and Au are most popular for VOCs complete oxidation, however, Rh and Ru catalysts have also shown high catalytic activity [1, 28].

1.3.1. Platinum based catalysts

Platinum (Pt) based catalysts have shown the highest catalytic activity for complete oxidation of VOCs, and so far, they are the most active for oxidation of benzene, toluene, ethylbenzene and xylene (BTEX), occurring between 150 – 350 ºC [29]. Complete oxidation of formaldehyde from room temperature to 120 ºC have been reported with Pt catalysts [30-33], although for alkanes, it has only been efficient for molecular weights higher than pentane's [34]. Complete oxidation of acetone, propane and dichloromethane over Pt catalysts occurred between 260 – 320 ºC, 360 – 500 ºC and 377 – 485 ºC, respectively [26, 35-37].

How active a Pt based catalyst can be greatly depends on the properties of the support such as specific surface area, pore structure, acidity, surface hydrophobicity, metal dispersion on support, metal – support interaction, Pt content, particle size on support and VOC adsorption. Pt supported on $\gamma - Al_2O_3$ have been the most investigated [34], however, Pt supported on MCM-41 mesoporous silica with higher surface area (1000 m^2/g) showed a higher catalytic activity compared to Pt/ $\gamma - Al_2O_3$ for oxidation of aromatic VOCs at 150 ºC; unfortunately, the presence of water vapour, either from the oxidation reaction or in the gas stream, easily condensed in the micro/mesopores of Pt/MCM-41 catalyst at low temperature, causing structural damage to the catalyst support which resulted in Pt sintering and decrease in catalytic activity [38, 39]. Hydrothermal stability therefore seems vital for mesoporous silica based catalysts in VOCs oxidation. Hydrothermal stability can be improved by introducing hydrophobicity to the mesoporous silica (although this may have adverse effects on the supported active phase), or increase the pore wall thickness during synthesis [40-42].

1.3.2. Palladium based catalysts

Palladium (Pd) is widely used for low temperature catalytic oxidation of VOCs and for elimination of other air pollutants in several industrial scale catalytic gas clean-up systems

[43, 44]. Reports reveal that Pd is cheaper and show higher resistance to hydrothermal sintering compared to Pt catalysts, thus prompting considerable attention for development of Pd based catalysts for VOCs oxidation [45, 46]. Research has shown that the choice of support material is crucial when synthesising supported Pd catalysts, as metal – support interaction significantly influences Pd catalyst performance in VOCs oxidation. For instance, porous supports enhance the confinement of Pd nano-particles in the pores, thereby reducing Pd agglomeration and catalyst deactivation [47, 48]. Acid – base property of support influences Pd oxidation state, as Pd loaded on acidic supports are easily oxidised (i.e. acidic supports with electrophilic character results in electron deficient character of Pd), whereas Pd on basic supports are difficult to oxidise (i.e. the electrophobic character of basic supports makes Pd particle electron sufficient) [49]. The catalytic activity of Pd catalysts in VOCs complete oxidation depends on the oxidation state of Pd. [50-52]. Propane complete oxidation over Pd catalysts occurs between 340 – 430 ºC [22, 53-55].

1.3.3. Silver based catalysts

Silver (Ag) based catalysts have been tested for catalytic elimination of VOCs. Reports confirm that smaller Ag nano-particles with good dispersion on support, in addition to high metal loading between 8 – 11 %, significantly increases catalytic activity of Ag based catalysts in complete oxidation of VOCs [56-58]. From publications so far, Ag catalysts have shown inferior catalytic performance for oxidation of benzene, toluene, ethylbenzene and xylene (BTEX) compared to other noble and transition metal oxide catalysts [29].

1.3.4. Gold based catalysts

Unfortunately, the extraordinary performance of supported gold-based catalysts towards oxidation of carbon monoxide below room temperature have not been replicated for the complete oxidation of volatile organic compounds. In fact, from existing publications, gold based catalysts performed poorly when compared to Pt and Pd based catalysts for the

oxidation of BTEX, which occurred at higher temperatures, in the range of 190 to 400 ºC [37]. However, on the positive note, no carbon deposition on gold based catalysts has ever been reported for complete oxidation of BTEX [37]. It therefore seems that an appropriate preparation method and choice of catalyst support which could unleash the power of gold have not been applied in complete oxidation of VOCs

1.4. Transition metal oxide catalysts

Supported or unsupported transition metal oxide catalysts for VOCs oxidation has attracted great attention due to their relative abundance and lower price compared to noble metal catalysts [59, 60]. The most active transition metals in complete oxidation of VOCs include vanadium, chromium, manganese, caesium, iron, cobalt and molybdenum [26, 35, 37]. Significant effort have been made to improve catalytic activity of transition metal oxide catalysts; however, there are still challenges. For instance, iron based catalysts, just like chromium, manganese, and copper oxides, are prone to poisoning, especially from chlorides in oxidation of chlorinated VOCs [61, 62]. Also, chromium is highly toxic and may be unsuitable for air purification systems meant to safeguard public health and the environment. There is also the issue of disposal problems associated with spent chromium based catalysts [20]. The corrosive nature of vanadium presents a problem especially when dealing with wet flue gas streams [20].

1.5. Alloy catalysts

Alloy catalysts consisting of two or more noble metals, noble and transition metals or only transition metals have been synthesised, taking advantage of their synergistic effects, which, in most reported cases, produced a catalyst with higher catalytic activity compared to their monometallic-based catalysts [63, 64].

CHAPTER 2. Project overview

2.1. Choice of Au/SBA-15 catalyst for VOC oxidation

In selecting a highly active metal for synthesis of a suitable catalyst for low temperature VOCs oxidation, noble metals were preferred over the transition metals due to their higher catalytic activity at lower temperatures. Among the list of potential noble metals, gold was chosen due to the immense potential gold-based catalyst possess compared to the rest in complete oxidation reactions as demonstrated by Haruta. Another reason for the choice of gold is that water vapour seems to enhance its catalytic activity as demonstrated in CO oxidation results [65-67]. Water is present in VOCs polluted gas streams and from VOCs oxidation reactions. Water is also quite beneficial in oxidation of chlorinated VOCs, as water reacts with chloride formed in the oxidation process, thereby removing chlorides and increasing HCl selectivity [68, 69]. It is more favourable to have HCl than chloride in treated gas streams since HCl is easily scrubbed off [70].

According to Haruta, the catalytic activity of gold is almost insensitive to the type of metal oxide support but depends strongly on the catalyst preparation method which produces very small gold particles less than 5 nm in size, with high dispersion, firmly attached to the support [5, 6]. To stabilise gold nanoparticles on the support to prevent agglomeration, SBA-15 mesoporous silica, though inert (poor oxygen storage capacity) was preferred as support material for the proposed gold catalyst. SBA-15 of very thick pore walls could potentially confine gold nano-particles in the pores, preventing their growth, agglomeration, sintering and eventual deactivation. Very thick pore walls also enhance catalyst structural and hydrothermal stability, which may improve catalyst durability in reactions [41, 71]. In addition, SBA-15 offer other exciting advantages in catalysis such as high surface area (usually within 700 – 900 m^2/g), large pore size and volume for high dispersion of active

phase [42, 72]. To the best of my knowledge, no publication at the time of writing this thesis exists for developed Au/SBA-15 catalyst tested for VOCs complete oxidation.

2.2. Synthesis of Au/SBA-15 catalysts

For supported gold on reducible supports, adsorbed oxygen on the support and strong interaction between gold and the support play crucial roles in their catalytic activity. However, for supported gold on inert supports such as SBA-15, very small gold particles with high dispersion on the support, coupled with strong Au attachment to the support mainly determine their catalytic activity as gold is the sole active site [73-75].

The conventional co-precipitation, deposition-precipitation and impregnation methods have successfully been used to deposit gold on both reducible and inert supports, except for silica support. This is because silica has low isoelectric point (1 – 2), which causes the surface charge to become highly negative in pH media > 2 (above its isoelectronic point). So, when SBA-15 silica is introduced into a basic media environment necessary to generate gold nanoparticles from hydrolysis of the frequently used chloroauric acid ($HAuCl_4$) gold precursor, which exists either in trihydrate or tetrahydrate form, produces negatively charged gold species which makes it difficult to precipitate onto the negatively charged silica support, due to like charges. A media with a minimum pH of 6 is required to sufficiently generate gold nano-particles from the $[AuCl_4]^-$ transformed to $[Au(OH)_nCl_4\text{-}n]^-$ during gold loading on the support from the dissolved gold precursor [73, 76], resulting in mobility of gold nano-particles which easily agglomerates and sinter, especially during calcination step, to produce low gold loading and inactive Au/SBA-15 catalyst [77]. For this reason, silica was ignored as support material for gold nano-particles, until Kobayashi and co-workers reported co-sputtering of gold on silica, then followed by Mitsutaka Okumura and co-workers in 1998 who successfully prepared active Au/SiO_2 catalyst for CO and H_2 oxidation by chemical vapour deposition (CVD) of organo-gold complex on the surface of SiO_2 [75]. Although co-

sputtering and CVD are both very cumbersome and less suitable to prepare large amounts of catalysts, these synthetic breakthroughs, encouraged other researches to explore simpler ways of depositing gold on silica to produce active Au/Silica catalysts. Alternative modified synthetic method to improve attraction of gold precursor on SBA-15 during impregnation was developed by Zhu and co-workers in 2006, with the synthesis of cationic gold precursor $[Au(en)_2]^{3+}$ (en= ethylenediamine) synthesized from $HAuCl_4$ and ethylenediamine. They synthesised highly active Au/SBA-15 catalyst, prepared by solution based technique with the gold cationic complex precursor immobilised on the negatively charged surface of SBA-15, in a pH media ~ 10, to produce Au/SBA-15 catalyst with 2.2 % wt. Au loading. Their catalyst was highly active for CO oxidation, even below 24 °C [78]. Yang and co-workers also reported another novel synthetic method aimed at attracting gold on SBA-15 – functionalisation of silica support with cationic organo-silane groups before loading gold on SBA-15 via $HAuCl_4$ precursor [79]. Some of the Au/SBA-15 catalysts were either reduced in flowing hydrogen at 200 °C or used in CO oxidation in their oxide (as-synthesised) forms [79]. Although Yang and co-workers reported high dispersion of gold on SBA-15 with 4.8 % gold loading, producing the most active Au/SBA-15 catalyst prepared by solution based technique as at 2003, unfortunately, their Au/SBA-15 catalysts sintered beyond 100 °C, resulting in significant drop in catalytic activity. Au/SBA-15 catalysts by Yang and co-workers were less active than those from CVD and were not as active as Haruta's gold catalysts (which were pre-treated even at temperatures as high as 500 °C) as they showed no CO catalytic activity at room temperature. In conclusion, Yang attributed the mobility of gold particles on the surface of SBA-15 to the relatively weak interaction between gold and the SBA-15 support [79]. With this setback notwithstanding, most researchers have toed the path laid down by Yang and co-workers with further improvements in an attempt to synthesise active and stable Au/SBA-15 catalyst, especially for oxidation reactions. It was

observed that neither Yang nor Zhu calcined their Au/SBA-15 catalysts. At least, calcination temperature of 400 °C is required to burn off the organic complexes attached to gold and SBA-15. The reason for avoiding high calcination temperature could be that they tried to prevent possible gold sintering of their catalysts during preparation stage; and so it is possible that the reported Au/SBA-15 catalysts by Yang and Zhu could not have attained their optimum catalytic potential, with the gold nano-particles trapped in the organic complex. It would have been interesting to note the catalytic activity of these catalysts in complete oxidation of VOCs.

This research goes further, beyond the pioneering works of Zhu and Yang, by attempting to develop improved catalyst preparation methods using synthesised cationic gold precursor $[Au(en)_2]^{3+}$ on SBA-15 and functionalisation of SBA-15 with cationic organosilanes of amine group (3-aminopropyl-trimethoxy-silane, APTMS) and thiol group (3-mercaptopropyl-trimethoxy-silane, MPTMS) on SBA-15 samples, before loading gold with $HAuCl_4$. An attempt was also made on the functionalisation of SBA-15 with a neutrally charged organo-phosphine ligand before loading $HAuCl_4$ gold precursor.

The desired objectives in the synthesis of Au/SBA-15 catalyst is to produce the best catalyst with the smallest gold particles, highly dispersed and strongly attached to SBA-15 support, to prevent agglomeration of gold particles and consequently, sintering and deactivation before or during VOC oxidation reactions. Physical characterisation was done to investigate the nature of the external and internal morphologies of the catalysts, surface area of the catalysts, gold particle sizes, degree of gold loading and dispersion on SBA-15 support using the following techniques: SEM, TEM, BET, Wide angle XRD and EDX.

CHAPTER 3. Support/Catalyst characterisation techniques

3.1. Introduction

Characterisation of heterogeneous catalysts is the investigation into the physical (structural, textural and composition) and chemical attributes of catalysts responsible for their catalytic performance. Characterisation helps formulation scientists develop more active, selective and durable catalysts and also optimise reaction conditions [80].

3.2. Physical characterisation techniques

Physical characterisation deals with [81]:

- Surface morphology of the catalyst
- Elemental composition either in bulk or on the surface of the catalyst
- Size, shape and dispersion of metal particles on the support
- Surface area, pore size and volume of the catalyst

The physical characterisation techniques used in this research project include:

3.2.1. Scanning Electron Microscopy (SEM) and Energy Dispersive X-ray Analysis (EDX)

SEM is useful in observing the external morphology of material sample surfaces magnified in three dimensional-like images from nanometre (nm) to micrometre (μm) scale. This is achieved by directing extremely fine beam of electrons at the specimen, scanning across it by the scan coils. As the specimen is exposed to the incident beam, it emits three types of electronic signals namely; backscattering electrons, with energy close to that of the incident beam, secondary electrons, with kinetic energy less than 50 eV and Auger electrons produced by de-excitation of atoms. Photons from the de-excitation of atoms are produced within the range of X-rays to visible emission domain. SEM working principle is illustrated in Figure 4

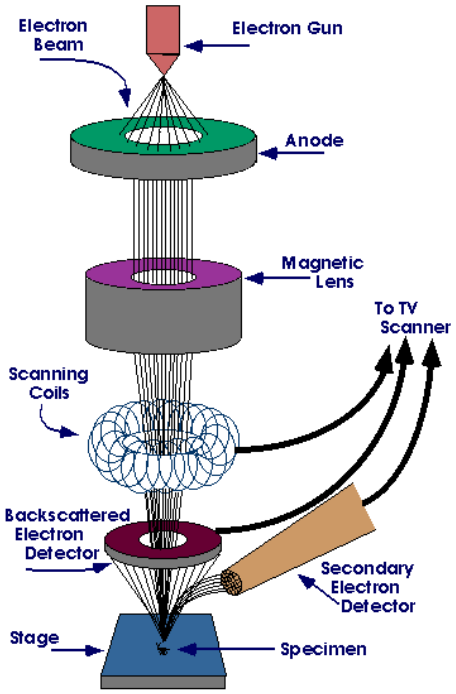

Figure 4. Working principle of SEM
https://www.purdue.edu/ehps/rem/rs/sem.htm

EDX is useful for elemental analysis of samples and is based on the fundamental principle of spectroscopy – the atomic structure of each element produces a unique set of peaks in the electromagnetic emission spectrum when they interact with X-rays. When high-energy beam of charged particles (electrons, protons or beam of x-rays) are focused on the sample, the incident beam may excite an electron in ground state (unexcited) from the inner orbit around the nucleus of the atom, ejecting it from the inner orbit and creating a vacancy. Another electron from an orbit further away in the atom then fills this vacancy. Such electron transitions between the obits results in characteristic X-rays used for either qualitative or quantitative EDX elemental analysis. Qualitative analysis in EDX involves identification of the unique peaks in the spectrum, while quantitative analysis (to determine the concentration of elements present) involves measuring the peak intensities for each element in the sample [82, 83]. EDX only penetrates about 1 – 2 micrometres in depth of sample, making it a useful technique in the determination of metal presence and loading on the surface of catalyst supports [82].

3.2.1.1. Experimental condition

Measurements were with Hitachi S-3400N scanning electron microscope operated at an accelerating voltage in the 15 – 20 kV. Adhesive carbon film on aluminium alloy stub was used to set and mount catalyst samples into the scanning microscope, coated by gold – palladium sputtering for clearer SEM images. No coating was done for EDX analysis.

3.2.2. Transmission Electron Microscopy (TEM)

TEM is useful for probing the internal structure of solids, which makes this technique widely utilised in the field of heterogeneous catalysis. TEM is an indispensable technique used to study gold nanoparticle morphology, size and shape and how well gold nanoparticles interact with the support. TEM images can also complement the determination of metal particle size from Scherrer equation fitted wide-angle XRD results.

Image formation in TEM is similar to that of optical microscope, except that it uses electrons instead of light. As illustrated in Figure 5, the electrons first emitted from the top column of the microscope via an electron gun travels through vacuum inside the column at an accelerated voltage, usually between 100 – 200 kV. The beam of electrons emitted by the gun also controls its diameter before it hits the specimen. A thin film of specimen is required in order to transmit the electron beam. An intermediate magnified image formed from the objective lenses is subsequently enlarged by projector lenses on a fluorescent screen and the image is then visualised by the operator who can also photograph the images with a camera attached to the microscope [84-86].

3.2.2.1. Experimental condition

TEM images were obtained using a JEOL 2100F FEG Transmission electron microscope operated at 200 kV. The catalyst samples were homogenously dispersed in pure acetone using ultrasonic bath and then deposited onto holey carbon grid. The acetone solvent was allowed to evaporate under vacuum before examination of the catalyst samples in TEM mode.

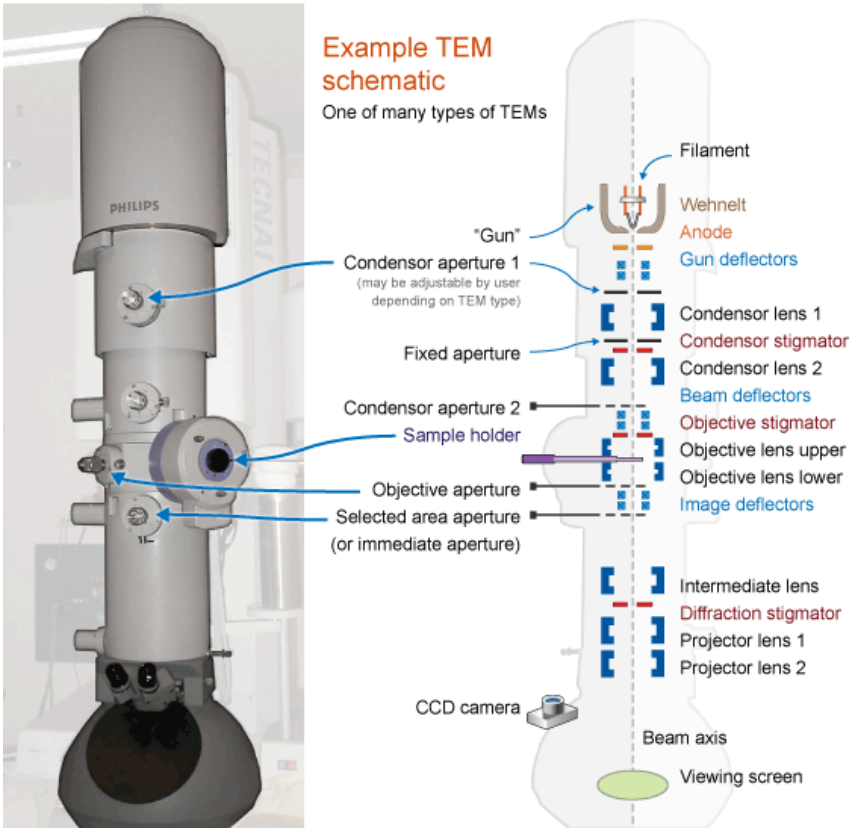

Figure 5. Working principle of TEM in the column
http://www.ammrf.org.au/myscope/tem/introduction/

3.2.3. X-ray Diffraction (XRD)

Solids can be classified either as crystalline or amorphous structures. A crystalline solid is a homogenous chemical compound with periodically long range ordered arrangements of their atoms, molecules or ions in three-dimensional geometrical structure. Amorphous solids on the other hand have no long-range regularity in their external structure (i.e. lacks crystalline structure). Many physical properties such as mechanical strength, thermal and electrical conductivity, refractive index, etc. are linked to the nature of crystallinity, and differ in amorphous forms of the solids [87]. Although silica is amorphous, it can be synthesised to have orderly regular repeating units (such as SBA-15), like a crystal.

XRD is a non-destructive analytical technique used in the determination of crystallinity of samples in fine powdered form (particle sizes less than 10 microns), also referred to as

powdered diffraction. XRD produces simple but unique patterns or peaks from Bragg's reflections associated with any given crystalline substance, based on the principle that: 'Every crystalline substance gives a pattern; the same substance always gives the same pattern; and in a mixture of substances each produces its pattern independently of the other' [88]. Therefore, XRD powder diffraction patterns of a sample only indicates its characteristic crystalline phase present and not its chemical elements or compounds.

The small group of atoms, molecules or ions that form the repeating pattern in a crystal is referred to as the unit cell of the structure. The unit cell builds up in a set of parallel equidistant planes, having a definite orientation and spacing, *d* [89]as shown in Figure 6.

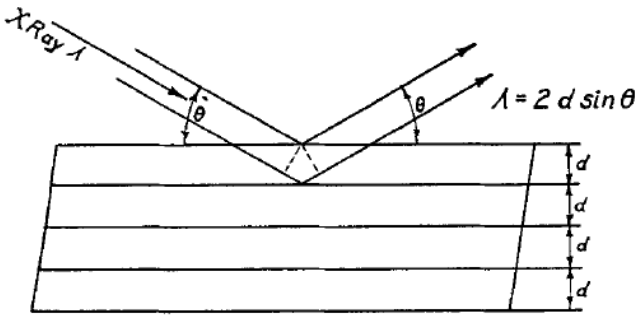

Figure 6. Diffraction by crystal planes [89]

In 1913, William Lawrence Bragg and his father, William Henry Bragg [90] first reported X-ray reflected patterns from a crystal. When an X-ray beam of certain wavelength (λ) falls or is incident on a crystal at an angle (θ) with a set of planes of spacing *d* (illustrated in Figure 6), it produces a Bragg peak if the reflection off the planes interfered constructively, which they expressed by their proposed Bragg's law: $\lambda = 2d \sin \theta$. Where: d = lattice interplanar distance of the crystal, θ = X-ray incidence angle (Bragg angle), λ = wavelength of the characteristic X-rays. If λ and θ (one-half of the diffracted angle) are known, it is possible to determine the perpendicular distance between lattice planes d and consequently, the unit cell (a) [91]

In the X-ray tube diffractometer (Figure 7), the high voltage maintained across the electrodes draws electrons towards the anode, which is a metal target, usually copper, because copper produces the strongest characteristic radiation at a wavelength of 0.154056 nm. These X-rays are collimated and directed onto the powdered sample.

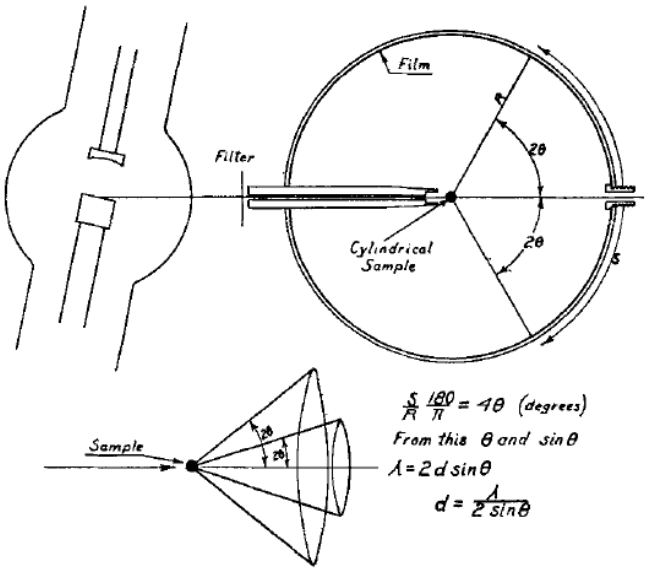

Figure 7. Schematic of X-ray diffractometer [89]

With Bragg's law satisfied, the constructive interference of the diffracted X-ray beams are picked up by a detector, and then is processed by a microprocessor electrically converting the signals to a count rate. The angle between the X-ray source, sample and detector can be changed at a controlled rate such as at low angle and wide angle, with each angle giving different information of the sample analysed [92]. Low angle XRD gives information on crystallinity, including lattice interplanar distances (*d*) and the unit cell of the structure (*a*). Wide angle XRD gives information on the crystal particle size and shape [85]. Scherrer equation is used to calculate crystal particle size as it relates particle size (in sub-micrometre) to the broadening of a peak in XRD diffraction pattern. Scherrer equation [93] is expressed as:

$$\Gamma = \frac{K\lambda}{\beta \, Cos\, \theta}$$

Where: Γ =Mean size of crystalline particle, K = Dimensionless shape factor, with value close to unity but varies slightly with crystallite shape, λ = wavelength of the characteristic x-rays, β = Half the maximum intensity (FWHM) of a broad XRD peak after subtracting the instrumental line broadening (in radians), θ = Bragg angle (in degrees)

3.2.3.1. Experimental condition

XRD patterns of samples were collected in a Siemens D500 diffractometer with Bragg-Brentano geometry, using nickel-filtered Cu-Kα radiation (λ = 0.15406 nm), at tube voltage of 40 kV and 20 mA current. Low angle XRD was from 0.9 – 3° over 2θ range at scanning rate of 1°/min. Wide angle XRD results were from 10 – 90 ° over 2θ range. Metal particle size on catalyst support was calculated using Scherrer equation.

3.2.4. Fourier-Transformed Infrared Spectroscopy (FT-IR)

With the discovery of infrared light in the 19th century, scientists established the fact that functional groups within a molecule exhibit characteristic absorption of infrared light when exposed to infrared radiation. This is because of selective absorption of radiation of specific wavelengths, which causes a change in their dipole moments, and as a result, the vibrational energy levels of samples transit from ground state to excited state. With the vibrational energy gap, the frequency of absorption peak is determined. FT-IR is a technique used to generate infrared spectrum from absorption or emission of a molecule in gas, liquid or solid phase via Fourier transform (a mathematical process) which converts intensity vs time spectrum into intensity vs frequency spectrum. FT-IR significantly provides a better resolution with improved signal to noise ratio compared to the classical continuous wave spectrometers used in ultraviolet-visible spectroscopy.

When a molecule exhibits a number of vibrational freedoms, it generates a corresponding number of absorption peaks. The absorption peak intensity is related to the change in dipole

moment and the transition of energy levels. Therefore, analysis of infrared spectrum of a sample gives structural information of a molecule with its presence and abundance.

Except for homonuclear diatomic molecules such as O_2, N_2, and Cl_2, which have zero dipole change, other molecules are infrared active. FT-IR operates mostly within 4000 to 400 cm^{-1} wave numbers, since most organic and inorganic compounds absorption radiation occur within this region.

Typical FT-IR spectrometer consists of a source, Michelson interferometer, sample compartment, detector, amplifier, A/D convector and a computer. Radiation generated from the source passes through the interferometer before passing through the sample and then to the detector. The signal is then amplified and converted to digital signal and transferred to the computer where Fourier transform is carried out. FT-IR working principle is illustrated in Figure 8.

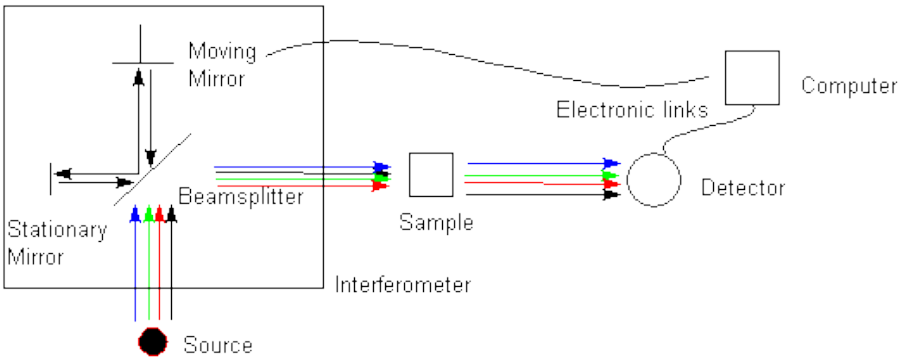

Figure 8. Working principle of FT-IR
http://chemistry.oregonstate.edu/courses/ch361-464/ch362/irinstrs.htm

Michelson interferometer, which consists of a beam splitter, stationary and moving mirrors, is the major difference between FT-IR spectroscopy and dispersive IR spectroscopy. The beam splitter sends light at right angles in two directions, so that one beam goes to the stationary mirror and back to the beam splitter, while the other beam goes to the moving mirror. The motion of the mirrors creates a total path length variable versus the stationary mirror beam, so that when the two meet up and combine at the beam splitter, they create

constructive and destructive interference (an interferogram), before passing through the sample. The sample absorbs all the different wavelengths characteristic of its spectrum and subtracts the specific wavelengths from the interferogram. The detector then reports energy (volts) versus time simultaneously for all wavelengths. A laser beam is superimposed to offer a reference for instrument operation. Fourier Transform thereby converts the energy versus time to intensity (% Transmittance or Absorbance) verse frequency (wavelengths) [94-96] as shown in Figure 9.

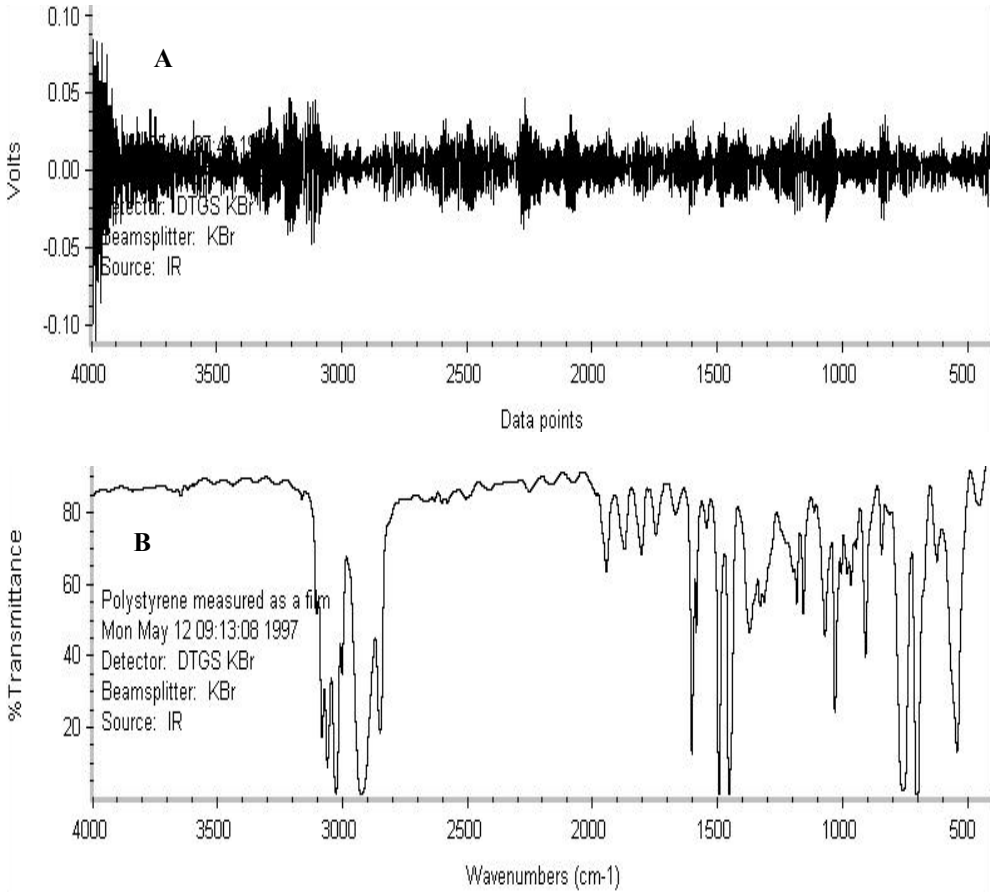

Figure 9. (A) FT-IR Interferogram, (B) FT-IR Interferogram
http://chemistry.oregonstate.edu/courses/ch361-464/ch362/irinstrs.htm

3.2.4.1. Experimental condition

FT-IR was used to confirm calcination was efficient in removing P123 surfactant template from the pores of SBA-15, in addition to detection of the functional groups present in the calcined and uncalcined SBA-15 samples. Spectra were recorded on 1760 Perkin-Elmer FT-IR spectrometer at 2 cm^{-1} resolution and 60 scans in normal conditions.

3.2.5. Nitrogen physisorption

The physical adsorption (physisorption) of nitrogen at 77 K on mesoporous materials (with pore diameter in the range of 2 – 50 nm) such as SBA-15, is widely used to determine surface area, pore size (diameter) and pore volume. Brunauer and Emmett first carried out the systematic measurements of nitrogen physisorption at 77K over eighty years ago [84]. Nitrogen is adsorbed on the surface of the solid sample held by weak Van der Waals forces and remains unchanged when adsorbed or desorbed from the sample surface which is an exothermic process [84].

In 1985, the IUPAC commission on Colloid and Surface Chemistry in addition to the five isotherms by Brunauer, added the sixth isotherm and therefore agreed on six types of isotherms (Figure 10) that corresponds to capillary evaporations and for heats of adsorption and phase transitions (capillary condensation and layer transitions) in pores [97].

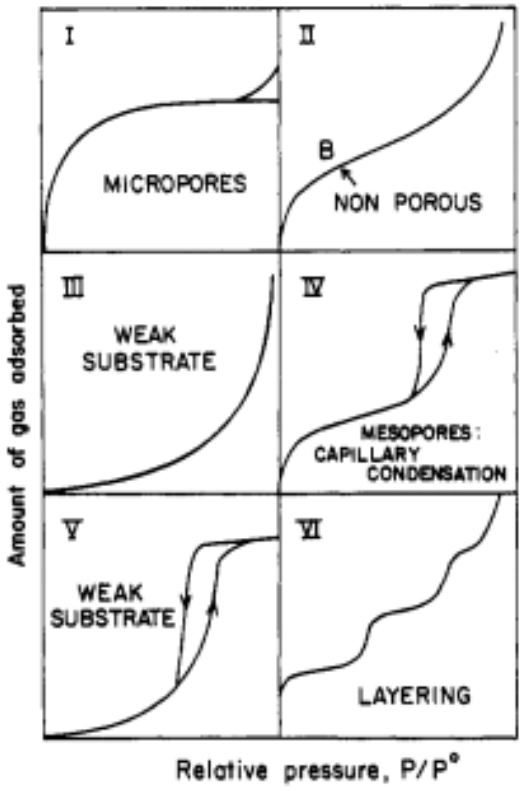

Figure 10. IUPAC types I - VI adsorption-desorption isotherm typical for surface area determination [97]
http://home.icpf.cas.cz/ivonez/papers/gubbinspore2.pdf

Type I (the Langmuir isotherm) is typical of many microporous adsorbents. Types II and III isotherms are common in non-porous materials with strong (type II) or weak (type III) fluid-wall attractive forces. Types IV and V are characterised by mesoporous materials for strong and weak fluid-wall forces, respectively and alongside capillary condensation, showing hysteresis loops. Materials with relatively strong fluid-wall forces show type VI isotherm.

To determine the surface area, the sample is first pre-treated to remove adsorbed contaminants from the atmosphere, such as water and carbon dioxide by using a combination of heat, vacuum and/or gas flow. The solid sample is then cooled to 77 K before dosing nitrogen incrementally. With each nitrogen dose, the pressure is allowed to equilibrate before calculating the quantity of adsorbed nitrogen. The quantity of adsorbed nitrogen at pressure and temperature relates to the adsorption isotherm, which is used to determine the quantity of nitrogen required to form a monolayer on the external surface of the sample. Brunauer, Emmet and Teller (BET) extended the Langmuir mechanism [98], a theory of monolayer molecular adsorption to multilayer adsorption which is expressed in BET equation for each monolayer in the multilayer as: $\frac{p}{n(p^0-p)} = \frac{1}{n_m C} + \frac{C-1}{n_m C} \text{ x } \frac{p}{p^0}$

Where: n = specific amount of gas adsorbed at equilibrium pressure, n_m= monolayer capacity, p^0 = saturation pressure, C = constant exponentially related to adsorption energy

BET plot will therefore be a straight line with slope of $\frac{C-1}{n_m C}$ and $\frac{1}{n_m C}$ as intercept.

The specific surface area, *a*(BET) can be determined from the BET monolayer capacity n_m using the relationship: $a(\text{BET}) = n_m \text{ L}\delta$ Where: L = Avogadro constant, δ = average area occupied by each molecule in the complete monolayer.

A further increase in nitrogen dose with pressure allowed to equilibrate causes the gas to condense to liquid and saturates the solid sample. The pressure is then reduced incrementally which causes the condensed nitrogen liquid to evaporate from the pores. The adsorption and

desorption of nitrogen relates to an isotherm with hysteresis in between the adsorption and desorption curves for mesoporous materials, revealing information on pore size and volume. Barrett, Joyner and Halenda (BJH) method is used to calculate pore size and volume from experimental isotherms using Kelvin model of pore filling which is most ideal for mesoporous and small range macroporous materials [85, 98].

3.2.5.1. Experimental condition

Nitrogen adsorption-desorption isotherms were obtained in a Micrometrics Tristar II 3020 Surface Area and Porosity Analyzer at 77 K. The samples were degassed at 350 °C, under vacuum, for two hours, before analysis. The surface area was calculated by BET method. The volume of mesopores was determined from BJH (adsorption isotherm). The pore wall thickness was calculated as: Pore wall thickness = Unit cell parameter (*a*) – Pore size diameter obtained from BJH [99].

3.3. Chemical characterisation techniques

Chemical characterisation of heterogeneous catalysts deals with the investigation of surface chemical properties of the catalyst such as [81]:

- Reducible – oxidable properties of the catalyst
- Acid – base property of the catalyst (This was not investigated since Au/SBA-15 catalyst has no acid or basic sites)
- Catalytic activity of the catalyst
- Selectivity
- Reaction stability

In this project, temperature programmed reactions: hydrogen Temperature Programmed Reduction (TPR) and Temperature Programmed Reaction (TPR_x) were carried out using Hiden Analytical Catlab system [100]. Catalytic micro-reactor system was used to study the

catalytic activity, selectivity and stability of VOC oxidation reaction over the best Au/SBA-15 catalyst.

3.3.1. Temperature Programmed Reduction (TPR)

John Ward Jenkins in 1975 perfected the technique of controlled reduction of catalysts, now popularly known as TPR, which involves subjecting an oxidised form of catalyst to a reducing environment, usually hydrogen, flown over the catalyst sample while steadily raising temperature versus time (ramp rate), to determine the optimum temperature condition required to reduce the catalyst [101, 102]. As hydrogen is consumed in TPR, a corresponding water formation can be observed in a gas chromatogram or a mass spectrum [100] .

3.3.1.1. Experimental condition

Hiden Analytical Catlab – Quadrupole Mass Spectrometer micro-reactor system with fixed bed (quartz tube reactor of 4mm internal diameter and 18.5 cm in length) was used for TPR TPRx and CFR. Before TPR, the catalyst in the reactor was pre-treated in 30 ml/min flow of argon at 200 °C for 1 hour, followed by flowing 30 ml/min 5 % H_2 in argon balance over the catalyst, with temperature raised from room temperature to 500 °C at 10 °/min ramp rate. Reduction in H_2 was continued for 1 hour at 500 °C before cooling back to room temperature in 30ml/min of Ar flow. TPRx or CFR was done immediately after TPR.

3.3.2. Temperature Programmed Reaction (TPRx)

TPRx is a reliable technique used in monitoring catalytic chemical reactions, and is useful in determination of rates of reaction, kinetic parameters and reaction mechanisms. TPRx involves increasing the reactor temperature at a constant rate in a continuous flow of reactants, over the catalyst. In most cases, the continuous sequence of catalytic conversion with corresponding product species distribution is monitored in real time over a selected temperature range using a mass spectrometer (MS) connected to a computer [103, 104].

3.3.2.1. Experimental condition

TPRx on the as-synthesised or reduced forms of the catalyst was carried out after catalyst pre-treatment at 200 °C for one hour. Gas Hourly Space Velocity (GHSV) of 45, 000 h^{-1} (20 mg of catalyst) was used for acetone oxidation, while for propane, BTEXB and dichloromethane TPRx, GHSV was 18, 450 h^{-1}. Acetone, dichloromethane and BTEXB were in three separate gas cylinders. Except for 1,3 – butadiene with 20 ppm, each of the BTEX VOC was 200 ppm, all in nitrogen balance. 40 ml/min flow rate from each VOC gas cylinder with 20 ml/min flowrate from air gas cylinder (zero grade), making a total flowrate of 60 ml/min were passed over the catalytic reactor for each set of TPRx experiments. For propane however, 1.5 ml/min flowrate of pure propane (99.9%) with 60 ml/min air (61.5 ml/min total flowrate) was passed over each 50 mg of catalyst for TPRx. For TPRx experiments, temperature of the reactor was raised from 28 °C to 400 °C at a constant rate of 10 °/min. A summary of the VOC composition and experimental conditions for catalyst testing are shown in Table 1.

Table 1. VOC composition and experimental testing conditions

VOC/Concentration	TPR	TPRx	GHSV (h^{-1})
Acetone (200ppm in N_2 balance)	5% H_2 in Ar balance Flowrate: 30 ml/min Temperature ramp: 28 - 500 °C at 10°/min	Flowrate: VOC: 40ml/min, Air: 20ml/min Temperature ramp: 28 – 400 °C at 10°/min	45,000
Propane (99.9% propane)		Flowrate: VOC: 1.5 ml/min, Air: 60ml/min Temperature ramp: 28 – 400 °C at 10°/min	18,450
BTEXB (820 ppm)		Flowrate: VOC: 40ml/min, Air: 20ml/min Temperature ramp: 28 – 400 °C at 10°/min	
Dichloromethane (200 ppm)			

CHAPTER 4. Synthesis and physical characterisation of SBA-15

4.1. Introduction

Catalyst formulation scientists are faced with the challenge of developing highly ordered mesoporous catalysts that can retain their structure, surface area and pore volume over a long period of time in a chemical reaction. This is because temperature reaction conditions and the presence of water vapour often causes irreversible structural damage to the catalyst which hampers its optimal performance [105]. For this reason, an attempt was made in this chapter to understand the synthetic parameters essential in the development of an optimised SBA-15 mesoporous silica support with high structural, thermal and hydrothermal stability, in addition to other desired properties such as high surface area, large pore size and volume for the design of the proposed Au/SBA-15 catalyst.

4.2. The importance of SBA-15 with thicker pore walls

Mesoporous supports such as SBA-15 offer high surface area for high dispersion of the metal active phase that could enhance catalytic activity. According to IUPAC, porous materials can have ordered or disordered structure and are classified as [106]:

Porous materials with pore diameter < 2 nm are known as microporous;

Porous materials with pore diameter between 2 nm and 50 nm are known as mesoporous;

Porous materials with pore diameter > 50 nm are known as macroporous.

Zeolite, an example of a microporous material with pores less than 1nm fall short in demand for separation or catalysis involving large molecules [107-109]. In addition, zeolites have a perfect crystalline morphology with pore sizes that are not easily tunable, prompting the growing research interest in controllable mesoporous materials with silica and alumina most common [110, 111]. The synthesis of mesoporous silica was first carried out in 1970 and the steps patented even though its usefulness was not recognized at the time, not until 1992 with

the discovery of Mobile Crystalline Material (MCM-41) and MCM-48 [112]. However, the quest to develop mesoporous materials with larger pore sizes for reactions or separations involving larger molecules lead to the synthesis of SBA-15.

In 1998, Zhao and co-workers at the University of California Santa Barbara reported the first synthesis of mesoporous silica with larger pores around 4.6 – 30 nm, using the surfactant known as non-ionic triblock polymer as template in acidic media which was named SBA-x (Santa Barbara Amorphous) where x corresponds to the number of specific pore structure and surfactant. For instance, they developed SBA-15 with hexagonally ordered cylindrical pore arrangement, by using P123 surfactant as structure directing agent (or template), and SBA-16 which has spherical pores arranged in a centred cubic structure synthesised with F127 surfactant as template [113]. Unlike the MCM-41, MCM-48 and SBA-16 mesoporous silica materials, SBA-15 with thicker pore walls is more hydrothermally stable compared to the rest [42, 72], which makes SBA-15 an excellent support material of choice for the proposed gold based catalyst.

Bore and co-workers [11] demonstrated that the sintering of gold nanoparticles on mesoporous silica is dependent on the pore size, pore wall thickness (strength of pores) and pore connectivity. They grafted gold nano-particles on various mesoporous silica, with different pore sizes, wall thicknesses and different pore structures (2D-hexagonal, 3D hexagonal and cubic) and testing them in CO oxidation from 25 to 400 °C, after reduction in hydrogen flow at 200 °C. Bore and co-workers observed that the 2D hexagonal mesoporous structures of MCM-41 and SBA-15 were best in retaining gold nanoparticles inside the pores. Subsequently, they compared the following 2D hexagonal mesoporous silica materials for sintering of gold particles: MCM – 41 (pore wall thickness of 1.0 nm), SBA-15 (pore wall thickness of 2.6 nm) and SBA-15 (pore wall thickness of 4.8 nm). The SBA-15 with the thickest pore wall was the most effective at controlling the growth of gold

particles. Mesoporous materials with thinner walls were most damaged in-between the gold particles, with MCM-41 (1.0 nm wall thickness) most crushed. It is important for mesoporous silica supports to have thicker, stronger pore walls to withstand the rigors of modification by functionalisation with organic groups and gold loading, to avoid crushing some of the meso- structure, which reduces the surface area of Au/SBA-15 catalyst. Thicker pore walls also increases the thermal and hydrothermal stability of SBA-15.

4.3. Synthesis of SBA-15

Mobil's scientists first proposed the true liquid-crystal templating process for the synthesis of mesoporous materials and later, the cooperative self-assembly templating process was proposed. These two main pathways are used to explain the possible synthetic mechanisms for the formation of ordered SBA-15 mesoporous materials as illustrated in Figure 11.

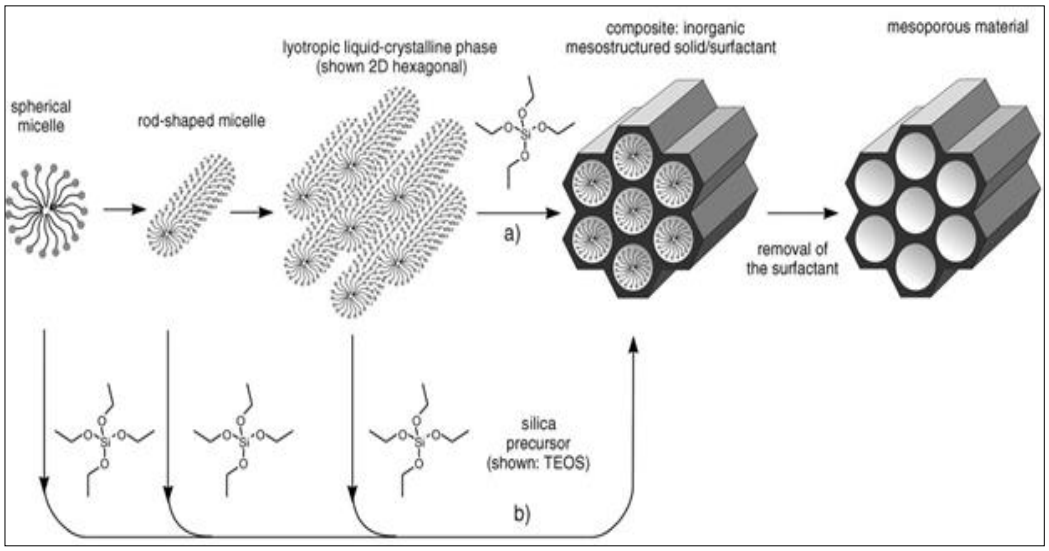

Figure 11: Formation of mesoporous materials by structure-directing agents: a) true liquid-crystal template mechanism, b) cooperative self-assembly template mechanism [112, 114]

SBA-15 synthesis is a sol-gel method. A liquid solution (Sol) is formed when a surfactant is dispersed in an aqueous solution to form micelles. Surfactants, meaning surface active agents, are amphiphilic molecules which consists of a polar hydrophilic head (water-loving or attracts water) and a non-polar hydrophobic tail (water-hating or repels water). Surfactants

could be classified by their head group as cationic, anionic and non-ionic. They are able to form micelles in aqueous solution due to their amphiphilic nature as illustrated in Figure 12:

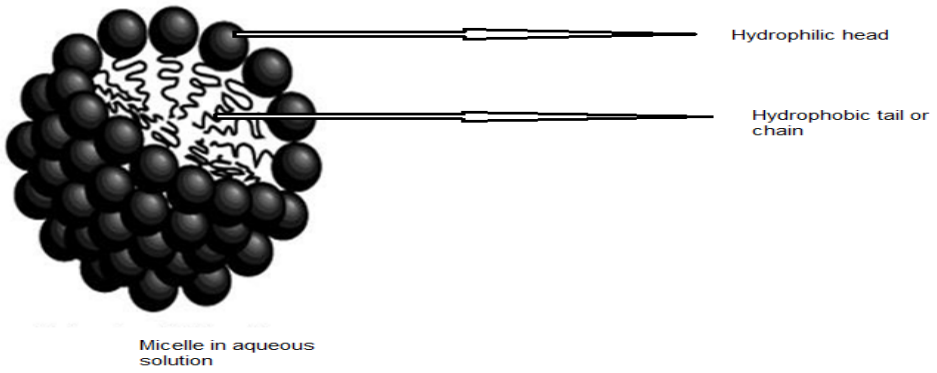

Figure 12: Spherical micelle formation in aqueous media
https://engineering.purdue.edu/MSE/research/reu/StudentPages/2004/hSpringer/index.html

The concentration of the surfactant and the temperature of the solvent play a critical role in the formation of micelles since the properties of the surfactants are temperature dependant [113]. For the purpose of this research, poly (alkylene oxide) triblock copolymer known as Poly (Ethylene Oxide) – Poly (Propylene Oxide) – Poly (Ethylene Oxide) (PEO-PPO-PEO), a non-toxic non-ionic amphiphilic surfactant, was used as template to form ordered mesoporous silica material. This surfactant is also referred to as P123 ($EO_{20}PO_{70}EO_{20}$). The PEO end is hydrophilic and the PPO end is hydrophobic. The first letter refers to physical appearance of the surfactant, (F) for flake, (P) for paste and (L) for liquid. The first one or two numbers multiplied with 300 refers to the molecular weight of the PPO block while the last number gives the PEO weight fraction, this means that P123 is a paste with 3600 g/mol PPO and 30wt% PEO. This differences gives rise to the variations in the pore structure of mesoporous materials; for example, the surfactant F127 gives spherical pores in a body centred cubic structure, whereas P123 gives hexagonally ordered cylindrical pores [113].

The next step in the synthesis of SBA-15 is the addition of a silica precursor to the dissolved surfactant. The concentration of reactants, temperature of the reaction, pH of solution, co-

solvents, additives and stirring can influence the morphology, surface area, pores size, pore volume and the thickness of the pore walls. The three most common silica precursors are the alkoxides:

1. Tetraethoxysilane (Tetraethyl orthosilicate), (TEOS), $Si(OC_2H_5)_4$
2. Tetramethoxysilane (Tetramethyl orthosilicate), (TMOS), $Si(OCH_3)_4$
3. Tetrapropoxysilane (Tetrapropyl orthoslicate), (TPOS), $Si(OC_3H_7)_4$

For this research, TEOS was used. TMOS is easier to use but very hazardous to the lungs and eyes [115]. However, they all are efficient as silica precursors.

When TEOS is added, it is hydrolysed by water in the solution and then undergoes condensation and polymerisation to form silica network around and inside the core of the micelles. Hydrolysis of TEOS requires an acid or base to take place and is directly proportional to the concentration of the acid or base so that the rate of hydrolysis and condensation can be controlled by varying the pH of the solution or by addition of salts or both [113]. SBA-15 have been formed in acid media with pH <1 with HCl, HBr, HI, HNO_3, H_2SO_4 and H_3PO_4. At pH values 2 – 6, which are above the isoelectric point of silica, no precipitation or formation of silica gel occurred [42, 72]. In other to form cylindrical pores in the SBA-15, the concentration and temperature of the surfactant in the solution is kept constant before TEOS is added. At minimum, a certain critical micelle concentration (CMC) and temperature (CMT) is required before micelles are formed [116-119]. Initially, micelles appear spherical as shown in Figure 12, but as TEOS is added to the solution, the hydrolysed TEOS which is also hydrophobic, enter the hydrophobic core of the micelles and adsorbs on P123 template [113]. As the TEOS is polymerised on the PEO chain, the water content on the PEO chain decreases, this changes the polarity and consequently leads to the elongation of the micelles.

4.3.1. Hydrothermal treatment

In the synthesis of SBA-15, an initial temperature between 35 °C – 80 °C while stirring is required. Poorly ordered structures are obtained below 35˚C and initial reaction temperature above 80 °C produces only silica gel [42]. Although the formation of SBA-15 is complete with the addition of a silica precursor, further treatment is required to manipulate its properties such as pores size, pore volume, surface area and pore wall thickness. This further treatment which involves increasing reaction temperature above 35 °C after about 24 hours, but not more than 140 °C, without stirring, is known as hydrothermal treatment or ageing. Swelling agents can also be introduced to increase pore size, but in this research, no swelling agent was used. The manipulation of the SBA-15 properties at this stage is possible because the properties of the surfactant, which serves as template, are temperature dependent. Hydrothermal treatment leads to the formation of the hexagonal structure, reduces the shrinkage of the silica walls during calcination, increases the pore size and changes the adsorptive properties. Pore size is increased because as the temperature is elevated, the PEO tails or chains become more hydrophobic and retract from the silica wall into the hydrophobic core of the micelles, consequently reducing micro-porosity, increasing pore size and reducing surface area [113]. Manipulating these properties can then be achieved by varying the hydrothermal temperature and time of the treatment.

4.3.2. Washing and drying

As-synthesised SBA-15 is obtained when the final solution from hydrothermal treatment is filtered, washed and dried. Drying can be done at room temperature or in the oven at an elevated temperature, but care must be taken not to destroy the ordered structure. Water is normally used for washing to remove the surfactant ($EO_{20}PO_{70}EO_{20}$) and acids before calcination. Thielemann and co-workers [99] demonstrated that washing SBA-15 with plenty of pure solvent, such as water or ethanol does not alter the homogeneity and order of

SBA-15 pores, whereas washing with plenty of mixed solvent, example, water and ethanol mixture, may increase SBA-15 surface area but also decrease the homogeneity of the pores. According to the authors, the detrimental effect of using plenty of mixed solvent quantity for SBA-15 washing may be attributed to hydrolysis and re-condensation reactions of the silica in the pore wall, which leads to narrowing or widening of certain pore sections [99]. It is therefore recommended that pure solvent or controlled amount of mixed solvent be used for SBA-15 washing.

4.3.3. Calcination

This is the final step in SBA-15 synthesis. Calcination is the most common method to remove the surfactant template, leaving the pores empty in SBA-15. Organic surfactants are completely oxidised or decomposed in oxygen or atmospheric air. Temperature programming is carefully done to prevent structural collapse of SBA-15. It has been reported that heating as-synthesised SBA-15 with the rate of 1-2 °C /min to 500 – 550 °C, keeping the temperature constant for 4-8 hours can completely remove triblock copolymer templates [42, 72]. Another alternative to calcination is Soxhlet extraction.

4.3.4. Soxhlet extraction

Soxhlet extraction laboratory apparatus was invented in 1879 by Franz von Soxhlet, originally designed for extraction of a lipid from a solid material [120]. It can be used as an alternative for calcination to remove P123 template from the pores of as-synthesised SBA-15 samples, using either ethanol or HCl-ethanol as solvent [121, 122]. One advantage of Soxhlet extraction over calcination of SBA-15 is that it preserves the high concentration of surface silanol groups on SBA-15 which is diminished to some extent by calcination, however, it has been reported that Soxhlet extraction does not sufficiently remove P123 template from the pores of SBA-15 as-synthesised samples [123-125]. This method is quite

suitable in removing P123 surfactant from functionalised SBA-15 material, by preserving the functionalised organic species which will burn off in calcination treatment [126, 127].

4.4. The chemistry of the formation of pore wall thickness in SBA-15

During the synthesis of SBA-15, TEOS (and the other metal alkoxides) undergo a transition by gelation, due to polymerisation of species from hydrolysis and condensation of TEOS to form a rigid non-fluid mass which after drying and calcination, produces SBA-15 mesoporous silica xerogel.

Metal alkoxides such as TEOS, $Si(OC_2H_5)_4$, tetramethyl orthosilicate (TMOS), $Si(OCH_3)_4$ and tetrapropoxysilane (TPOS), $Si(OC_3H_7)_4$ are popular silica precursors because they readily react with water (hydrolysis) with the – OH group from water, attaching directly to the Si metal atom [128]:

$$Si(OR)_4 + H_2O \rightarrow HO - Si(OR)_3 + ROH \quad (1)$$

The R represents alkyl group. Acid acts as a catalyst for the reaction. The reaction can also undergo complete hydrolysis to form silicic acid:

$$Si(OR)_4 + 4H_2O \rightarrow Si(OH)_4 + 4ROH \quad (2)$$

Two partially hydrolysed molecules (Equation 3) or a partially hydrolysed molecule and TEOS/TMOS/TPOS molecule (Equation 4) could link together in a condensation reaction as shown below:

$$(OR)_3Si - OH + HO - Si(OR)_3 \leftrightarrow (OR)_3Si - O - Si(OR)_3 + H_2O \quad (3)$$

$$(OR)_3Si - OR + HO - Si(OR)_3 \leftrightarrow (OR)_3Si - O - Si(OR)_3 + ROH \quad (4)$$

Water or alcohol is produced from the condensation reaction. The condensation product, $(OR)_3Si - O - Si(OR)_3$ continues to build up by polymerisation around the micelles to form the silica wall thickness.

Hydrolysis and condensation produce different siloxane particles ranging from 1 nm to 1 μm in size (oligomers: colloidal suspension or sol) suspended in water.

Further hydrolysis of the surface alkyl functional groups after polymerisation and washing with water introduces – OH on the surface of SBA-15, which displaces all alkyl groups on the surface and, eventually, from the entire SBA-15 material. Higher concentrations of acid will speed up the hydrolysis of partially hydrolysed $(OR)_3Si-OH$ species, together with condensation and polymerisation reactions to form SBA-15 with thicker pore walls, compared to a sol-gel synthesis with lower acid concentrations. According to Zhao, the macroscopic morphology of SBA-15 (as observed in SEM, Figure 15) is dependent on the local curvature energy between the inorganic silica and block copolymer template, which develops alongside the internal meso-structural properties during synthesis. High acid concentrations will promote faster condensation rates of silica which results in high energy curvature to form elongated worm-like morphology with segments joined together. Low acid concentrations causes slower silica condensation rates to form curved SBA-15 morphology in the form of bent tube or spherical morphologies [129-134].

In addition to the need for thicker pore walls, hydrothermal treatment is also a necessity to reduce microporosity and produce a denser wall thickness.

To study the effect of pore wall thickness on hydrothermal stability of SBA-15, four samples of SBA-15 (A – D) were synthesised. SBA-15 Sample A was prepared with high HCl concentration, while SBA-15 samples B – D were prepared with low HCl concentration. The effect of hydrothermal treatment (aging) time on the wall thickness was also investigated by comparing Sample B, aged for 24 hours, with Sample C, aged for 48 hours, with all other parameters the same for samples B and C. Finally, the effect of aging temperature on wall thickness was studied by comparing Sample C, aged at 80 °C, and Sample D, aged at 90 °C.

The hydrothermal stability of the four SBA-15 samples were tested by flowing pure steam over the samples in a reactor at 800 °C, for one hour.

4.5. Experimental

4.5.1. Materials

The synthesis of SBA-15 was carried out using the procedure described by Zhao et al. [42, 72], as a guide. Triblock copolymer $EO_{20}PO_{70}EO_{20}$ (Pluronic® P123, Aldrich, MW~5800) was used as structure directing agent or template. Tetraethyl orthosilicate (TEOS, Acros Organics, 98 %) was used as silica source and hydrochloric acid (Fisher Scientific, 2M) as catalyst for the reaction.

4.5.2. Synthesis of SBA-15 samples

Four different samples of SBA-15 mesoporous silica were synthesised as follows: SBA-15 sample A was synthesised by dissolving 4 g of triblock copolymer (P123) in 30 ml water with 120 g of 2M HCl (final solution had 1.60 mol/l HCl) added and stirred at 35 °C for 2 hours. 8.5 g of TEOS was then introduced drop wise with the solution stirred for 20 hours at 35 °C. After the 20 hours of initial reaction time where hydrolysis, condensation and polymerisation takes place, stirring was stopped and the solution was aged for 24 hours (hydrothermal treatment). After aging, the solution was filtered, washed with water, air dried for three days before calcination in air at 500 °C, for 6 hours, at 1°/min ramping rate. SBA-15 sample B was synthesised just as SBA-15 sample A, except that less amount of 2M HCl was introduced (9 g HCl, final solution had 0.14 mol/l HCl), with same 4g of P123 and 8.5g of TEOS added. Samples C and D had the same low acid concentrations (9 g HCl, final solution had 0.14 mol/l HCl) as sample B, however, Sample C was aged at 80 °C for 48 hours, while Sample D was aged at 90 °C for 48 hours. For all SBA-15 samples, the initial

reaction temperature was 35 °C and all were stirred for 20 hours at this temperature. In summary, the experimental conditions are listed in Table 2:

Table 2. Summary of experimental conditions for SBA-15 synthesis studied

SBA-15	HCl conc.(mol/l)	Ageing temperature (ºC)	Ageing time (h)
Sample A	1.60	80	24
Sample B	0.14	80	24
Sample C	0.14	80	48
Sample D	0.14	90	48

4.6. Physical characterisation of SBA-15 samples

The physical characterisation of the SBA-15 samples was performed using FT-IR, SEM/EDX, TEM, N_2 physisorption and low-angle XRD, under the conditions described in Chapter 3, section 3.2, along with hydrothermal stability tests, performed under the conditions described below:

4.6.1. Hydrothermal stability test

Hydrothermal stability test was done by flowing steam at 100 °C and at 1 atmospheric pressure (density = 0.6 Kg/m^3) over each of the four SBA-15 sample packed as fixed bed in a stainless-steel tube reactor connected to a steam generator. The temperature of the furnace was maintained at 800 °C throughout the one-hour test duration.

4.7. Results and discussion

All four SBA-15 samples were characterised before and after hydrothermal stability tests to compare the stability of the SBA-15 samples.

4.7.1. FT-IR

FT-IR result (Figure 13) show that the calcination procedure followed was sufficient in removing P123 polymer template which appears around 2975 – 2875 cm^{-1} in the uncalcined SBA-15, but disappeared after calcination.

FT-IR spectra also confirmed the nature of functional groups present in SBA-15 such as: Si-OH (3490 – 3173 cm^{-1}), Si-O-Si (1253 – 998 cm^{-1}) and Si-O (977 – 440 cm^{-1}), present in both calcined and uncalcined SBA-15.

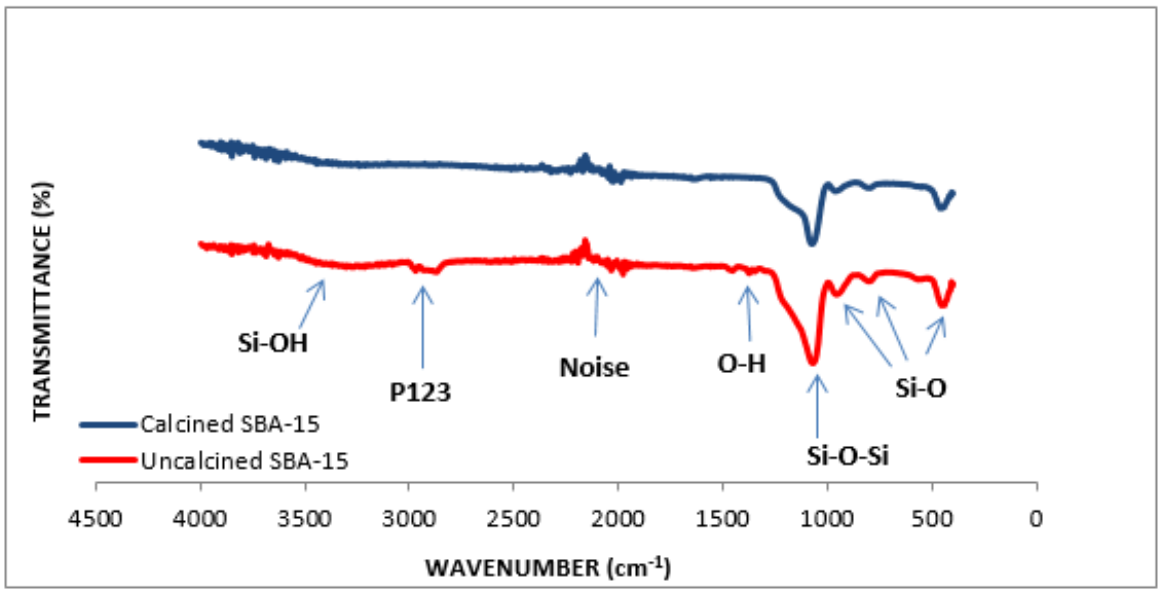

Figure 13. FT-IR spectra of calcined and uncalcined SBA-15 samples

4.7.2. Morphology and elemental analysis of SBA-15

EDX analysis (Figure 14) confirms SBA-15 Sample A as a silica material, of silicon and oxygen atoms only. Same results were obtained on the Samples B – D (results not shown).

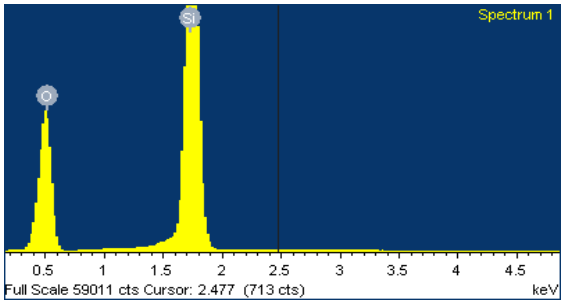

Figure 14: EDX of SBA-15 Sample A

Figure 15 show SEM images of the different SBA-15 samples. Sample A has long worm-like morphology, with primary particles of about 0.4 – 0.6 µm in width and 1.2 – 3.1 µm lengths attached end-to-end. Samples B – D have the same morphology, as short separate bended tubes of about 0.4 – 0.7 µm width and 0.9 – 1.7 µm lengths. The concentration of the acid during synthesis, significantly influenced the morphology of the samples with Sample A of high acid concentration having elongated worm-like morphology; whereas using less acid concentration resulted in shorter bended tube morphology for Samples B – D. Changes in hydrothermal temperature or time during synthesis did not affect the morphology.

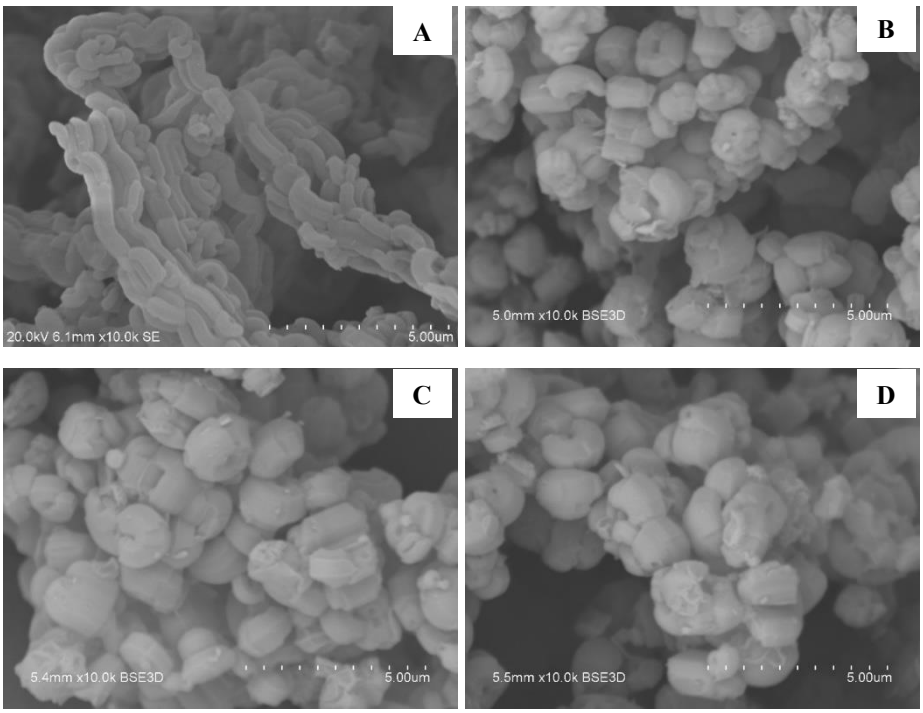

Figure 15: SEM images of SBA-15 Samples A – D

4.7.3. TEM images of SBA-15

TEM was performed only for the SBA-15 Sample A, as TEM had to be outsourced. TEM vertical view (A), in Figure 16, reveals the ordered hexagonal mesoporous structure and the presence of rather thick walls around the cylindrical pores. TEM viewed from the horizontal plane (B), reveals the arrays of narrow cylindrical pores with silica pore walls in between. The TEM images are another evidence of the hexagonally ordered mesoporous SBA-15 arrangement with thick pore walls. The pore size was estimated as 5.23 nm, the unit cell parameter was estimated as 9.8 nm, while the thickness of the pore wall thickness was estimated as 4.8 nm using the TEM images. The estimated TEM values for pores size, unit cell parameter and pore wall thickness are similar to results obtained using nitrogen physisorption and low angle XRD (Table 3)

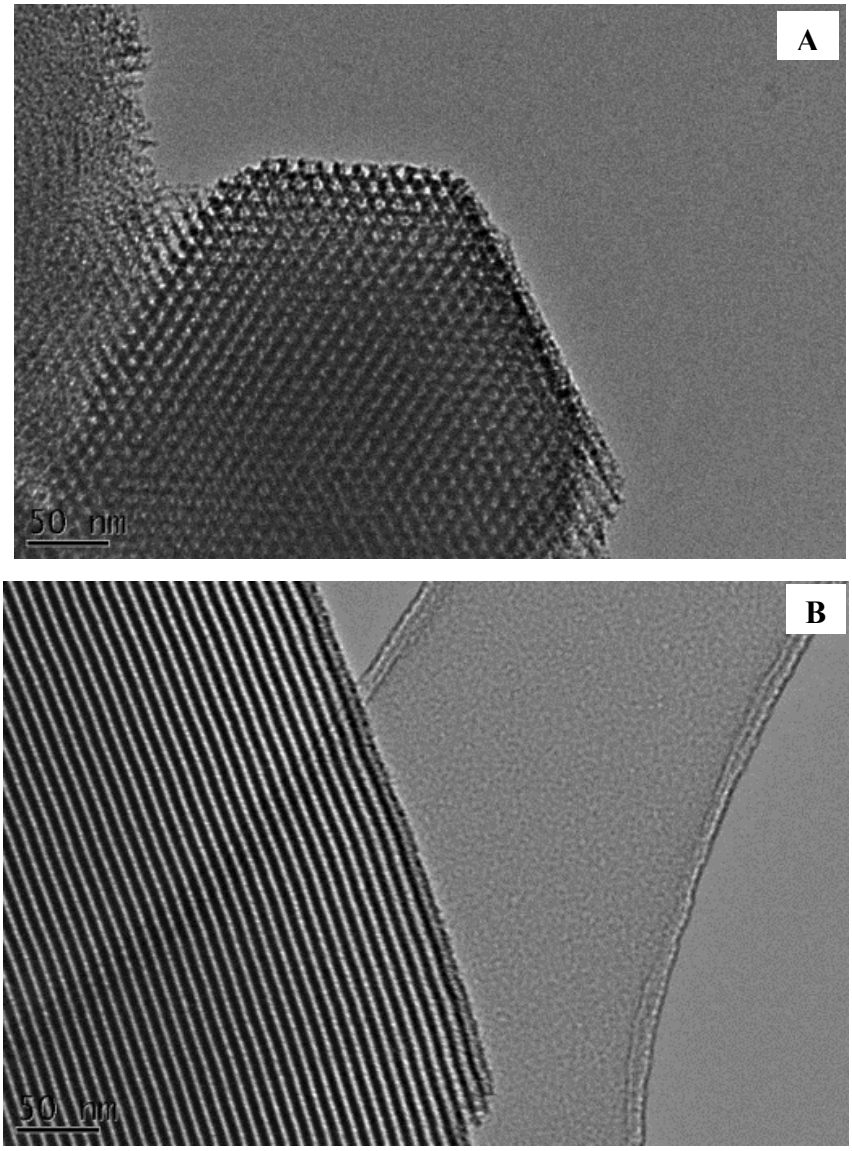

Figure 16: TEM images of SBA-15 Sample A

4.7.4. Nitrogen physisorption of SBA-15 samples before stability test

Figure 17 show the nitrogen adsorption-desorption isotherms for different SBA-15 samples. All samples exhibit type IV isotherms characteristics with H1 hysteresis loop, with steep parallel adsorption/desorption isotherms, which means that all the pores are filled at adsorption and emptied at desorption and it is characteristic of mesoporous materials with uniform pores.

Differences in the shapes of the isotherms and hysteresis loops (Figure 17) are due to the differences in pore volumes and pore sizes of the samples. As the adsorption of N_2 in

Samples B – D happened at almost the same relative pressure indicates that these three samples should have the same pore diameter (Figures 18 – 21). It is worth to mention that the existence of a plateau at large relative vapour pressures, indicates the incidence of a limiting porous volume and also that the SBA-15 samples are mostly mesoporous solids; a macropore contribution can be practically ruled out due to the failure of the sorption curves in adopting an asymptotic behaviour near $p/p_o \sim 1$. A detailed analysis of these isotherms evidenced the presence of microporosity in all samples. What is more, as the isotherms of Samples B – D are steeper and at higher relative pressures than that of Sample A, which supports the statement that the use of less concentrated acid led to wider pores but with narrow pore size distribution.

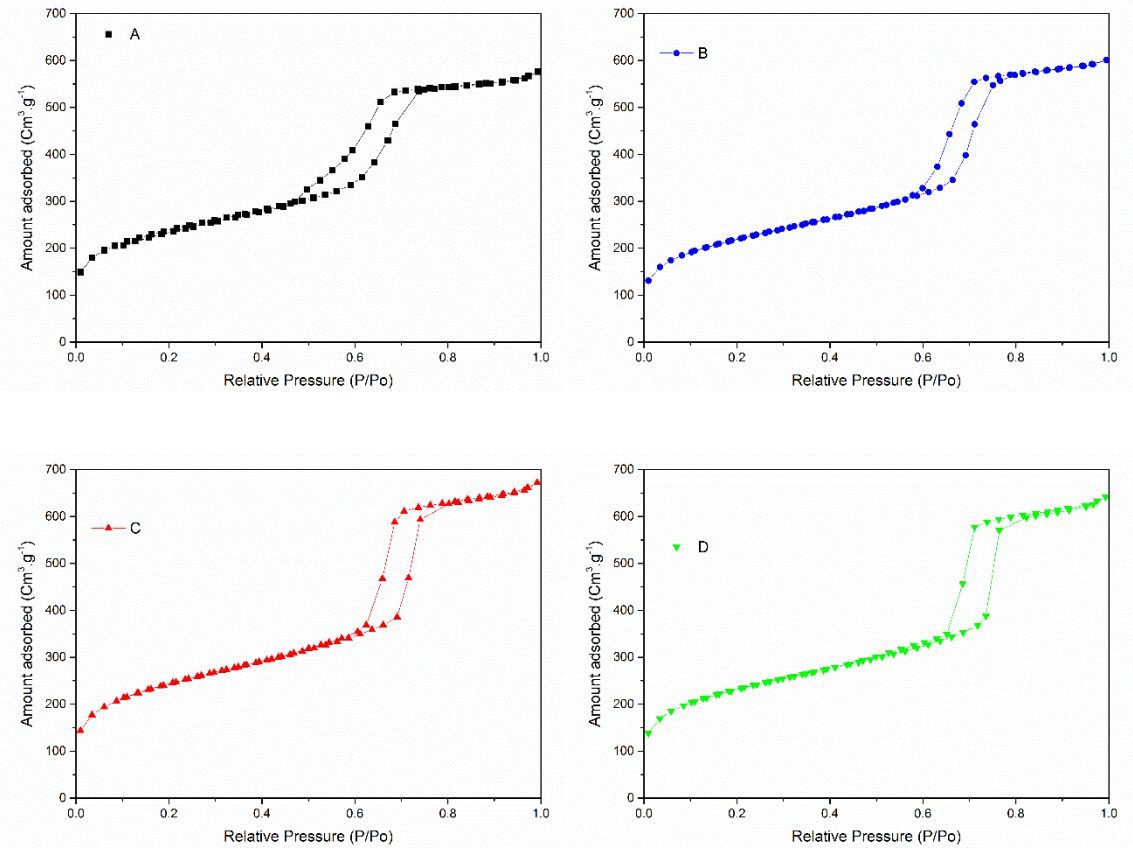

Figure 17: Nitrogen physisorption of SBA-15 Samples A – D, before hydrothermal stability test

Figures 18 – 21 show the BJH pore size distribution of Samples A – D, calculated from both adsorption and desorption branches of the isotherms.

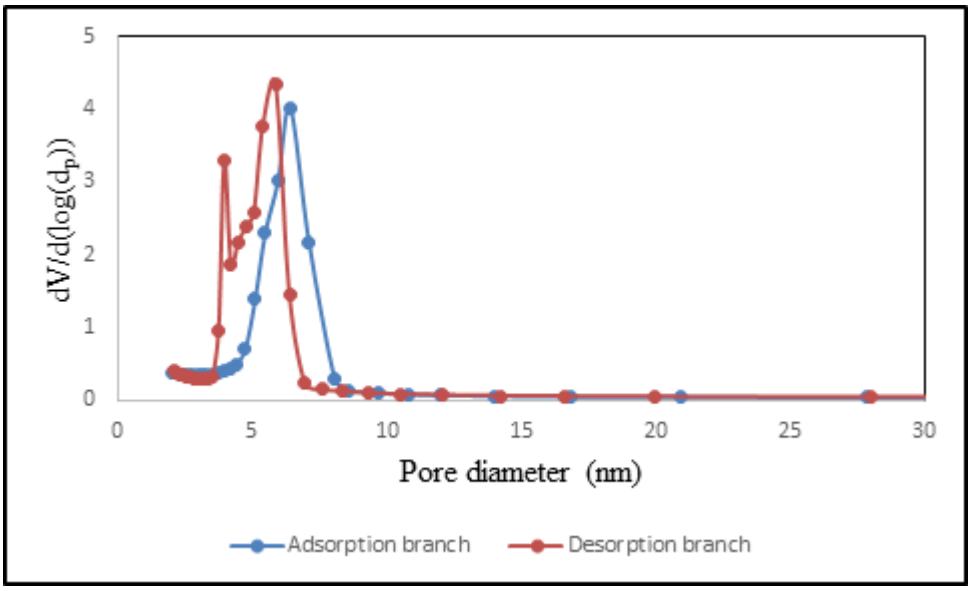

Figure 18. BJH pore size distribution for SBA-15 Sample A calculated from the adsorption and desorption branch of the isotherms

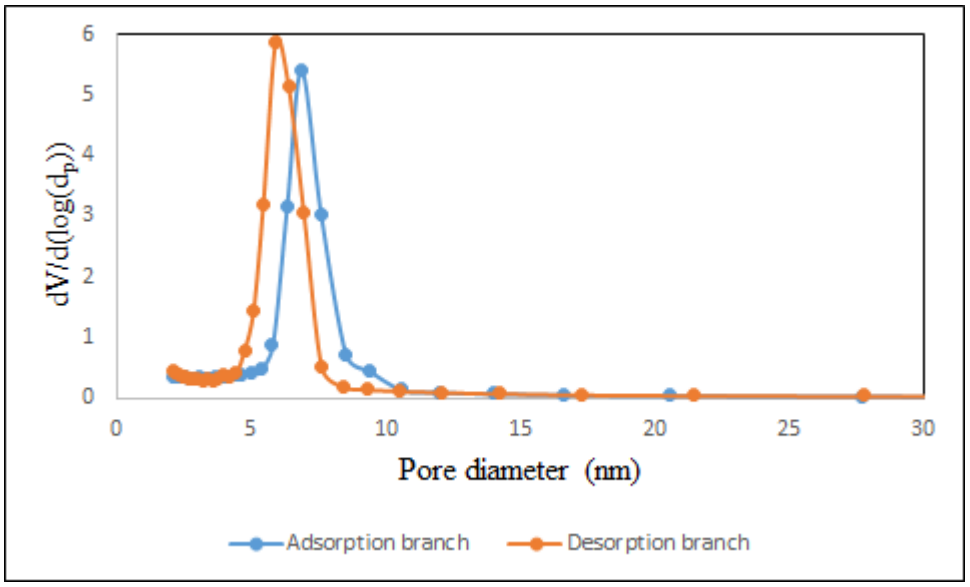

Figure 19. BJH pore size distribution for SBA-15 Sample B calculated from the adsorption and desorption branch of the isotherms

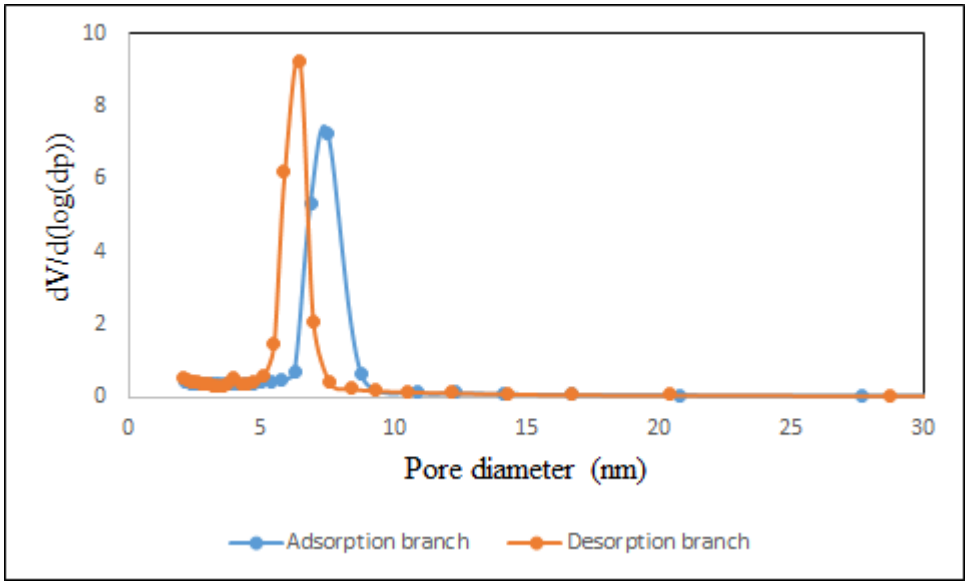

Figure 20. BJH pore size distribution for SBA-15 Sample C calculated from the adsorption and desorption branch of the isotherms

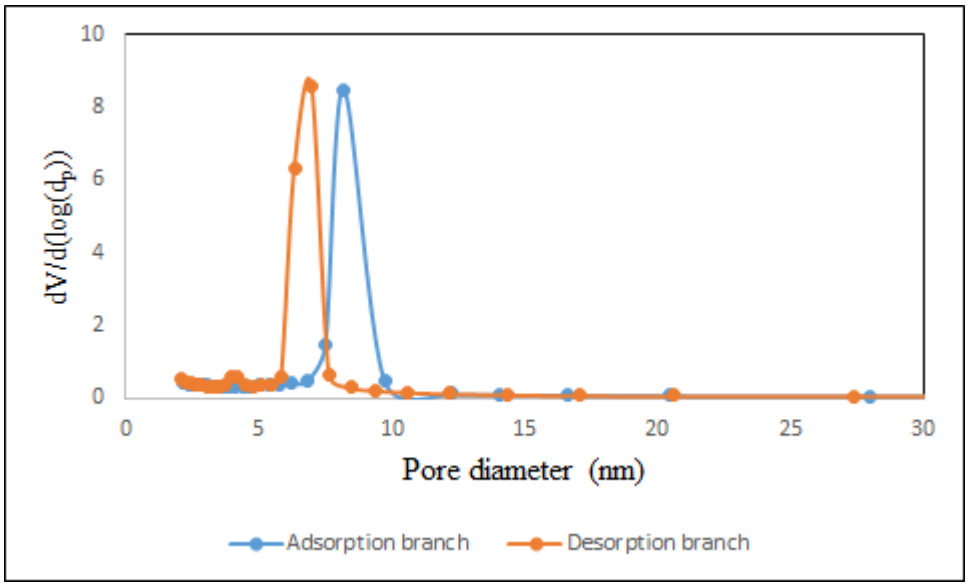

Figure 21. BJH pore size distribution for SBA-15 Sample C calculated from the adsorption and desorption branch of the isotherms

4.7.5. Low-angle XRD before hydrothermal stability test

Figure 22 show low angle XRD of SBA-15 samples. The four synthesised samples exhibited characteristic low-angle XRD peaks (1 0 0), (1 1 0) and (2 0 0), associated with uniform 2D hexagonally ordered SBA-15 meso-phase. The time of hydrothermal treatment during synthesis appear to have effect on the crystallinity of SBA-15. As observed, Samples A and B aged for 24 hours appear more crystalline (higher ordered pore structure) than Samples C and D which were aged for a longer time of 48 hours, as XRD results for Samples C and D (Figure 22) show poor crystalline materials (broader, less intense 100 peak). It therefore suggests that aging time beyond 24 hours reduces the orderly structure of SBA-15.

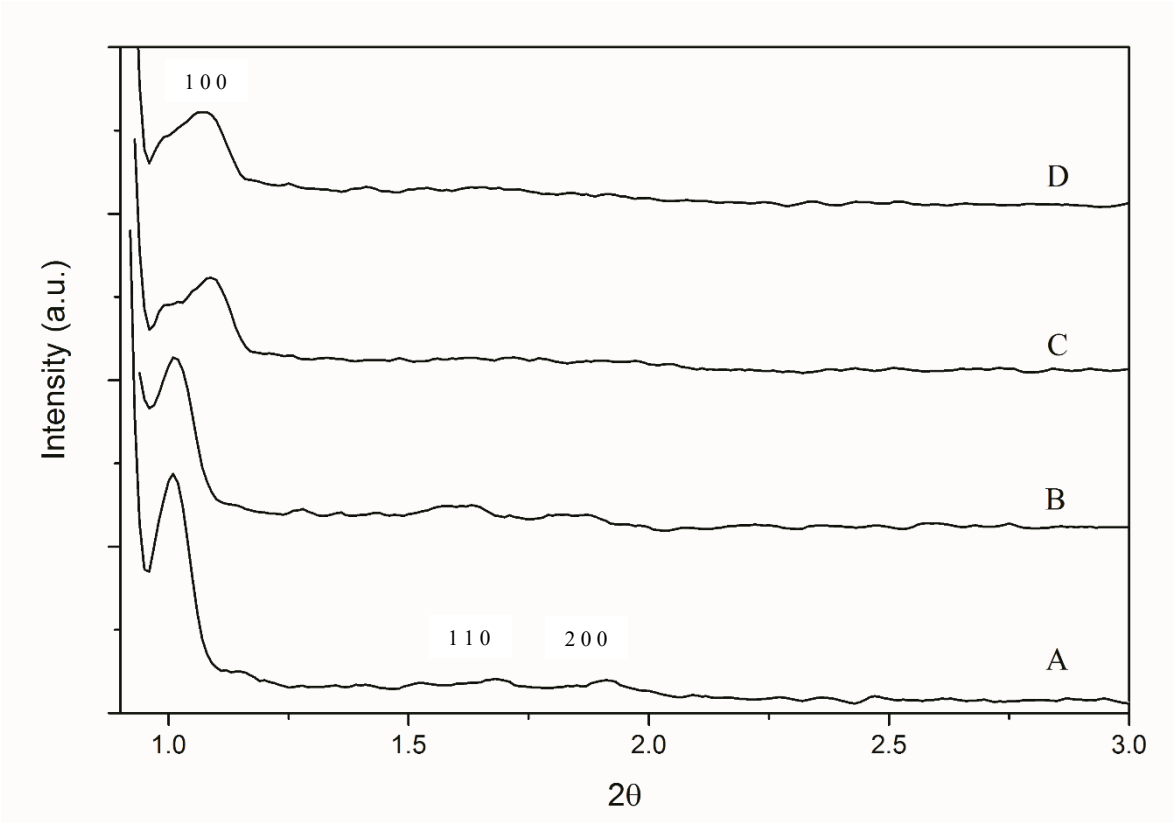

Figure 22. Low-angle XRD of SBA-15 Samples A – D before hydrothermal stability test

A summary of the properties of the different SBA-15 samples, as determined from the nitrogen physisorption and XRD low-angle measurements is presented in Table 3. SBA-15 Sample A has the thickest pore wall of 5.0 nm which interestingly, is much thicker than most of the reported SBA-15 reported in literature. It seems that most researchers paid more emphasis on the synthesis of SBA-15 with higher surface area and larger pore diameters, while taking for granted the need to further increase the thickness of the pore walls, to enhance the structural strength of SBA-15 which, according to Bore [11], stabilises gold nanoparticles in the pores. Also, thicker pore walls increases SBA-15 resistance to damage from water and high temperatures during calcination or reaction.

Table 3. Properties of synthesised SBA-15 samples

Sample name	BET surface area (m^2/g)	Pore size (nm)	Pore Volume (cm^3/g)	d_{100} (nm)	a (nm)	Wall Thickness (nm)
A	794	5.4	0.86	9.02	10.42	5.0
B	744	6.0	0.91	8.43	9.73	3.7
C	823	6.2	1.00	8.20	9.47	3.3
D	780	6.6	0.81	8.20	9.47	2.9

* Using BJH method

$d_{100} = \frac{\lambda}{2sin\theta}$ (Interplaner spacing)

$a = \frac{2}{\sqrt{3}} d_{100}$ (Hexagonal unit cell parameter)

λ = 0.1542

$Pore\ wall\ thickness\ = hexagonal\ unit\ cell\ parameter\ (a)\ - Pore\ size$

There is a good agreement between TEM (Figure 16) and data in Table 3 above regarding SBA-15 Sample A.

4.7.6. Low-angle XRD after hydrothermal stability test

Low-angle XRD results of SBA-15 Samples A – D in Figure 19 show the characteristic peak associated with SBA-15 mesoporous structure. However, except for the SBA-15 Sample A, there were significant detrimental changes to SBA-15 Samples B – D as they had poor crystalline structures, an evidence of their poor hydrothermal stability. Comparing Samples

B – D however, Sample B with shorter ageing time of 24 hours was more damaged than Samples C and D aged for 48 hours, which suggests that longer hydrothermal treatment time increased the pore wall densities and consequently, the strength and stabilities of Samples C and D.

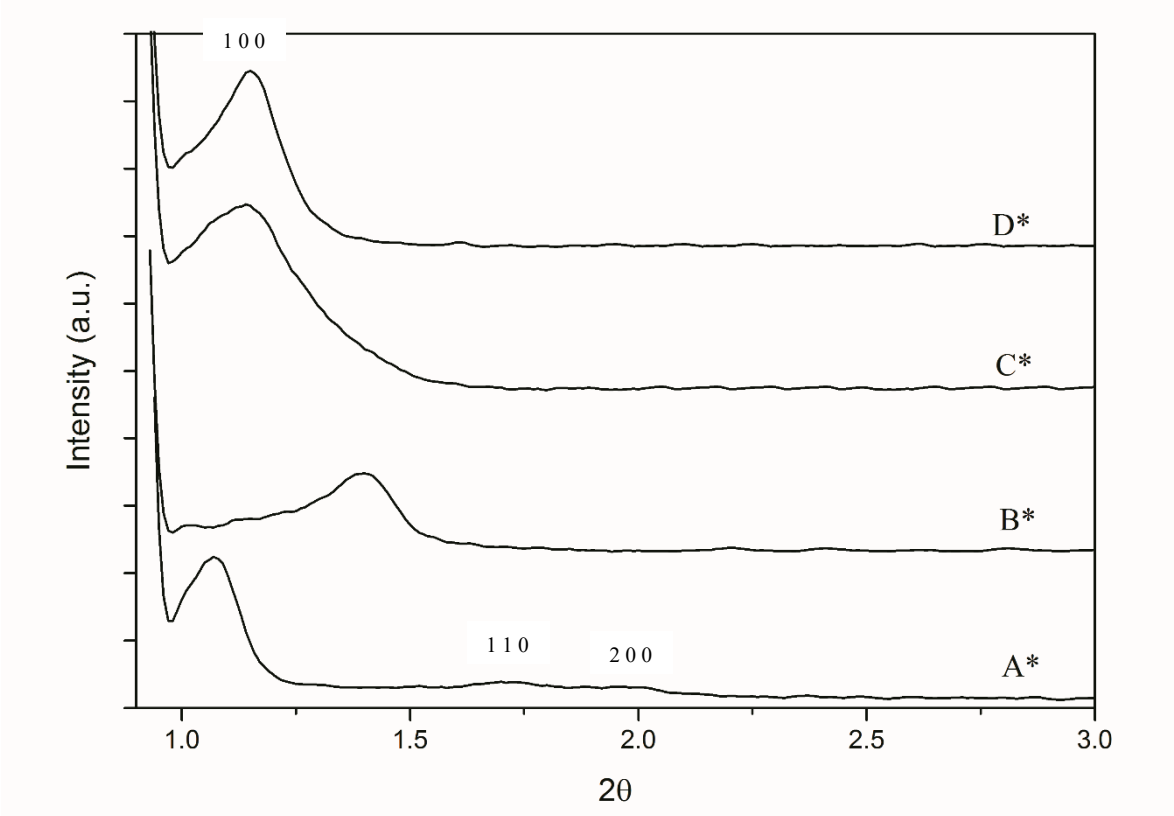

Figure 23. Low-angle XRD for SBA-15 Samples *A – *D after hydrothermal stability test

4.7.7. Nitrogen physisorption of SBA-15 samples after stability test

Nitrogen adsorption-desorption experiments were done on the four samples after hydrothermal stability tests. From the isotherms in Figure 24, the decrease in the amount of adsorbed nitrogen for Samples B – D is attributed to a decrease in their pore volumes, with Sample B having the lowest value. The adsorbed nitrogen and shape of Sample A's hysteresis loop remained almost the same before and after hydrothermal stability test, an

indication of its higher stability compared to the rest of SBA-15 samples. This is an expected result, as Sample A has the thickest pore wall.

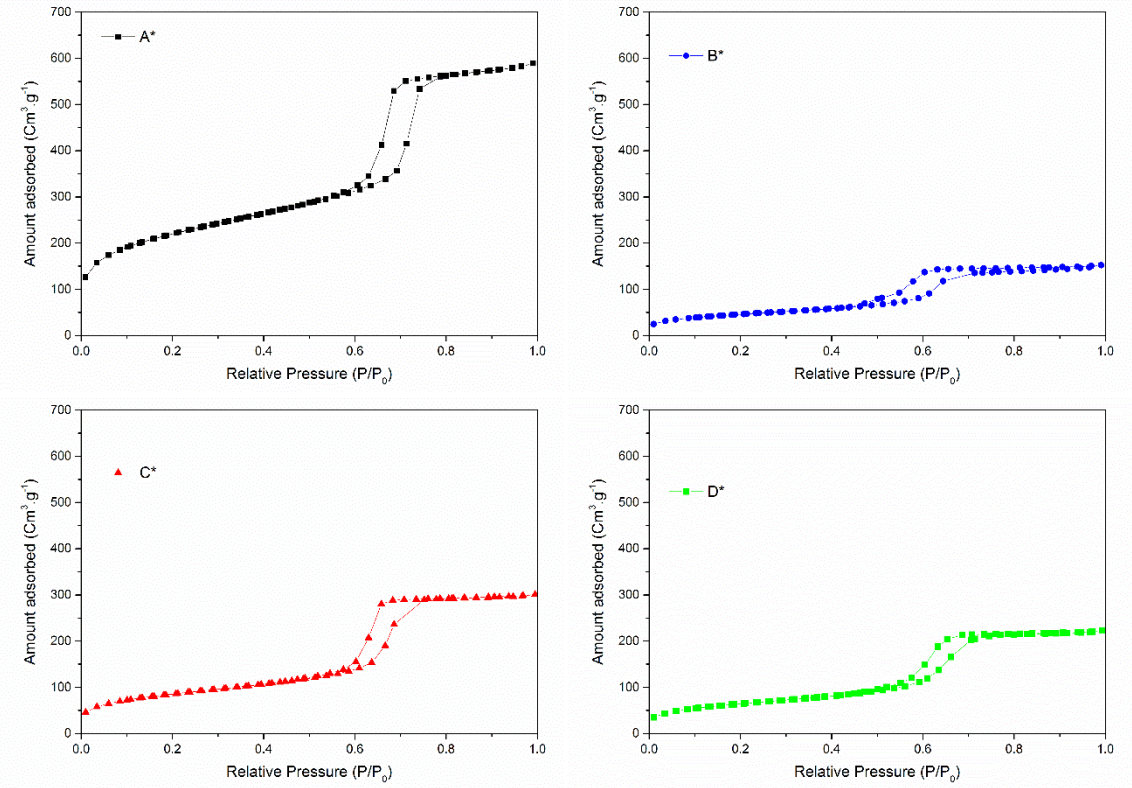

Figure 24. Nitrogen physisorption of SBA-15 Samples *A – *D after hydrothermal stability test

The surface area, pore volume and the percentage reduction in surface area and pore volume after hydrothermal stability test for all samples are summarised in Table 4.

Table 4. Properties of SBA-15 samples after hydrothermal test

Sample name	BET surface area (m^2/g)	Reduction in BET surface area (%)	Pore Volume (cm^3/g)	Reduction in Pore Volume (%)
A	748	6	0.89	0
B	162	78	0.21	77
C	293	64	0.46	54
D	232	70	0.32	60

SBA-15 Sample A with the thickest pore wall of 5.0 nm proved to be highly stable when pure steam at 800 °C was flown over the sample for an hour. The surface area, and pore

volume did not record significant changes, a confirmation that thicker pore wall is necessary for the stability of mesoporous silica as catalyst support material. From the isotherms in Figure 24, it is observed that SBA-15 Sample C is the second most stable SBA-15, with wall thickness of 3.3 nm. Although SBA-15 Sample B has the thickest pore walls, of 3.7 nm, among Samples B – D, it is the least stable. The reason for this is that the longer hydrothermal time of 48 hours for Sample C produced a much denser material which was more stable than SBA-15 Sample B with hydrothermal time of 24 hours. The same reason explains why SBA-15 Sample D produced by hydrothermal time of 48 hours was more stable than SBA-15 Sample B, even though, it has thinner wall thickness of 2.9 nm. Therefore, the acid concentration and to some extent, hydrothermal treatment determines SBA-15 stability. For low acid concentrations, a longer hydrothermal treatment time beyond 24 hours is therefore necessary to increase the wall density for better stability. As shown in Figure 24, the walls microporosity for samples prepared with less concentrated acid almost disappeared because of the hydrothermal testing, however, this research findings also show that hydrothermal treatment time beyond 24 hours reduces the orderly structure of SBA-15.

4.8. Conclusion

The acid concentration added during the synthesis of SBA-15 mesoporous silica, and to some extent, the duration of hydrothermal treatment has strong effects on the formation of thicker and stronger pore walls. Higher acid concentrations speeds up partial hydrolysis of silica species from TEOS needed for condensation and polymerisation to form thicker pore walls, while longer hydrothermal treatment increases the density of SBA-15 material. Further increase in the acid concentration could possibly produce SBA-15 mesoporous silica with thicker pore walls beyond 5.0 nm; however, tests proved that sample A was highly stable in pure steam even at 800 °C, which is a harsh environmental condition, sufficient to cause colossal damage to the physical properties of catalysts, which eventually affects their

overall catalytic performance. The use of highly stable catalytic support material is a crucial step in the design and preparation of highly efficient heterogeneous catalysts able to withstand harsh environmental reaction conditions.

The best SBA-15 sample (Sample A) was used to prepare the six Au/SBA-15 catalysts discussed in Chapter 5.

CHAPTER 5. Synthesis and physical characterisation of Au/SBA-15 catalysts

5.1. Introduction

Six solution based preparation methods were explored to develop six different Au/SBA-15 catalysts with the aim of screening out the best in low temperature oxidation of VOCs. The six preparation methods and Au/SBA-15 catalysts include:

1. Cationic gold precursor $Au(en)_2Cl_3$ (en=ethylenediamine) on SBA-15 (labelled as Au-en/SBA-15 catalyst).
2. Post functionalisation of SBA-15 with MPTMS before loading with $HauCl_4$ (labelled as Au-M0.8/SBA-15 catalyst).
3. Post functionalisation of SBA-15 with APTMS before loading with $HauCl_4$ (labelled as Au-A0.8/SBA-15 catalyst).
4. One pot synthesis of SBA-15 with MPTMS before loading with $HauCl_4$ gold precursor (labelled as Au-0.6Mdp/SBA-15 catalyst).
5. One pot synthesis of SBA-15 with APTMS before loading with $HauCl_4$ gold precursor (labelled as Au-0.6Adp/SBA-15 catalyst).
6. Post functionalisation of SBA-15 with organo-phosphine ligand $(-N(CH_2PPh_2)_2$ before loading with $HauCl_4$ gold precursor (labelled as Au-P/SBA-15 catalyst).

5.1.1. Cationic gold precursor on SBA-15

In this synthesis, organic functional group is used to incorporate gold nano-particles on the mesoporous silica material, starting with tetrachloroauric acid as gold precursor for the synthesis of the cationic gold-organo-complex. Although active gold catalyst have been produced using this method, it may lead to some defects on the meso-structure due to the grafting of the organic functional groups and the ligand removal, with high calcination temperature, could lead to a decrease in catalytic activity. Block and Bailar in 1951[135]

found that tetrachloroauric acid reacts with ethylenediamine (en) to form gold complex $[Au(en)_2]Cl_3$ after precipitation with ethanol. This complex behaves as an acid by losing a proton from the coordinated amine group, under basic conditions. Zhu and co-workers carried out deposition- precipitation of this complex in alkaline media on prepared SBA-15, as the negatively charged mesoporous silica material surface readily attracted the $[Au(en)_2]^{2+}$ cations by deprotonation reaction of Au-ethylenediamine ligand [77].

The experimental procedure by Zhu and co-workers was followed to produce Au-en/SBA-15 catalyst [78], however, calcination of the prepared catalyst at 500 °C was introduced to burn off the organic ligand, so as to properly activate the catalyst. A summary of the synthetic procedure is shown in Figure 25, but the detailed experimental procedure is outlined in Section 5.3.1 of this Chapter.

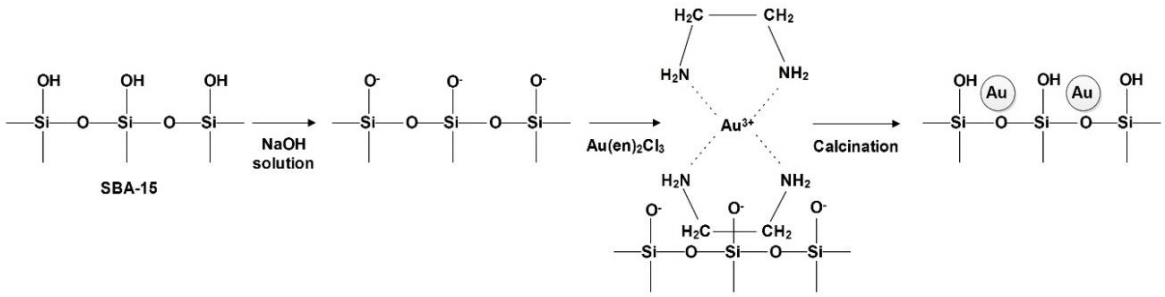

Figure 25. Schematic procedure for synthesis of Au-en/SBA-15 catalyst

5.1.2. Post functionalisation of SBA-15 with MPTMS/APTMS before gold loading

Similar experimental procedure by Yang and co-workers [79] was followed in the surface functionalisation of prepared SBA-15 with either the thiol or amine cationic organosilanes - MPTMS or APTMS before loading gold on the functionalised SBA-15 using $HAuCl_4$ gold precursor. Unlike Yang, calcination at 500 °C was introduced. The full experimental details

are outlined in Section 5.3.2 of this Chapter, however, the synthetic procedure is illustrated in Figure 26:

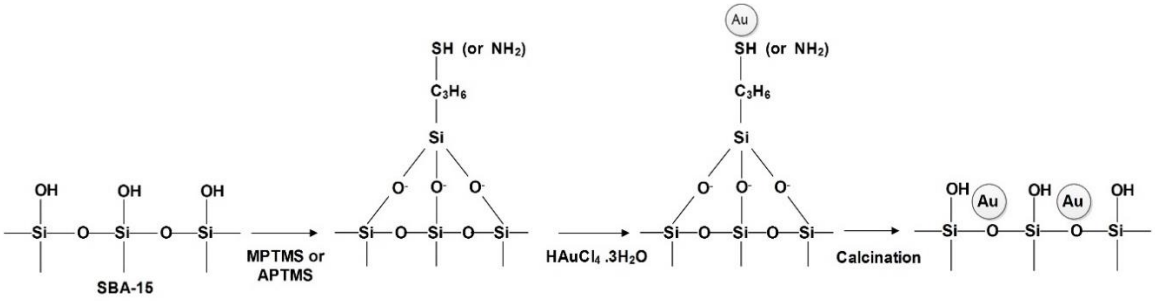

Figure 26. Schematic procedure for synthesis of Au-M0.8/SBA-15 and Au-A0.8/SBA-15 catalysts

The major challenge in using this synthetic method is that it is difficult to achieve homogenous distribution of the organo-silanes both inside the long SBA-15 cylindrical pores and on the external surface; this consequently affects the uniformity in dispersion of gold nano-particles on the SBA-15 [136]. It is also difficult to determine the right amount of organosilanes to use for functionalisation. Reported Au/SBA-15 catalysts prepared by post functionalisation of organosilanes before gold loading have recorded significantly reduced specific surface areas and pore volumes compared to the original SBA-15 which may be as a result of pore blockage and collapse of some of the meso-structures of the catalyst [137]. An attempt was made in this project to determine an estimated amount of MPTMS/APTMS required for optimum functionalisation of ready-made SBA-15 without causing much damage to SBA-15 material. This is discussed in Section 5.3.2 of this Chapter.

5.1.3. One pot synthesis of SBA-15 with MPTMS/APTMS before gold loading

This method is also known as self-assembly functionalisation of SBA-15 before gold loading. Organosilane (in this case, MPTMS or APTMS) is added directly into SBA-15 during its sol – gel synthesis. Co-hydrolysis and polycondensation of the silica precursor (TEOS) with the organosilane takes place in the presence of P123 template. The advantage

of this method is that homogenous functionalisation can be achieved as the organosilane is part of the silica matrix which also eliminates the issue of pore blockage [114]. The disadvantage of this method is that it is difficult to determine the right amount of organosilane sufficient to functionalise SBA-15 without inhibiting hydrolysis and polycondensation of silica precursors, which affects the formation of its ordered meso-structure, as an increase in the amount of added organosilane increases the inhibition of hydrolysis and polycondensation [114, 138].

An attempt was made in this project to estimate the right amount of MPTMS/APTMS required to functionalise SBA-15 without causing much damage to SBA-15 meso-structure. The synthetic schematic scheme is same as in Figure 26. The experimental details of the procedure is discussed in Section 5.3.3.

5.1.4. Post functionalisation of SBA-15 with organo-phosphine ligand before gold loading

For the first time, neutrally charged organo-phosphine ligand was synthesised and used to functionalise SBA-15 before gold loading. Phosphorus has previously been reported to form complexes with gold [139, 140]. The idea was to investigate if the attraction between phosphorus and gold could lead to the generation of very small gold particles on SBA-15. The full details of experiment is discussed in Section 5.3.4, but the synthetic procedure is illustrated in Figure 27.

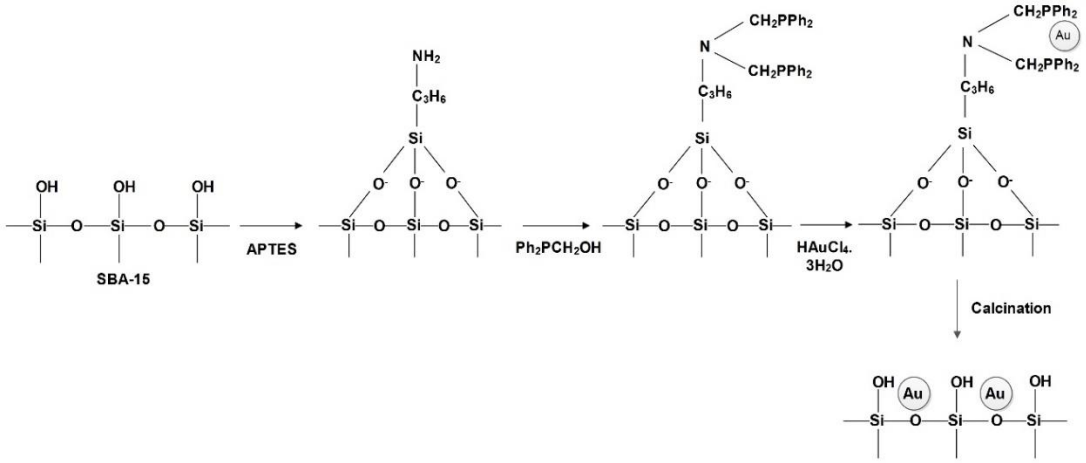

Figure 27. Schematic procedure for synthesis of Au-P/SBA-15 catalyst

5.2. Experimental

5.2.1. Synthesis of Au-en/SBA-15 catalyst

The synthesis of $Au(en)_2Cl_3$ (cationic gold precursor) was done as described by Zhu and co-workers [78]. 2 g of $HAuCl_4.3H_2O$ was dissolved in 20 ml deionised water and 0.90 ml ethylenediamine was slowly added and stirred for 30 minutes. 140 ml ethanol was added and the white suspension formed was stirred for 20 minutes and then filtered. The solid was washed with ethanol, dried in vacuum at 40 ºC overnight. To synthesis Au-en/SBA-15 catalyst, 0.1g of the cationic gold complex $Au(en)_2Cl_3$ was dissolved in 50 ml water. 1 g of SBA-15 was then added to the solution and the pH was adjusted to 10 using 0.1M NaOH solution, to form the Au-en-SBA-15 complex. The suspension was stirred at 65 ºC for 2 hours, filtered and washed with acetone. The product was dried in vacuum at 70 ºC for 5 hours then calcined at 500 ºC, for 6 hours at 1 ºC/min ramping, to burn off the ethylenediamine ligand, leaving gold nano-particles on SBA-15.

5.2.2. Synthesis of Au-M0.8/SBA-15 and Au-A0.8/SBA-15 catalysts

Post-functionalisation of SBA-15 with MPTMS or APTMS was performed as follows: 2 g of calcined SBA-15 was added to 60 ml toluene. A predetermined amount of MPTMS/APTMS (0.8 g) was added into the solution and kept under starring at 25 ºC for 1 hour, then increased temperature to 40 ºC and kept under stirring for 5 hours. The suspension was filtered under vacuum, washed with acetone and dried at 80 ºC overnight. 1 g of functionalised support was suspended in 80 ml of distilled water and stirred for 30 minutes at 80 ºC. To synthesise the catalysts, 0.08 g of $HAuCl_4.3H_2O$ was dissolved in 10 ml water. The solution rapidly became colourless in the case of MPTMS, an indication that deposition of gold has occurred on the surface of SBA-15. After 20 minutes, the solution was allowed to cool at room temperature for 20 minutes while stirring, then recovered by filtration, washed with acetone before air drying in a fume cupboard for 18 hours, and then at 60 ºC for 24 hours in an oven. The samples were calcined at 500 ºC for 6 hours at 1º/min ramp rate, to burn off the organic ligands. The catalysts were labelled as Au/M0.8-SBA-15 for MPTMS functionalised catalyst and as Au/A0.8-SBA-15 for the APTMS functionalised catalyst.

5.2.3. Synthesis of Au-0.6Mdp/SBA-15 and Au-0.6Adp/SBA-15 catalysts

One-pot functionalisation of SBA-15 with MPTMS or APTMS was done as follows: A predetermined amount of MPTMS or APTMS (0.6g) was added after 2 hours pre-hydrolysis of TEOS during the synthesis of SBA-15. After SBA-15 synthesis, the suspension was filtered under vacuum, washed with water, then acetone and dried at 80 ºC overnight. P123 template removal from as-synthesised SBA-15-SH and SBA-15-NH_2 was done by placing 3 g of the functionalised SBA-15 into 200 ml of ethanol in Soxhlet extraction for 48 hours. Recovered sample was dried at 60 ºC for 24 hours. 1 g of functionalised support was then suspended in 80 ml of distilled water and stirred for 30 minutes at 80 ºC before adding 0.08

g of $HAuCl_4.3H_2O$ dissolved in 10 ml water. The solution gradually turned from light yellow to colourless within 5 minutes for MPTMS sample. After 20 minutes, the solution was allowed to cool at room temperature for 20 minutes while stirring, then recovered by filtration, washed with acetone before air drying in a fume cupboard for 18 hours and then kept at 60 ºC for 24 hours in an oven. The samples were finally calcined at 500 º C for 6 hours at 1º/min ramp rate to burn off the organic ligands, leaving gold nano-particles on SBA-15. The new catalysts were labelled as Au/0.6Mdp-SBA-15 for MPTMS and as Au/0.6Adp-SBA-15 for APTMS, respectively.

5.2.4. Synthesis of Au-P/SBA-15 catalyst

SBA-15 was functionalised with 3-aminopropyltriethoxysilane, which basically gives Si-O_3Si-$CH_2CH_2CH_2$-NH_2. This was then reacted with Ph_2PCH_2OH. The P-CH_2OH groups are highly reactive towards amines, losing water to form a P-CH_2-N bond and Si-O_3Si-$CH_2CH_2CH_2$-$N(CH_2PPh_2)_2$ is formed. To synthesis the catalyst, 1 g of functionalised support was suspended in 80 ml of distilled water and stirred for 30 mins at 80 ºC before adding 0.08 g of $HAuCl_4.3H_2O$ dissolved in 10 ml water. The solution gradually turned from light yellow to red within 7 minutes. The solution was cooled to room temperature for 20 minutes while stirring, then recovered by filtration, washed with acetone before air drying for 18 hours and then kept in an oven at 60 ºC for 24 hours. The sample was calcined at 500 ºC for 6 hours at 1º/min ramp rate, to burn of the phosphine ligand and to form gold nano-particles on SBA-15. The catalyst was labelled as Au/P-SBA-15.

5.3. Results and discussions

5.3.1. SEM images of Au/SBA-15 catalysts

SEM images of pure SBA-15 (A) and the six Au/SBA-15 catalysts (1 – 6) are shown in Figure 28. The different preparation methods used did not destroy the initial worm-like

morphology of SBA-15 support. The primary particle sizes of the catalysts (1.2 - 3.1µm lengths and 0.4 – 0.6 µm widths) remained the same with that of SBA-15 support.

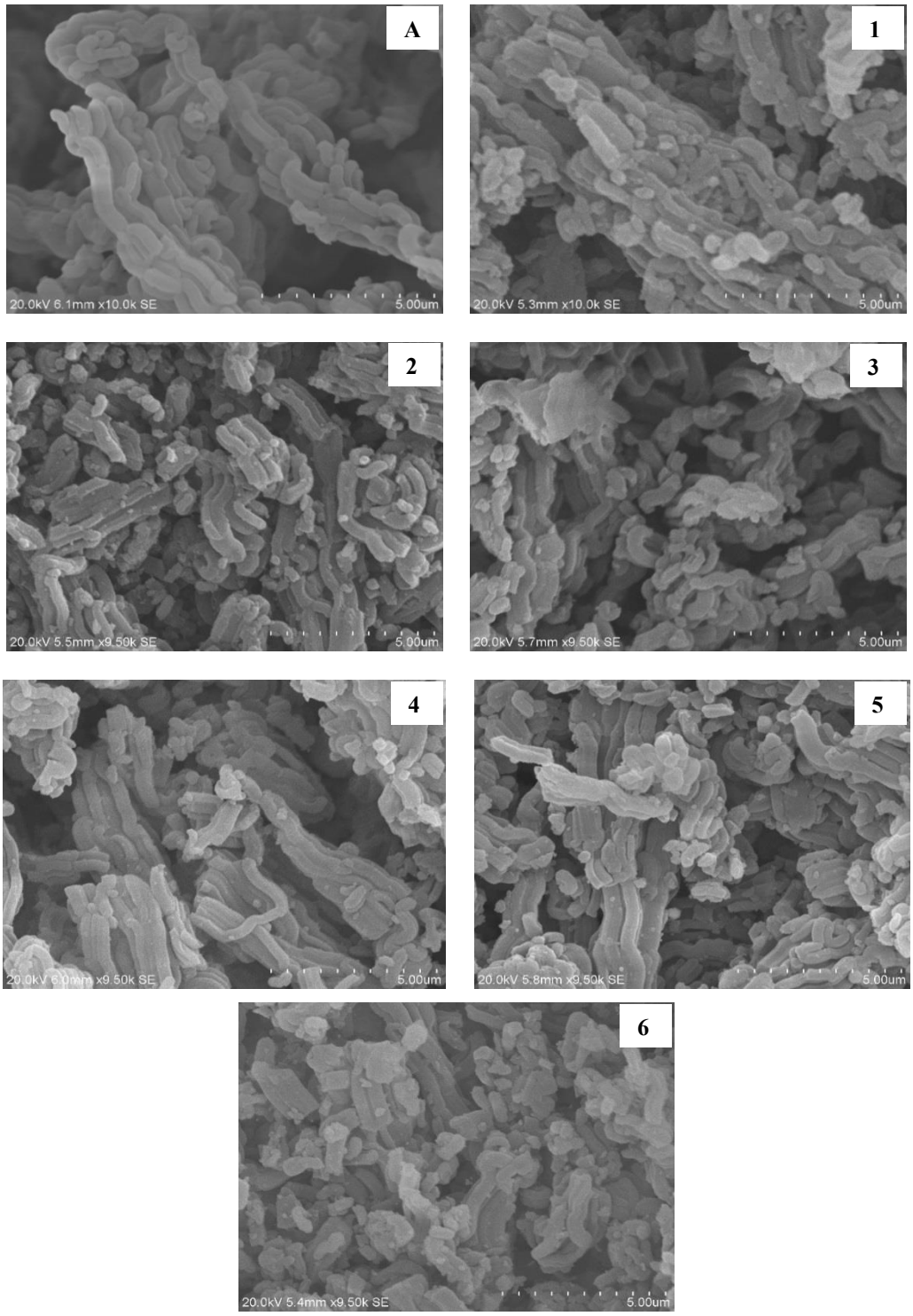

Figure 28. SEM of SBA-15 (A), Au-en/SBA-15 (1), Au-M0.8/SBA-15 (2), Au-A0.8/SBA-15 (3), Au-0.6Mdp/SBA-15 (4), Au-0.6Adp/SBA-15 (5) and Au-P/SBA-15 (6)

5.3.2. EDX analysis

EDX results are presented in Figures 29 – 41. Figures 30 and 35 confirm that SBA-15 was successfully functionalised with MPTMS by post and one-pot synthesis respectively. Equally successful was the post functionalisation of SBA-15 with the organo-phosphine group (Figure 40). Gold loading on SBA-15 using the cationic gold precursor $Au(en)_2Cl_3$ (en=ethylenediamine) was achieved, producing Au wt % as high as 5.08 % (Figure 25), although small amount of sodium (0.32 %) was present, most likely from NaOH added during synthesis. Sulphur and gold are clearly seen on Au-M0.8/SBA-15 and Au-0.6Mdp/SBA-15 as-synthesised samples before calcination (Figures 30 and 36), which suggests that SBA-15 functionalised with MPTMS is able to attract gold. After calcination treatment at 500 ºC, MPTMS was successfully burnt off, leaving only gold on SBA-15 (Figures 32 and 37). Although nitrogen in APTMS cannot be detected using EDX, Figures 33 - 34, and 38 - 39 confirm that gold was successfully loaded on SBA-15 functionalised with APTMS by post and one-pot synthesis. Au-0.6Adp/SBA-15 catalyst prepared by one-pot synthesis with APTMS produced the lowest gold loading of 1.35 wt. %. Chlorine was seen in the as-synthesised Au-A0.8/SBA-15 and Au-0.6Adp/SBA-15 catalysts (Figures 33 and 38), however, calcination treatment at 500 ºC was sufficient to remove the chlorine (Figures 34 and 39). Gold loading on SBA-15 functionalised with organo-phosphine group was successful, with Au-P/SBA-15 catalyst of 2.30 Au wt. %.

In all the samples, some carbon was observed either due to adsorbed CO_2 from the atmosphere or from some left over carbon after calcination because of burning off the organic groups, or a combination of both. High carbon content of 23.38 wt % was peculiar to post functionalised SBA-15 with organo-phosphine group (Figure 40) which reduced drastically to 3.62 wt % after calcination, suggesting that the organo-phosphine group with high carbon content was burnt off during calcination.

Overall, the functionalisation of SBA-15, followed by gold loading and calcination to burn off the organic groups were all successful from EDX point of view.

Element	Weight %
C	2.64
O	54.44
Na	0.32
Si	37.52
Au	5.08
Total	100

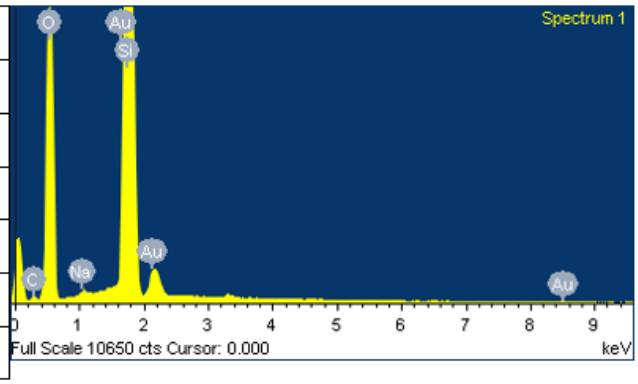

Figure 29. EDX of Au-en/SBA-15 catalyst (calcined)

Element	Weight %
O	49.03
Si	46.60
S	4.37
Total	100

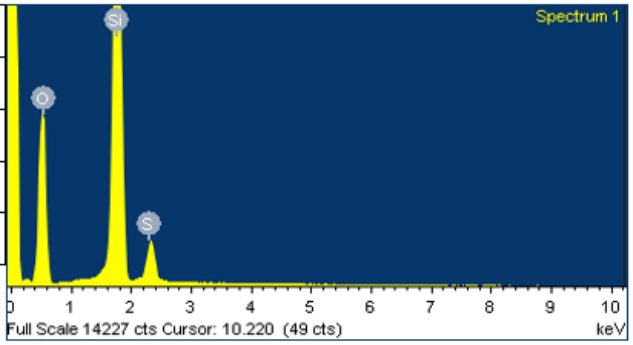

Figure 30. EDX of SBA-15 post functionalised with MPTMS

Element	Weight %
C	6.62
O	53.47
Si	34.82
S	2.66
Au	2.44
Total	100

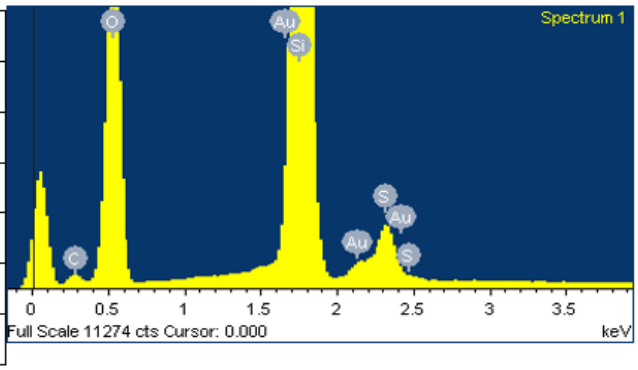

Figure 31. EDX of Au-M0.8/SBA-15 catalyst (before calcination)

Element	Weight %
C	7.11
O	56.47
Si	34.27
Au	2.15
Total	100

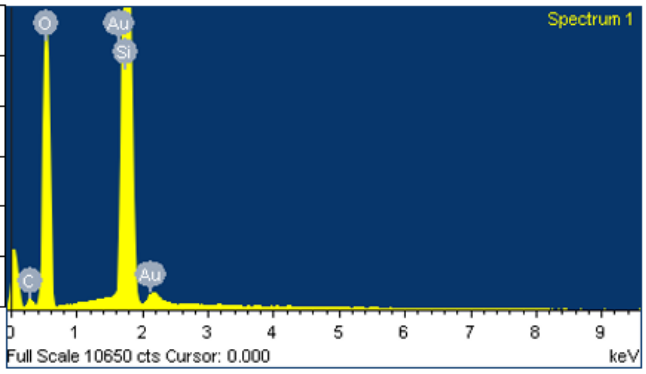

Figure 32. EDX of Au-M0.8/SBA-15 catalyst (after calcination)

Element	Weight %
O	52.39
Si	43.55
Cl	0.33
Au	3.73
Total	100

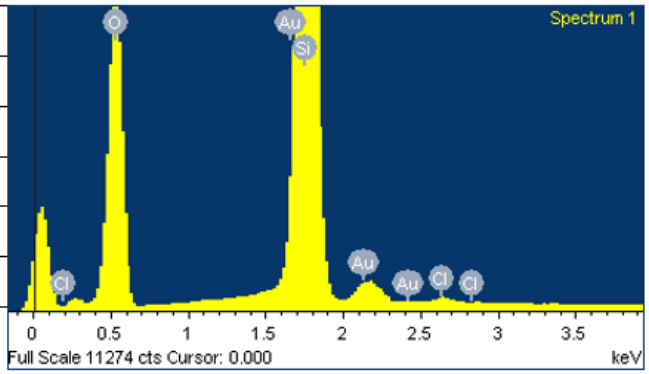

Figure 33. EDX of Au-A0.8/SBA-15 catalyst (before calcination)

Element	Weight %
C	3.59
O	54.51
Si	38.40
Au	3.50
Total	100

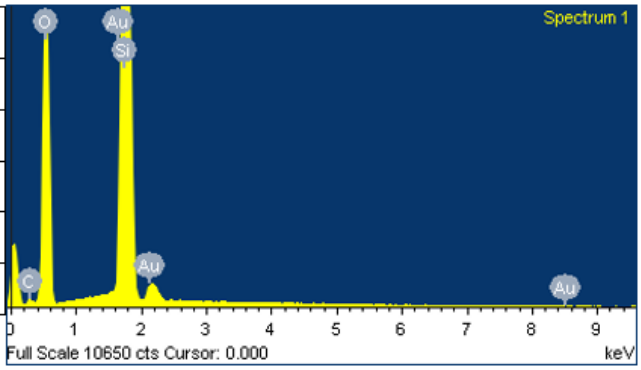

Figure 34. EDX of Au-A0.8/SBA-15 catalyst (after calcination)

Element	Weight %
C	17.47
O	57.52
Si	23.96
S	1.06
Total	100

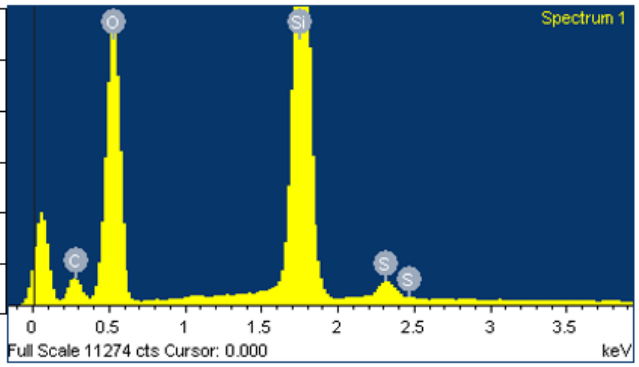

Figure 35. EDX of one-pot synthesis of SBA-15 with MPTMS

Element	Weight %
C	8.72
O	52.50
Si	33.02
S	1.99
Au	3.78
Total	100

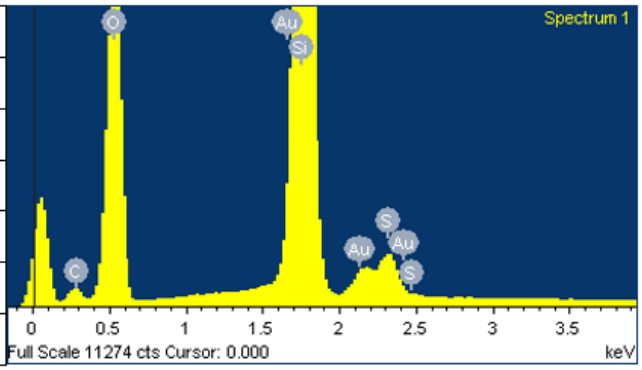

Figure 36. EDX of Au-0.6Mdp/SBA-15 catalyst (before calcination)

Element	Weight %
C	6.40
O	52.96
Si	37.16
Au	3.48
Total	100

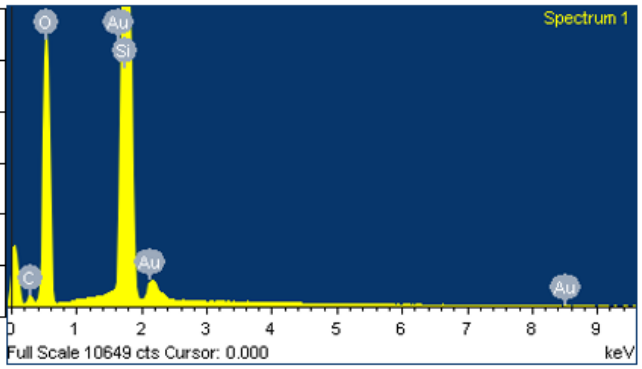

Figure 37. EDX of Au-0.6Mdp/SBA-15 catalyst (after calcination)

Element	Weight %
O	62.02
Si	34.81
Cl	0.71
Au	2.46
Total	100

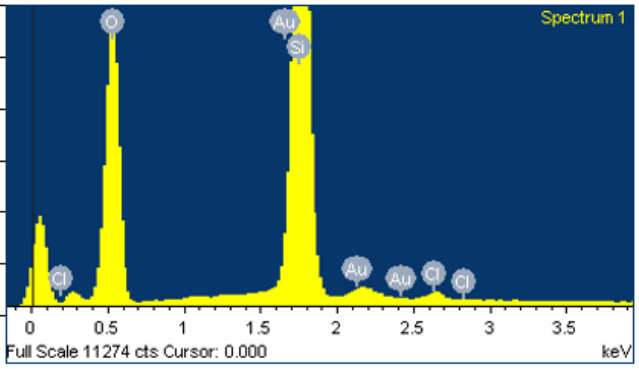

Figure 38. EDX of Au-0.6Adp/SBA-15 catalyst (before calcination)

Element	Weight %
C	10.65
O	56.56
Si	31.44
Au	1.35
Total	100

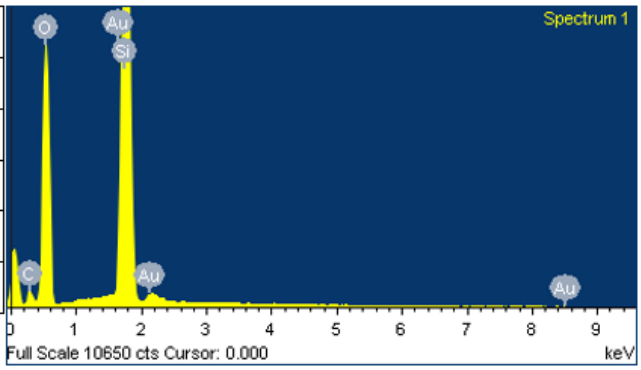

Figure 39. EDX of Au-0.6Adp/SBA-15 catalyst (after calcination)

Element	Weight %
C	23.38
O	42.59
Si	31.70
P	2.33
Total	100

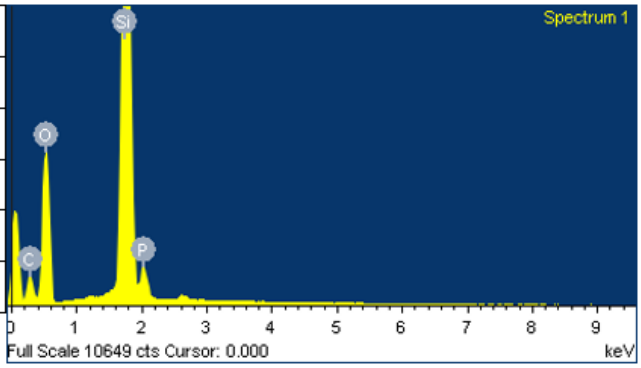

Figure 40. EDX of post functionalisation of SBA-15 with phosphine group

Element	Weight %
C	3.62
O	54.10
Si	39.98
Au	2.30
Total	100

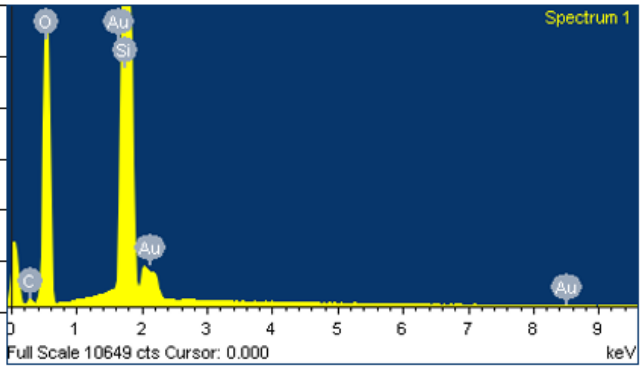

Figure 41. EDX of Au-P/SBA-15 catalyst (after calcination)

The EDX results confirm that the improved synthetic methods used in depositing gold on SBA-15 achieved the desired target, which is to sufficiently load gold on the support, as loading was in the range of 1.35 – 5.08 wt. % . However, other techniques such as wide angle XRD and TEM are required to study gold particle sizes and the extent of gold dispersion on SBA-15 support. XRD and TEM results are reported in sections 5.3.3 and 5.3.5.

5.3.3. Wide-angle XRD

Wide-angle XRD of the six Au/SBA-15 catalysts (Figure 42 and 43) confirm the presence of cubic shaped gold nano-particles, which have characteristic 2 theta peaks at 38°, 44°, 64°, 78° and 82°, respectively [141]. Au-0.6Mdp/SBA-15 catalyst (Clearly shown in Figure 43) has gold nano-particles so small, it only shows a small broad peak at 38°, while Au-P/SBA-15 catalyst has very narrow, most intense peak at 38°, an indication it has the largest gold particle size. Gold particle sizes calculated from the XRD line broadening at half the maximum intensity (FWHM) value and substituted into Scherrer equation [142], gives gold average sizes for the six catalysts as shown in Table 5, with Au-0.6Mdp/SBA-15 catalyst having the smallest gold particle size of 1.3 nm (Clearly shown in Figure 43) and Au-P/SBA-15 catalyst having the largest gold particle size of 79 nm. The XRD results are in agreement with TEM (Figures 44 – 49), also shown in Table 5:

Table 5. Gold particle size determination using XRD and TEM

Technique	Au-en/	Au-M0.8/	Au-A0.8/	Au-0.6Mdp/	Au-0.6Adp/	Au-P
XRD (nm)	5.5	3.4	10.0	1.3	30.0	79.0
TEM (nm)	5.5	4.0	9.0	1.3	30.0	81.0

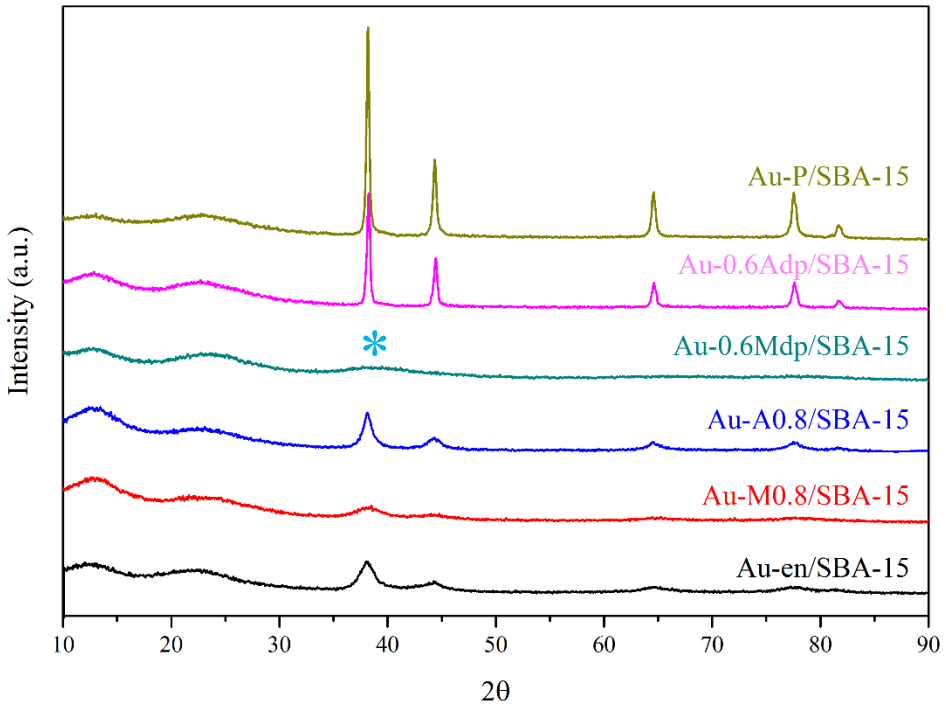

Figure 42: Wide-angle XRD of Au/SBA-15 catalysts

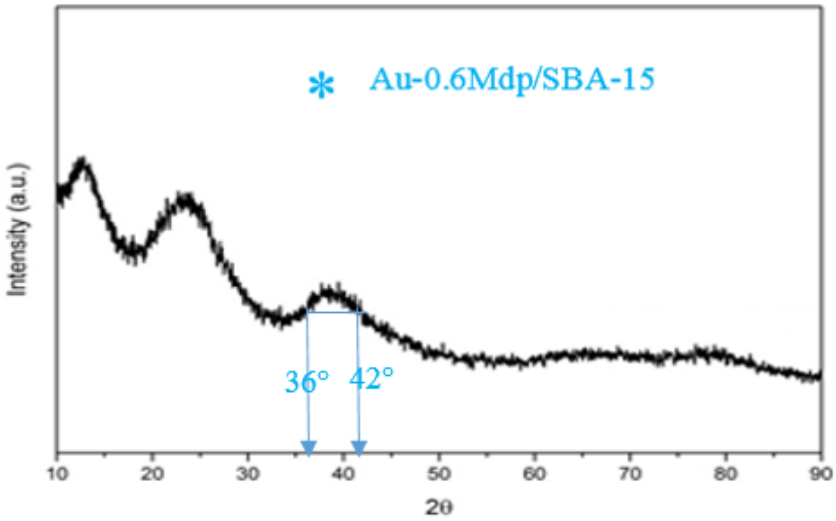

Figure 43. Wide-angle XRD of Au-0.6Mdp/SBA-15 catalyst

5.3.4. Physical properties

Table 5 lists some of the characteristic properties of SBA-15 support and the six Au/SBA-15 catalyst samples, measured by N_2 adsorption/desorption isotherms, wide-angle XRD and EDX. Au/P-SBA-15 catalyst prepared from post-functionalisation of calcined SBA-15 with organo-phosphine group ($-N(CH_2PPh_2)_2$ has the largest Au particles of 79 nm with 2.30 wt.% Au loading. BET surface area of SBA-15 decreased significantly, by 44%, from 794 to 441 m^2/g, after functionalisation with phosphine ligand and gold loading. In the case of one- pot synthesis of SBA-15 with APTMS (Au-0.6Adp/SBA-15), although surface area remained high (673 m^2/g), it had the lowest Au loading of 1.35 wt. %, with rather large gold particles of 30 nm. One-pot synthesis of SBA-15 with MPTMS (Au-0.6Mdp/SBA-15) produced a catalyst with high surface area (726 m^2/g) and small gold particles of 1.3 nm, with 3.5 wt. % gold loading. Au-0.6Mdp/SBA-15 catalyst had the best desired physical properties of all the catalysts prepared. SBA-15 post-functionalised with APTMS before gold loading (Au/A0.8-SBA-15) had a significant reduction in its surface area (395 m^2/g) compared to SBA-15, with 3.5 wt.% gold loading and Au particle size of 10 nm. After gold loading on SBA-15 post-functionalised with MPTMS (Au-M0.8/SBA-15), the surface area of the resulting

catalyst did not change significantly compared to SBA-15, with 2.2 wt. % gold loading and 3.4 nm Au particle size obtained. Au-en/SBA-15 catalyst had 54% reduction in surface area compared to SBA-15 (366 m^2/g), with 5.1 %wt. gold loading and Au particle size of 5.5 nm. Summary of physical properties of the six catalysts are shown in Table 6.

Table 6. Physical properties of SBA-15 and Au/SBA-15 catalysts

Support/ Au/SBA-15 catalysts	BET surface area (m^2/g)	Au loading (%wt.)	Au size (nm)
SBA-15	794	-	-
Au-en/SBA-15	366	5.1	5.5
Au-M0.8/SBA-15	789	2.2	3.4
Au-A0.8/SBA-15	395	3.5	10.0
Au-0.6Mdp/SBA-15	726	3.5	1.3
Au-0.6Adp/SBA-15	673	1.4	30.0
Au-P/SBA-15	441	2.3	79.0

5.3.5. TEM images

Figures 44 - 49 shows the TEM images of the six Au/SBA-15 catalysts. TEM results are in good agreement with those obtained by XRD regarding the size of the gold nanoparticles. Furthermore, TEM images show the particle size distribution as well. For instance, although XRD wide-angle recorded large particle sizes for AuA0.8/SBA-15 (10 nm), Au-0.6Adp/SBA-15 (30 nm) and Au-P/SBA-15 (79 nm) catalysts, which are also seen in TEM, there still exists as well, some small gold particles of various sizes in these catalysts. Also, although Au-M0.8/SBA-15 catalyst recorded 3.4 nm gold size in XRD, TEM images (2A – 2C) show a vast array of sizes with some larger gold particules loosely attached to SBA-15 support also present. Au-en/SBA-15 (1A – 1C) and Au-0.6Mdp/SBA-15 catalysts have the most uniformly sized gold particles, with the latter having the smallest gold particle size (in agreement with XRD) and the highest dispersion without any large gold particle observed.

It therefore means that one-pot synthesis of SBA-15 with an appropriate amount of MPTMS uniformly functionalised the inner pore walls and the external surface of SBA-15 which promoted high dispersion of gold particules uniformly dispersed on SBA-15.

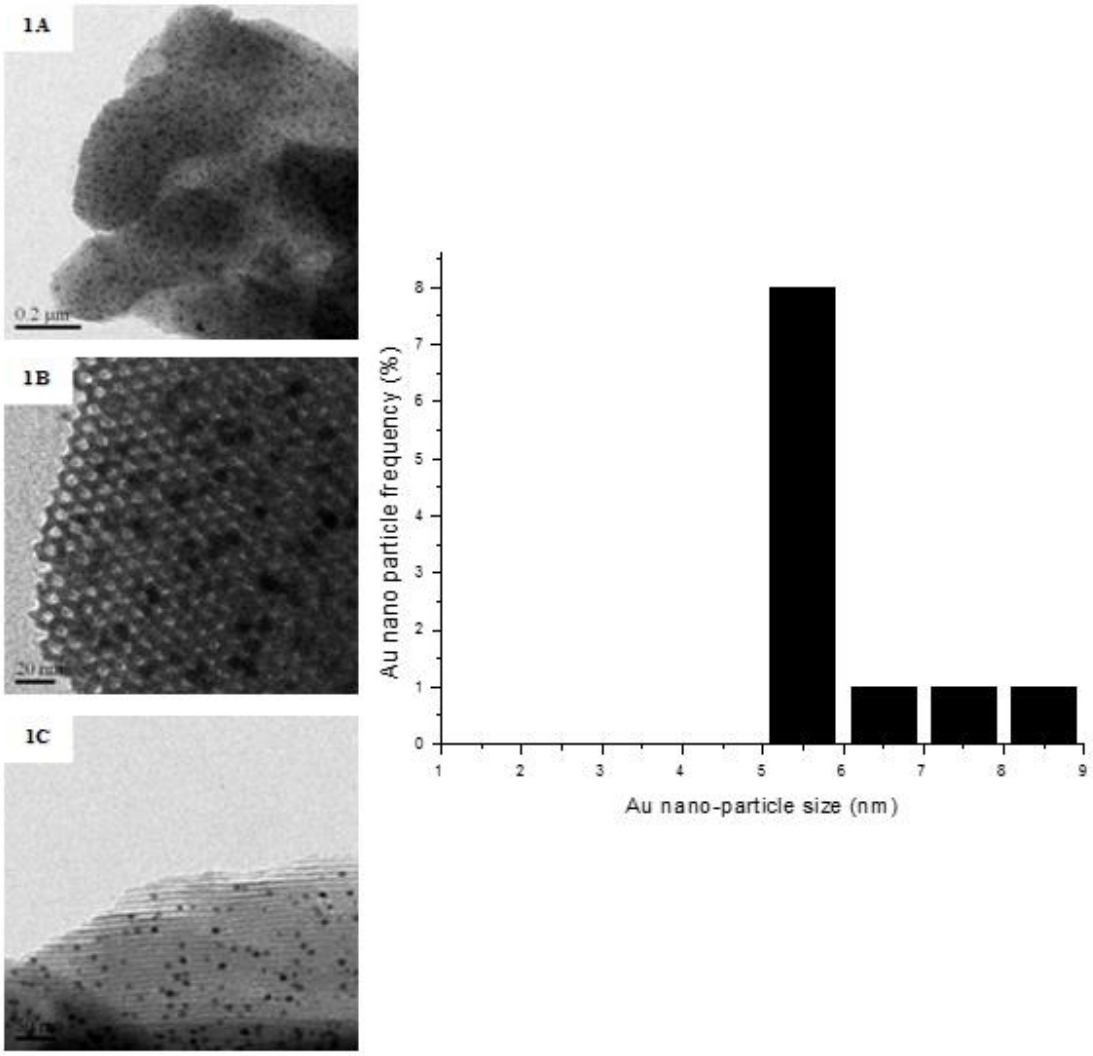

Figure 44. TEM (1A – C) and Au particle size distribution for Au-en/SBA-15 catalyst

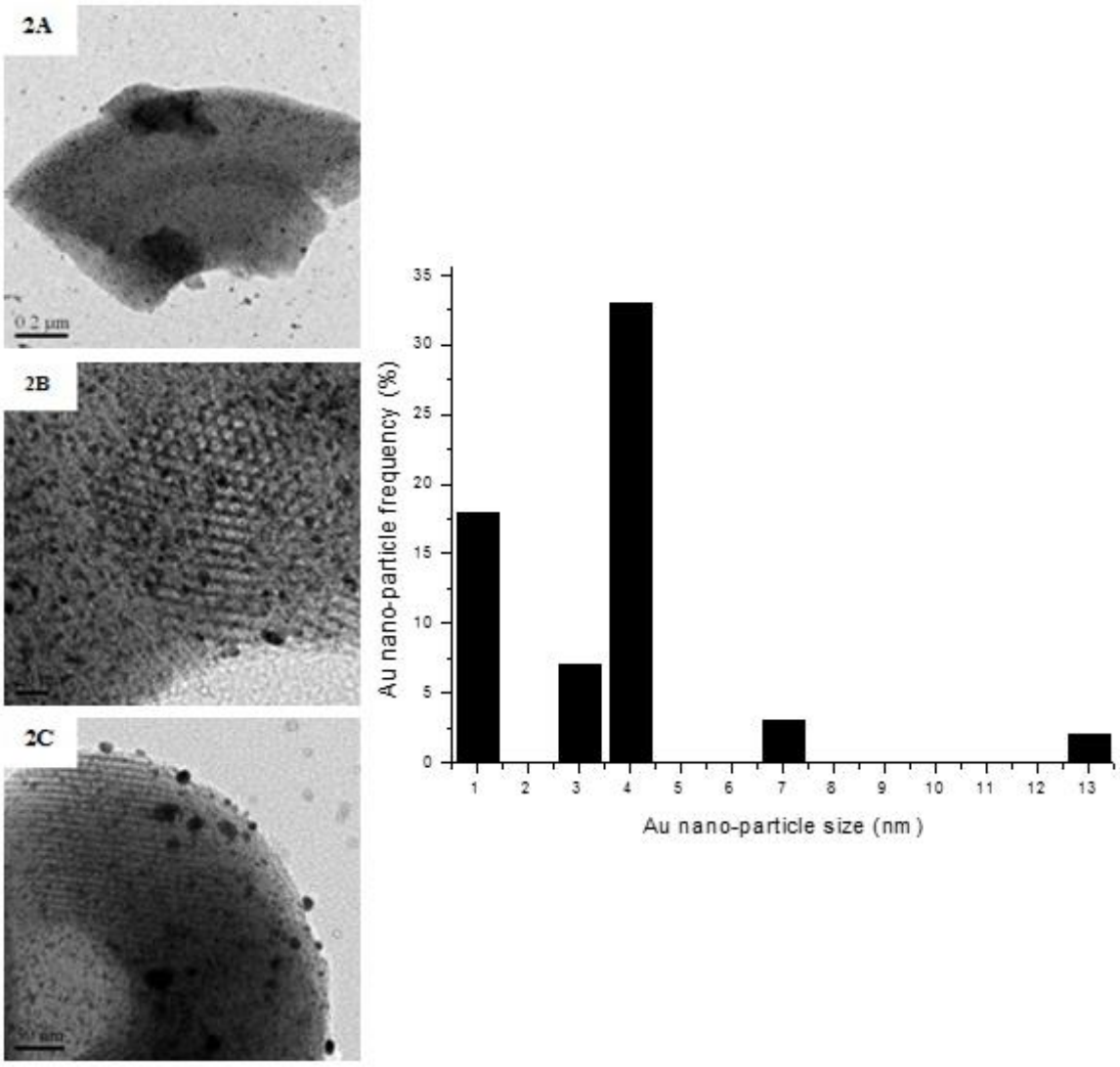

Figure 45. TEM (2A – C) and Au particle size distribution for Au/M0.8-SBA-15 catalyst

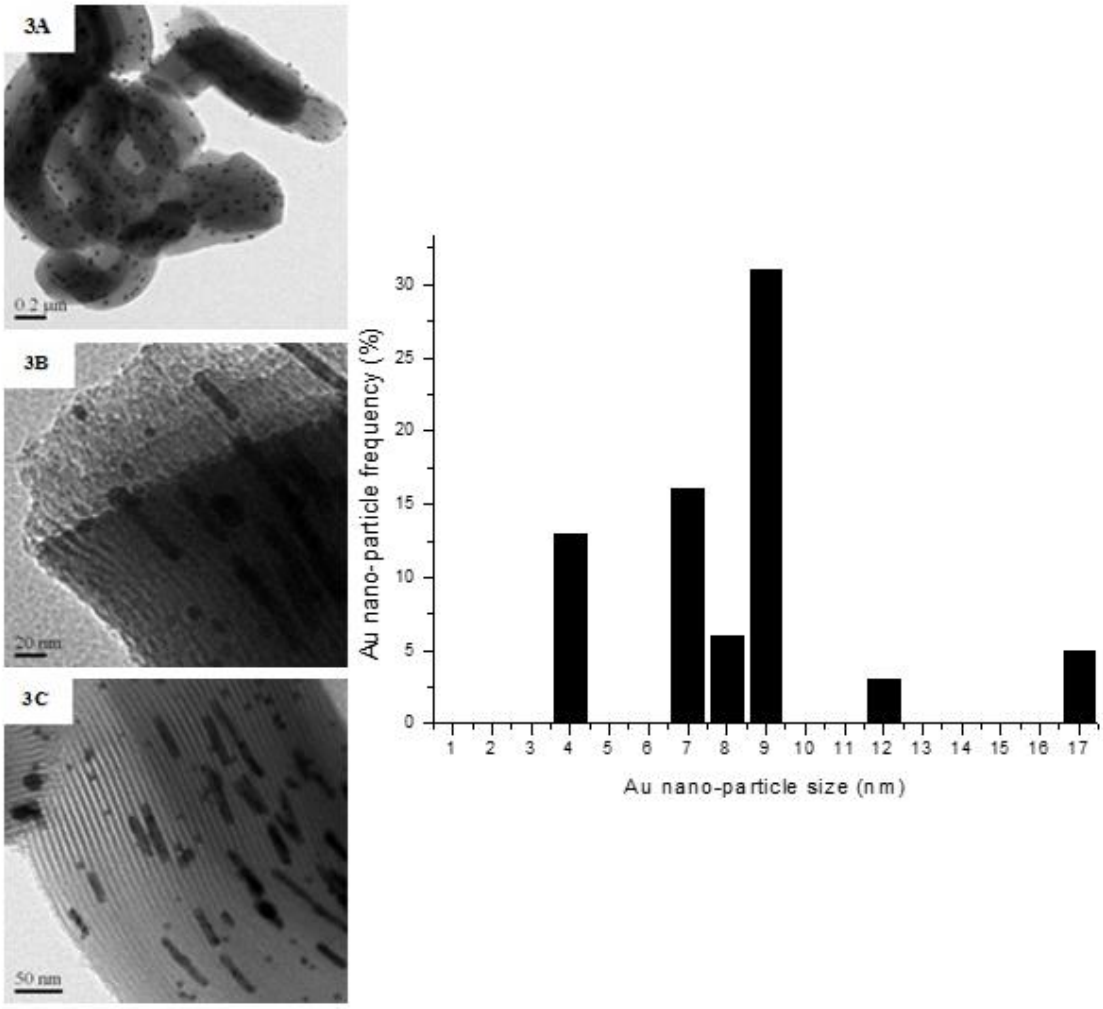

Figure 46. TEM (3A – C) and Au particle size distribution for Au/A0.8-SBA-15 catalyst

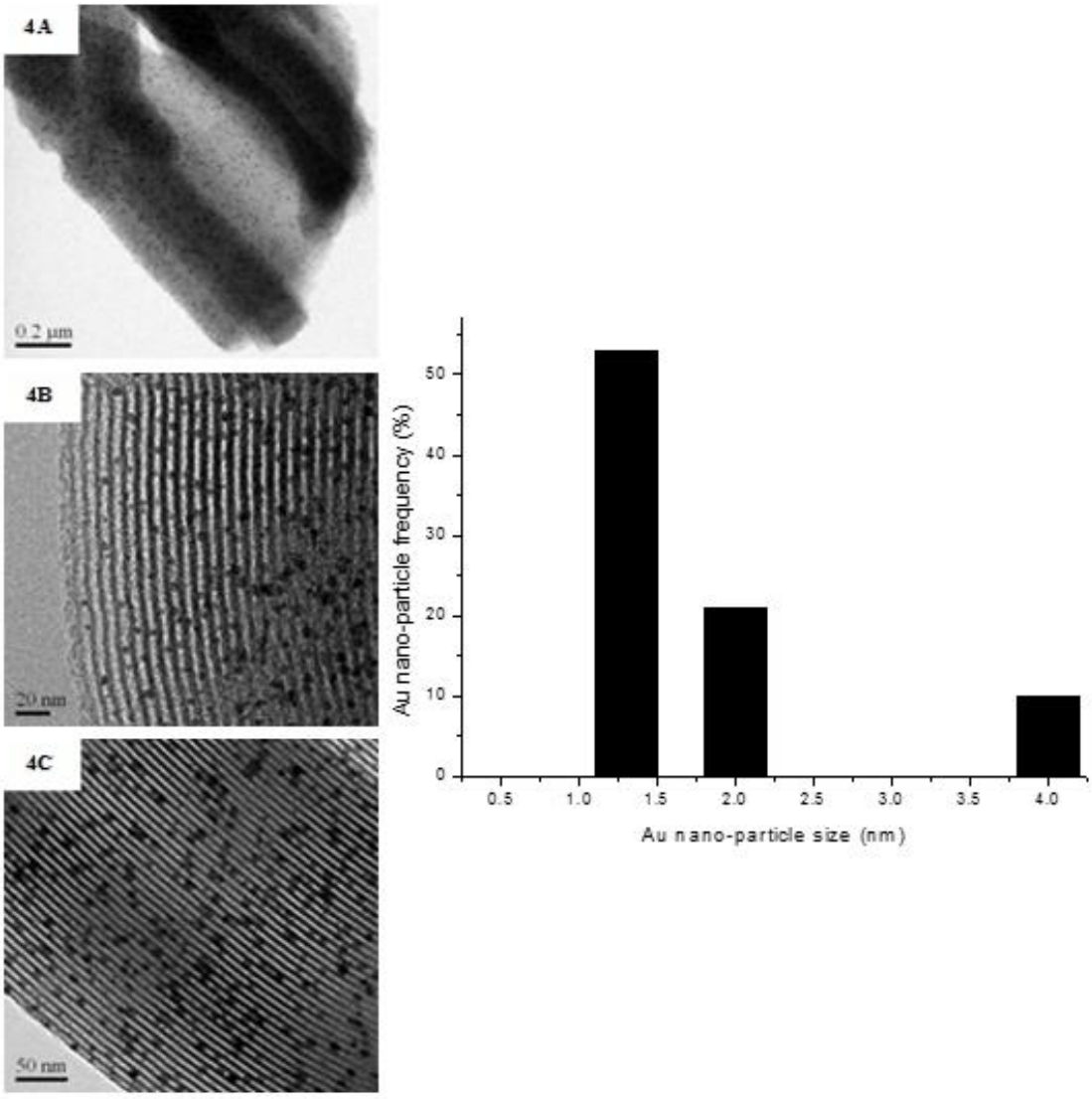

Figure 47. TEM (4A – C) and Au particle size distribution for Au/0.6Mdp-SBA-15 catalyst

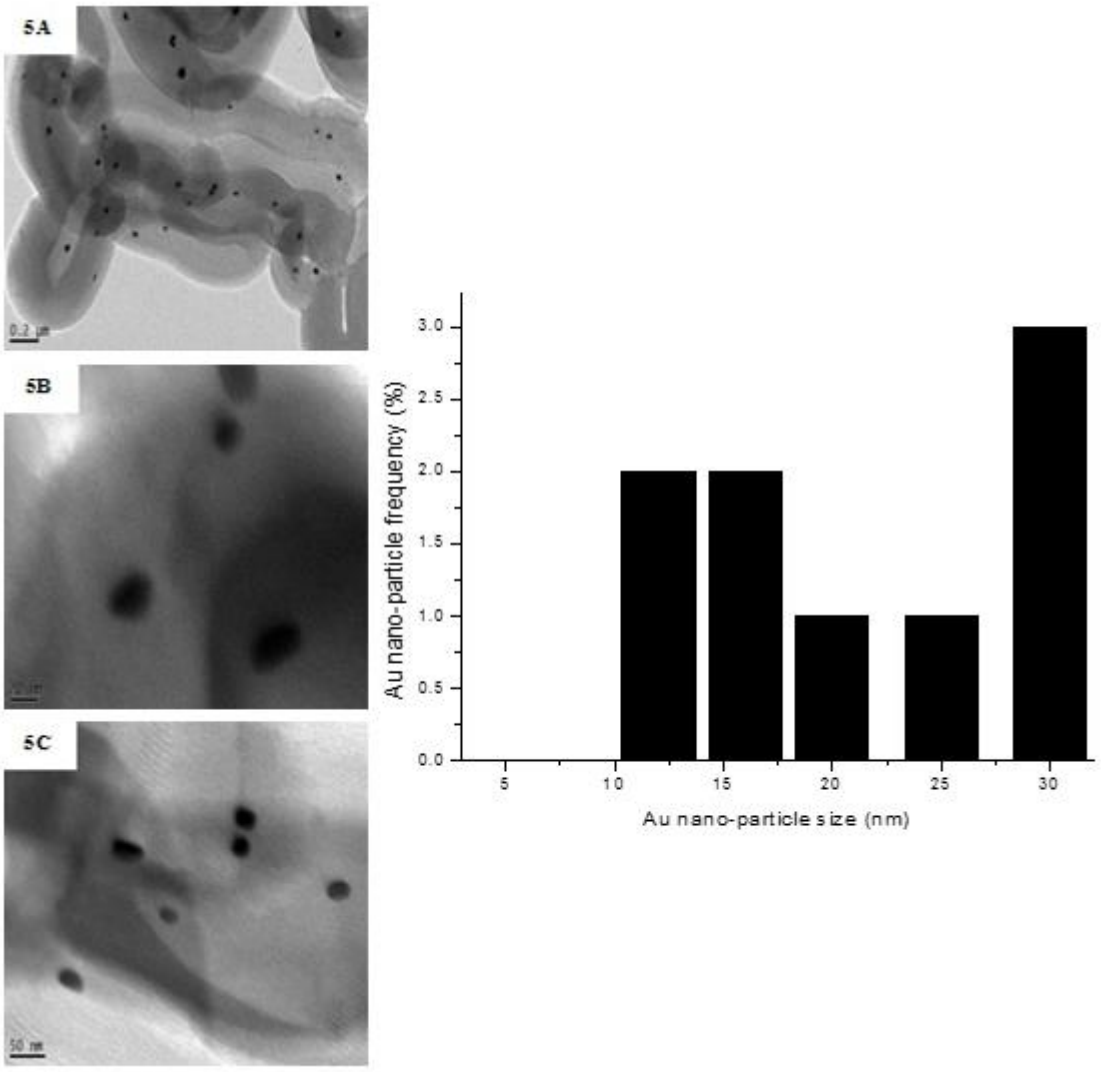

Figure 48. TEM (5A – C) and Au particle size distribution for Au/0.6Adp0.6-SBA-15 catalyst

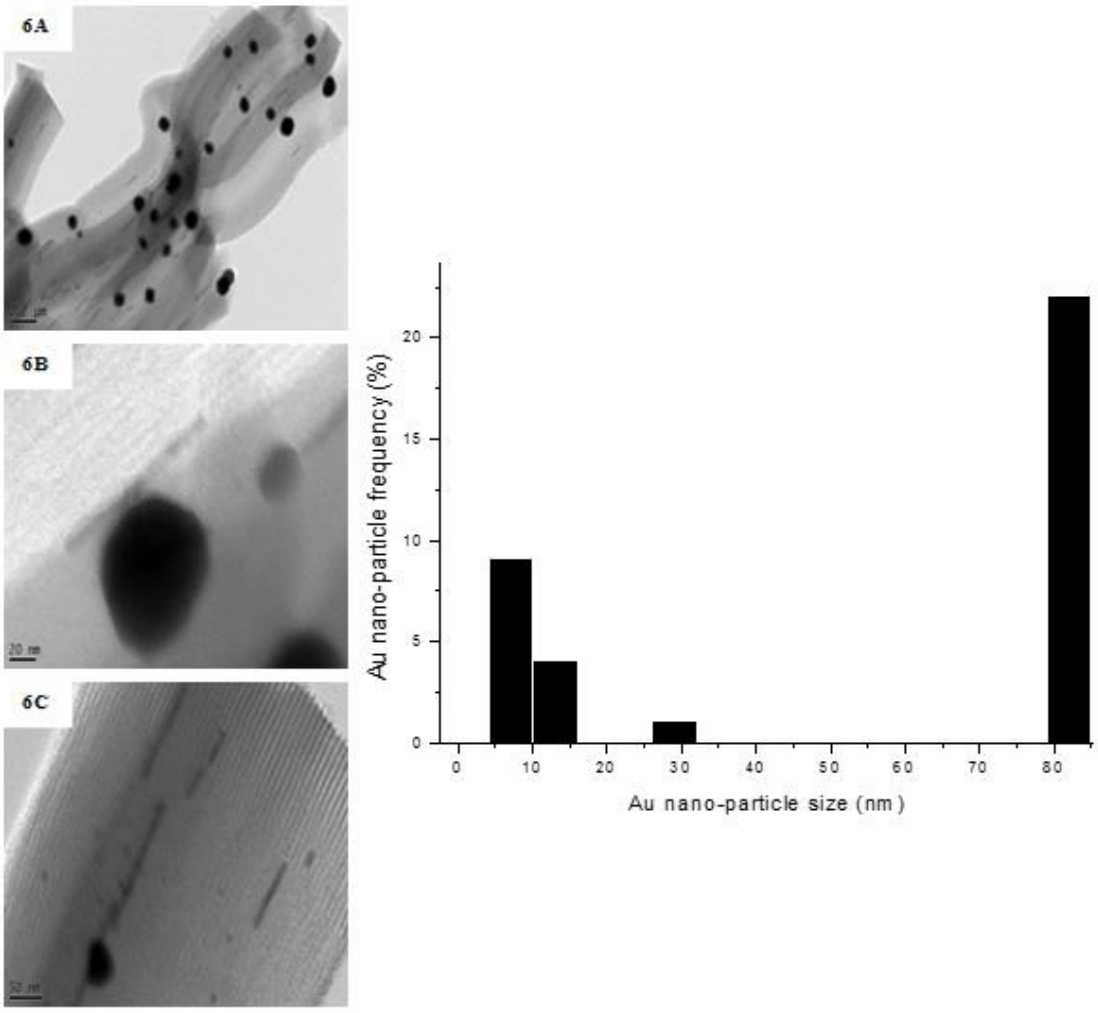

Figure 49. TEM (6A – C) and Au particle size distribution for Au/P-SBA-15 catalyst

5.4. Conclusion

After exploring six different preparation methods to synthesise six Au/SBA-15 catalysts, physical characterisation has revealed the best desired Au/SBA-15 catalyst – Au-0.6Mdp/SBA-15- with high gold loading of 3.5 wt. % and gold particles as small as 1.3 nm, uniformly dispersed and strongly attached to the SBA-15 support. The catalyst has a high surface area of 726 m^2/g, which makes it one of the best, if not the best reported Au/SBA-15 catalyst with such desired characteristics. Other Au/SBA-15 catalysts such, as Au-M0.8/SBA-15 and Au-en/SBA-15, also appear very promising since both have high surface areas and small particles sizes between 3.5 – 5.5 nm.

The next part of this project is the development of an appropriate coating technique to introduce the best Au/SBA-15 catalyst onto the channels of a novel metal machined micro-reactor designed and fabricated by Odiba [143]. This will be followed by catalytic evaluation or chemical characterisation of the six Au/SBA-15 catalysts, including the Au/SBA-15 coated micro-reactor in complete oxidation of selected VOC model compounds (Chapter 7).

CHAPTER 6. Coating Au/SBA-15 catalyst in a micro-reactor

6.1. Introduction

A metal machined micro-reactor with eleven channels of dimensions 0.3 mm x 0.5 mm x 100 mm (width x depth x length) was designed and fabricated by Odiba [143] for the purpose of coating the best Au/SBA-15 catalyst from this project for elimination of VOCs by complete oxidation at low temperatures. For the best micro-reactor design, in terms of geometric shapes and fluid dynamics, Odiba used Computational Fluid dynamics (CFD) module of COMSOL Multi-physics simulation software to obtain the optimum micro-reactor design with gas flow profiles that are most appropriate for VOC/air gas mixtures across the micro-reactor channels. This Chapter briefly discusses the design and fabrication of the micro-reactor by Sunday Odiba [143], with more emphasis on the investigation into the development of a suitable coating technique necessary to produce a thin, uniform and firmly adhered Au/SBA-15 catalyst on the walls of the micro-reactor channels. It is also important to choose coating techniques that do not destroy or inhibit Au/SBA-15 catalyst activity. Scanning electron microscopy and light microscopy images were used to check each coating technique for catalyst uniformity, adhesion and cracks. The best catalyst coated micro-reactor was later tested for elimination of VOCs by complete oxidation at low temperatures, using propane as model VOC compound [143].

6.2. Micro-reactors

Micro-reactors are devices in which chemical reaction takes place in narrow confinement typically less than 100 μm. Unlike the large traditional reactors, micro-reactors house chemical reactions to the scale of 5 – 100 ml. Micro-reactors are constructed from a network of miniaturised reaction channels. The main distinctions between micro-reactors and traditional chemical reactors are directly related to their size. Besides a larger ratio of surface area to volume, micro-reactors also allow one to drive highly exothermic reactions while

avoiding hot-spot formation, since they have a high heat transfer rate. Even though micro-reactors are small, units can tolerate temperatures and pressures as high as 650 ºC and 25 bars. This allows micro-reactors to carry out, on a small scale, reactions that are too exothermic or explosive to run at large scale [144-146]. Fast mixing and diffusion can be achieved easily in micro-reactors due to small characteristic size and low volume. Moreover, the avoidance of mass-transfer limitation is one of the main objective in the development of micro-reactors. For reactions that are mass transfer limited in traditional macro-scale systems, the improved mass transfer in micro-reactor can lead to higher observed reaction rates [145, 147, 148].

6.3. Experimental

6.3.1. Micro-reactor fabrication

The designed micro-reactor was fabricated in stainless steel (type 316L) plate of 8 mm thickness, by using a CNC (Computer Numerical Control) micro-milling machine. Two micro-channel plates (Figure 50) were fabricated by micro-milling 11 rectangular slots of 1mm x 1mm x 100 mm (width x depth x length) with a semi-circular inlet and outlet manifolds in SS 316L plates. This dimension will be reduced to 0.5 mm x 0.5 mm x 100mm due to the catalyst coating on the micro-channel wall. In-depth description of the construction, testing and commissioning of the gas rig with the micro-reactor are contained in Odiba's work [143].

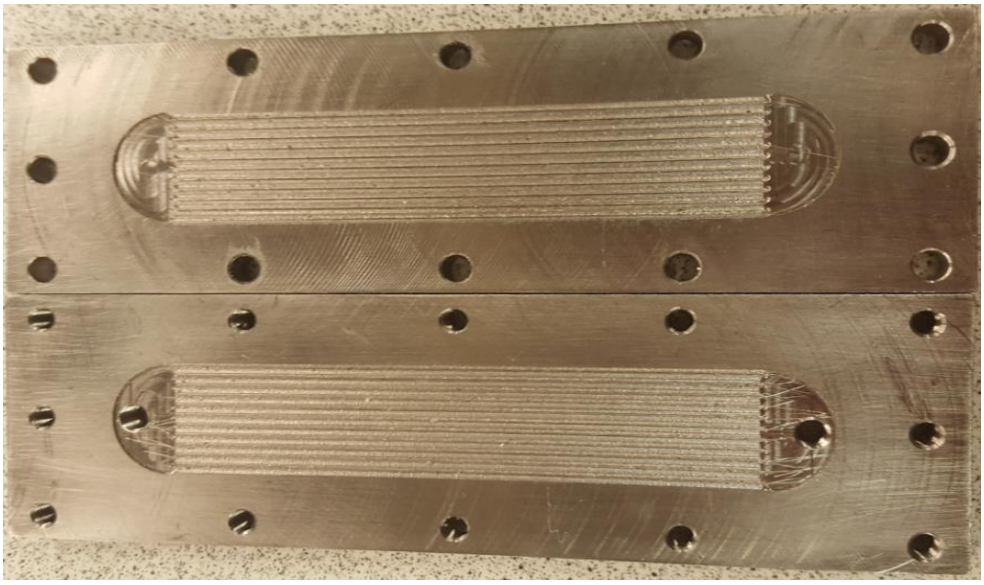

Figure 50. Photos of 2 fabricated micro-reactor plates having 11 rectangular parallel micro-channels/slots and inlet and outlet manifolds on stainless steel 315L [143]

6.3.2. Preparation of Au/SBA-15 catalyst slurry and coating techniques

Although significant progress has been made in terms of the design and fabrication of micro-channelled reactors, the introduction of the active catalyst in thin, firm and uniform layer which does not flake off from the channel walls of the micro-reactor, intended for gas phase reactions remain a big challenge [149]. To analyse how well the support or catalysts binds to the metal surface; Scanning Electron Microscopy (SEM) is normally used to characterise the coatings which reveals if there are cracks or flaking of the catalyst coatings from the micro-reactor channels. In addition, light microscopy (GXCAM-5 microscope) images were used alongside SEM for characterisation in this thesis.

Despite several publications on Au/SBA-15 catalysts and the unusually high activity of gold catalysts towards oxidation and hydrogenation reactions at lower temperatures [5, 150, 151], no publication was found for coating Au/SBA-15 catalyst in micro-reactor channels. In choosing catalyst binders necessary for coating the developed Au/SBA-15 catalyst on the walls of the micro-reactor, inorganic binders such as alumina, titania, zirconia, natural clays

like bentonite, sepiolite, kaolin, montmorillonite and palygorskite were avoided, since they contain metal impurities or acid-base properties which can significantly change the properties of the original powdered catalyst, thereby introducing possible inhibitory effects in the catalytic performance of the coated catalyst. For this reason, only organic binders (that can be burnt off during calcination to re-activate the catalyst before reaction) and colloidal silica (a neural inorganic binder with pH of 7 and no metal impurities) were used to formulate catalyst slurry for coatings.

To develop the best coating technique on the stainless steel machined micro-reactor which offer thin, firm and uniform deposition of the Au/SBA-15 catalyst, three different coating methods where explored, namely:

1. Manually injecting a slurry made of Au/SBA-15 catalyst, polyvinyl alcohol (as binder), acetic acid and water into the channels of the micro-reactor using a syringe (Technique 1).

2. Spraying slurry from Technique 1 (Au/SBA-15 catalyst, polyvinyl alcohol, acetic acid and water) at room temperature using a manual fine airbrush with 0.3 mm nozzle (Technique 2).

3. Spraying slurry made of Au/SBA-15 catalyst, colloidal silica (inorganic binder), methyl cellulose (organic binder) and water, using a manual fine airbrush with 0.3 mm nozzle on micro-reactor heated up to 150 °C (Technique 3).

For Technique 1, a small amount of Au/SBA-15 catalyst was added to water, polyvinyl alcohol as binder with acetic acid in the ratio of 10:84:5:1. The mixture, while stirring, was heated at 65 ºC for 3 hours and left to stir at room temperature for 1 hour to achieve a homogenous solution. A syringe was manually used to fill each channel to the brim. The

coated plate was then dried at room temperature before heat treatment at 500 °C with ramping at 1 °C/minute to remove the polyvinyl alcohol organic binder.

For Technique 2, the same catalyst slurry was used; however a manual air brush with 0.3 mm nozzle and 2 bar air pressure was used to spray the catalyst slurry into all the channels of the micro-reactor. The coated plated was air dried before heat treatment at 500 °C to remove the polyvinyl alcohol organic binder.

Technique 3 was a mixture of 10 mg catalyst, 7g colloidal silica, 7g methyl cellulose and 6g of water (10:7:7:6 ratio). Homogeneity of the mixture for Technique 3 was achieved within 30 minutes of stirring at room temperature as shown in Figure 51 A. The reactor plate was heated at 150 °C before spraying with the manual airbrush as shown in Figure 51 B. The coated plated was air dried before heat treatment at 500 °C to remove methyl cellulose organic binder as shown in Figure 51 C. Excess catalyst outside the channels in all cases were easily wiped off.

To improve the adherence of the catalyst layers onto the micro-channels, the micro-reactor was rinsed with acetone followed by deionized water and dried in an oven at 65 °C to remove organic material from the surface prior to catalyst deposition steps.

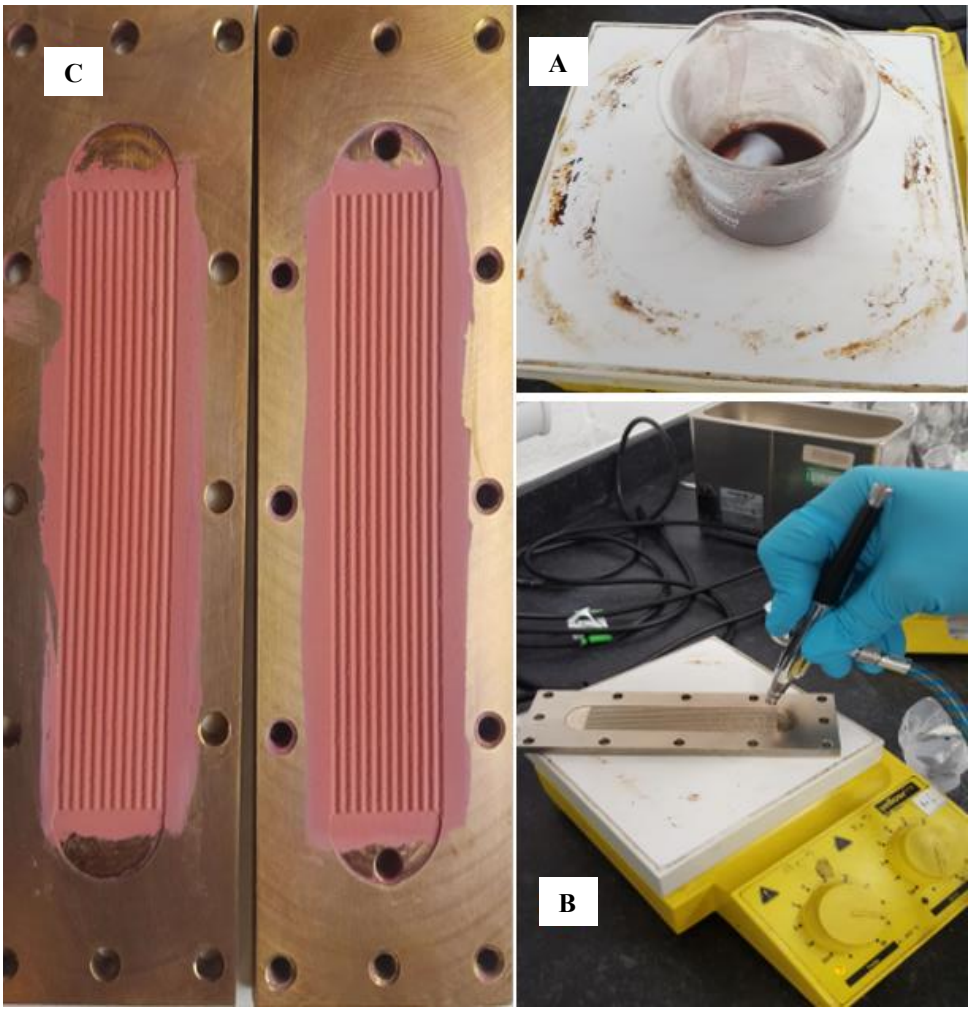

Figure 51. Catalyst preparation and spraying in the micro-channels

6.4. Results and discussions

6.4.1. SEM/Microscopy images of catalyst coated micro-reactor

The catalyst-coated micro-channels using these three coating techniques were characterised by GXCAM-5 light microscope and Scanning Electron Microscopy (SEM) Hitachi S-3400 N variable.

Technique 1

From the images in Figure 52, it can be seen that coating Technique 1 failed to produce firmly adhered catalyst coating on the walls of the micro-reactor as cracks are seen

everywhere in the channels which can easily flake off and block the channels of the micro-reactor during reaction.

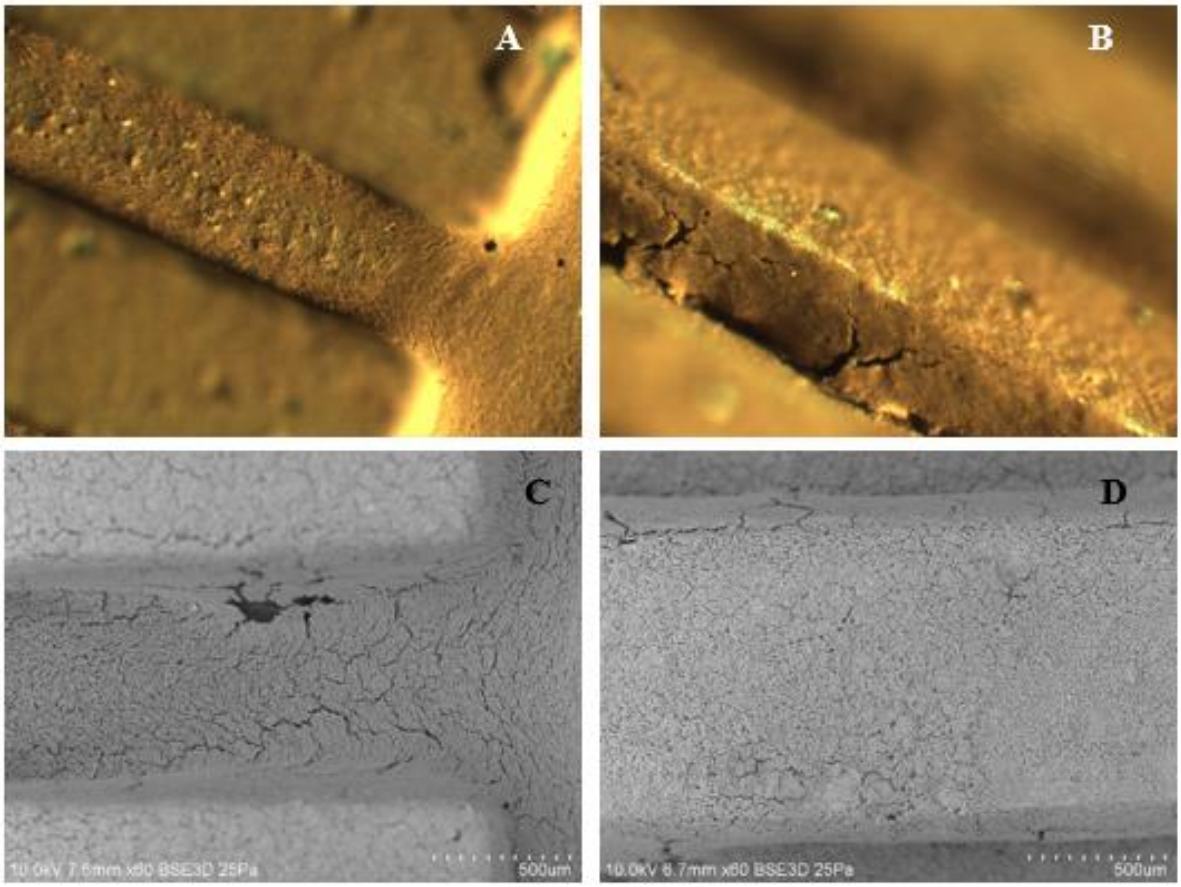

Figure 52. Technique 1: GXCAM-5 light microscope images (**A** and **B**) and SEM images (**C** and **D**) of Au/SBA-15 catalyst coating in the channels of the micro-reactor after coating and calcination at 500 °C

Technique 2

Technique 2 developed deeper cracks all over the channels of the micro-reactor as shown in Figure 53. The coatings flaked from the walls of the reactor, and so just like Technique 1, Technique 2 will not be suitable as a coating method to introduce Au/SBA-15 catalyst in the micro-reactor.

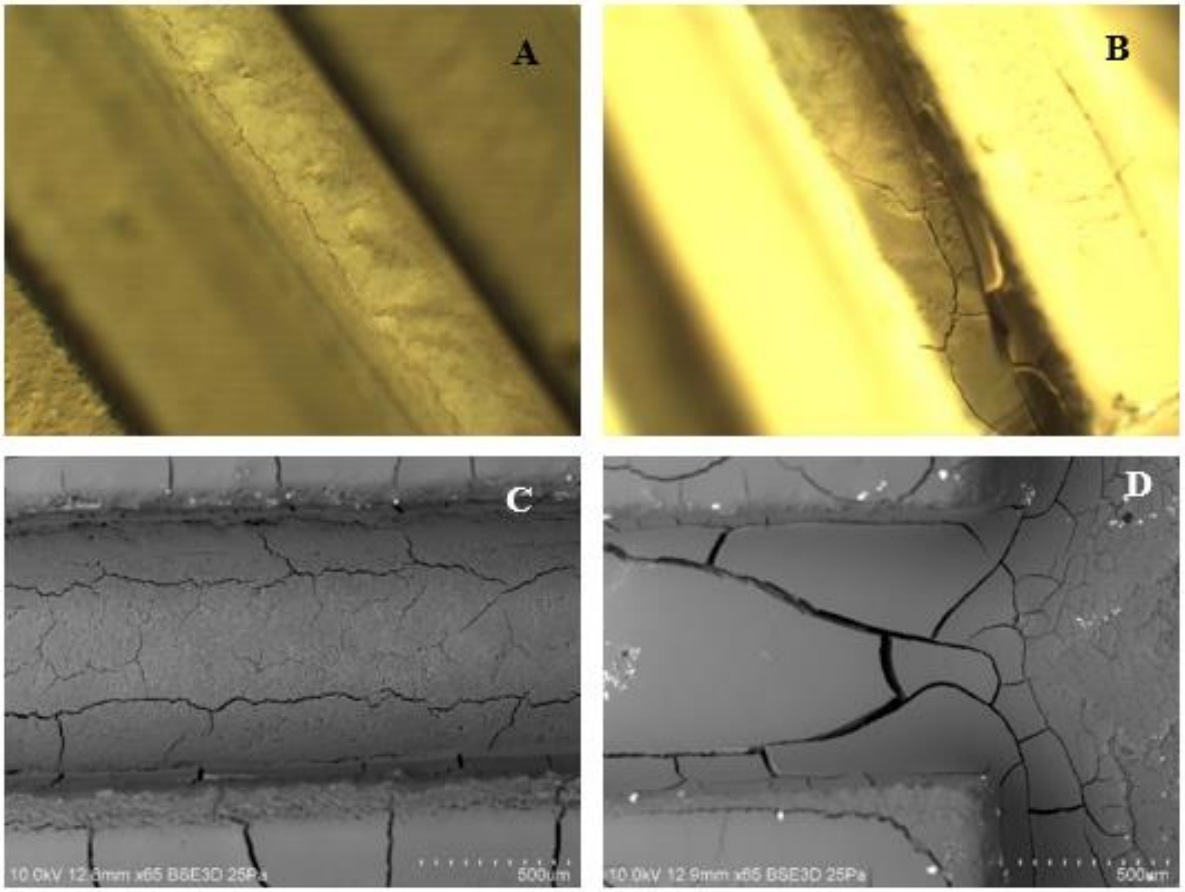

Figure 53. Technique 2: GXCAM-5 light microscope images (A and B) and SEM images (C and D) of Au/SBA-15 catalyst coating in the channels of the micro-reactor after coating and calcination at 500 °C

Technique 3

As seen in Figure 54, Technique 3 produced a uniform, thin, sponge-like Au/SBA-15 coating that appear to be firmly adhered to the walls of the micro-reactor. No cracks or flaked off catalyst coating was observed in all the channels.

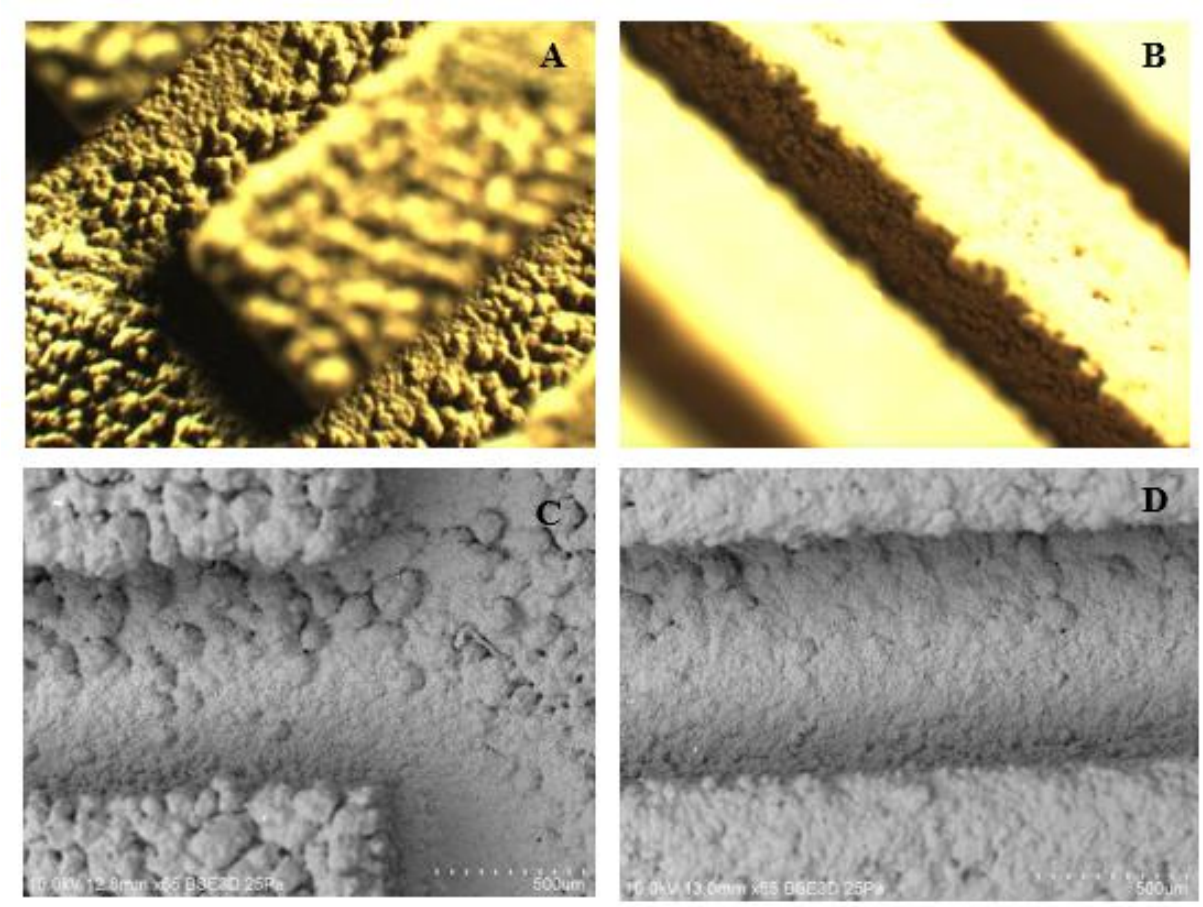

Figure 54. Technique 3: GXCAM-5 light microscope images (A and B) and SEM images (C and D) of Au/SBA-15 catalyst coating in the channels of the micro-reactor after coating and calcination at 500 °C

6.5. Conclusion

An optimised metal machined micro-reactor was successfully designed and fabricated for the purpose of eliminating VOCs in indoor air streams by complete catalytic oxidation at lower temperatures. The use of micro-reactor instead of conventional chemical reactors is aimed at efficiently using less energy to generate enough heat for significantly higher VOC

conversion rates at lower temperatures. This is possible due to higher heat transfer rates, improved mass transfer to achieve higher rates of reaction, in addition to a greater degree of VOCs/air mixture rates and higher residence time distribution of reactants offered by the catalytic micro-reactor. However, to introduce a thin film of firmly adhered Au/SBA-15 catalyst in the micro-reactor required the development of a novel catalyst coating procedure. Technique 3 as shown by SEM and light microscopy characterisation, proved to be highly effective in producing a uniformly firm Au/SBA-15 catalyst coating in the micro-reactor channels devoid of any cracks. Also important is the fact that the nature of binders used (colloidal silica and methyl cellulose) do not contain metal impurities or acid-base properties that could possibly interfere with the catalytic performance of the prepared Au/SBA-15 catalyst. Propane was selected as a model VOC compound because the alkanes are one of the most difficult hydrocarbons to oxidise due to their high stability [22-25, 152-154]. Only the most active catalytic systems can oxidise propane at temperatures below 200 °C.

In addition, the test results of the six prepared Au/SBA-15 catalysts in powdered form using conventional fixed bed reactor for complete oxidation of VOCs are discussed in Chapter 7, with the aim of screening out the best Au/SBA-15 catalyst to be coated in the micro-reactor.

CHAPTER 7. Complete oxidation of VOCs over Au/SBA-15 catalysts

7.1. Introduction

The catalytic performance of the six Au/SBA-15 catalysts, namely: Au-en/SBA-15 catalyst, Au-M0.8/SBA-15 catalyst, Au-A0.8/SBA-15 catalyst, Au-0.6Mdp/SBA-15 catalyst, Au-0.6Adp/SBA-15 catalyst and Au-P/SBA-15 catalyst were tested using a wide range of VOCs model molecules namely, acetone, propane, BTEXB (a gas mixture of benzene, toluene, ethylbenzene, xylene and 1,3-butadiene) and dichloromethane, in total oxidation with air, by Temperature Programmed Reaction (TPRx) and steady state reaction (SSR) over each catalyst in a fixed bed reactor system. Hydrogen Temperature Programmed Reduction (TPR) studies were done to understand the behaviour of the catalysts in reducing environment and to determine the optimum temperature required to reduce the oxide form of the catalysts from cationic gold (Au^{+} and Au^{3+}) to metallic gold (Au^{0}). After reducing the catalysts in hydrogen at 500 ° C for one hour, the six catalysts were then tested for oxidation of VOCs starting with acetone. Four of the best catalysts (Au-en/SBA-15 catalyst, Au-M0.8/SBA-15 catalyst, Au-A0.8/SBA-15 catalyst, and Au-0.6Mdp/SBA-15 catalyst) were tested in oxidation of propane. The best Au/SBA-15 catalyst was later tested in BTEXB oxidation, followed by the oxidation of dichloromethane. A comparison of the catalytic activities of the as-synthesised catalysts with the reduced catalysts were carried out to determine the active oxidation state of gold, cationic (Au^{+}/Au^{3+}) or metallic (Au^{0}), in VOCs oxidation. Reaction stability test with Au/SBA-15 catalyst in VOCs complete oxidation at constant temperatures for 25 hours was also carried out. The details of experimental procedure for catalytic evaluation was discussed in Chapter 3, section 3.3.

The best Au/SBA-15 catalyst was successfully coated in a micro-reactor as described in Chapter 6. The catalytic performance of the catalyst coated micro-reactor using propane as

VOC model compound was tested by S,Odiba [143], and the result compared with other published catalysts propane oxidation in Appendices pages.

7.2. Experimental set-up

7.2.1. Catalytic evaluation of Au/SBA-15 catalysts

The catalytic characterisation of the selected catalysts were performed using the Catlab (Hiden Analytical) system. A schematic diagram of the experimental system is shown in Figure 51.

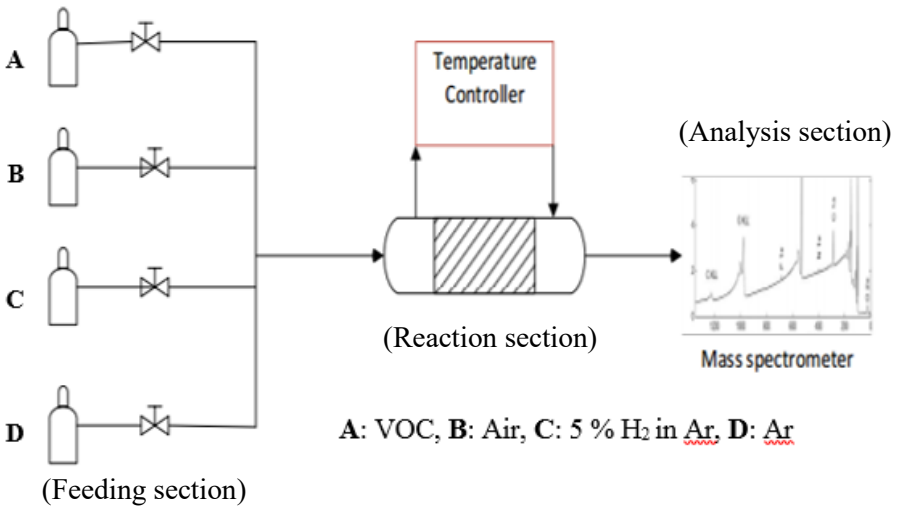

Figure 55. Hiden Analytical Catlab system consists of three sections namely: feeding, reaction and analysis (with mass spectrometer) sections

For all the experiments, the measured partial pressure readings of the M-S instrument (in torr) were correlated to the gas concentrations in ppm (initial M-S gas partial pressure reading before reaction was regarded as the reading for the known initial VOC concentration from each VOC gas bottle from the feeding section). The percentage VOC conversions (%X) were calculated as:

$$\%\,X = \frac{Inital\ VOC\ concentration\ -\ Final\ VOC\ concentration\ at\ T^{o}C}{Inital\ VOC\ concentration}\ x\ 100 \qquad (1)$$

Where % X is percentage conversion and $T^{\circ}C$ is temperature in Celsius.

With non-chlorinated VOCs as the limiting reactant in excess oxygen (in air), complete oxidation to CO_2 and H_2O is expected. However, for chlorinated VOCs, Cl/HCl is also expected in addition to CO_2 and H_2O [155]. Previous monitoring of propane oxidation over excess oxygen with mass spectrometer in TAP reactor at The University of Tokyo, Japan confirmed CO_2 and H_2O as the only final products. No carbon monoxide was detected.

Product formation (CO_2) was calculated as percentage mole fraction after CO_2 calibration.

Table 7 contains the selected mass-to-charge ratio (m/z) of ions monitored in the VOC complete oxidation experiments using quadrupole mass spectrometer:

Table 7. Ions detected at m/z values

Ions	**m/z**
Acetone	43
Propane	29
Dichloromethane	49
Oxygen	32
Carbon dioxide	44
Water	18

7.3. Results and discussions

The catalytic performance of the six Au/SBA-15 catalysts are reported and discussed in this section

7.3.1. TPR of Au/SBA-15 catalysts

There are still disputes in literature regarding which oxidation state of gold is the active form in gold based catalysts. Is it the metallic (Au^0) or cationic (oxidised) gold species (Au^+, Au^{3+}) [156] or a combination of both the metallic and cationic species? [157-159]. No literature was found that clearly explained hydrogen reduction behaviour of oxidised gold on inert supports such as SBA-15 silica. However, studies conducted by Ying and co-workers [160] on oxidation state of gold on a series of Au/ceria catalysts using X-ray photoelectron

spectroscopy (XPS), suggests that both cationic (Au^{+}, Au^{3+}) and metallic gold species (Au^{0}) were present on the as-synthesised gold/ceria catalysts. According to Ying and co-workers [160], the calcination temperature in the catalyst preparation determined the gold specie distribution. The higher the calcination temperature, the higher the percentage of Au^{0}. It is therefore possible that all the Au species (Au^{+}, Au^{3+}, Au^{0}) are present in the as-synthesised Au/SBA-15 catalysts.

The hydrogen TPR results of the six Au/SBA-15 catalysts are shown in Figures 56 - 61. TPR for all the catalysts started off from room temperature, with readings measured from around 50 ºC, and gradually raised to 500 ºC, at 10 º/minute ramp rate. The M-S partial pressure readings for hydrogen and water were represented as arbitrary units (a.u), with initial water partial pressure reading corresponding to zero mark (a.u). Hydrogen and water M-S partial pressures signals drifted continuously with on observed hydrogen consumption peak with corresponding water formation peak, which suggests that no observable reduction occurred between 50 – 500 ºC for all the six Au/SBA-15 catalysts.

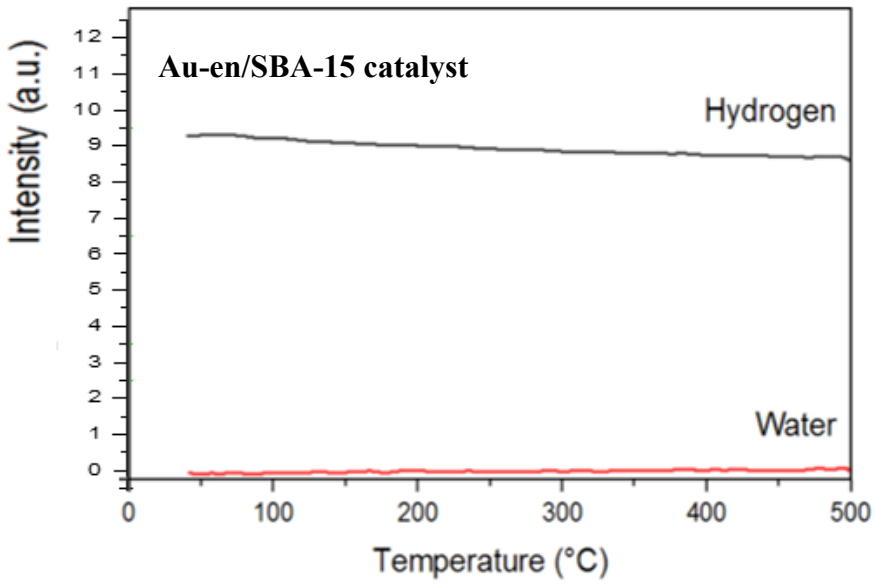

Figure 56. H_2 TPR of Au-en/SBA-15 catalyst

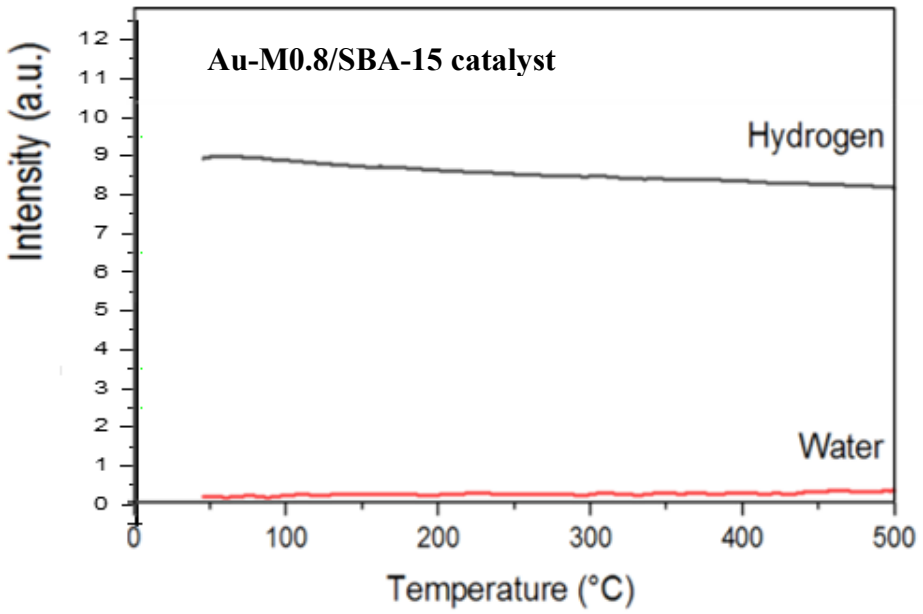

Figure 57. H_2 TPR of Au-M0.8/SBA-15 catalyst

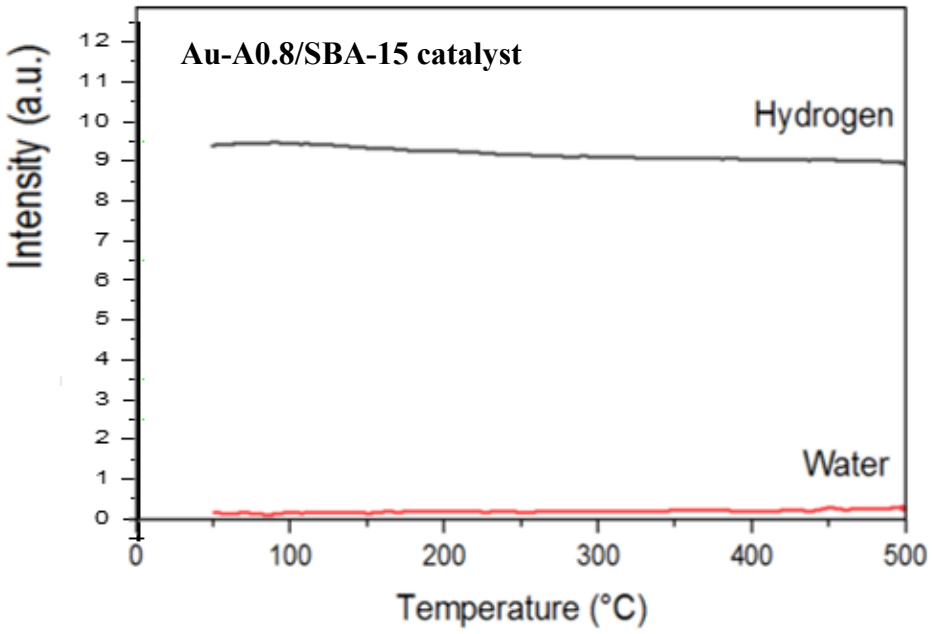

Figure 58. H_2 TPR of Au-A0.8/SBA-15 catalyst

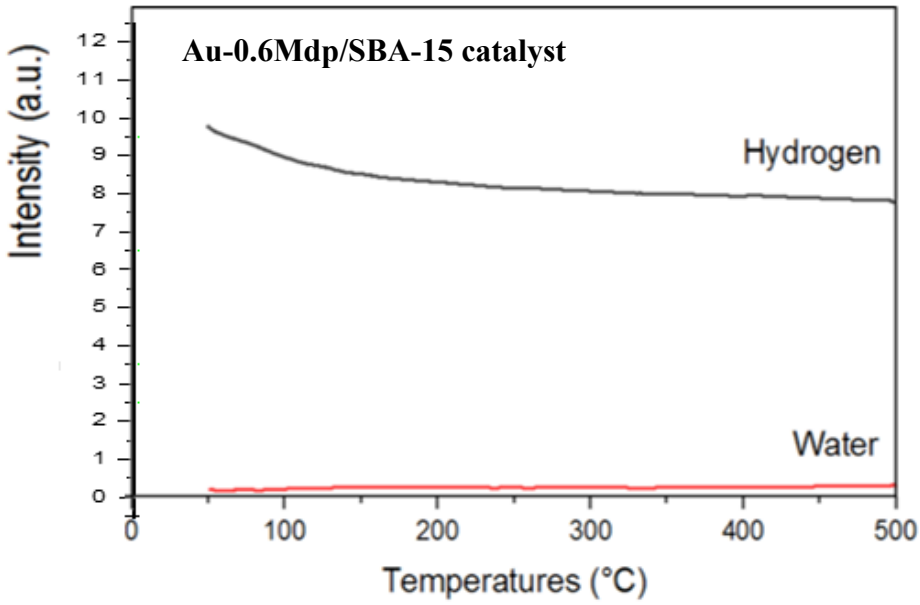

Figure 59. H_2 TPR of Au-0.6Mdp/SBA-15 catalyst

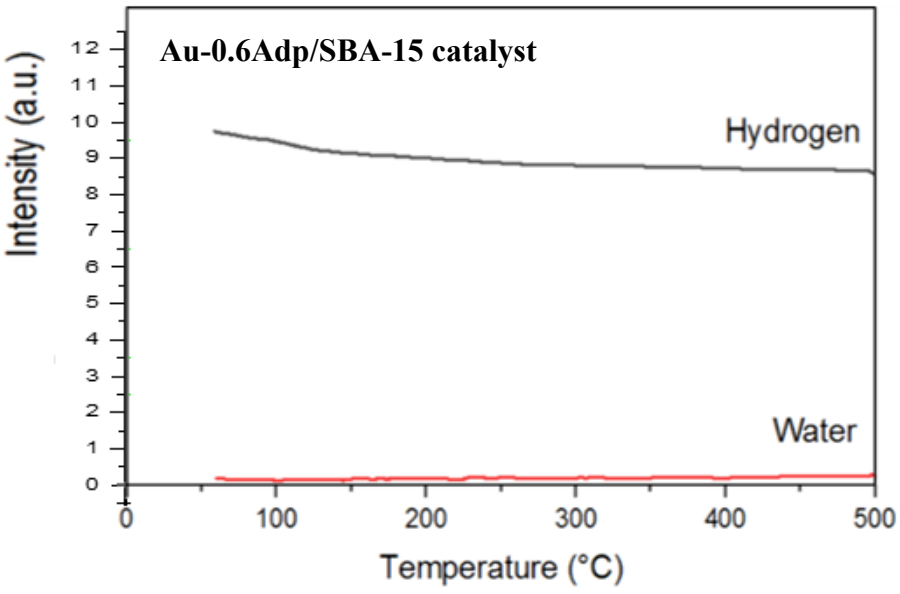

Figure 60. H_2 TPR of Au-0.6Adp/SBA-15 catalyst

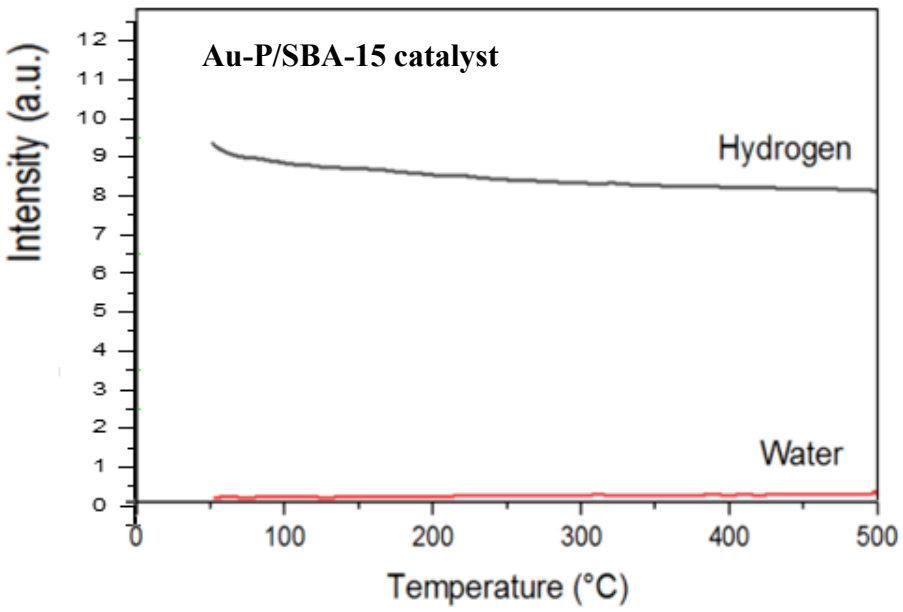

Figure 61. H_2 TPR of Au-P/SBA-15 catalyst

The TPR results shown in Figures 56 – 61 could suggest the following conclusions:

1. It is possible that hydrogen reduction only occurred at low temperatures (less than 50 °C). If this assumption is true, then metallic gold (Au^0) may be the dominant specie on the hydrogen reduced Au/SBA-15 catalysts.
2. Considering suggestion by Ying [160], since all the catalysts were calcined in air at high temperatures (500 °C), it is possible that most of the gold species already exist as Au^0 , therefore, no observable reduction was seen in H_2 TPR.
3. It is also possible that no reduction took place at all, even after hydrogen flow for up to 500 °C, as TPR results in Figures 56 – 61 seem to suggest.

7.3.2. Acetone complete oxidation

Acetone is one of the most common and abundant indoor type VOC, and so, any catalyst designed to eliminate indoor VOCs must be able to destroy acetone.

7.4. Reference standard

Acetone oxidation TPRx from room temperature to 400 °C was carried out over quartz wool in Catlab fixed bed reactor (without catalyst) as reference standard to compare with Au/SBA-15 catalytic oxidation of acetone. This was to ascertain if the oxidation was based on complete catalytic oxidation or merely a thermal oxidation phenomenon. As shown in Figures 62, no acetone oxidation occurred below 280 °C. Acetone oxidation started off at 300 °C, at 22 % acetone conversion. Initial partial pressure of acetone remained constant at 8.3E-14 torr up to 290 °C, an indication that no acetone oxidation took place before 290 °C. Acetone oxidation rapidly increased from 22% to 93 % between 300 – 400 °C. Observed acetone oxidation between 300 – 400 °C was followed by corresponding CO_2 formation (Figure 63). Water partial pressure (Fig. 64) remained constant at 4.0E – 12 from room temperature to 400 °C, which suggests that the observed thermal oxidation of acetone beyond 290 °C was only partial oxidation as no water was formed.

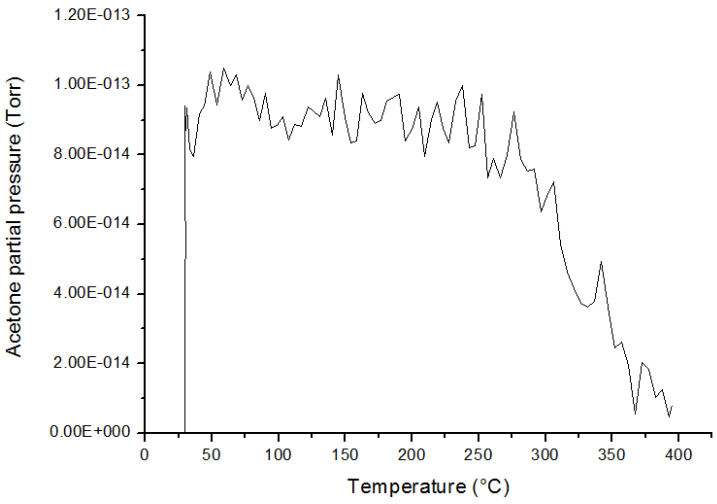

Figure 62. Acetone TPRx on quartz wool reference standard

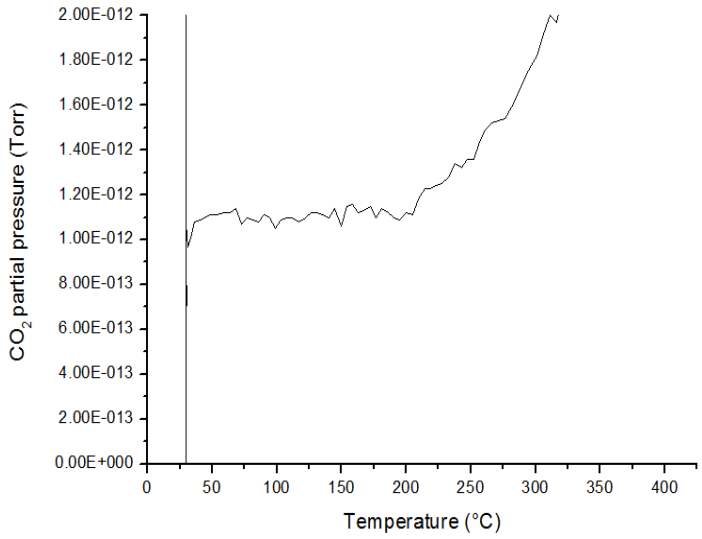

Figure 63. Acetone TPRx (CO_2 response) on quartz wool reference standard

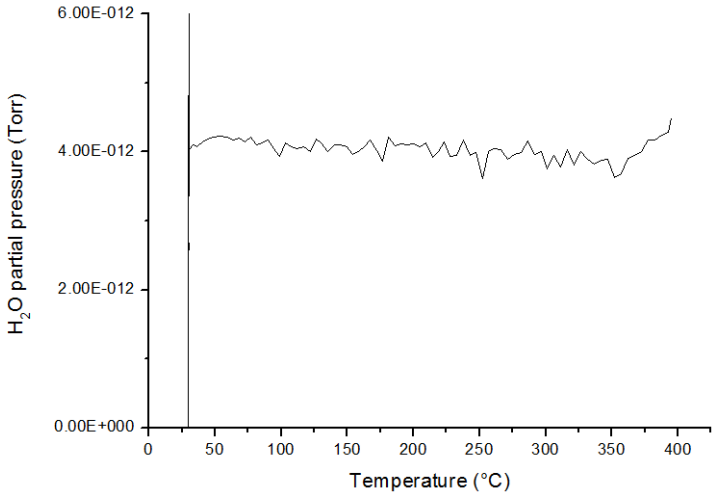

Figure 64. Acetone TPRx (H_2O response) on quartz wool reference standard

For Propane, BTEXB and dichloromethane, no oxidation was observed in the reactor with quartz wool (without catalyst) upto 400 °C.

7.5. Acetone TPRx over as-synthesised (oxidised) and reduced Au/SBA-15 catalysts

Figures 65 - 82 contains all the MS raw data for acetone TPRx over the as-synthesised and reduced forms of the six Au/SBA-15 catalysts

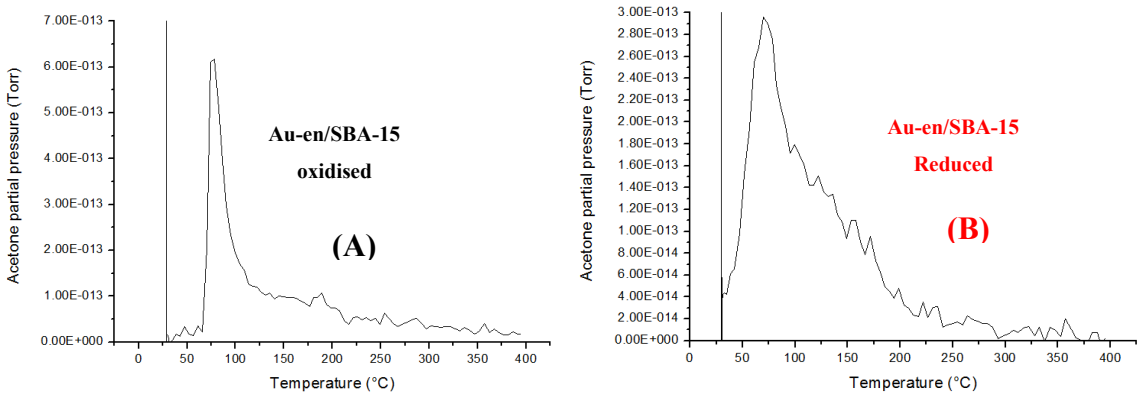

Figure 65. Acetone TPRx over oxidised (A) and reduced (B) Au-en/SBA-15 catalyst (MS raw data)

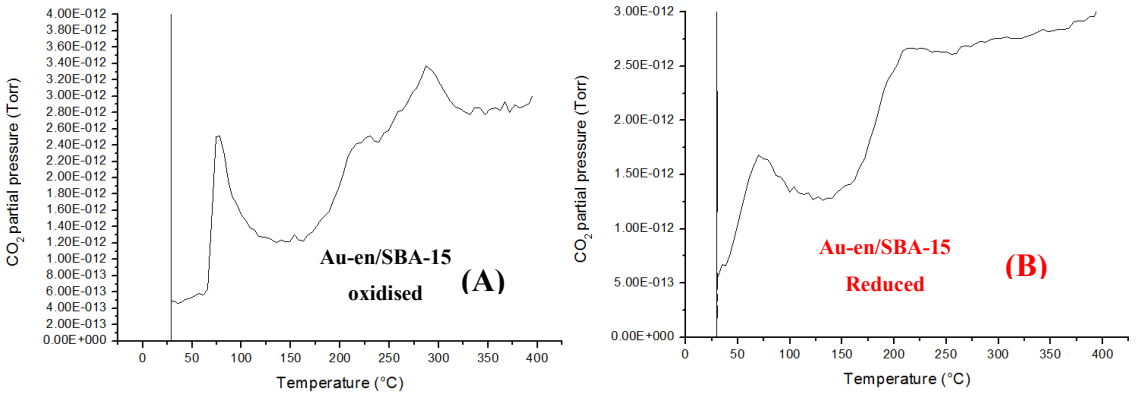

Figure 66. Acetone TPRx (CO_2 response) over oxidised (A) and reduced (B) Au-en/SBA-15 catalyst (MS raw data)

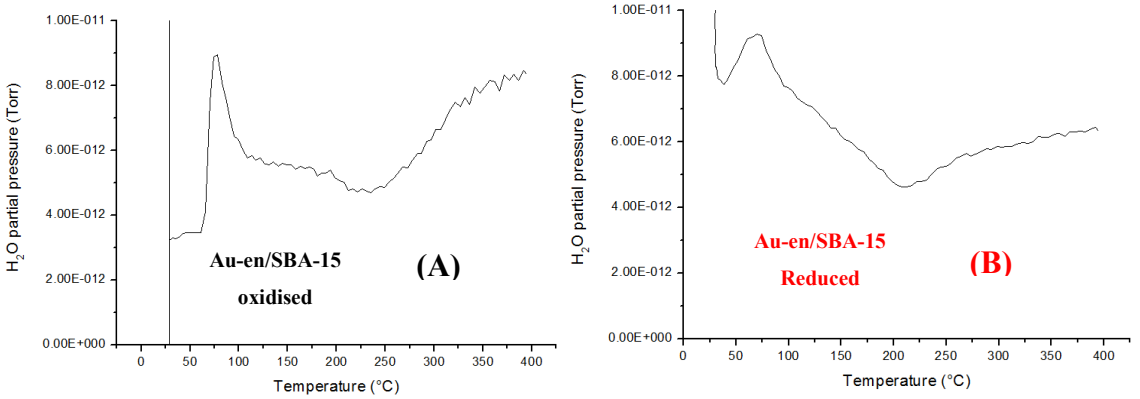

Figure 67. Acetone TPRx (H_2O response) over oxidised (A) and reduced (B) Au-en/SBA-15 catalyst (MS raw data)

TPRx results in Figures 65 – 67 shows that only the reduced form of Au-en/SBA-15 catalyst attained 100 % acetone conversion at 280 – 400 °C. Although the synthesised (oxidised) form of the catalyst did not attain 100 % acetone conversion, it was also very active in acetone complete oxidation.

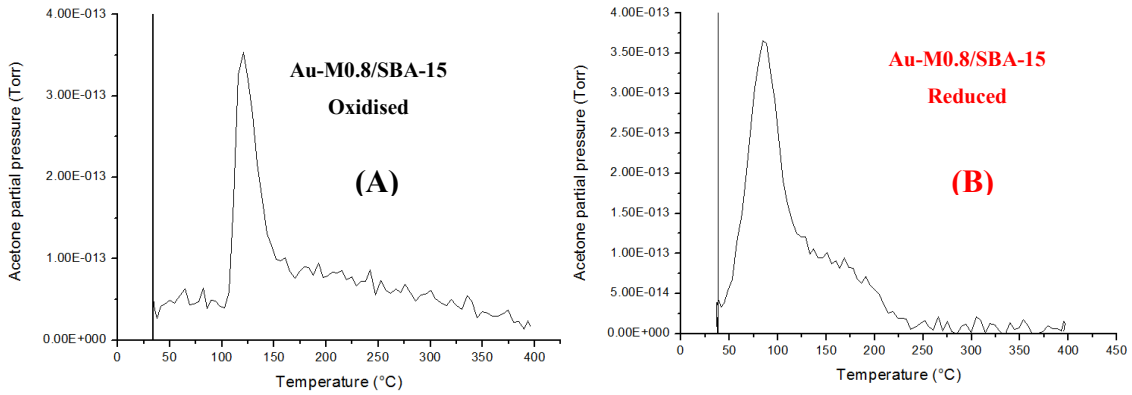

Figure 68. Acetone TPRx over oxidised (A) and reduced (B) Au-M0.8/SBA-15 catalyst (MS raw data)

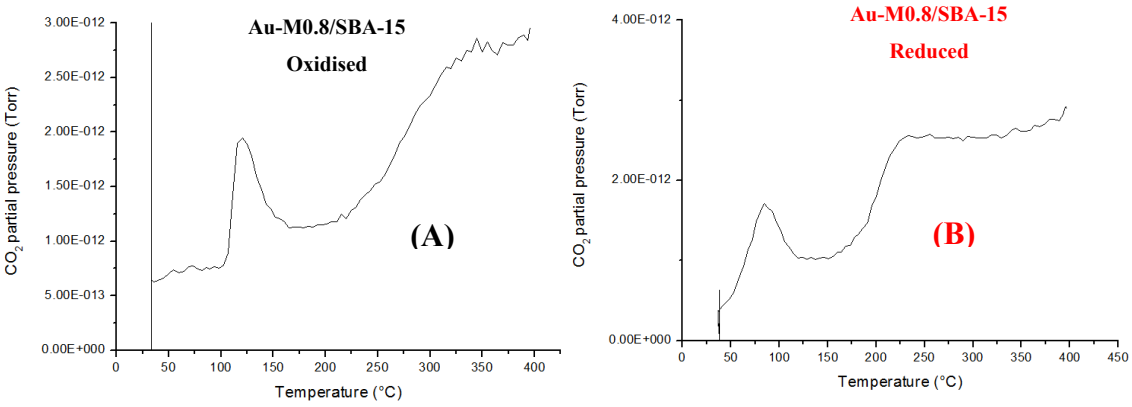

Figure 69. Acetone TPRx (CO_2 response) over oxidised (A) and reduced (B) Au-M0.8/SBA-15 catalyst (MS raw data)

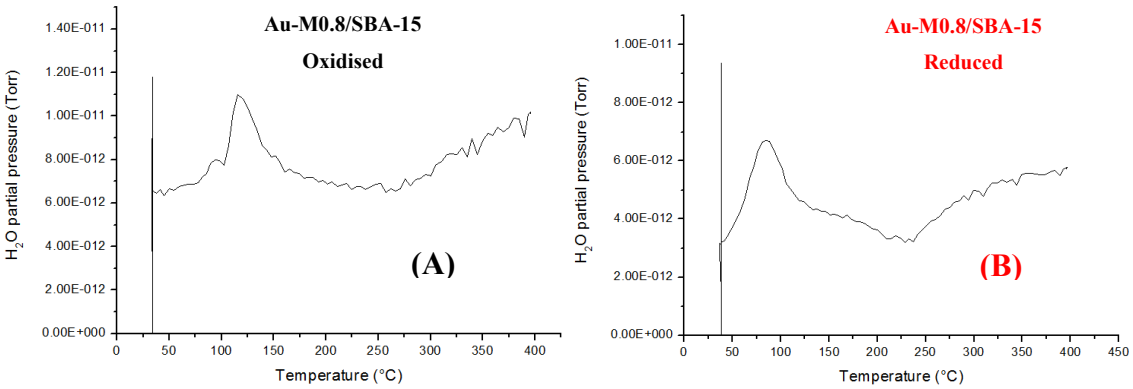

Figure 70. Acetone TPRx (H_2O response) over oxidised (A) and reduced (B) Au-M0.8/SBA-15 catalyst (MS raw data)

Although both the synthesised and reduced forms of Au-M0.8/SBA-15 catalyst were very active in acetone complete oxidation (Figures 68 – 70), only the reduced form attained 100 % acetone conversion at 260 – 400 °C.

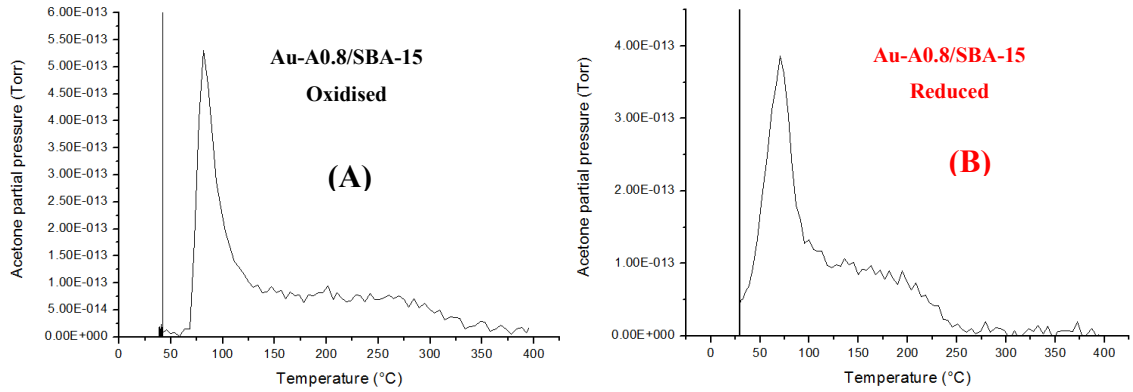

Figure 71. Acetone TPRx over oxidised (A) and reduced (B) Au-A0.8/SBA-15 catalyst (MS raw data)

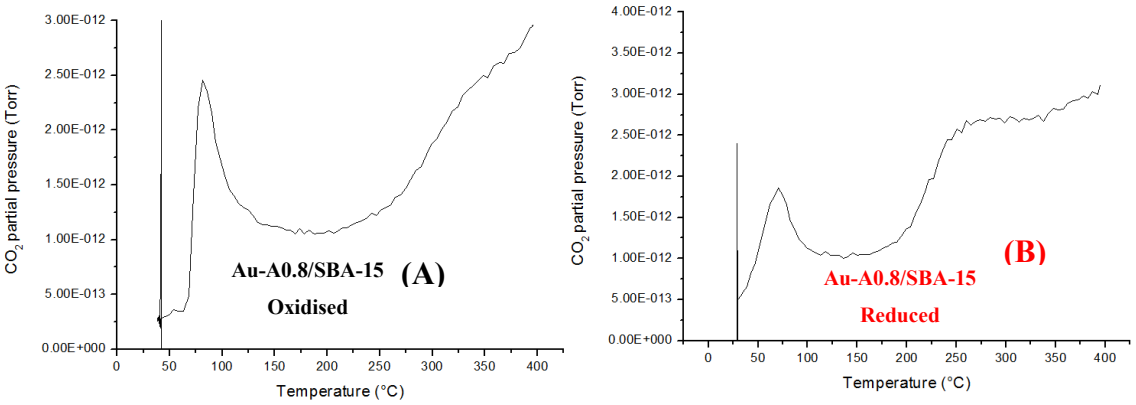

Figure 72. Acetone TPRx (CO_2 response) over oxidised (A) and reduced (B) Au-A0.8/SBA-15 catalyst (MS raw data)

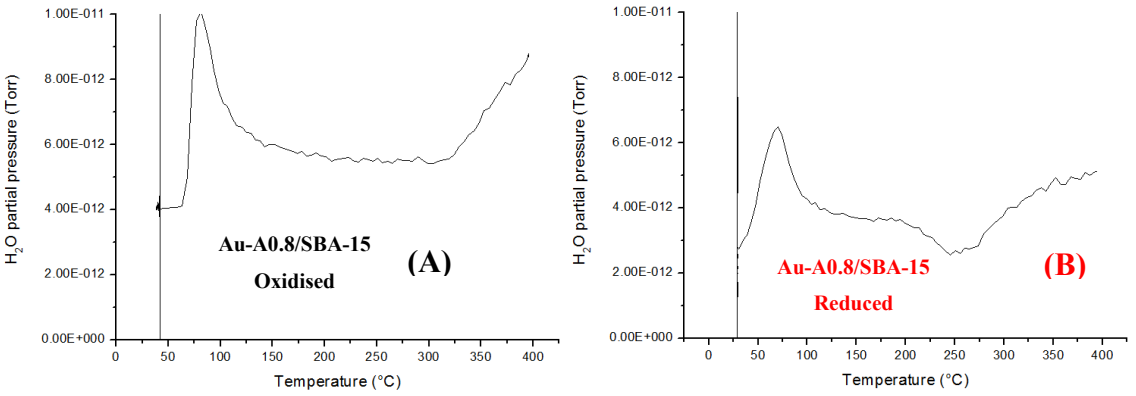

Figure 73. Acetone TPRx (H_2O response) over oxidised (A) and reduced (B) Au-A0.8/SBA-15 catalyst (MS raw data)

The reduced form of Au-A0.8/SBA-15 catalyst was more active than the as-synthesised form (Figures 71 -73), attaining 100 % acetone conversion from 280 - 400 °C. The as-synthesised form of the catalyst was only close to 100 % acetone conversion at 380 °C.

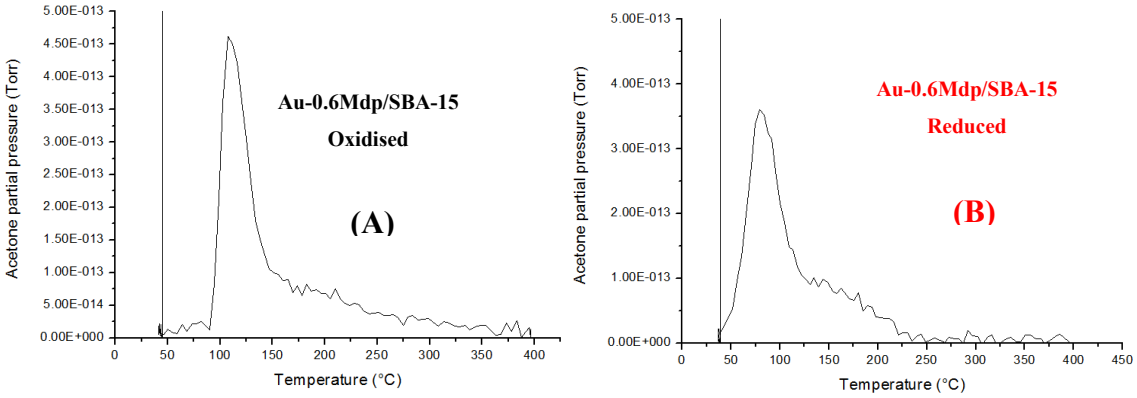

Figure 74. Acetone TPRx over oxidised (A) and reduced (B) Au-0.6Mdp/SBA-15 catalyst (MS raw data)

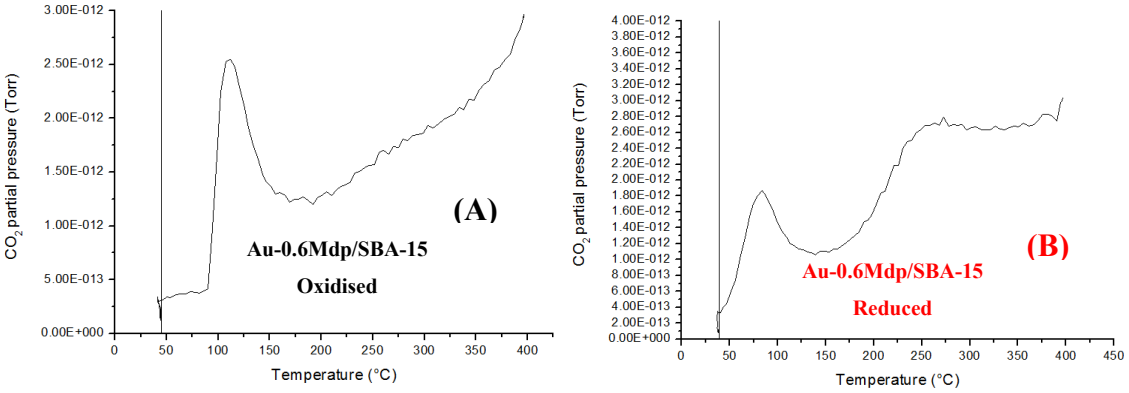

Figure 75. Acetone TPRx (CO_2 response) over oxidised (A) and reduced (B) Au-0.6Mdp/SBA-15 catalyst (MS raw data)

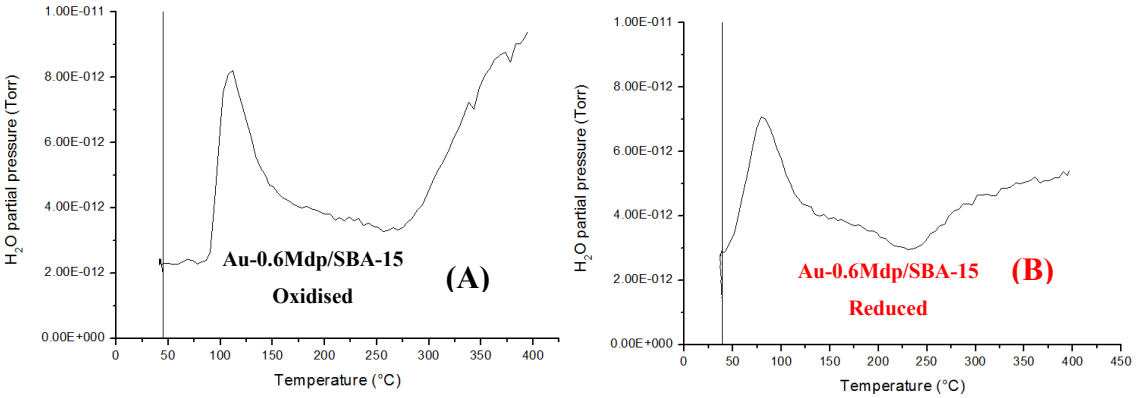

Figure 76. Acetone TPRx (H_2O response) over oxidised (A) and reduced (B) Au-0.6Mdp/SBA-15 catalyst (MS raw data)

The reduced form of Au-0.6Mdp/SBA-15 catalyst was the most active of all the Au/SBA-15 catalysts (Figure 74B – 76B), attaining 100 % acetone conversion as low as 250 °C.

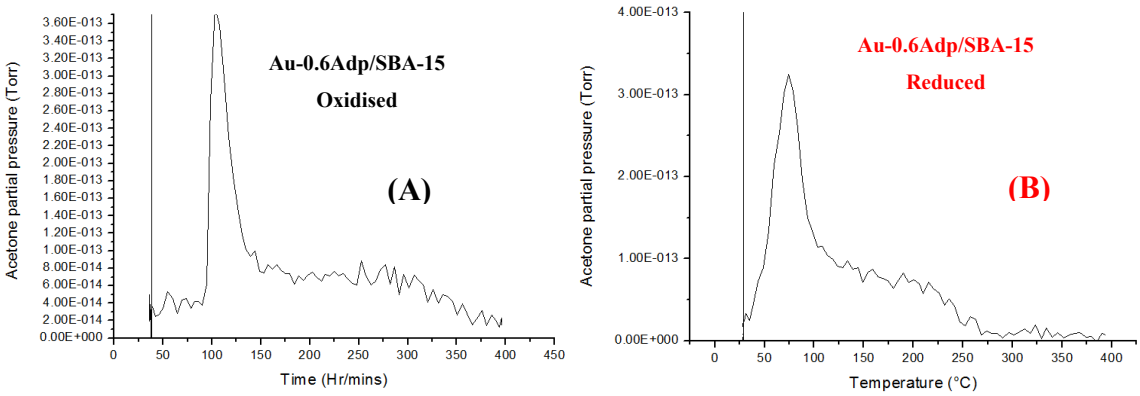

Figure 77. Acetone TPRx over oxidised (A) and reduced (B) Au-0.6Adp/SBA-15 catalyst (MS raw data)

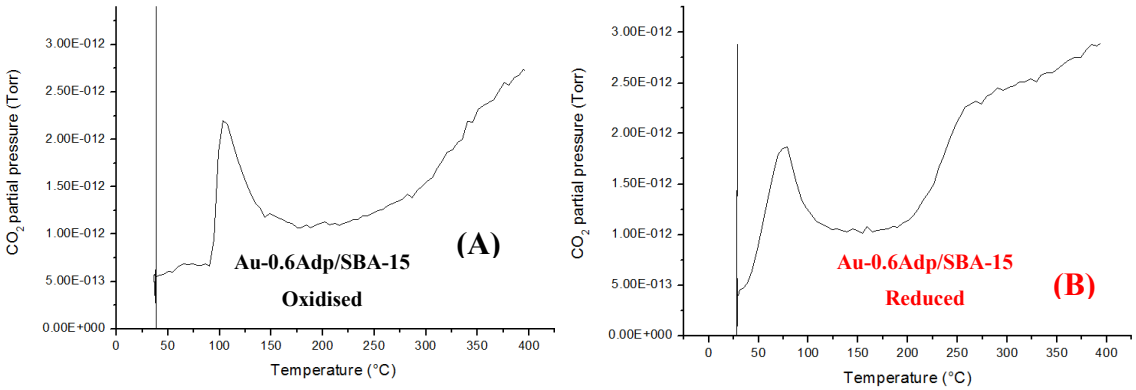

Figure 78. Acetone TPRx (CO_2 response) over oxidised (A) and reduced (B) Au-0.6Adp/SBA-15 catalyst (MS raw data)

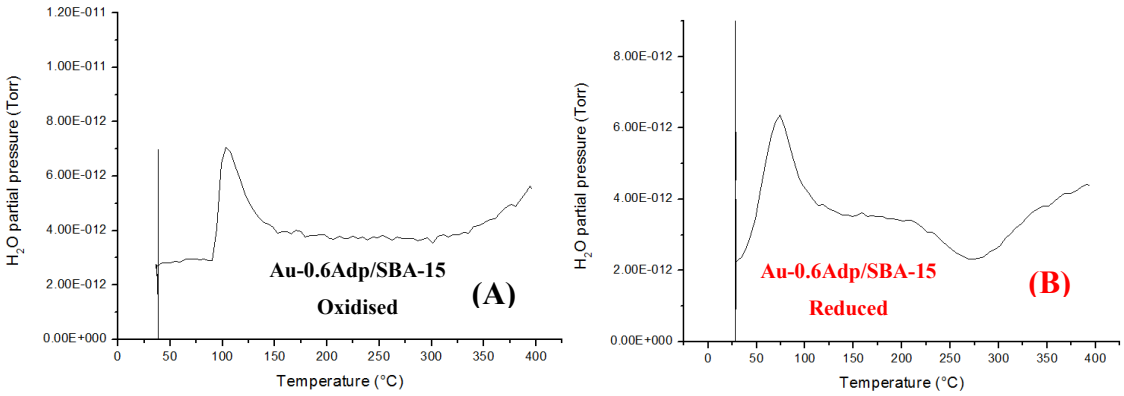

Figure 79. Acetone TPRx (H_2O response) over oxidised (A) and reduced (B) Au-0.6Adp/SBA-15 catalyst (MS raw data)

Only the reduced form of Au-0.6Adp/SBA-15 catalyst (Figure 77B – 79B) attained 100 % acetone conversion at 280 – 400 °C.

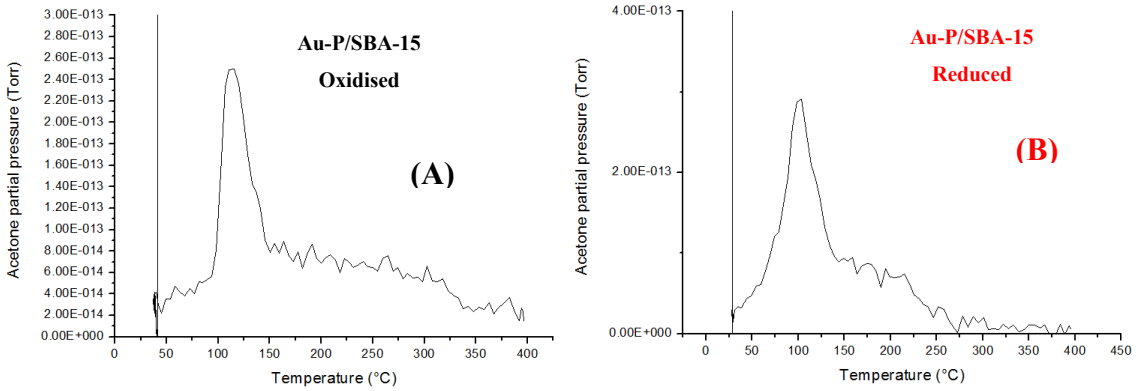

Figure 80. Acetone TPRx over oxidised (A) and reduced (B) Au-P/SBA-15 catalyst (MS raw data)

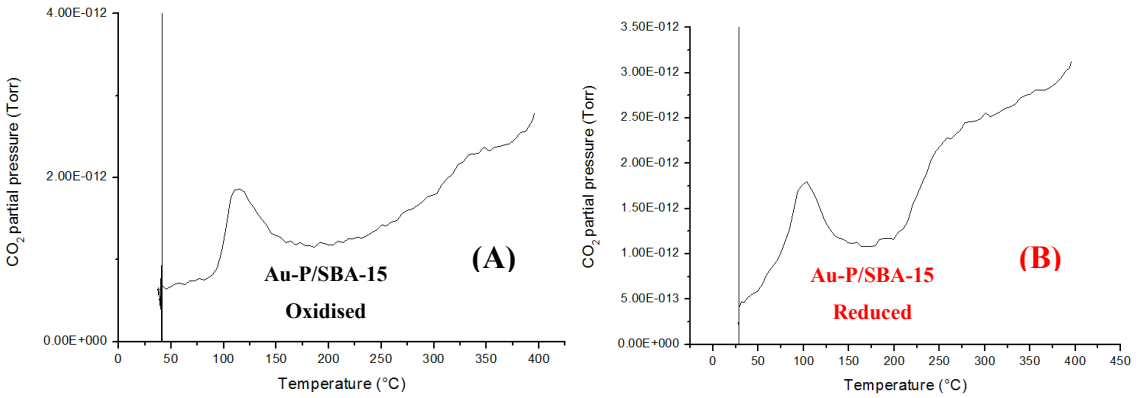

Figure 81. Acetone TPRx (CO_2 response) over oxidised (A) and reduced (B) Au-P/SBA-15 catalyst (MS raw data)

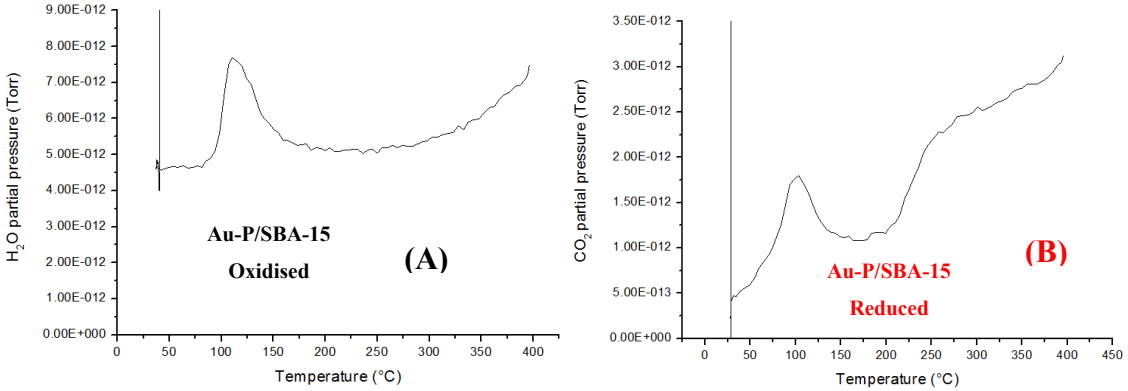

Figure 82. Acetone TPRx (H_2O response) over oxidised (A) and reduced (B) Au-P/SBA-15 catalyst (MS raw data)

The reduced form of Au-P/SBA-15 catalyst was far more active than the synthesised form (Figures 80 - 82), attaining 100 % acetone conversion at 300 – 400 ºC.

Although complete consumption of acetone in TPRx was observed from 250 - 400 ºC (with the most active catalyst – Au-0.6Mdp/SBA-15 showing 100 % conversion at 250 ºC), TPRx was not reliable in reading acetone oxidation values below 225 ºC. This is because an intense peak appeared at the beginning of acetone TPRx. The intense peak was simultaneously observed also in the corresponding CO_2 and H_2O MS signals. The reason of the peak is suspected to be due to initial acetone adsorption (at room temperature) and desorption (~ 60

- 70 ºC) phenomena on the Au/SBA-15 catalysts. It seems below 50 °C, acetone strongly adsorbed on the catalysts, and as the reactor was heated in gas flow at about 60 - 70 °C, acetone desorbed (with small reaction which produced CO_2 and H_2O), causing a sudden increase in the gas MS partial pressures for acetone, CO_2 and H_2O. If this is the case, then it means that the Au/SBA-15 catalysts have a strong affinity for acetone (the adsorption-desorption phenomenon was not observed on the quartz wool). It will therefore be interesting to study in details, acetone adsorption – desorption behaviour on Au/SBA-15 catalysts as no publication was found with such experimental observation or explanation.

In order to be able to measure catalytic activity of the catalysts from low to high temperatures (80 – 280 ºC), steady state reaction (SSR) for one hour at 80 ºC, 180 ºC and 250 ºC or 260 ºC or 280 ºC was used for catalytic evaluation of acetone oxidation.

7.6. Acetone Steady State Reaction over as-synthesised (oxidised) and reduced Au/SBA-15 catalysts

Steady State Reaction (SSR) for one hour was used to measure and calculate the percentage conversion of acetone in complete oxidation with air over the six Au/SBA-15 catalysts. TPRx (Section 7.5) was not reliable in monitoring reactions below 225 °C as previously discussed. Since no acetone oxidation occurred without catalyst below 300 °C (Reference standard), three temperatures (80 °C, 180 °C and 280 °C) were selected for SSR test. Initial acetone concentration was 200 ppm. The M-S signal's partial pressure at 80 °C was regarded as the initial VOC concentration (200 ppm - no significant oxidation occurred at this temperature) and used to calculate acetone conversion at selected temperatures based on Equation (1). From the instrument's M-S readings, there was a corresponding CO_2 and H_2O formation with all acetone converted as reaction temperature increased beyond 80 °C, which confirmed that complete VOC oxidation occurred.

The MS raw data for all the SSR experiments for as-synthesised and reduced forms of the six Au/SBA-15 catalysts at 80 °C, 180 °C and 280 °C are shown in Figures 83 – 136, which also compares the catalytic activity of the as-synthesised and reduced forms of the six Au/SBA-15 catalysts.

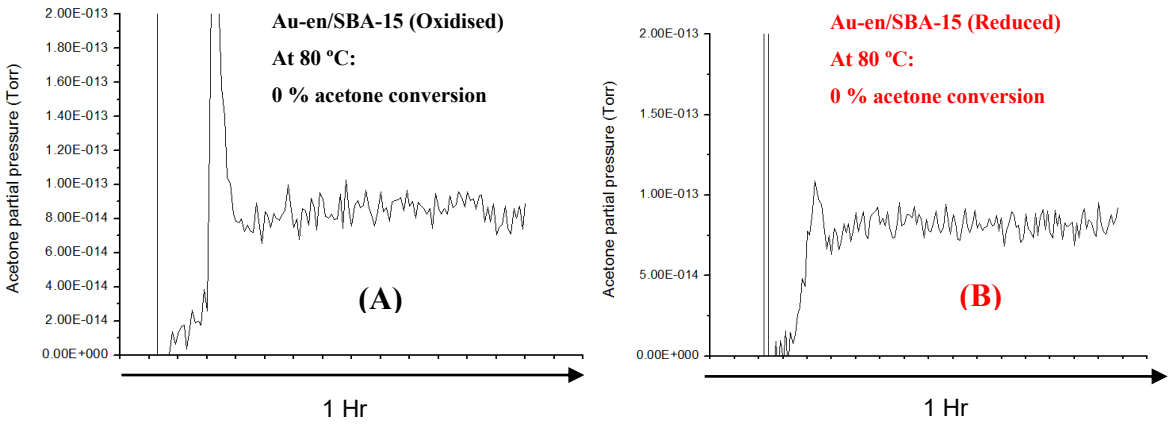

Figure 83. Acetone SSR over oxidised (A) and reduced (B) Au-en/SBA-15 catalyst at 80 °C (MS raw data)

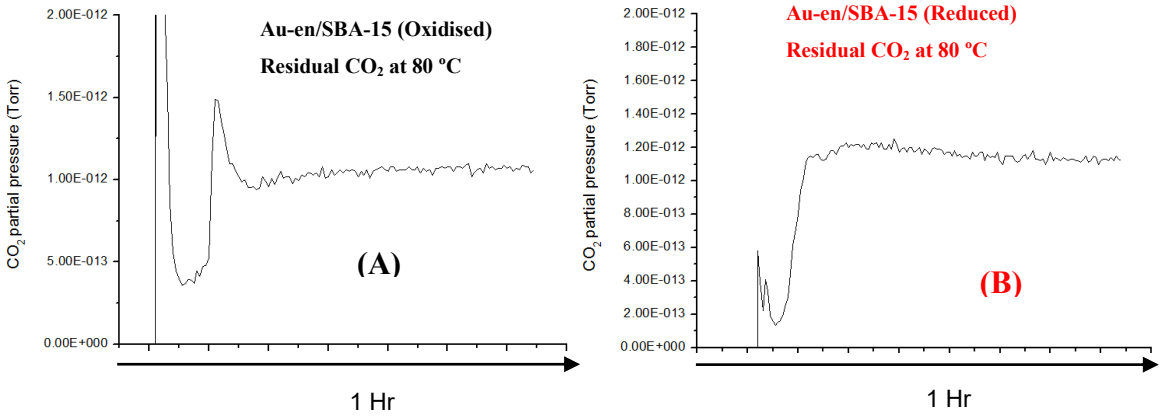

Figure 84. Acetone SSR (CO_2 response) over oxidised (A) and reduced (B) Au-en/SBA-15 catalyst at 80 °C (MS raw data)

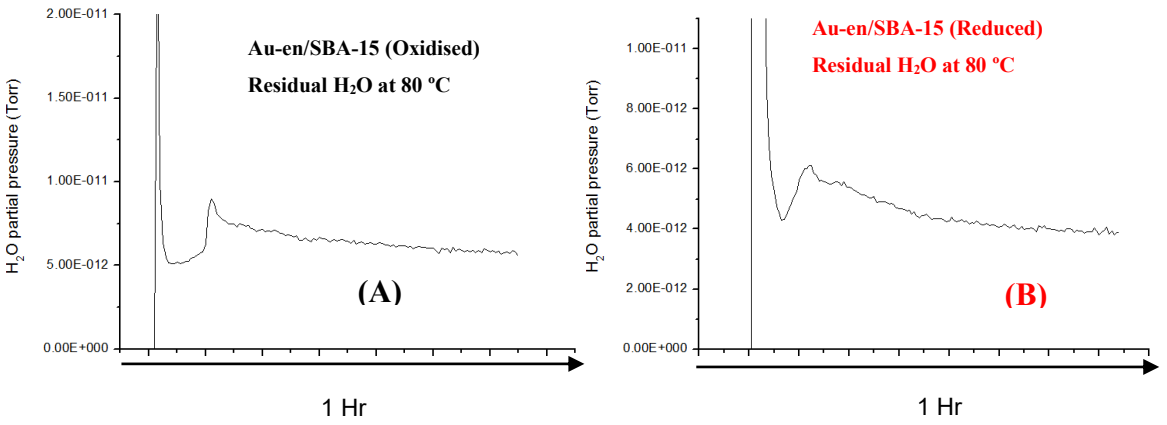

Figure 85. Acetone SSR (H_2O response) over oxidised (A) and reduced (B) Au-en/SBA-15 catalyst at 80 °C (MS raw data)

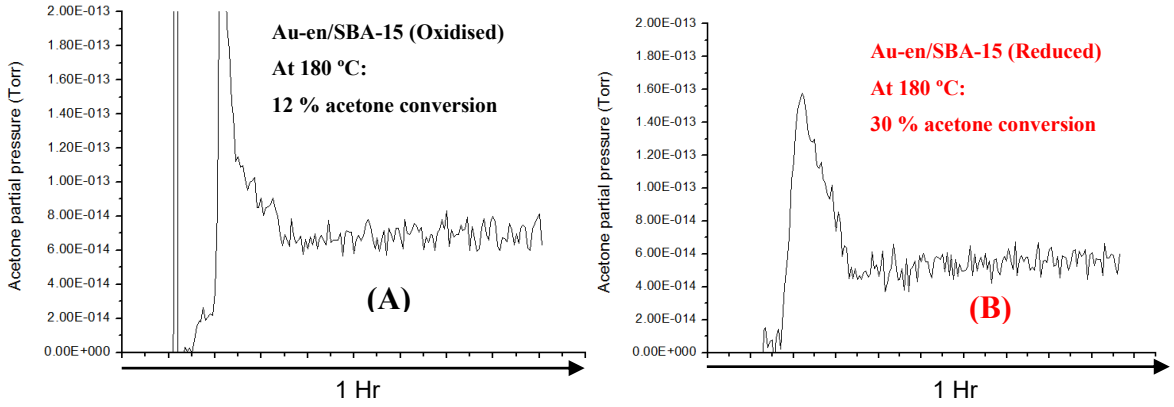

Figure 86. Acetone SSR over oxidised (A) and reduced (B) Au-en/SBA-15 catalyst at 180 °C (MS raw data)

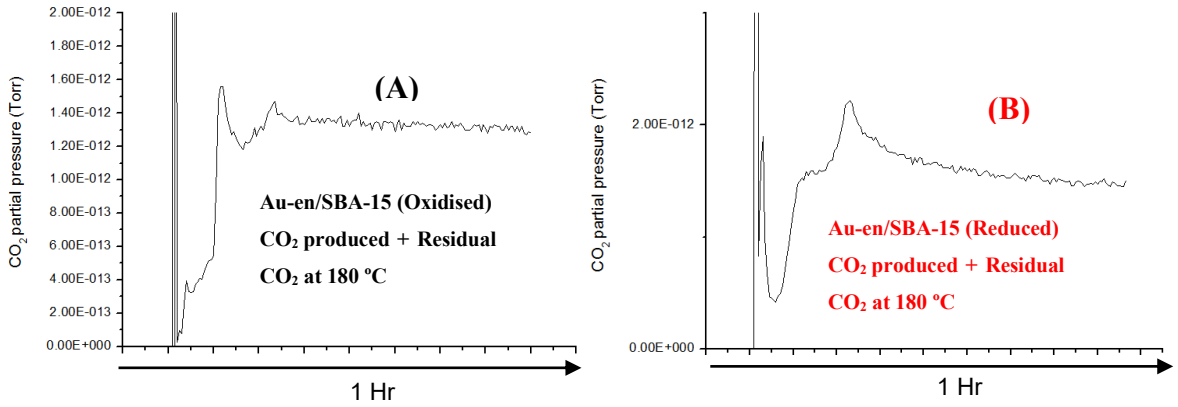

Figure 87. Acetone SSR (CO_2 response) over oxidised (A) and reduced (B) Au-en/SBA-15 catalyst at 180 °C (MS raw data)

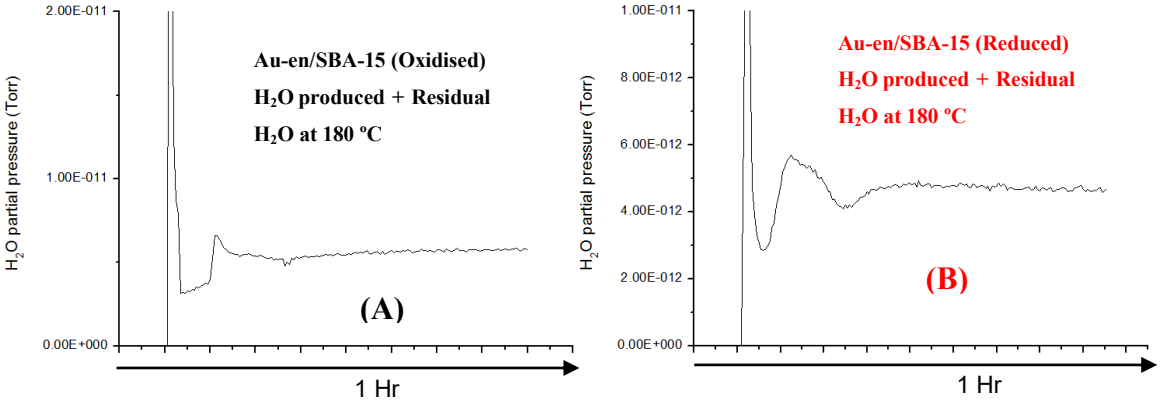

Figure 88. Acetone SSR (H_2O response) over oxidised (A) and reduced (B) Au-en/SBA-15 catalyst at 180 °C (MS raw data)

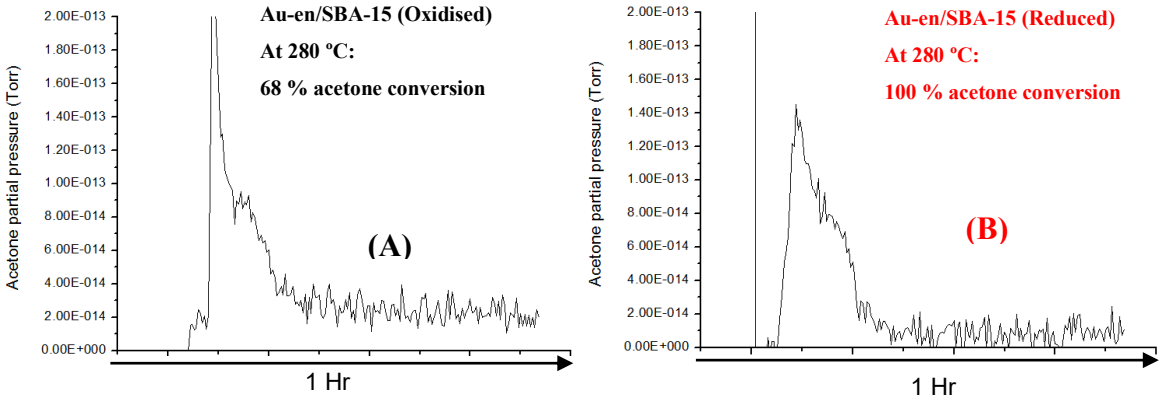

Figure 89. Acetone SSR over oxidised (A) and reduced (B) Au-en/SBA-15 catalyst at 280 °C (MS raw data)

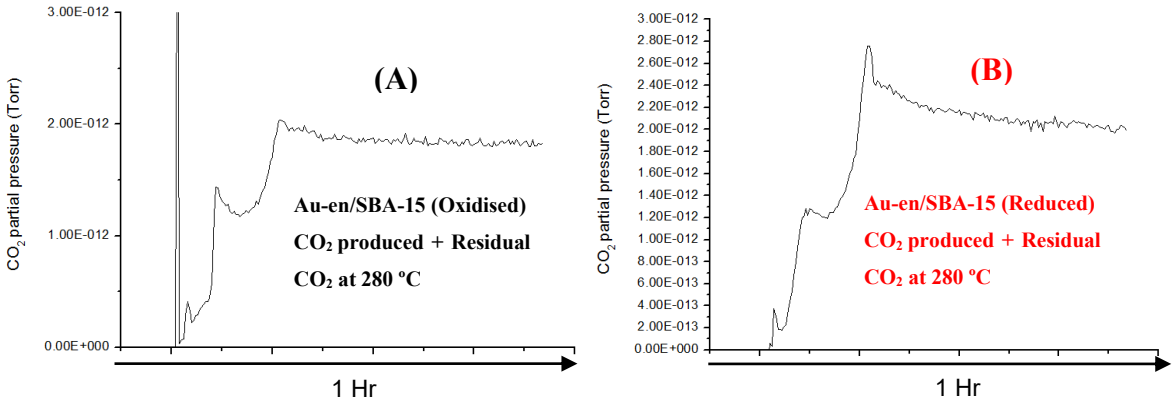

Figure 90. Acetone SSR (CO_2 response) over oxidised (A) and reduced (B) Au-en/SBA-15 catalyst at 280 °C (MS raw data)

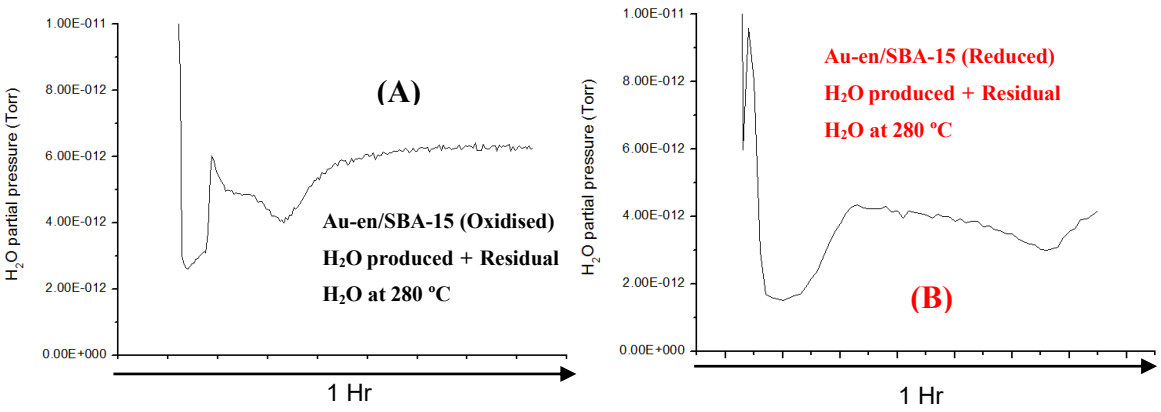

Figure 91. Acetone SSR (H_2O response) over oxidised (A) and reduced (B) Au-en/SBA-15 catalyst at 280 °C (MS raw data)

From the results in Figures 83 – 91, The reduced Au-en/SBA-15 catalyst was more active than the as-synthesised form (SSR in agreement with TPRx), attaining 30 % at 180 ° C and 100 % at 280 ° C acetone conversion, compared to the as-synthesised form – 12 % at 180 ° C and 68 % at 280 ° C.

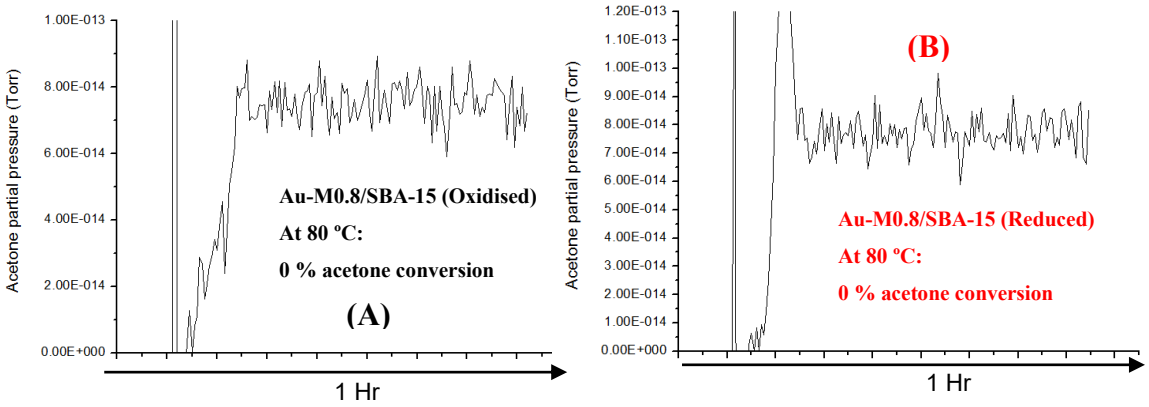

Figure 92. Acetone SSR over oxidised (A) and reduced (B) Au-M0.8/SBA-15 catalyst at 80 °C (MS raw data)

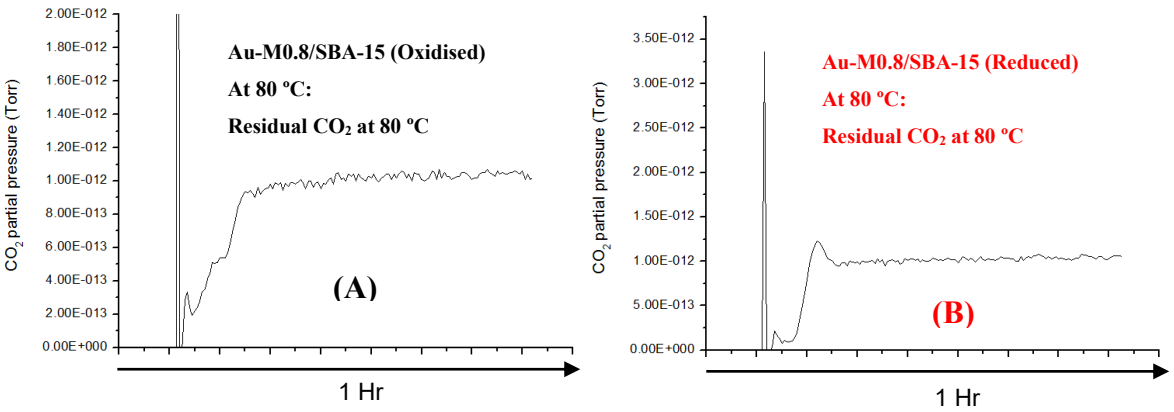

Figure 93. Acetone SSR (CO_2 response) over oxidised (A) and reduced (B) Au-M0.8/SBA-15 catalyst at 80 °C (MS raw data)

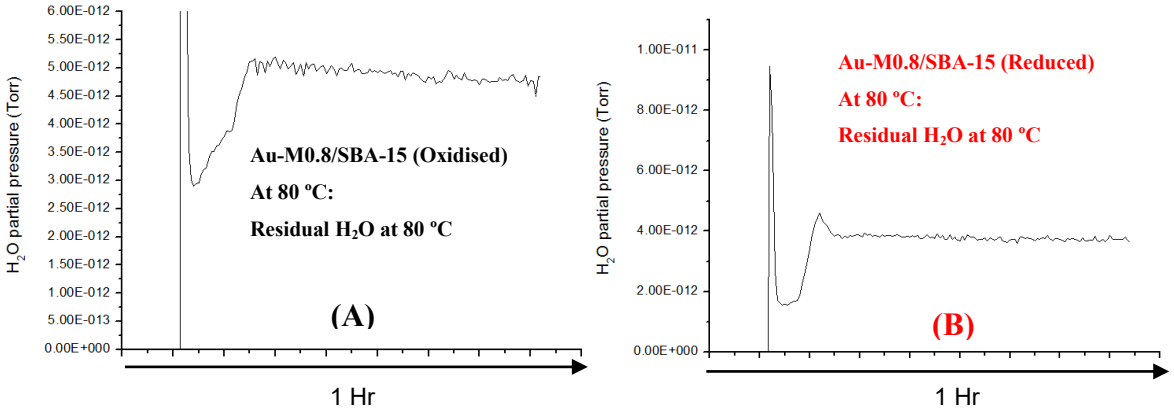

Figure 94. Acetone SSR (H_2O response) over oxidised (A) and reduced (B) Au-M0.8/SBA-15 catalyst at 80 °C (MS raw data)

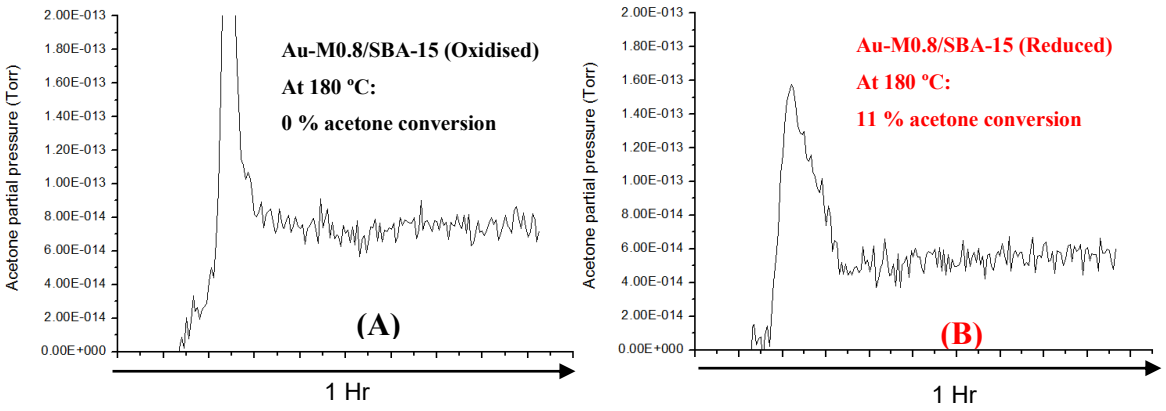

Figure 95. Acetone SSR over oxidised (A) and reduced (B) Au-M0.8/SBA-15 catalyst at 180 °C (MS raw data)

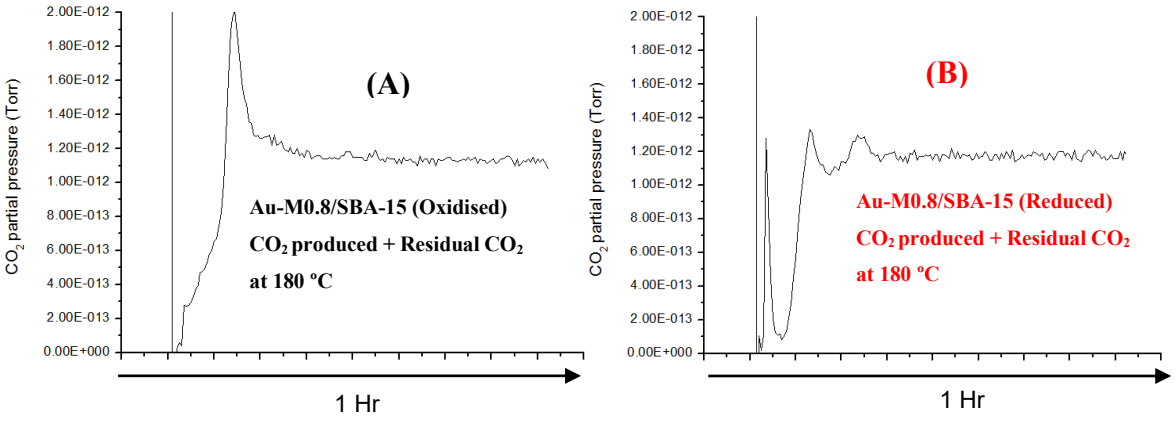

Figure 96. Acetone SSR (CO_2 response) over oxidised (A) and reduced (B) Au-M0.8/SBA-15 catalyst at 180 °C (MS raw data)

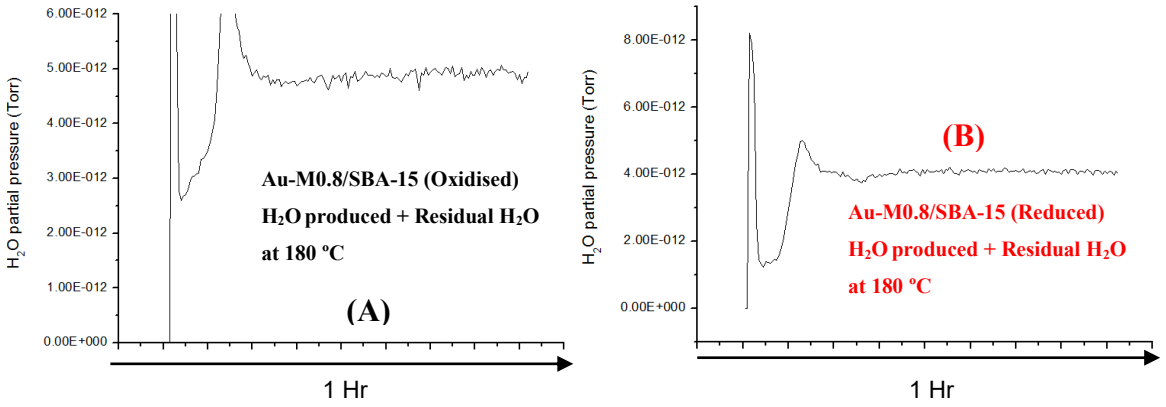

Figure 97. Acetone SSR (H_2O response) over oxidised (A) and reduced (B) Au-M0.8/SBA-15 catalyst at 180 °C (MS raw data)

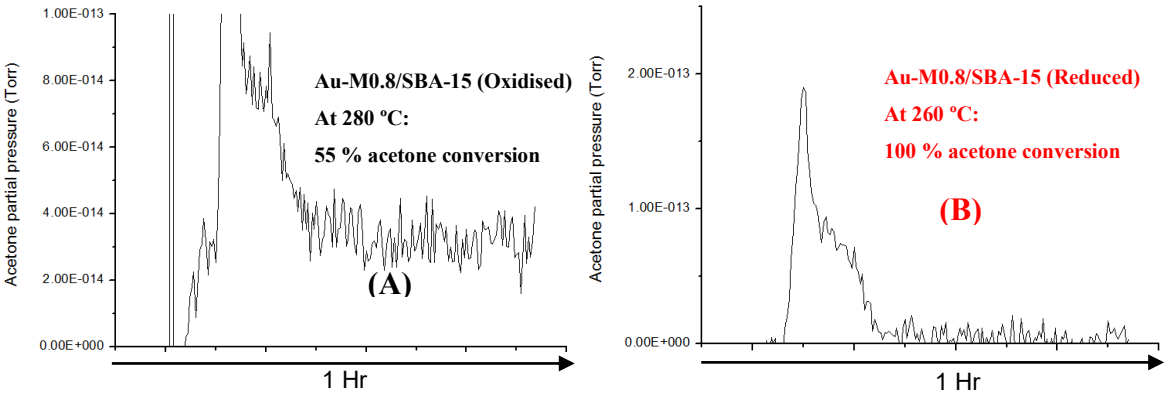

Figure 98. Acetone SSR over oxidised (A) and reduced (B) Au-M0.8/SBA-15 catalyst at 280 °C (MS raw data)

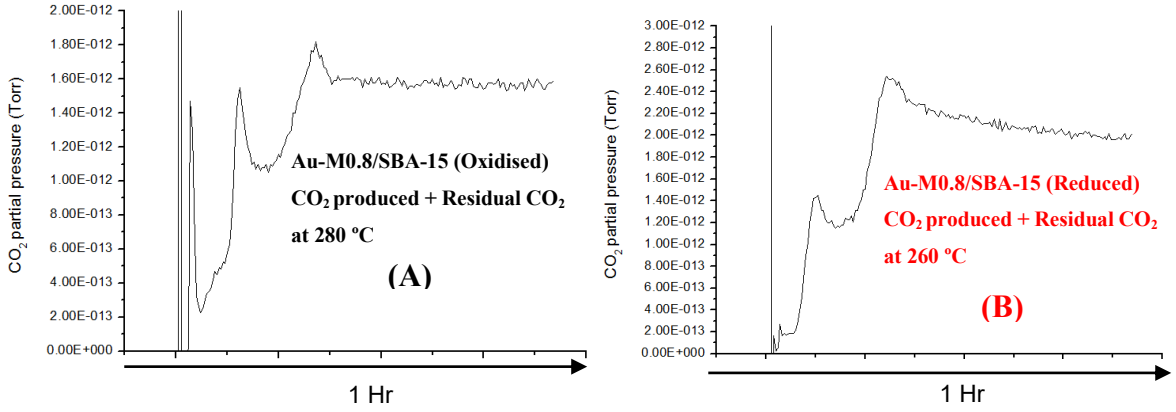

Figure 99. Acetone SSR (CO_2 response) over oxidised (A) and reduced (B) Au-M0.8/SBA-15 catalyst at 280 °C (MS raw data)

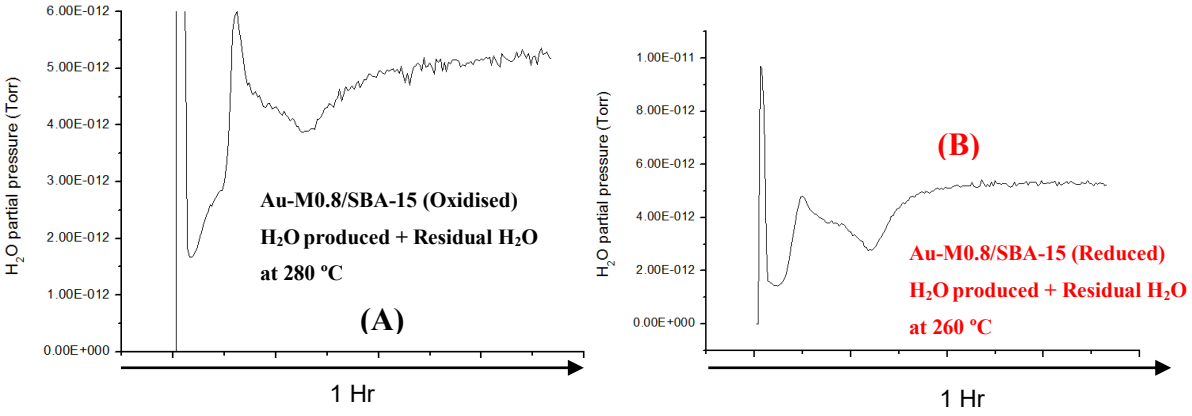

Figure 100. Acetone SSR (H_2O response) over oxidised (A) and reduced (B) Au-M0.8/SBA-15 catalyst at 280 °C (MS raw data)

The reduced Au-M0.8/SBA-15 catalyst was more active than the as-synthesised form (SSR in agreement with TPRx) as shown in Figures 92 – 100, attaining 11 % at 180 ° C and 100 % at 280 ° C acetone conversion, compared to the as-synthesised form – 0 % at 180 ° C and 55 % at 280 ° C.

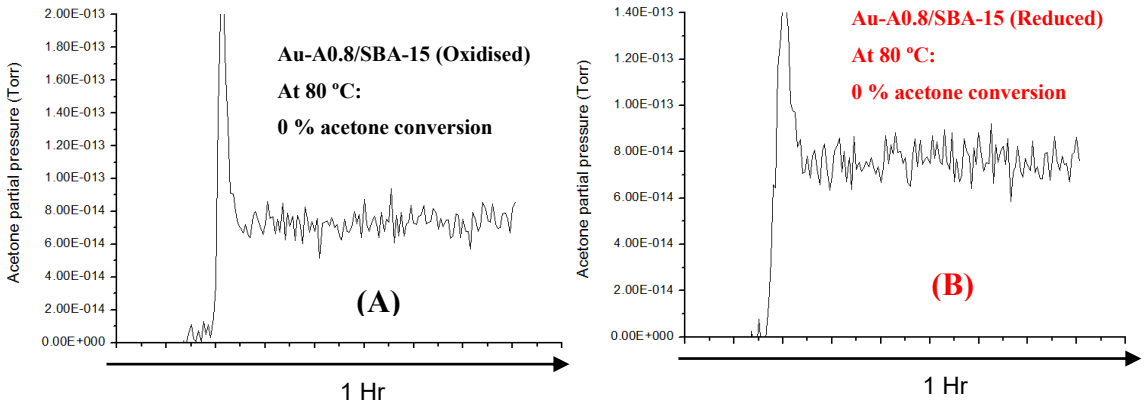

Figure 101. Acetone SSR over oxidised (A) and reduced (B) Au-A0.8/SBA-15 catalyst at 80 °C (MS raw data)

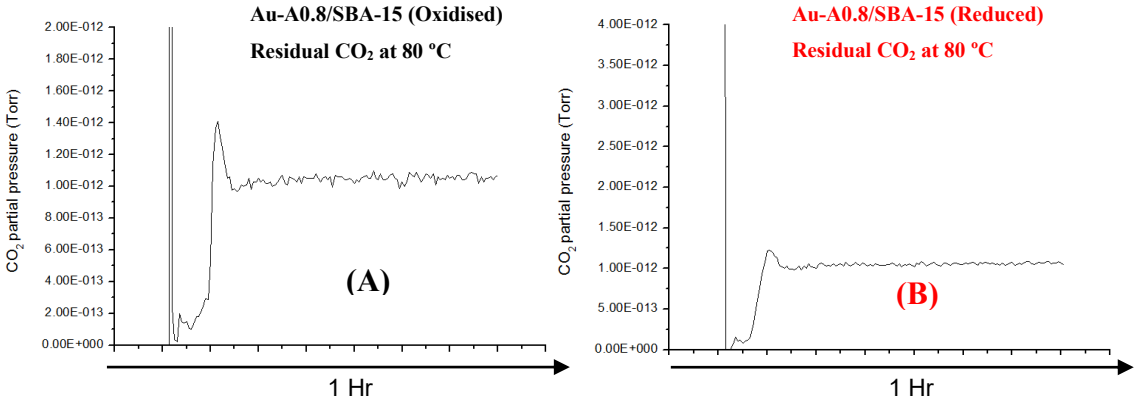

Figure 102. Acetone SSR (CO_2 response) over oxidised (A) and reduced (B) Au-A0.8/SBA-15 catalyst at 80 °C (MS raw data)

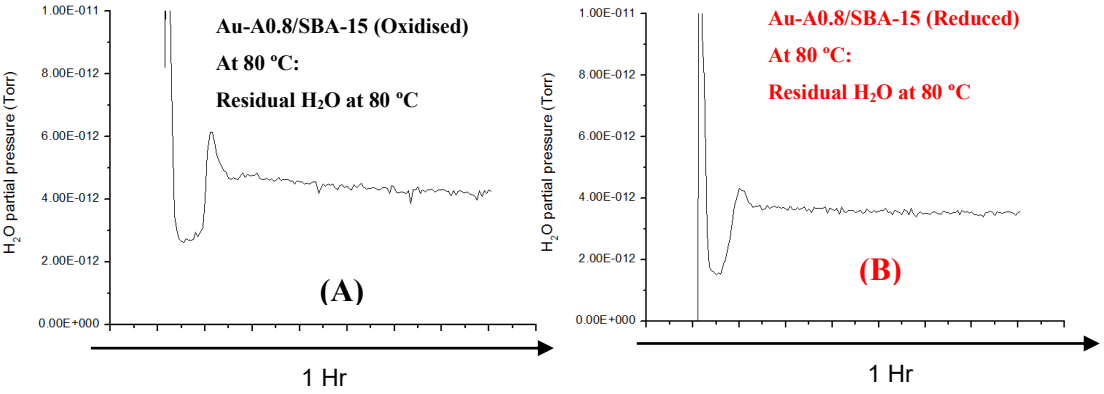

Figure 103. Acetone SSR (H_2O response) over oxidised (A) and reduced (B) Au-A0.8/SBA-15 catalyst at 80 °C (MS raw data)

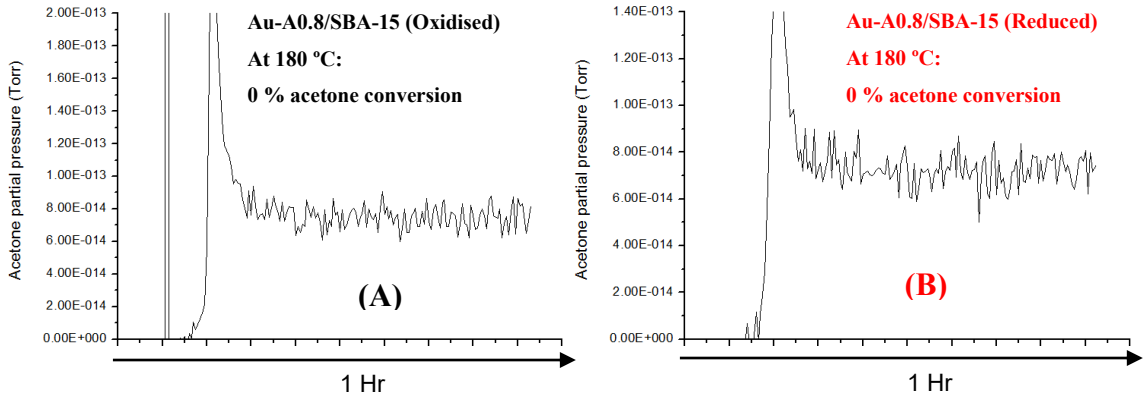

Figure 104. Acetone SSR over oxidised (A) and reduced (B) Au-A0.8/SBA-15 catalyst at 180 °C (MS raw data)

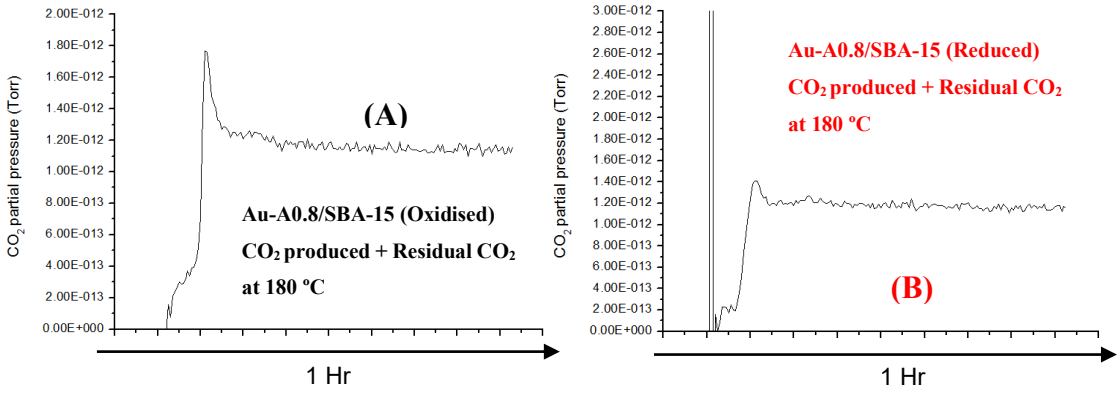

Figure 105. Acetone SSR (CO_2 response) over oxidised (A) and reduced (B) Au-A0.8/SBA-15 catalyst at 180 °C (MS raw data)

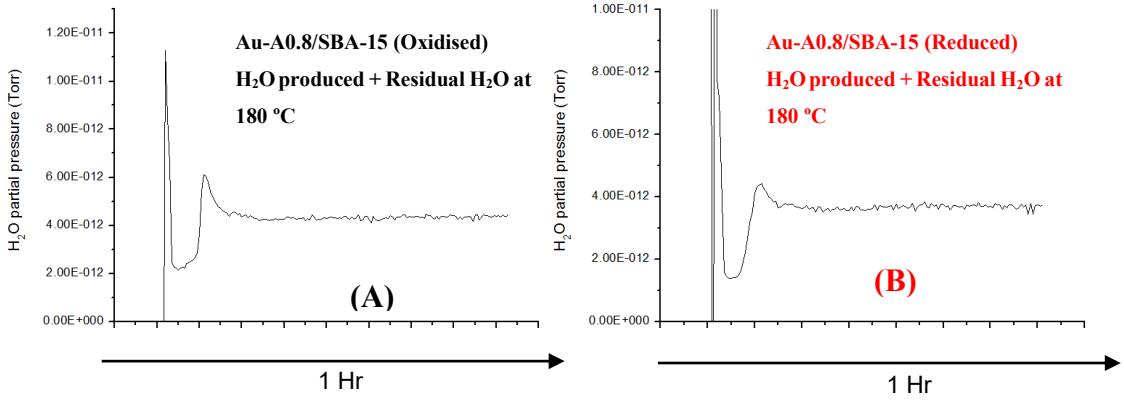

Figure 106. Acetone SSR (H_2O response) over oxidised (A) and reduced (B) Au-A0.8/SBA-15 catalyst at 180 °C (MS raw data)

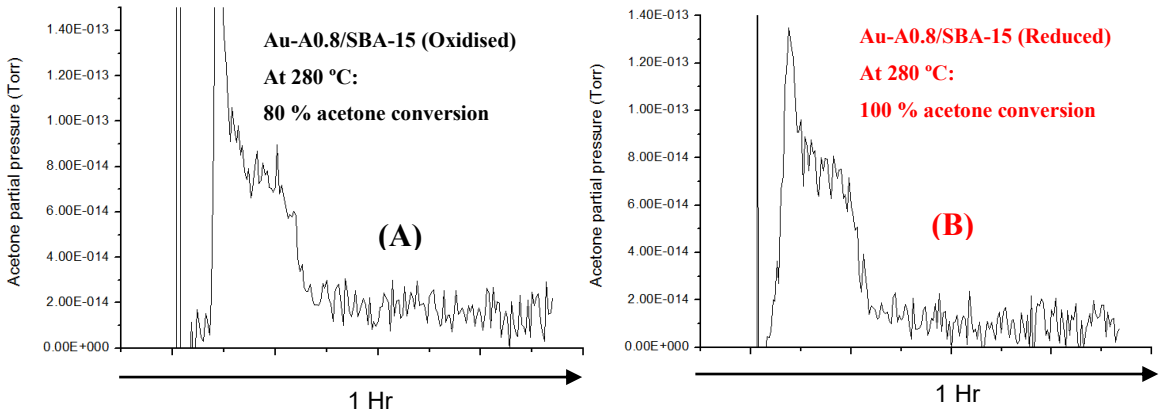

Figure 107. Acetone SSR over oxidised (A) and reduced (B) Au-A0.8/SBA-15 catalyst at 280 °C (MS raw data)

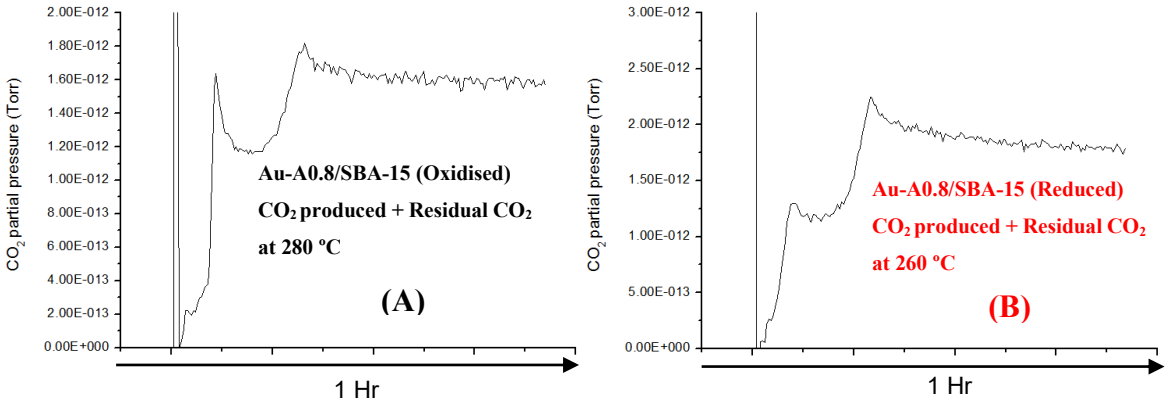

Figure 108. Acetone SSR (CO_2 response) over oxidised (A) and reduced (B) Au-A0.8/SBA-15 catalyst at 280 °C (MS raw data)

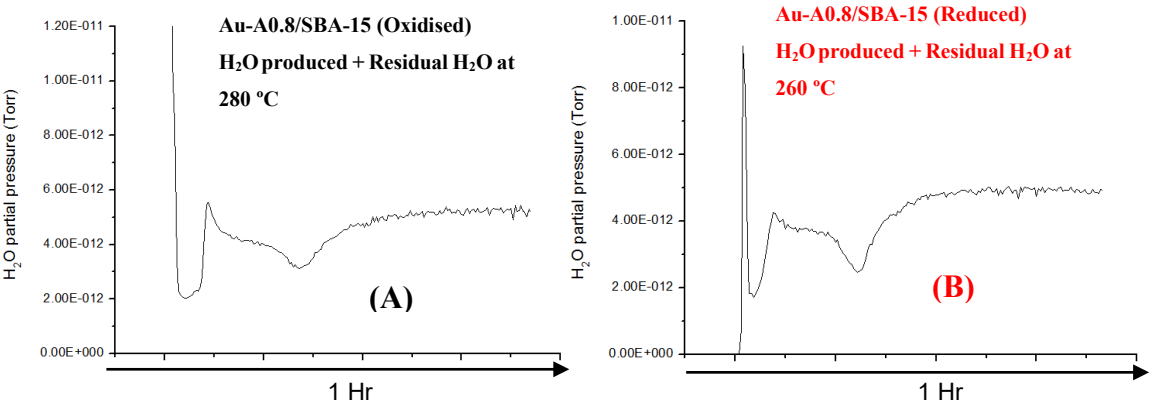

Figure 109. Acetone SSR (H_2O response) over oxidised (A) and reduced (B) Au-A0.8/SBA-15 catalyst at 280 °C (MS raw data)

Both the reduced and as-synthesised Au-A0.8/SBA-15 catalyst (Figures 101 – 109) were inactive at 180 ° C. At 280 ° C, the reduced was more active, attaining 100 % acetone conversion, while the as-synthesised form attained 80 % acetone conversion at 280 ° C.

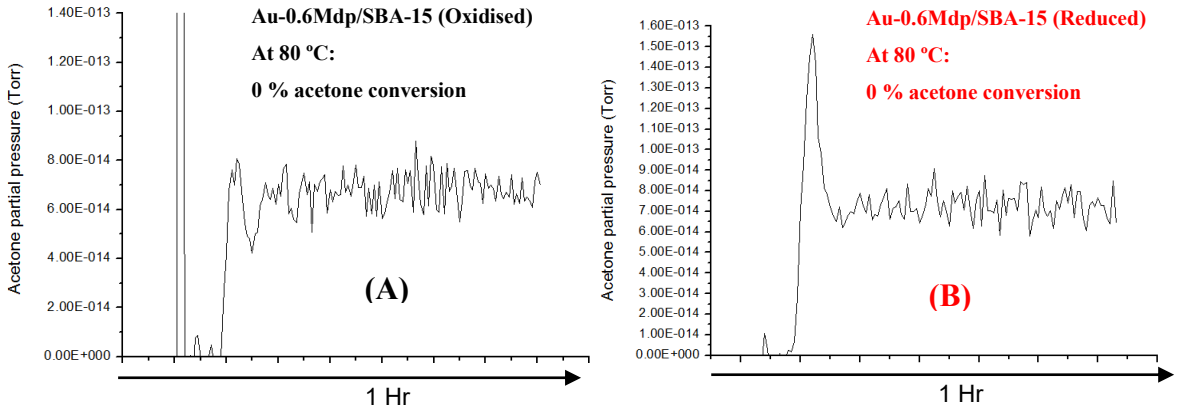

Figure 110. Acetone SSR over oxidised (A) and reduced (B) Au-0.6Mdp/SBA-15 catalyst at 80 °C (MS raw data)

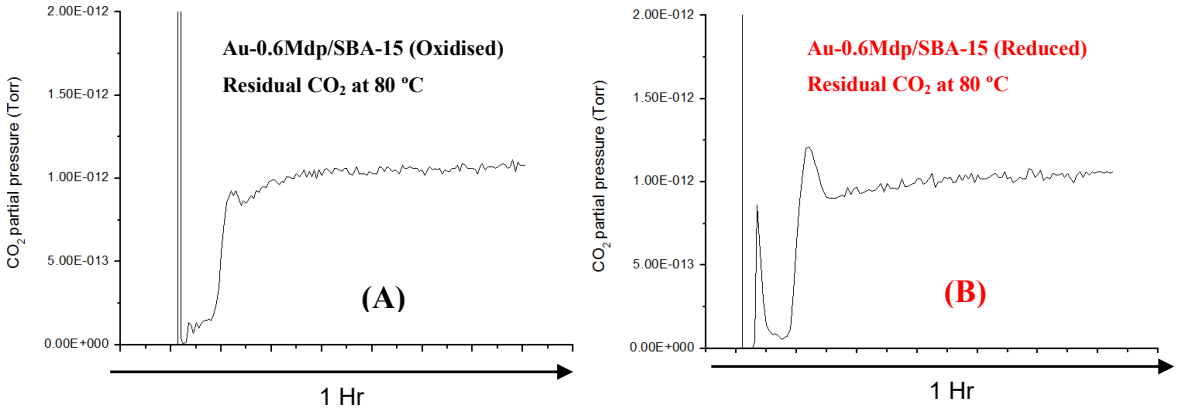

Figure 111. Acetone SSR (CO_2 response) over oxidised (A) and reduced (B) Au-0.6Mdp/SBA-15 catalyst at 80 °C (MS raw data)

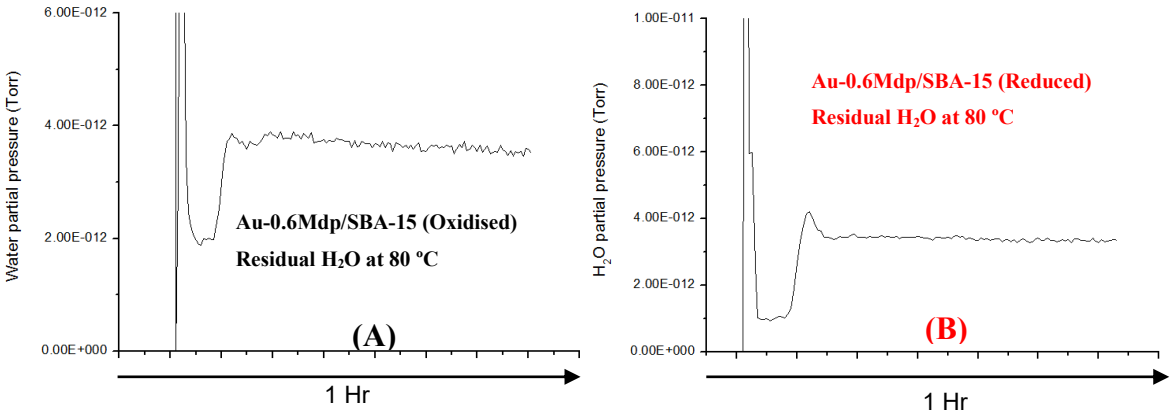

Figure 112. Acetone SSR (H_2O response) over oxidised (A) and reduced (B) Au-0.6Mdp/SBA-15 catalyst at 80 °C (MS raw data)

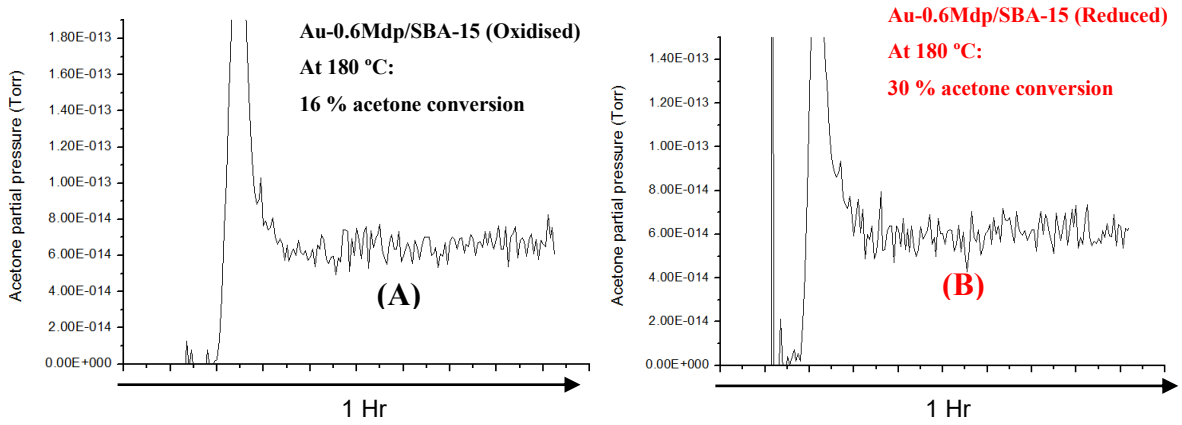

Figure 113. Acetone SSR over oxidised (A) and reduced (B) Au-0.6Mdp/SBA-15 catalyst at 180 °C (MS raw data)

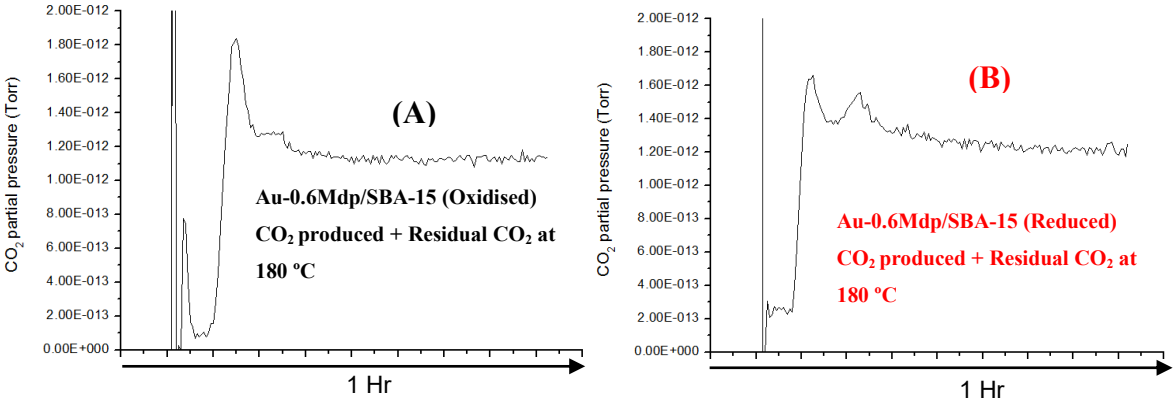

Figure 114. Acetone SSR (CO_2 response) over oxidised (A) and reduced (B) Au-0.6Mdp/SBA-15 catalyst at 180 °C (MS raw data)

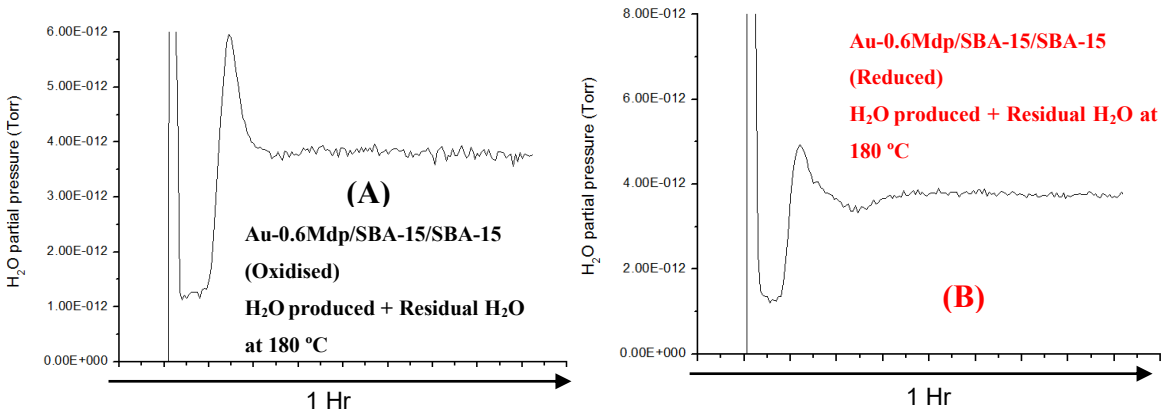

Figure 115. Acetone SSR (H_2O response) over oxidised (A) and reduced (B) Au-0.6Mdp/SBA-15 catalyst at 180 °C (MS raw data)

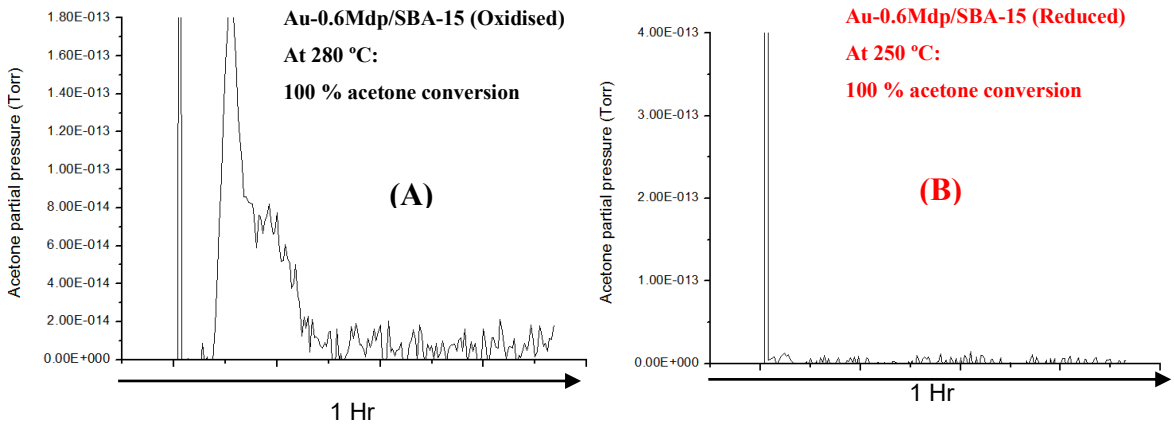

Figure 116. Acetone SSR over oxidised (A) and reduced (B) Au-0.6Mdp/SBA-15 catalyst at 280 °C (MS raw data)

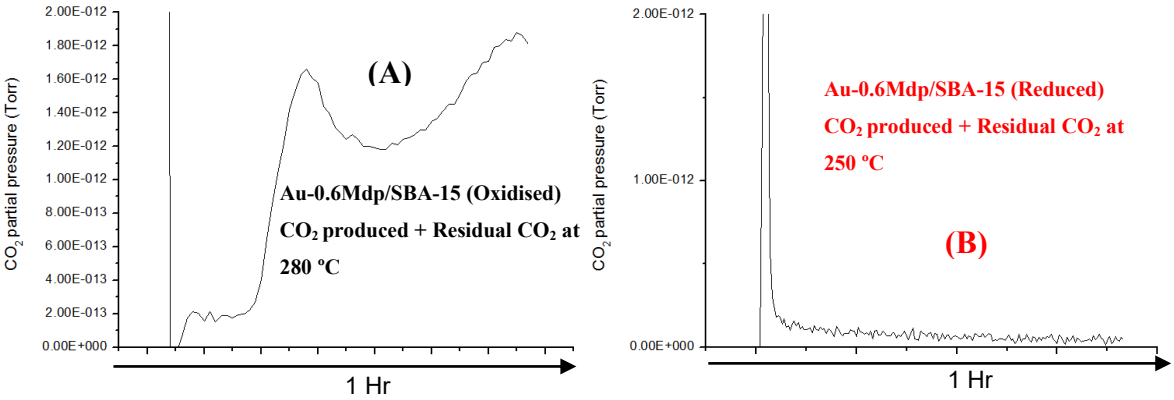

Figure 117. Acetone SSR (CO_2 response) over oxidised (A) and reduced (B) Au-0.6Mdp/SBA-15 catalyst at 280 °C (MS raw data)

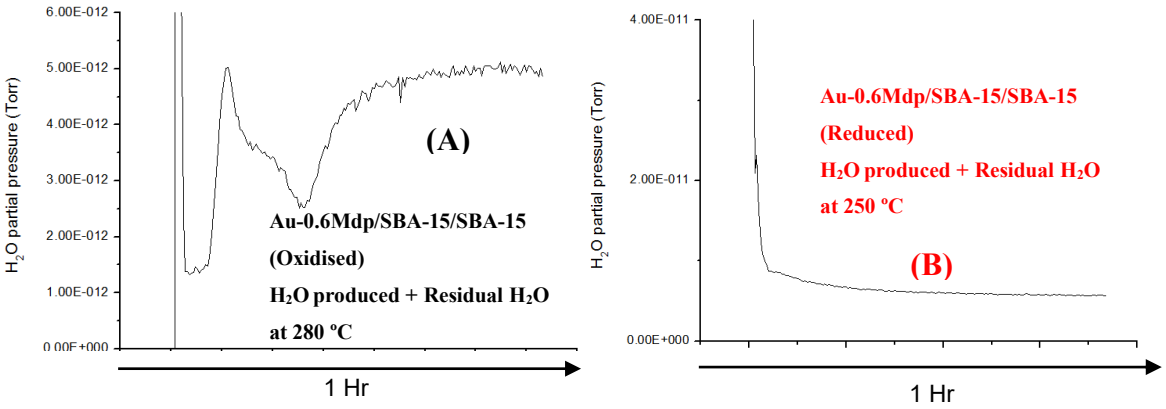

Figure 118. Acetone SSR (H_2O response) over oxidised (A) and reduced (B) Au-0.6Mdp/SBA-15 catalyst at 280 °C (MS raw data)

The SSR results (Figures 110 - 118) show that the as-synthesised Au-0.6Mdp/SBA-15 catalyst was the only as-synthesised Au/SBA-15 catalyst that attained 100 % acetone conversion at 280 °C. The reduced Au-0.6Mdp/SBA-15 catalyst was the overall best catalyst, attaining 100 % acetone conversion at the lowest temperature – 250 °C.

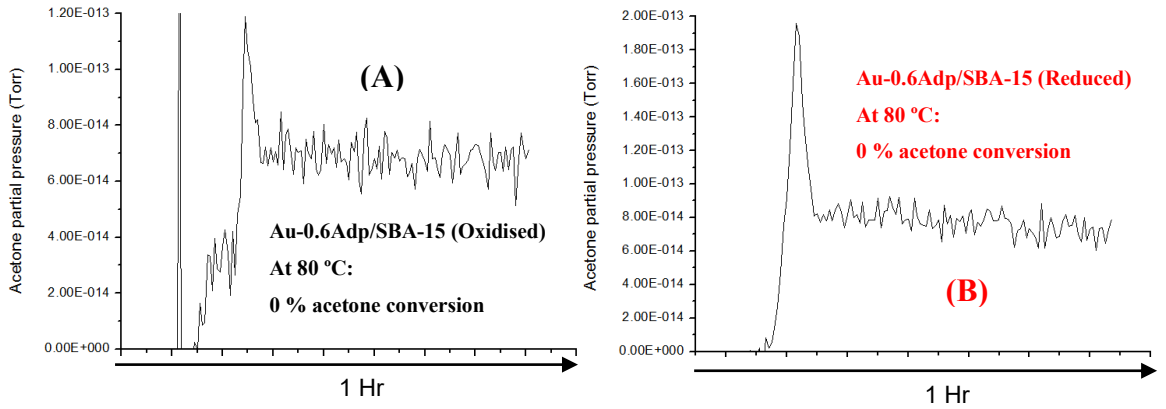

Figure 119. Acetone SSR over oxidised (A) and reduced (B) Au-0.6Adp/SBA-15 catalyst at 80 °C (MS raw data)

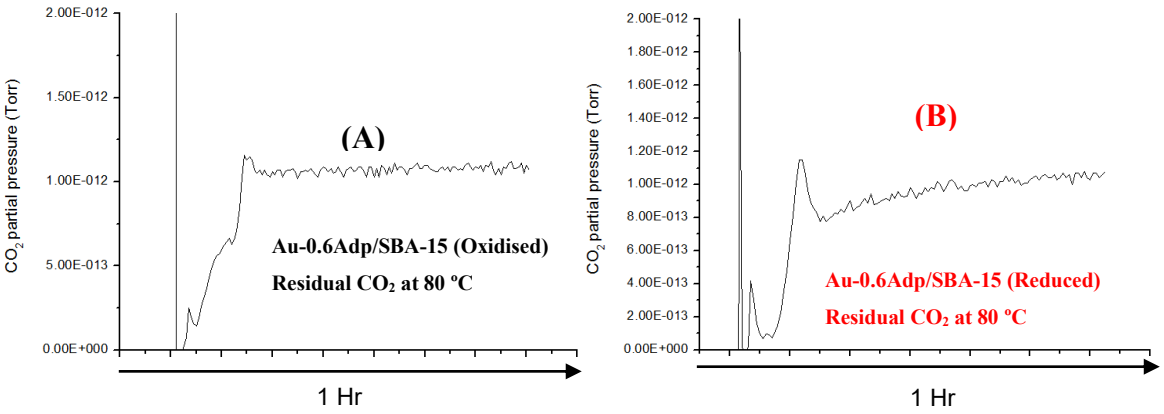

Figure 120. Acetone SSR (CO_2 response) over oxidised (A) and reduced (B) Au-0.6Adp/SBA-15 catalyst at 80 °C (MS raw data)

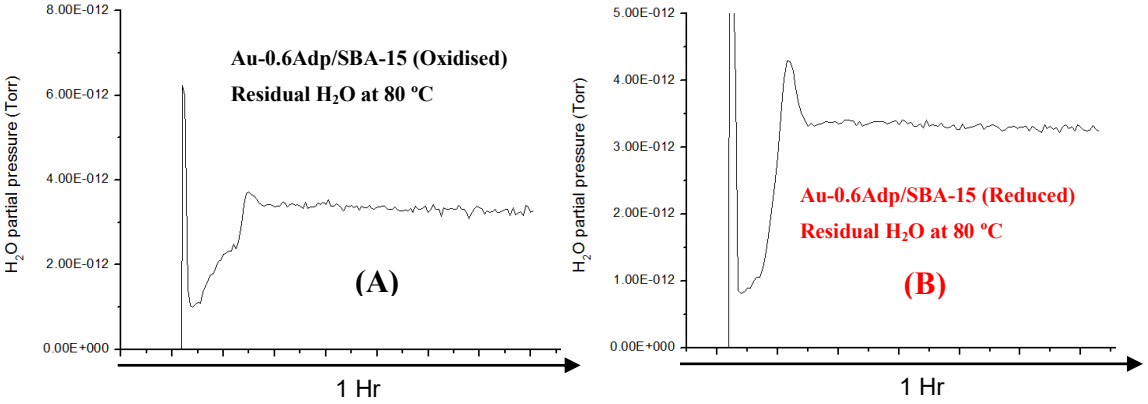

Figure 121. Acetone SSR (H_2O response) over oxidised (A) and reduced (B) Au-0.6Adp/SBA-15 catalyst at 80 °C (MS raw data)

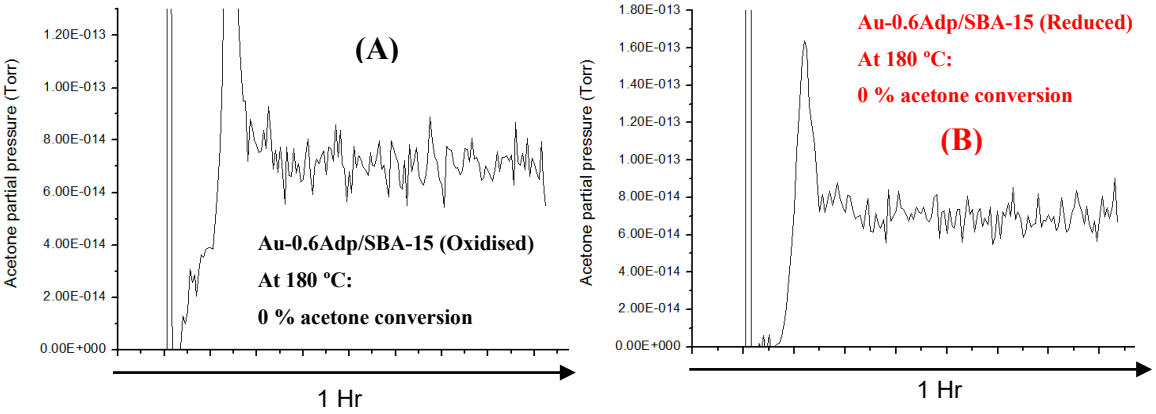

Figure 122. Acetone SSR over oxidised (A) and reduced (B) Au-0.6Adp/SBA-15 catalyst at 180 °C (MS raw data)

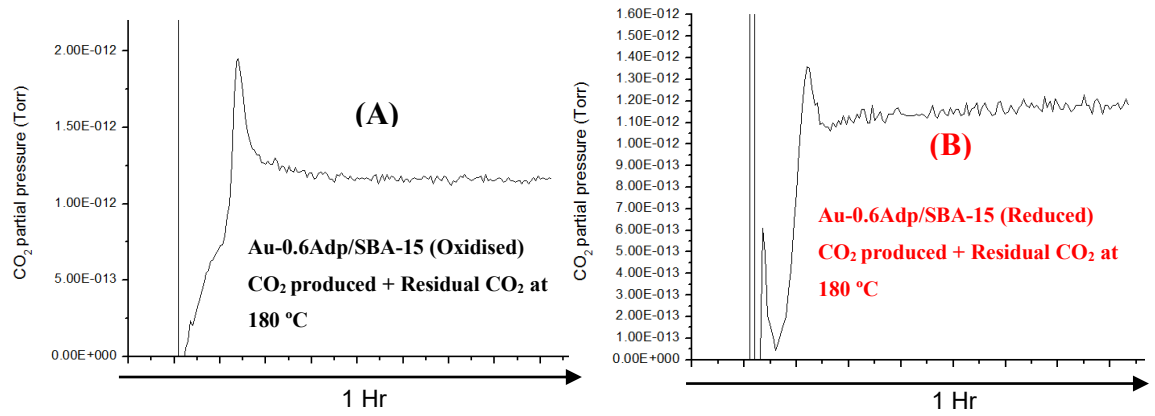

Figure 123. Acetone SSR (CO_2 response) over oxidised (A) and reduced (B) Au-0.6Adp/SBA-15 catalyst at 180 °C (MS raw data)

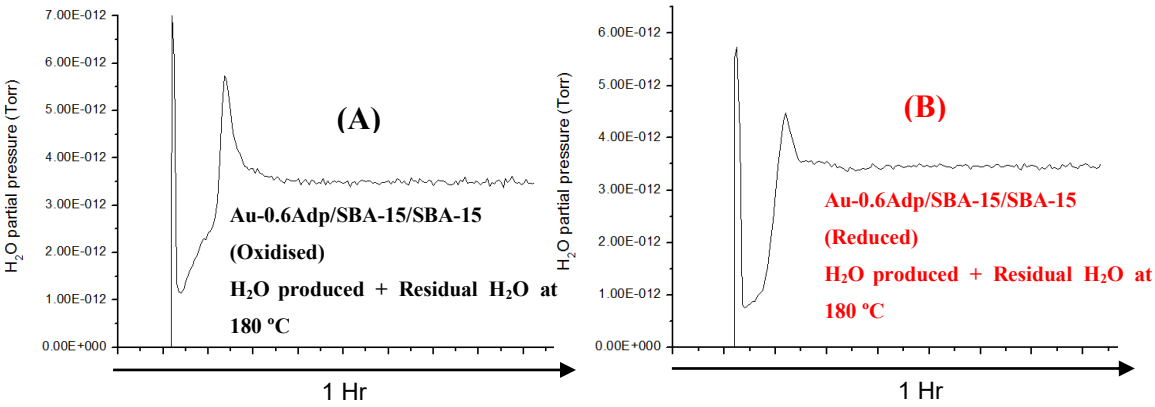

Figure 124. Acetone SSR (H_2O response) over oxidised (A) and reduced (B) Au-0.6Adp/SBA-15 catalyst at 180 °C (MS raw data)

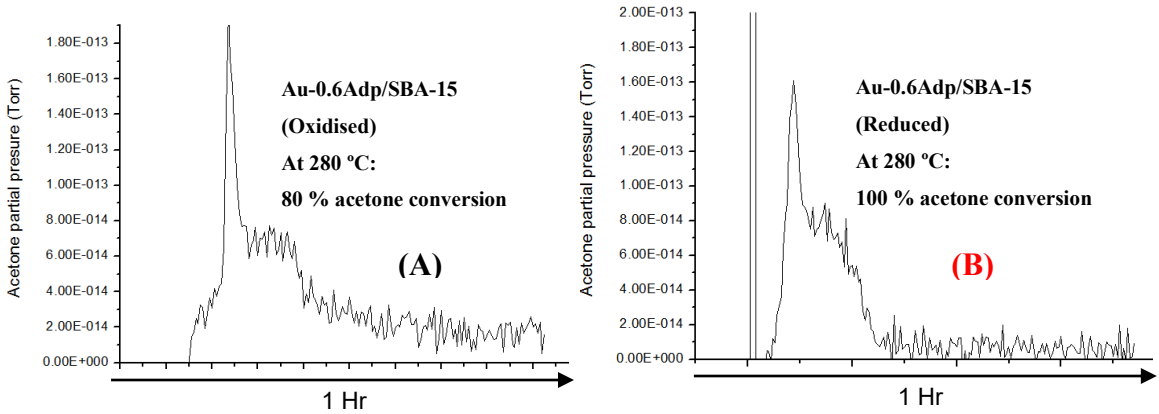

Figure 125. Acetone SSR over oxidised (A) and reduced (B) Au-0.6Adp/SBA-15 catalyst at 280 °C (MS raw data)

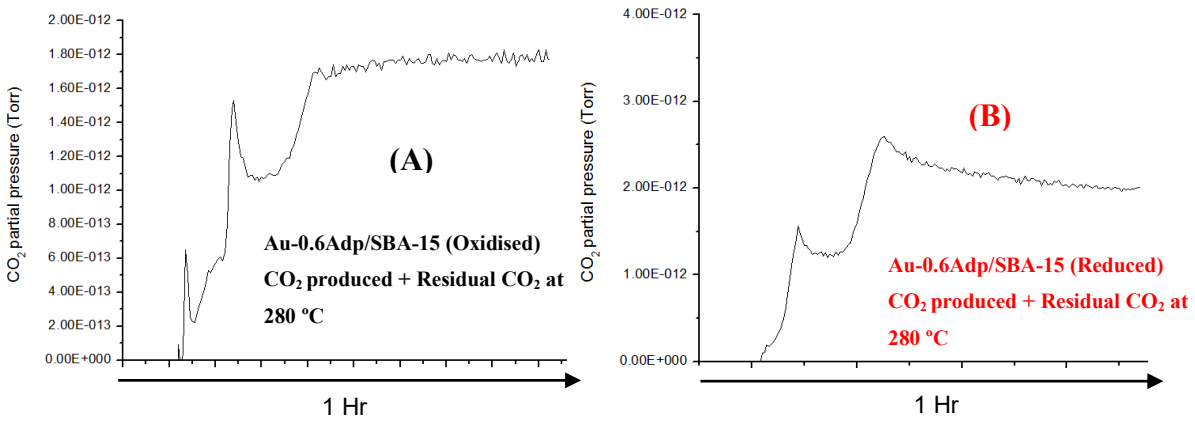

Figure 126. Acetone SSR (CO_2 response) over oxidised (A) and reduced (B) Au-0.6Adp/SBA-15 catalyst at 280 °C (MS raw data)

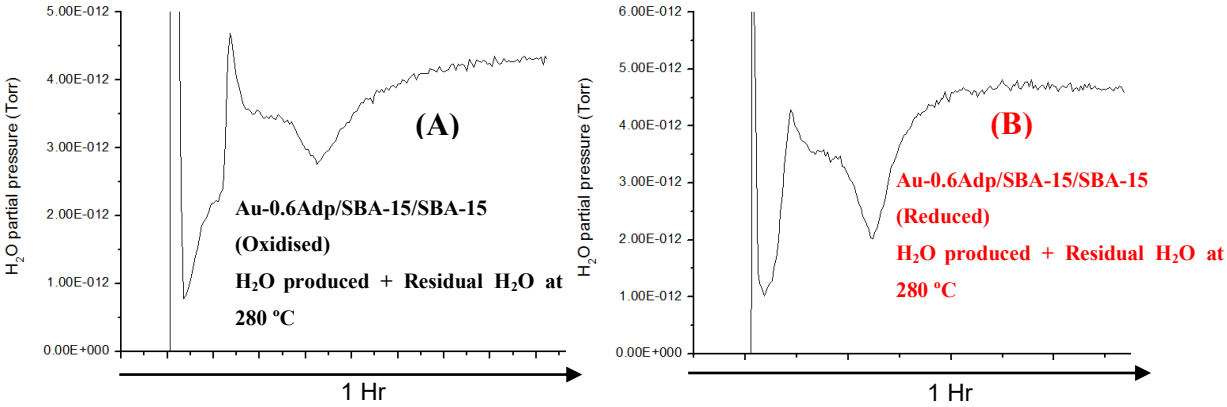

Figure 127. Acetone SSR (H_2O response) over oxidised (A) and reduced (B) Au-0.6Adp/SBA-15 catalyst at 280 °C (MS raw data)

Both the as-synthesised and reduced forms of Au-0.6Adp/SBA-15 catalysts were inactive at 180 °C. However, at 280 °C, the reduced catalyst was more active, attaining 100 % acetone conversion, while the as-synthesised attained 80 % at 280 °C.

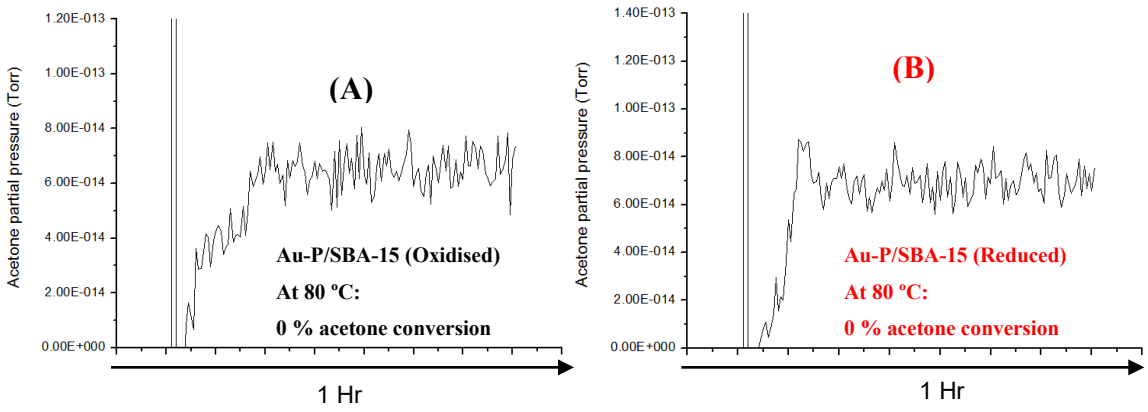

Figure 128. Acetone SSR over oxidised (A) and reduced (B) Au-P/SBA-15 catalyst at 80 °C (MS raw data)

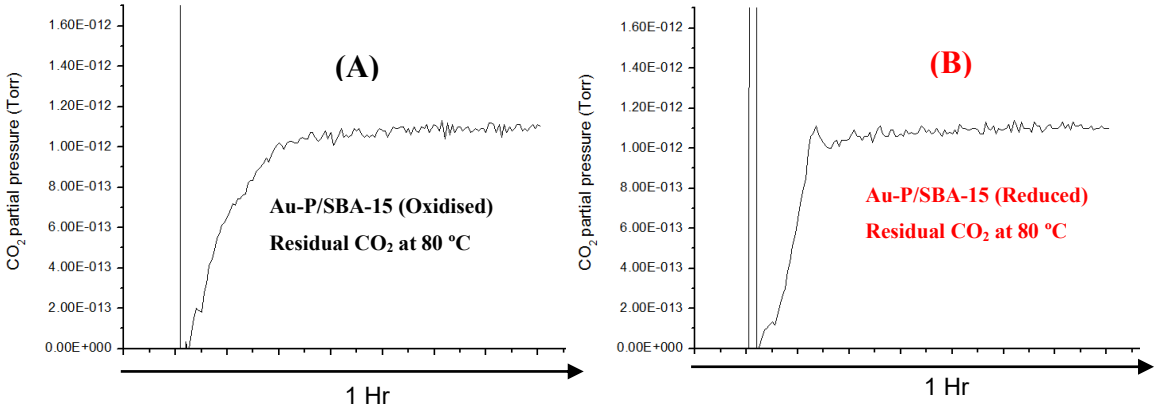

Figure 129. Acetone SSR (CO_2 response) over oxidised (A) and reduced (B) Au-P/SBA-15 catalyst at 80 °C (MS raw data)

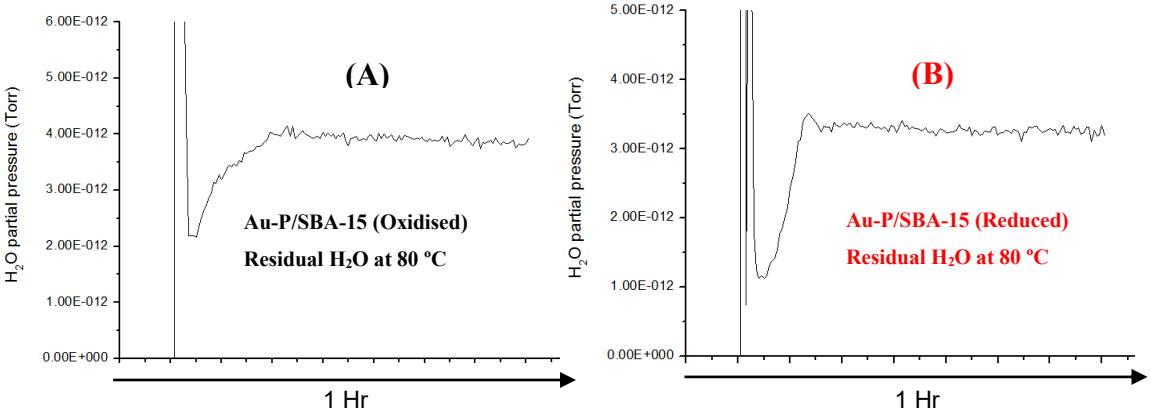

Figure 130. Acetone SSR (H_2O response) over oxidised (A) and reduced (B) Au-P/SBA-15 catalyst at 80 °C (MS raw data)

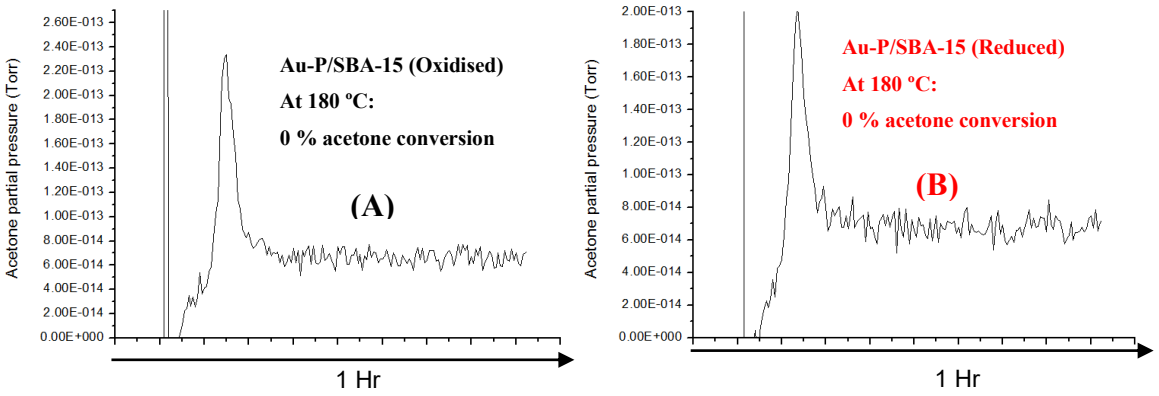

Figure 131. Acetone SSR over oxidised (A) and reduced (B) Au-P/SBA-15 catalyst at 180 °C (MS raw data)

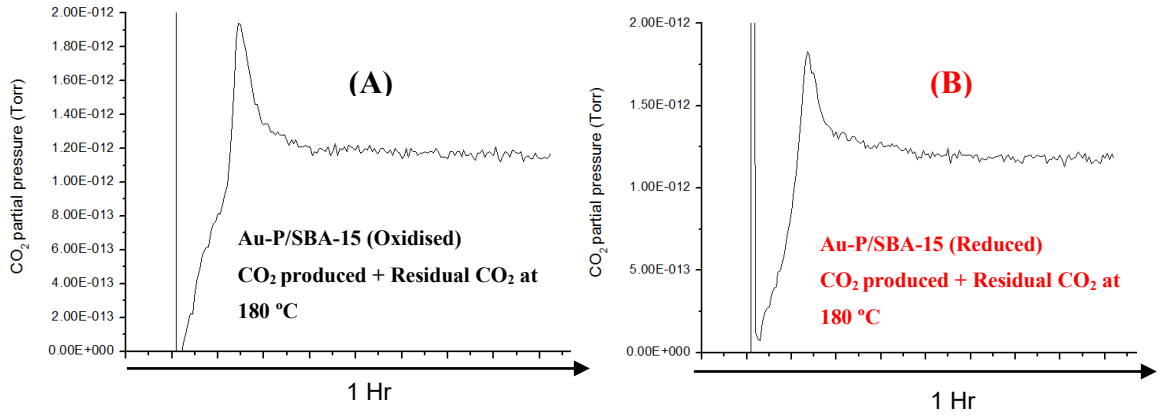

Figure 132. Acetone SSR (CO_2 response) over oxidised (A) and reduced (B) Au-P/SBA-15 catalyst at 180 °C (MS raw data)

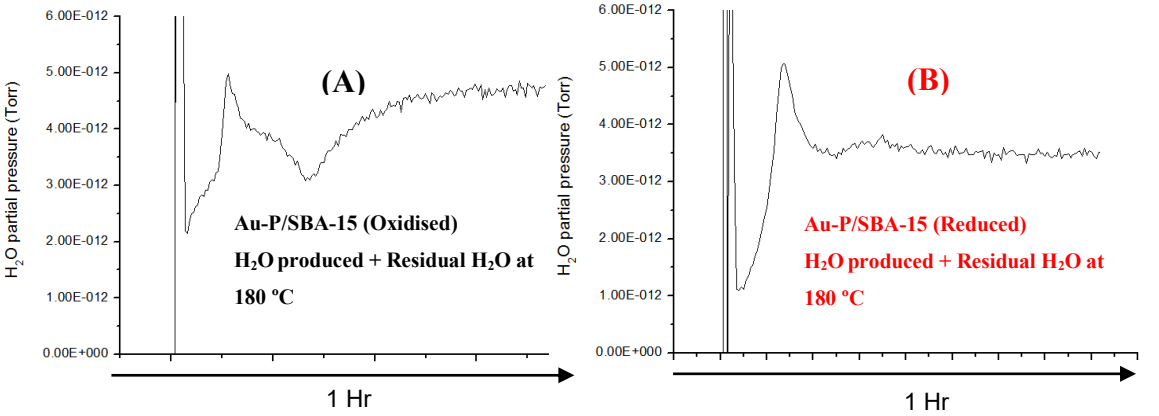

Figure 133. Acetone SSR (H_2O response) over oxidised (A) and reduced (B) Au-P/SBA-15 catalyst at 180 °C (MS raw data)

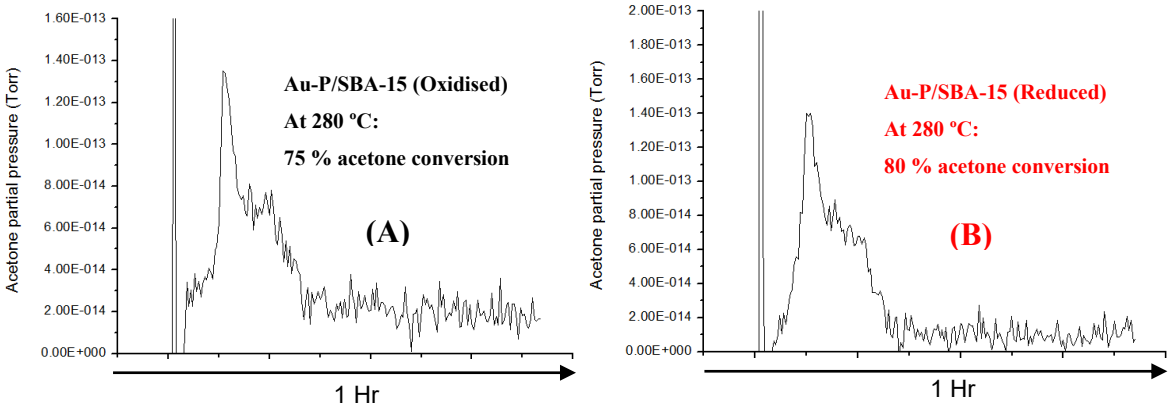

Figure 134. Acetone SSR over oxidised (A) and reduced (B) Au-P/SBA-15 catalyst at 280 °C (MS raw data)

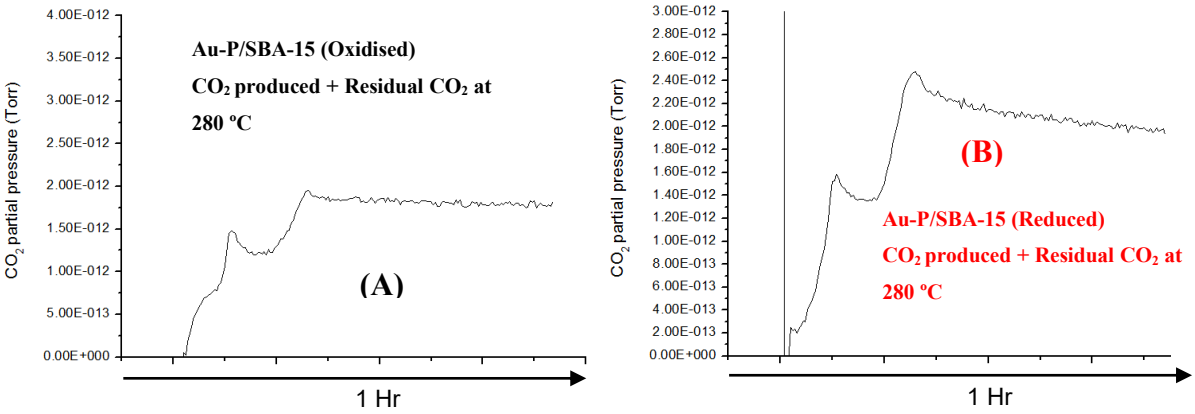

Figure 135. Acetone SSR (CO_2 response) over oxidised (A) and reduced (B) Au-P/SBA-15 catalyst at 280 °C (MS raw data)

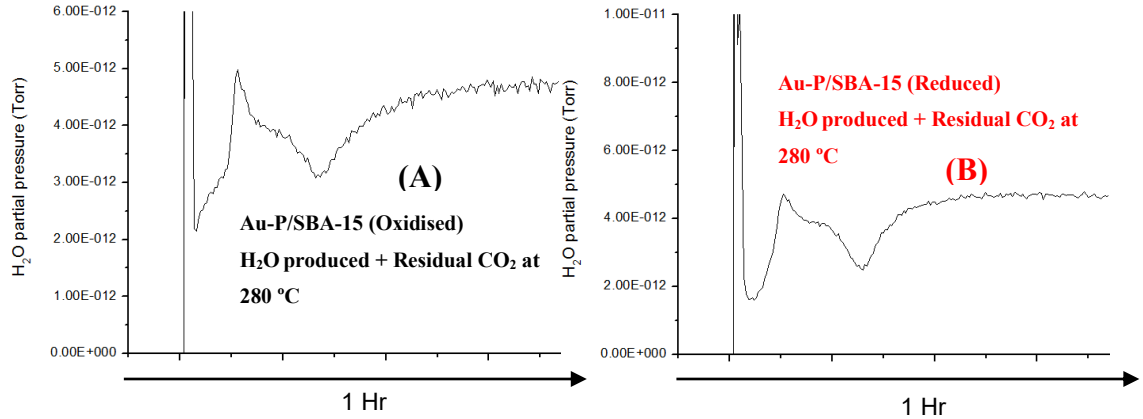

Figure 136. Acetone SSR (H_2O response) over oxidised (A) and reduced (B) Au-P/SBA-15 catalyst at 280 °C (MS raw data)

The catalytic activities of the as-synthesised and reduced forms of Au-P/SBA-15 catalysts were quite similar (Figures 128 – 136). Both forms of the catalyst were inactive at 180 °C. At 280 °C, the reduced catalyst was slightly more active, attaining 80 % acetone conversion, while the as-synthesised attained 75 % at 280 °C.

7.6.1. Plots for acetone Steady State Reaction over oxidised and reduced Au/SBA-15 catalysts

Although qualitative analysis of water is possible using GC-MS (as seen in MS raw data), it is usually difficult to quantify its formation since some water condensation do occur in the lines. For this reason, only VOC conversions (Equation1) and CO_2 formation (calculated in % mole fractions) were used for quantitative analysis of complete oxidation experiments.

The mole fractions in CO_2 formation from complete oxidation of acetone were calculated as follows:

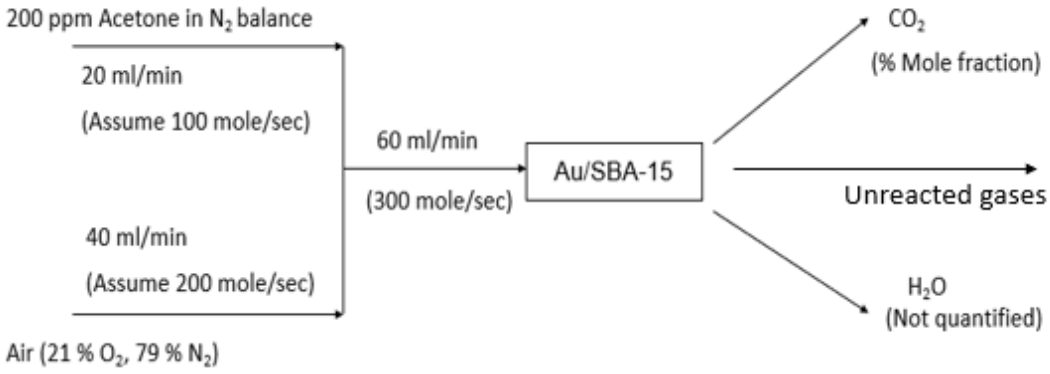

$$C_3H_6O + 4O_2 \longrightarrow 3CO_2 + 3H_2O$$

By stoichiometry, 1 mole of acetone (0.02 moles in the case of 200 ppm acetone) will produce 3 moles of CO_2 (0.06 moles of CO_2) if 100 % acetone conversion takes place by complete oxidation.

100 mole/sec of 200 ppm acetone in N_2 balance will contain:

$$\text{Mole fraction of acetone} = \frac{200}{1000000} = 2 \times 10^{-4}$$

$$\text{Mole fraction of } N_2 \text{ balance} = 1 - \frac{200}{1000000} = 0.9998$$

200 mole/sec of air will contain:

$$\text{Mole fraction of } O_2 = \frac{42}{200} = 0.21 \text{ (i.e. Moles of } O_2 = 0.21 \times 200 = 42 \text{ moles)}$$

$$\text{Mole fraction of } N_2 = \frac{158}{200} = 0.79 \text{ (i.e. Moles of } N_2 = 0.79 \times 200 = 158 \text{ moles)}$$

Mole fraction of CO_2 produced from 100 % acetone conversion will be:

$$\text{Mole fraction of } CO_2 = \frac{0.06}{300} = 2 \times 10^{-4} \text{ (by reaction)}$$

MS CO_2 signal obtained from 100 % acetone conversion in all the steady state experiments is 2×10^{-12}, which corresponds to CO_2 produced after reaction (2×10^{-4}), plus the residual mole fraction of CO_2 present in air (4×10^{-4}).

The residual CO_2 present in air gave MS signal of 1.3×10^{-12}, which corresponds to 4×10^{-4} mole fraction of residual CO_2

With the calculations above, CO_2 sensitivity factor for acetone was plotted as shown below:

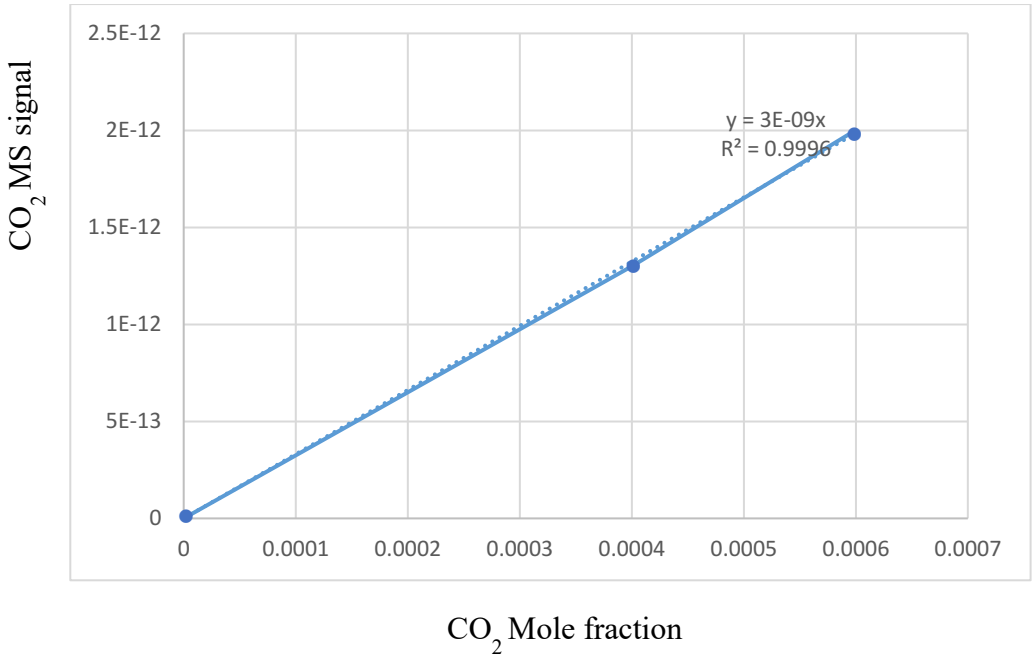

Figure 137. Calibration for CO_2 formation in mole fraction

Every CO_2 mole fraction plot was done by subtracting CO_2 mole fraction of reaction from the residual CO_2 value.

The plots for acetone conversion and the corresponding CO_2 formation plots are shown in Figures 138 - 143

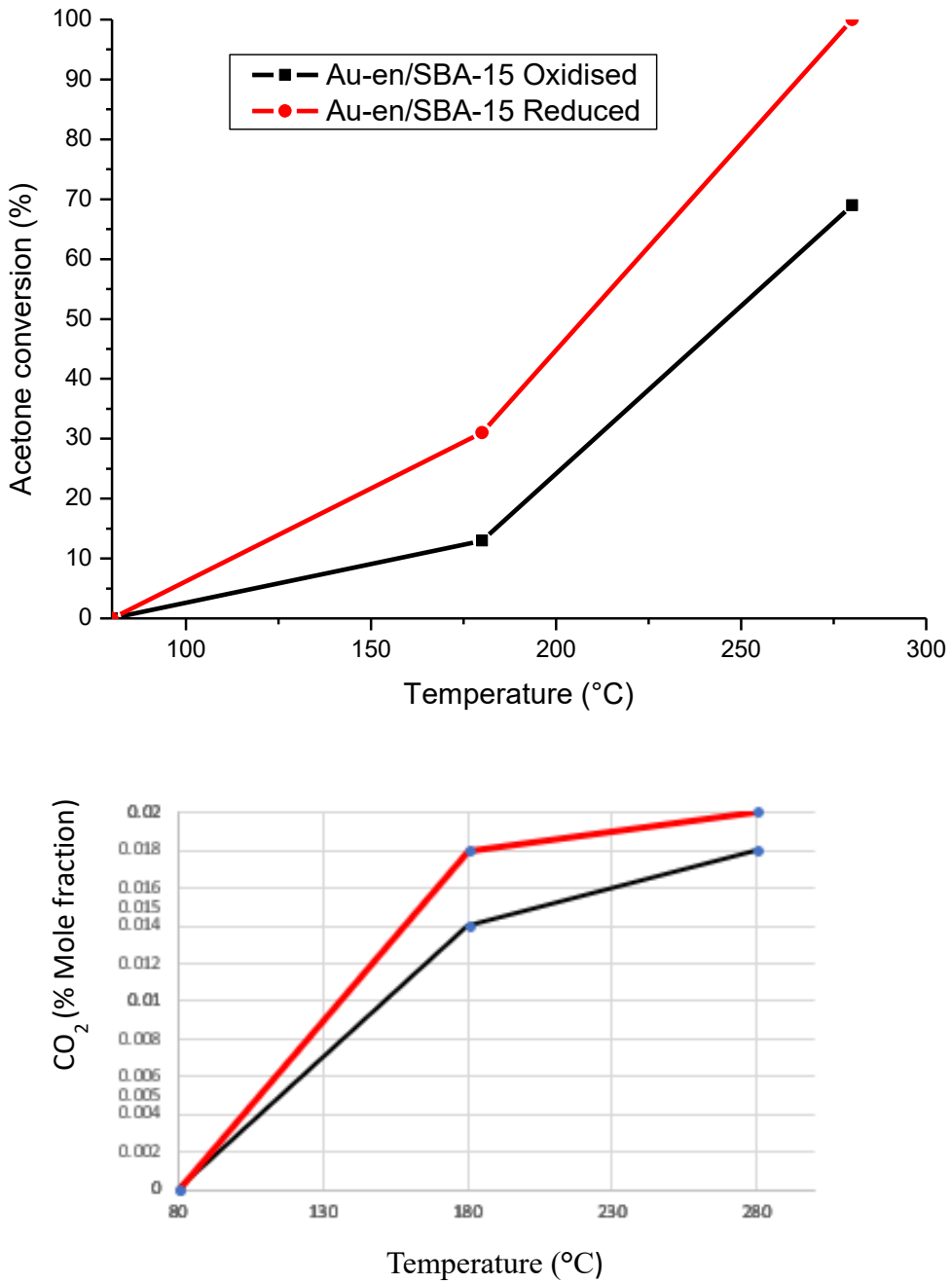

Figure 138. Complete oxidation of acetone over as-synthesised and reduced forms of Au-en/SBA-15 catalyst with corresponding CO_2 formation

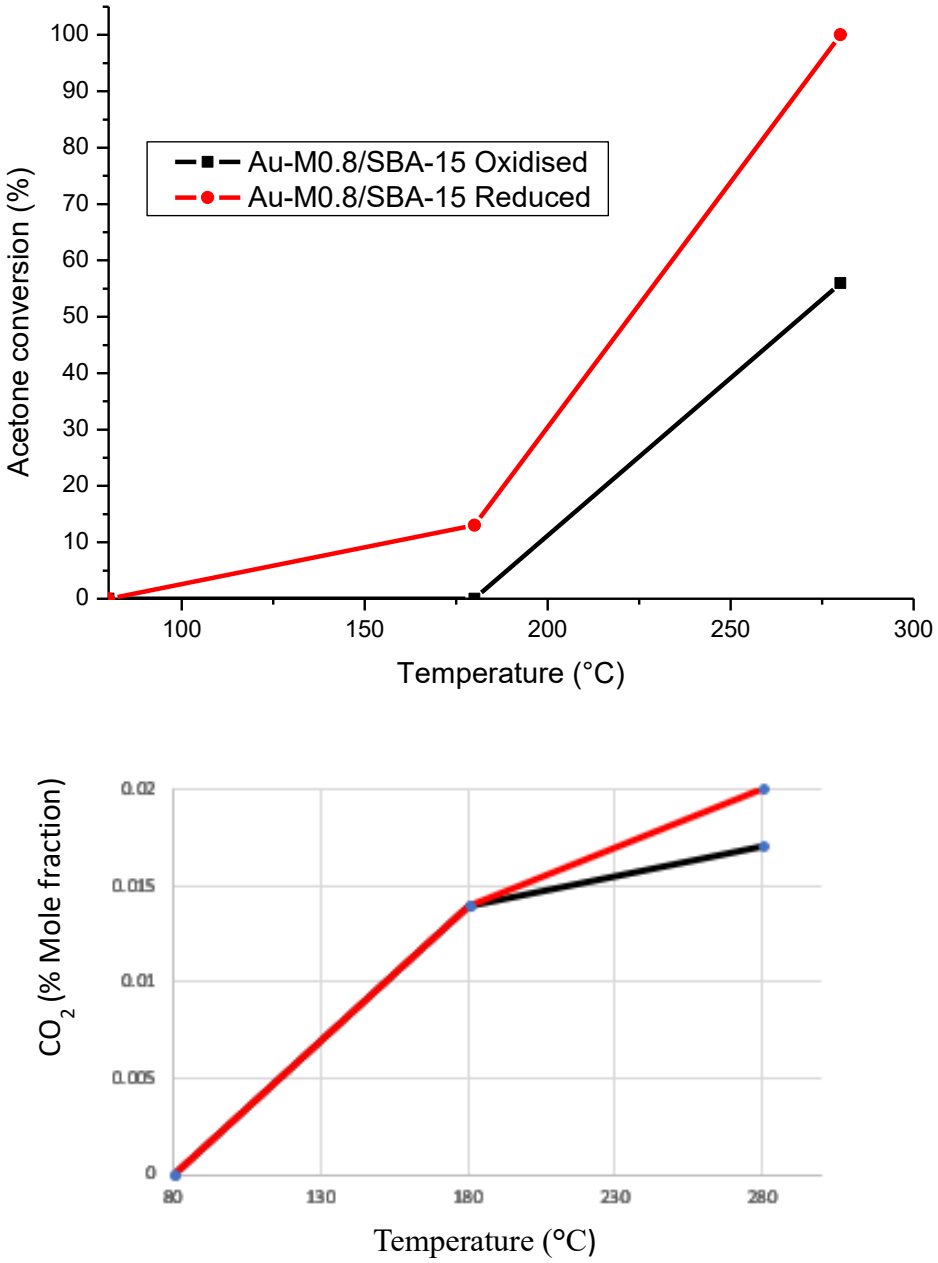

Figure 139. Complete oxidation of acetone over as-synthesised and reduced forms of Au-M0.8/SBA-15 catalyst with corresponding CO_2 formation

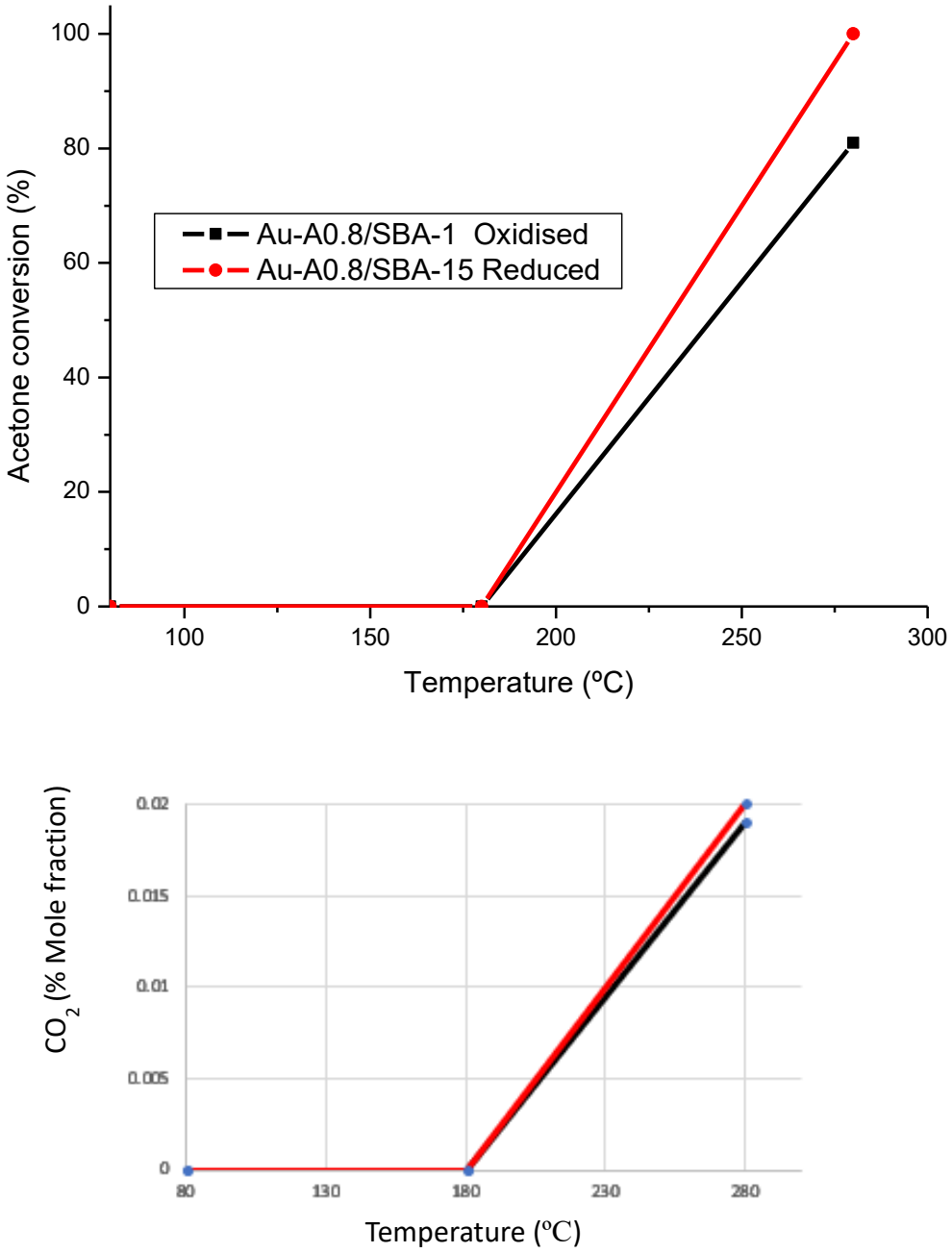

Figure 140. Complete oxidation of acetone over as-synthesised and reduced forms of Au-A0.8/SBA-15 catalyst with corresponding CO_2 formation

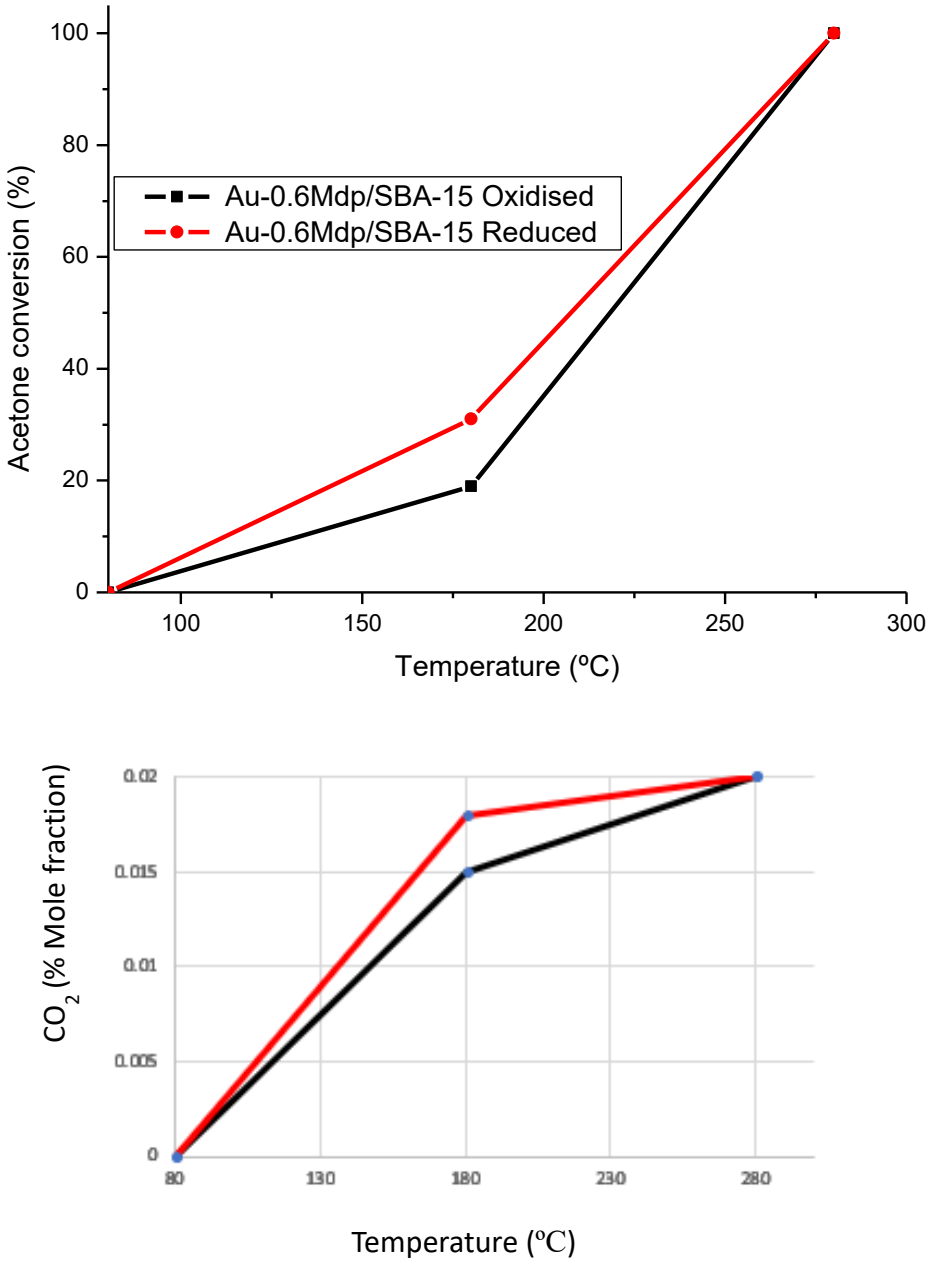

Figure 141. Complete oxidation of acetone over as-synthesised and reduced forms of Au-0.6Mdp/SBA-15 catalyst with corresponding CO_2 formation

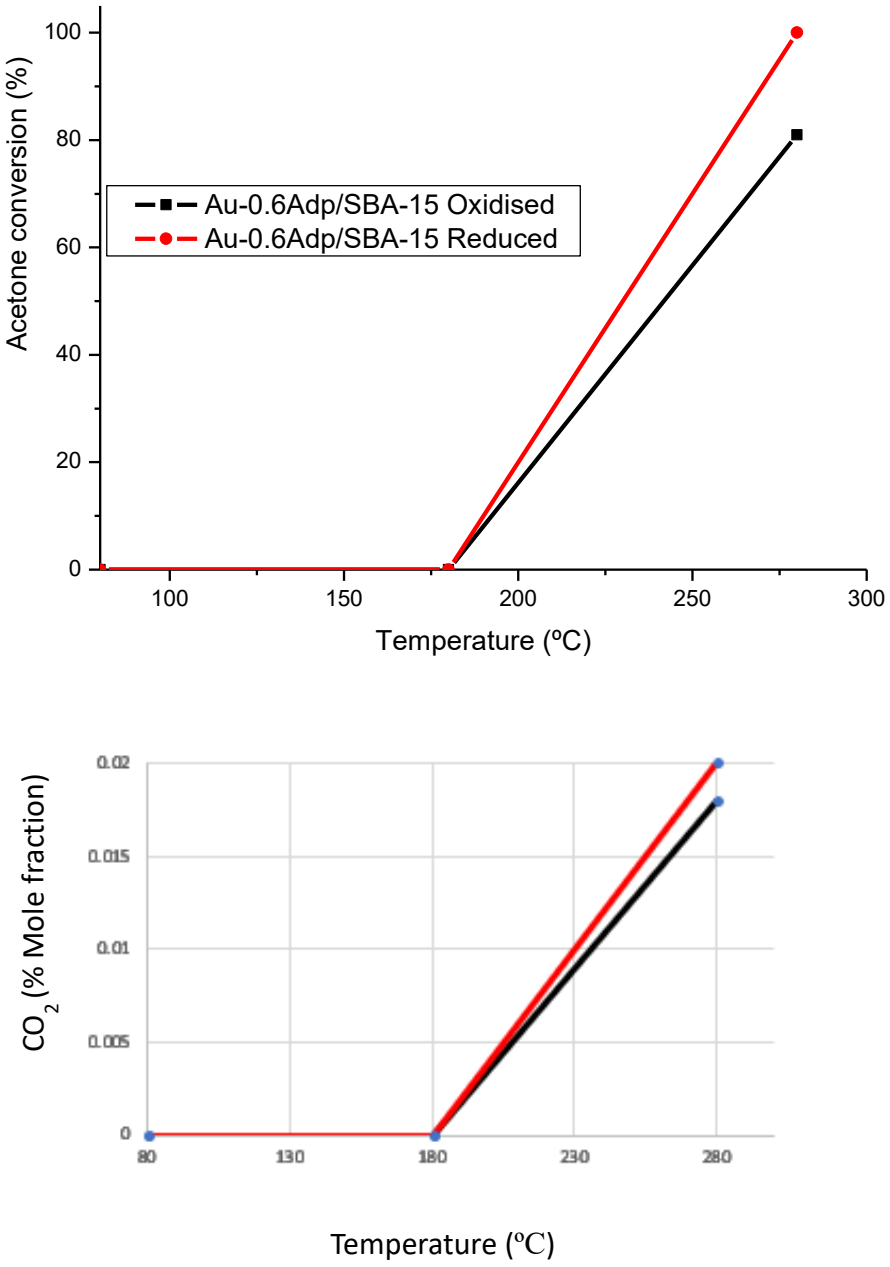

Figure 142. Complete oxidation of acetone over as-synthesised and reduced forms of Au-0.6Adp/SBA-15 catalyst with corresponding CO_2 formation

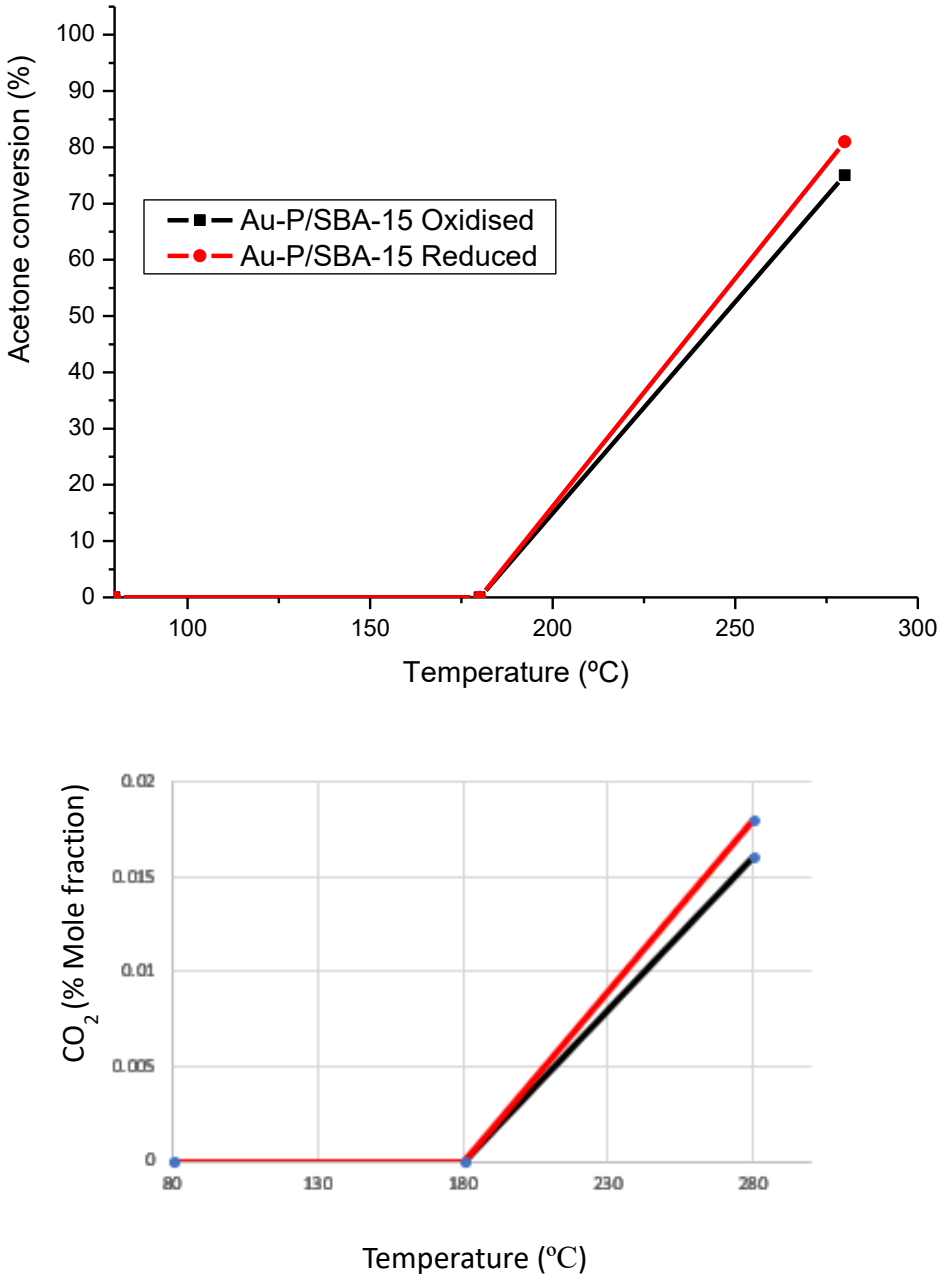

Figure 143. Complete oxidation of acetone over as-synthesised and reduced forms of Au-P/SBA-15 catalyst with corresponding CO_2 formations

All SSRs were done at GHSV of 45, 000 h^{-1}. The results in Figures 138 – 143 clearly show that oxidation state and particle size of gold had significant influence on catalytic activity in complete oxidation of acetone with Au/SBA-15 catalysts. In terms of oxidation state, there was a clear difference between the catalytic activity of the as-synthesised and reduced Au/SBA-15 catalysts. Although both the as-synthesised and reduced forms of Au/SBA-15

catalysts were highly active, the reduced catalysts showed a higher catalytic activity, which indicates that there is a clear difference between the hydrogen reduced catalysts and the fresh catalysts without reduction. Could it be that hydrogen reduction occurred at lower temperature and increased the amount of metallic gold (Au^0)?. Particle size of gold also had pronounced influence on catalytic activity. For instance, Au-0.6Mdp/SBA-15 catalyst with most of its gold particle sizes at 1.3 nm (smallest gold particle size) was the only catalyst to attain 100 % acetone conversion in Au/SBA-15 as-synthesised form at 280 °C. The other as-synthesised Au/SBA-15 catalysts only attained 55 – 80 % acetone conversion at 280 °C. Also, the reduced Au-0.6Mdp/SBA-15 catalyst (1.3 nm Au size) proved to be the most active, attaining 100 % acetone conversion as low as 250 °C. The other reduced Au/SBA-15 catalysts, except for reduced Au-0.6Adp/SBA-15 and Au-P/SBA-15 catalysts, achieved 100 % acetone conversion at 280 °C. Au-0.6Adp/SBA-15 and Au-P/SBA-15 catalysts with the biggest gold particle sizes at 30 and 79 nm respectively were the least active, attaining less than 100 % (80%) at 280 °C, however, the presence of some smaller gold particle sizes (5 – 15 nm) in these catalysts might have been responsible for its high catalytic activity at 80 %.

Au-0.6Mdp/SBA-15 catalyst with the highest number of the smallest gold particle sizes of 1.3 nm which are well dispersed and firmly attached to SBA-15 support proved to be the best Au/SBA-15 catalyst in complete oxidation of acetone.

The reaction stability of acetone complete oxidation over the as-synthesised and reduced forms of Au-0.6Mdp/SBA-15 catalyst (catalyst life time test) was done in later done in Steady State Reaction (SSR) for 25 hours at 270 °C and 220 °C, respectively with GHSV of 45,000 h^{-1}

7.6.2. Catalyst life time test for the best Au/SBA-15 catalyst

Catalyst life time test in acetone complete oxidation for 25 hours was carried out for the best Au/SBA-15 catalyst (Au-0.6Mdp/SBA-15 catalyst) in its as-synthesised form at 270 °C, and for the reduced form at 220 °C. The results are shown in Figures 144 - 147.

Stable operation of the as-synthesised Au-0.6Mdp/SBA-15 catalyst (Figures 144A and 146) was achieved after a period of about 18 hours at about 50 % acetone conversion, while the reduced catalyst (Figure 144B and 147) was stable after 4 hours. The result show there is a transient behaviour of the oxidised and reduced catalysts upon exposure to reaction stream. During this transient period, as explained by Avgouropoulous and co-workers [161], the carbon mass balance is deficient, indicating deposition/adsorption of acetone derived species on the catalyst surface. As soon as the catalyst surface is saturated, the carbon mass balance is satisfied, and the catalyst exhibits stable behaviour. Once reaction stability was attained, the catalytic activities of the two catalysts remained stable.

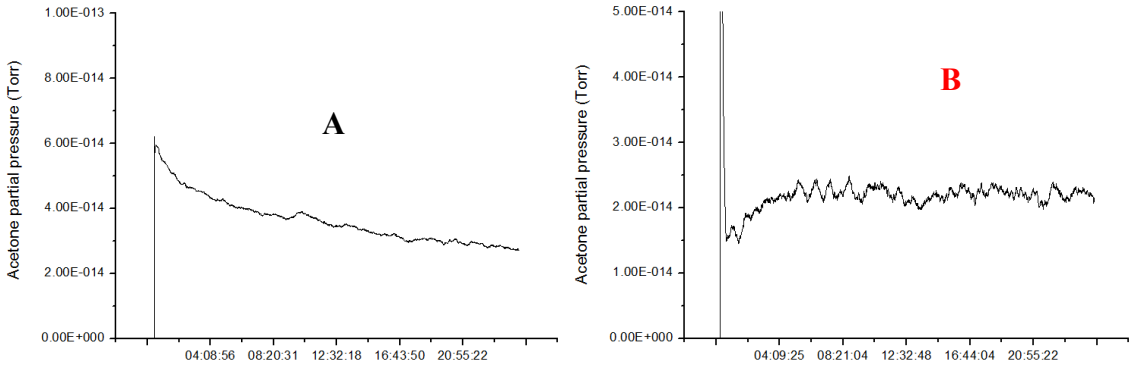

Figure 144. Catalyst life time test for as-synthesised (A) and reduced Au-0.6Mdp/SBA-15 catalyst (B) at 270 ºC and 220 ºC for 25 hrs respectively (MS raw data)

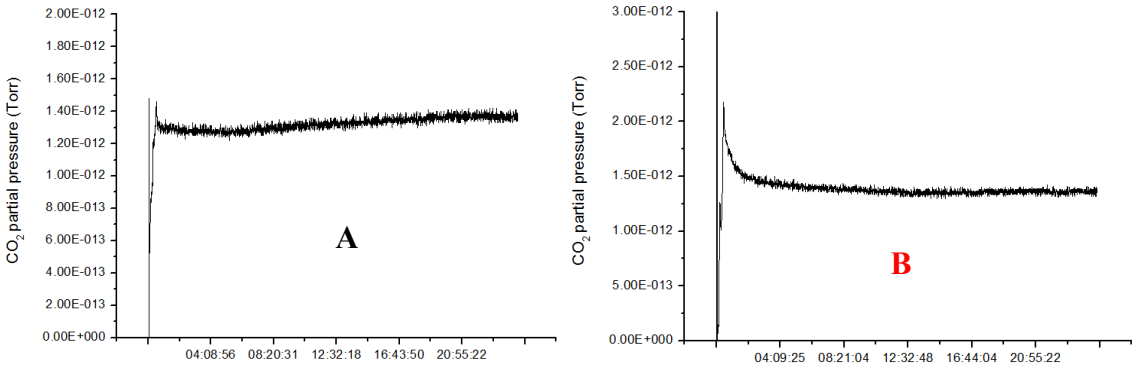

Figure 145 Catalyst life time test (CO_2 response) for as-synthesised (A) and reduced Au-0.6Mdp/SBA-15 catalyst (B) at 270 ºC and 220 ºC for 25 hrs respectively (MS raw data)

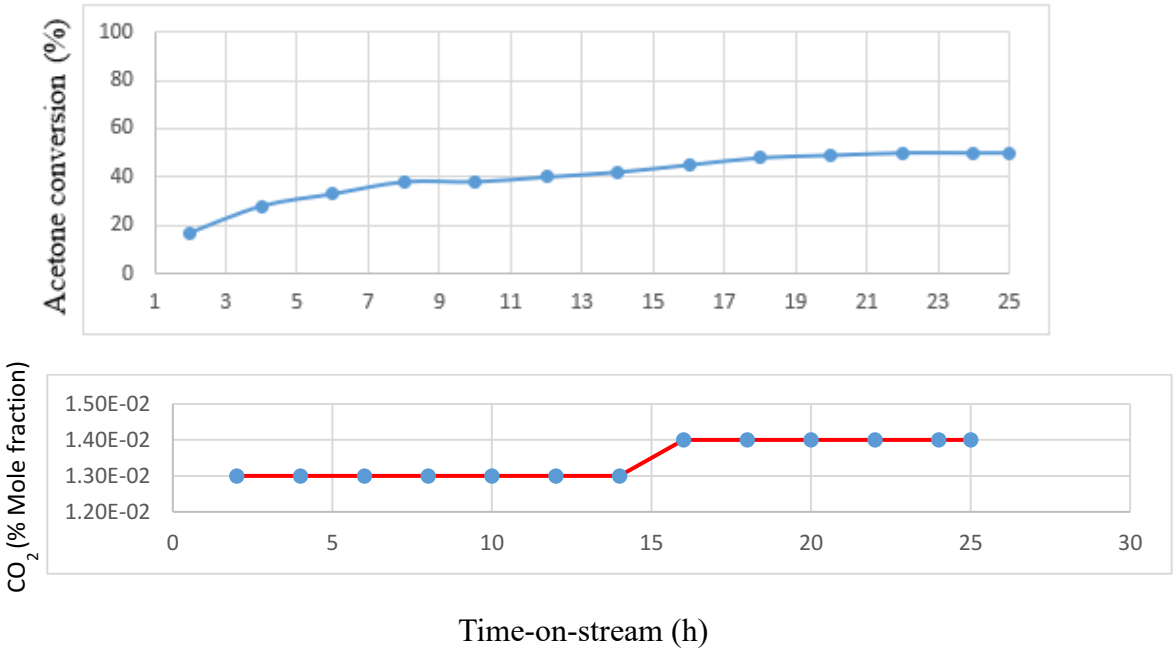

Figure 146. Catalyst life time test for as-synthesised Au-0.6Mdp/SBA-15 catalyst in acetone complete oxidation at 270 °C showing CO_2 response

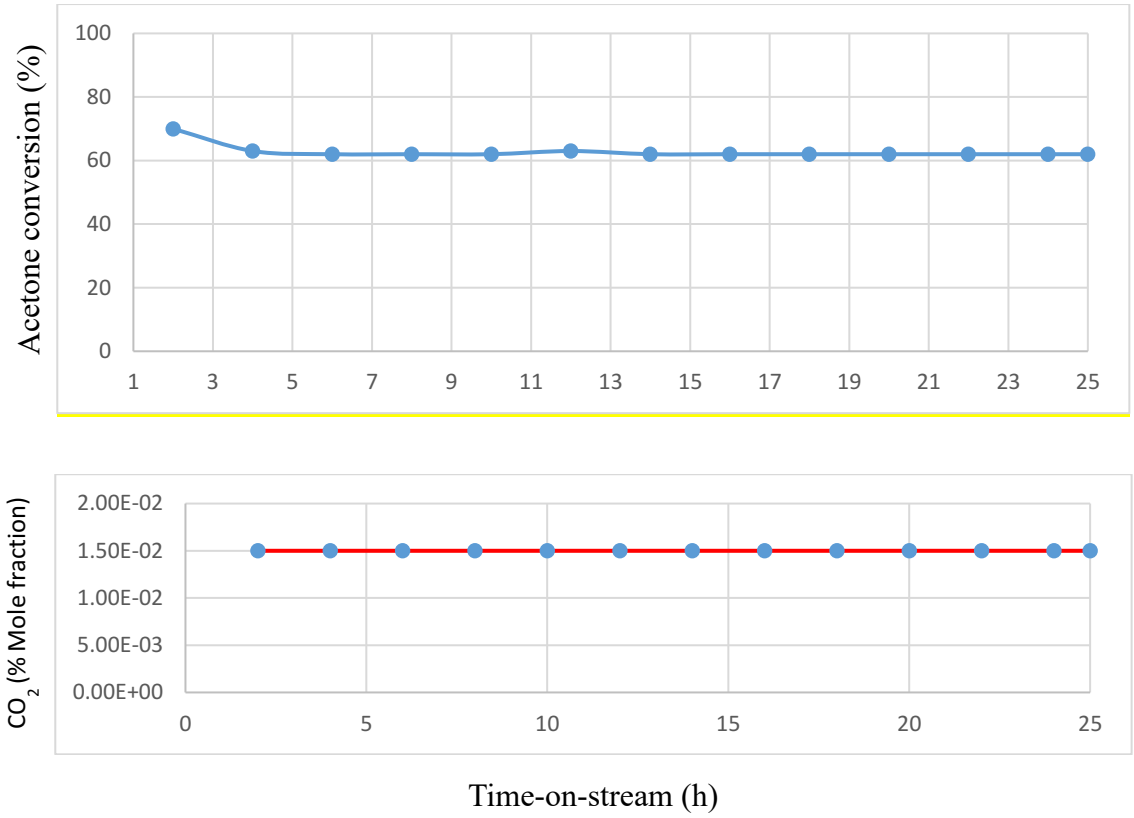

Figure 147. Catalyst life time test for reduced Au-0.6Mdp/SBA-15 catalyst in acetone complete oxidation at 220 °C showing CO_2 response

7.7. Propane complete oxidation

It has been reported that the alkane group of VOCs are one of the hardest to oxidise due to their high stability [152], and so any catalyst designed to eliminate VOCs at low temperature must be capable of dealing with the alkanes. Propane (alkane group) was tested as VOC model compound over the best four reduced Au/SBA-15 catalysts tested in acetone oxidation. The catalytic performance of the best out of the four catalysts was compared to its as-synthesised form to determine the most active state. Catalytic stability test for 25 hours at 300 °C was later carried out on the best Au/SBA-15 catalyst.

7.7.1. Propane TPRx over reduced Au/SBA-15 catalysts

As explained in Chapter 3, TPRx for propane oxidation was done using 1.5 ml/min flow rate of pure propane (99.9 %) with 60 ml/min flow rate of air over each 50 mg of Au/SBA-15

catalyst (GHSV = 18, 450 h^{-1}), which corresponds to 2.4 % volume of propane in air (24, 000 ppm of propane). The TPRx results for propane complete oxidation over Au/SBA-15 catalysts are shown in Figures 148 -149 and 150. No catalytic activity was observed below 120 °C, and so the M-S partial pressure reading at 100 °C was regarded as the initial propane concentration corresponding to 24,000 ppm of propane. Propane conversion between 100 - 400 °C was then calculated using Equation 1. From the instrument's M-S readings, there was a corresponding CO_2 and H_2O formation with propane conversion as shown in Figures 148 - 149.

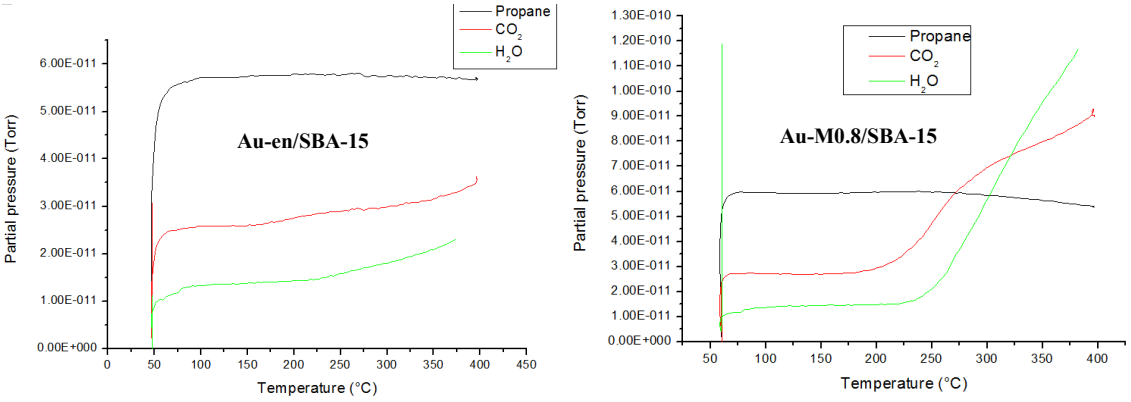

Figure 148. Raw MS data for propane TPRx over four Au/SBA-15 catalysts

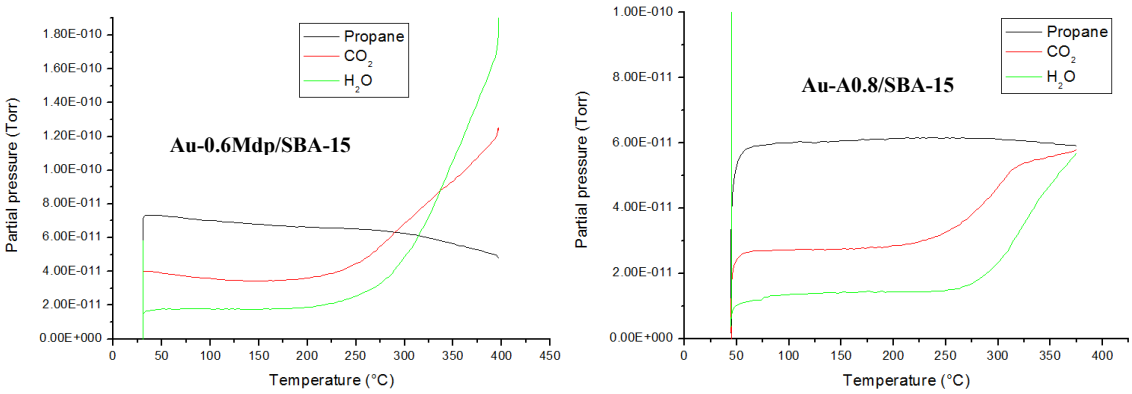

Figure 149. Raw MS data (CO_2 response) for propane TPRx over four Au/SBA-15 catalysts

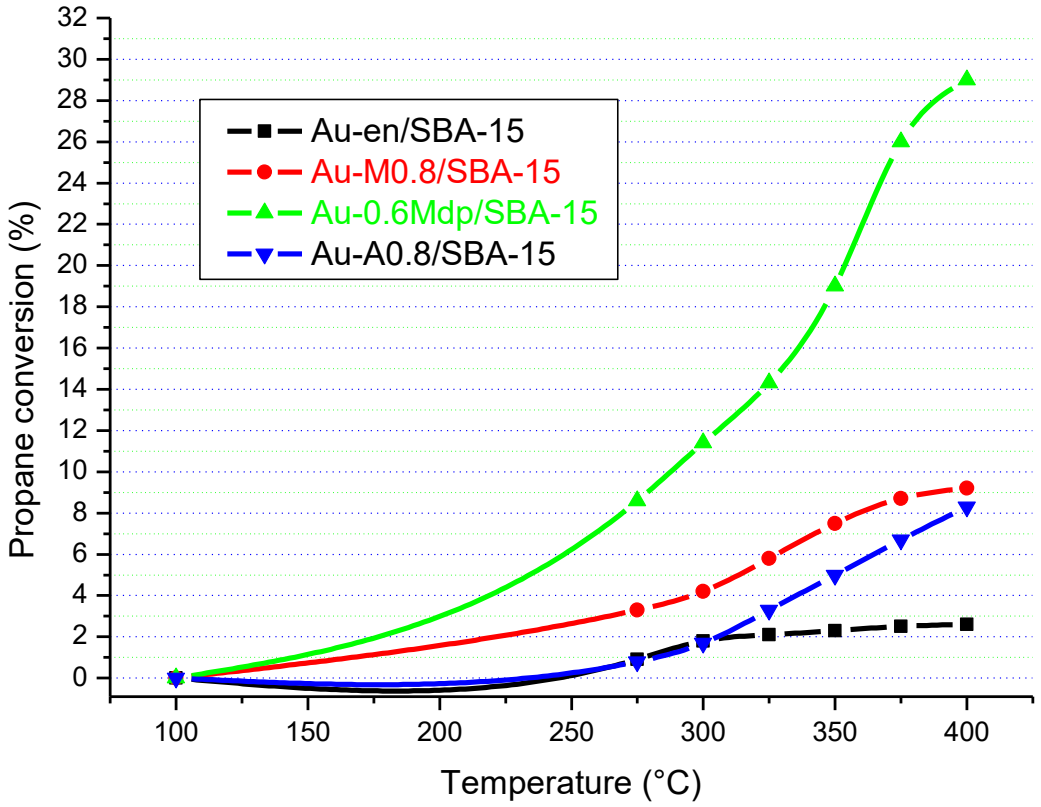

Figure 150. Propane TPRx plots of the r four reduced Au/SBA-15 catalysts

The mole fractions in CO_2 formation from complete oxidation of propane were calculated as follows:

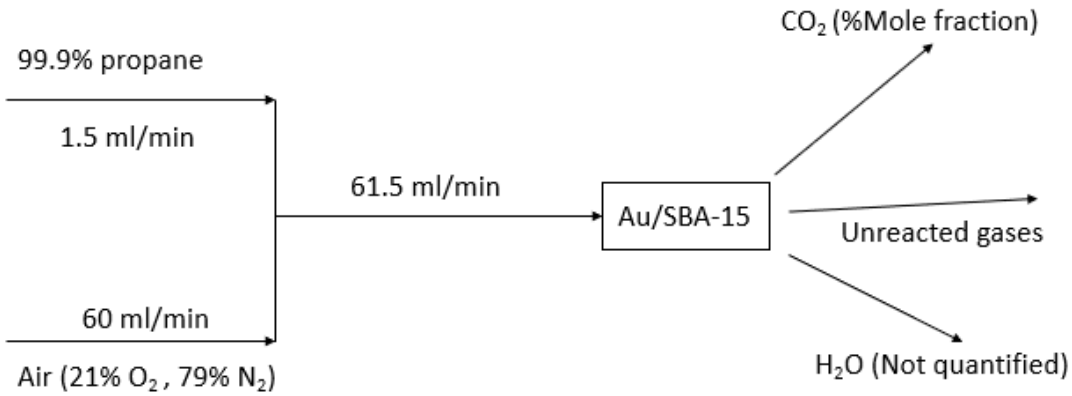

$$C_3H_8 + 5O_2 \longrightarrow 3CO_2 + 4H_2O$$

By stoichiometry, 1 mole of propane will produce 3 moles of CO_2 for complete propane oxidation.

Since 22.4 litres (Volume of 1 mole of any gas) contains 1 mole of propane

1.5×10^{-3} L will contain:

$$= \frac{1.5 \times 10-4}{22.4} = 6.69 \times 10^{-5} \text{ mole of propane}$$

Mole fraction of N_2 balance = $1 - \frac{200}{1000000} = 0.9998$

Since 22.4 L air contains 1 mole air,

6.0×10^{-3} L will contain = 2.68×10^{-3} mole air

Therefore, total moles in 61.5ml/min flow: $2.68 \times 10^{-3} + 6.69 \times 10^{-5} = 2.75 \times 10^{-3}$ moles

Mole fraction of propane = $\frac{6.69 \times 10-5}{2.75 \times 10-3} = 0.02$

Therefore, mole fraction of CO_2 = 0.06 (100% propane conversion)

At 400 °C, the most active Au-SBA-15 catalyst (Au-0.6Mdp/SBA-15) attained the highest propane conversion of 29 %, with corresponding MS CO_2 signal of 1.25E – 10. CO_2 formation (% mole fraction) was calibrated as follows:

Moles of propane = 6.69×10^{-5}

29 % propane converted at 400 °C = $0.29 \times 6.69 \times 10^{-5}$

$= 1.94 \times 10^{-5}$ moles converted

Moles of CO_2 produced = $(1.94 \times 10^{-5)} \times 3 = 5.8 \times 10^{-5}$

Mole fraction of CO_2 by reaction $= \frac{5.8 \times 10-5}{2.68 \times 10-3} = 0.022$

CO_2 residual $= \frac{0.04}{100} \times 2.68 \times 10^{-3} = 1.07 \times 10^{-6}$

$= \frac{1.07 \times 10-6}{2.68 \times 10-3} = 4.0 \times 10^{-4}$

For CO_2 calibration, a plot of MS signal for residual CO_2 (3E – 12) and CO_2 produced (1.25E – 10) against mole fractions of residual CO_2 $(4.0 \times 10^{-4)}$ and CO_2 produced (0.022) is shown below

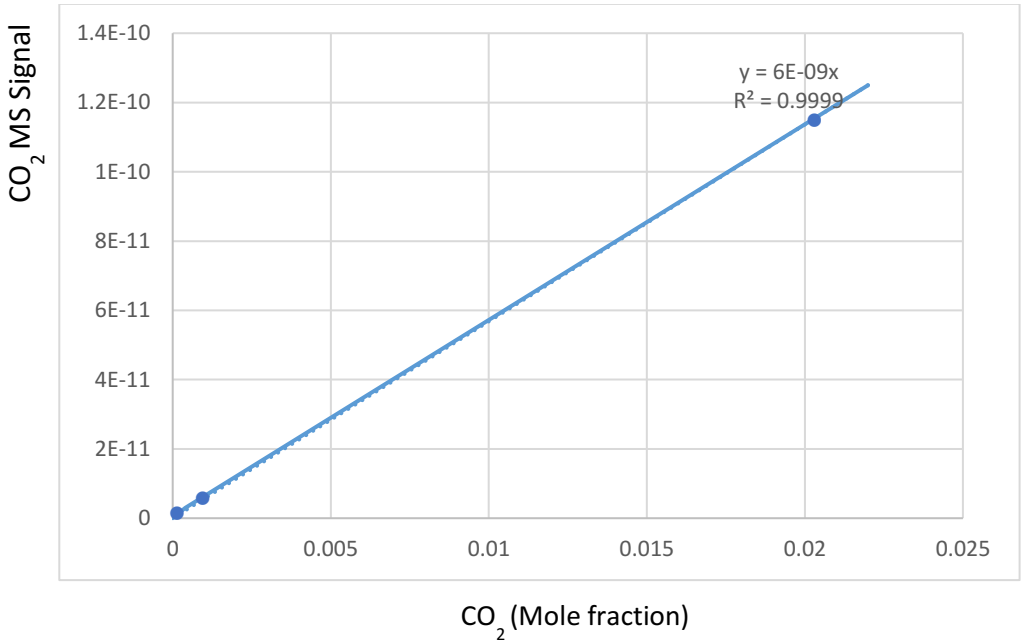

Figure 151. CO_2 calibration for propane oxidation

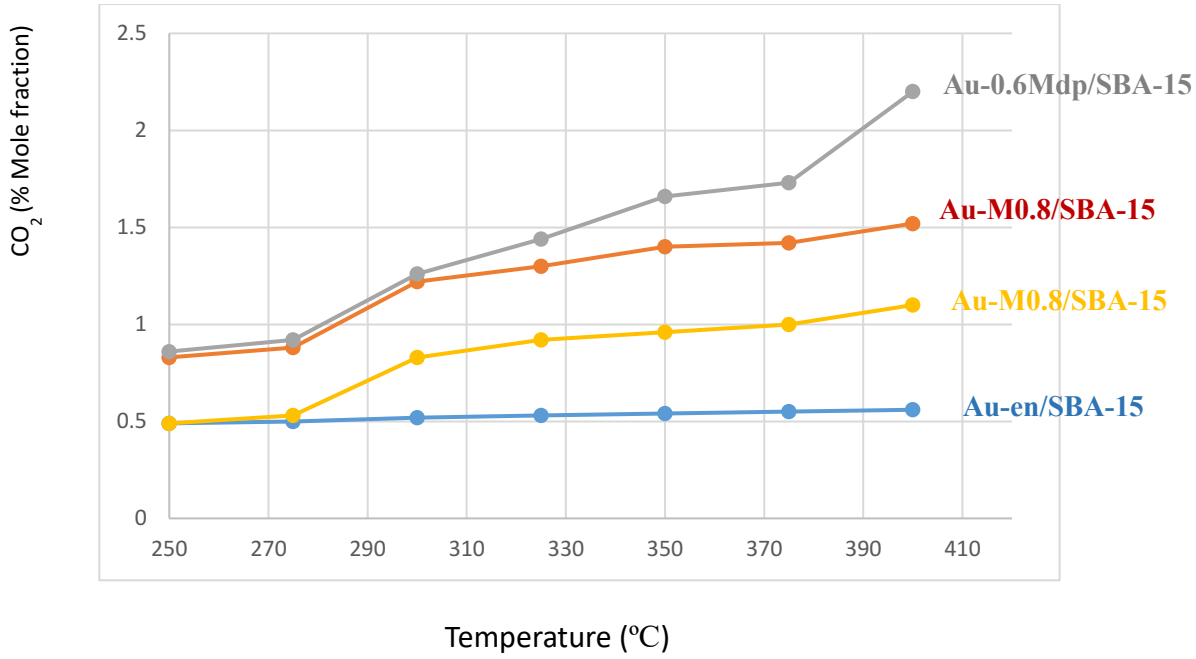

Figure 152. CO_2 response over four reduced Au/SBA-15 catalysts in propane oxidation

The results in Figure 150 show that particle size of gold had a major influence on how active Au/SBA-15 catalyst can be in propane complete oxidation. The catalyst with most of the smallest gold particle size of 1.3 nm (Au-0.6Mdp/SBA-15 catalyst) was the most active, with light off temperature from around 275 °C, which increased steadily with increase in temperature to 29 % propane conversion at 400 °C. The second most active catalyst – Au-M0.8/SBA-15 catalyst with most of its gold particle sizes at 3.5 nm, attained 3.3 % propane conversion at 275 °C, which increased steadily to 9.2 % at 400 °C. The third most active catalyst – Au-A0.8/SBA-15 with most of its gold particles in the range of 4 -17 nm, attained 0.8 % propane conversion at 275 °C, and 8.3 % at 400 °C. The fourth and least active catalyst – Au-en/SBA-15 catalyst, with its gold nano-particles mostly at 5.5 nm, with few other gold particles between 6.5 – 8.5 nm attained 0.9 % propane conversion at 275 °C, and 2.6 % at 400 °C.

Au-0.6Mdp/SBA-15 catalyst proved to be the most active catalyst in propane complete oxidation (this catalyst was also the most active in acetone complete oxidation).

A comparative study was done to compare the catalytic activity of the reduced Au-0.6Mdp/SBA-15 catalyst with its as-synthesised form in propane complete oxidation.

7.7.1. Comparison between reduced and as-synthesised Au-0.6Mdp/SBA-15 catalyst in propane complete oxidation TPRx

The TPRx results in Figure 153 - 154 show that the reduced Au-0.6Mdp/SBA-15 catalyst was more active than its as-synthesised form, attaining 8.6 %, 14.3% and 29 % at 275 °C, 325 °C and 400 °C, respectively. The as-synthesised form of the catalyst attained 1.2 %, 2.4 % and 4.3 % at 275 °C, 325 °C and 400 °C, respectively.

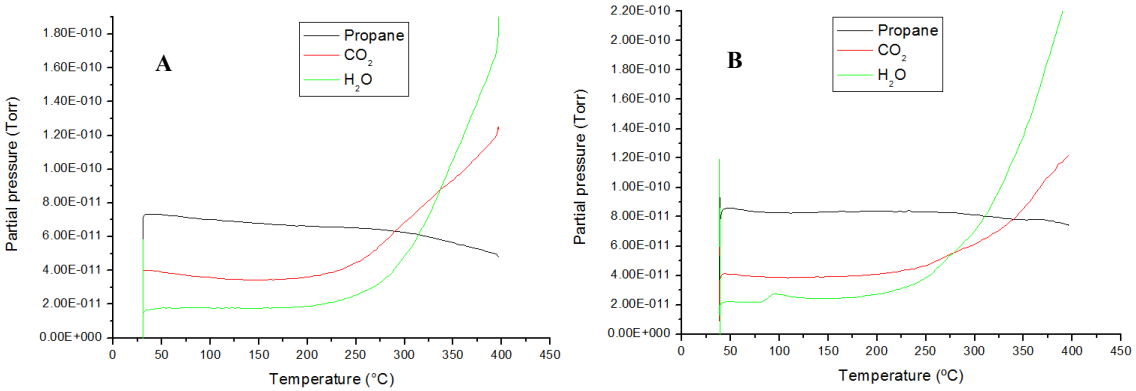

Figure 153. Comparison between the catalytic activity of reduced (A) and as-synthesised Au-0.6Mdp/SBA-15 catalyst (B) in propane oxidation TPRx (Raw MS data)

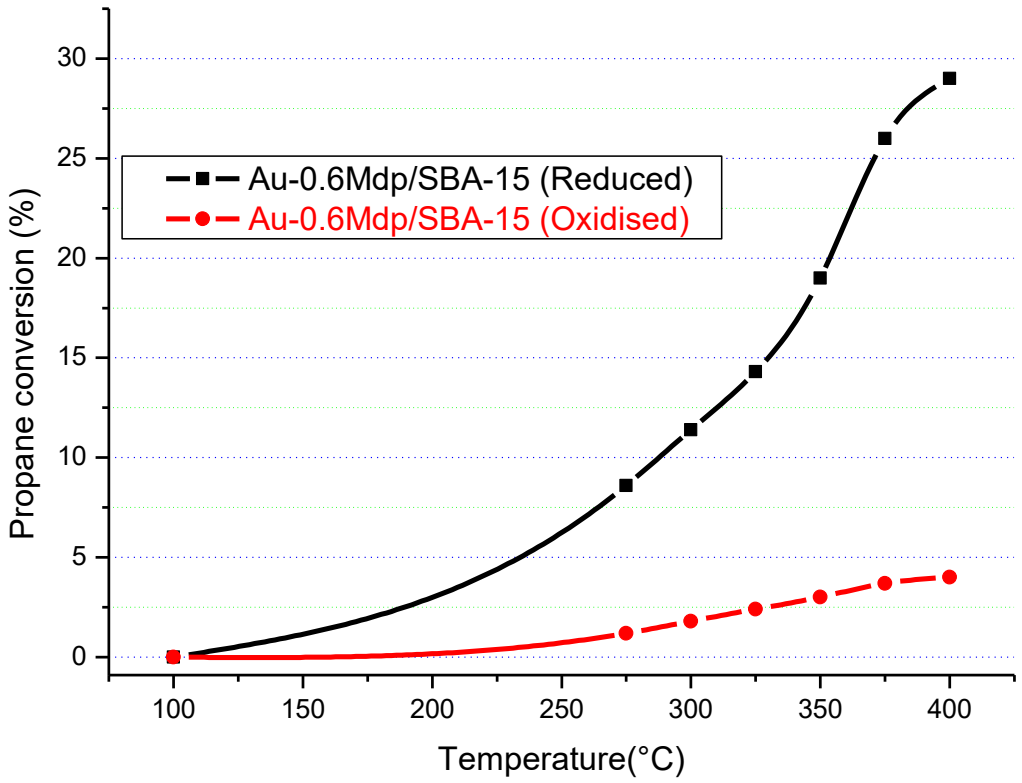

Figure 154. Comparison between the catalytic activity of reduced and as-synthesised Au-0.6Mdp/SBA-15 catalyst in propane oxidation

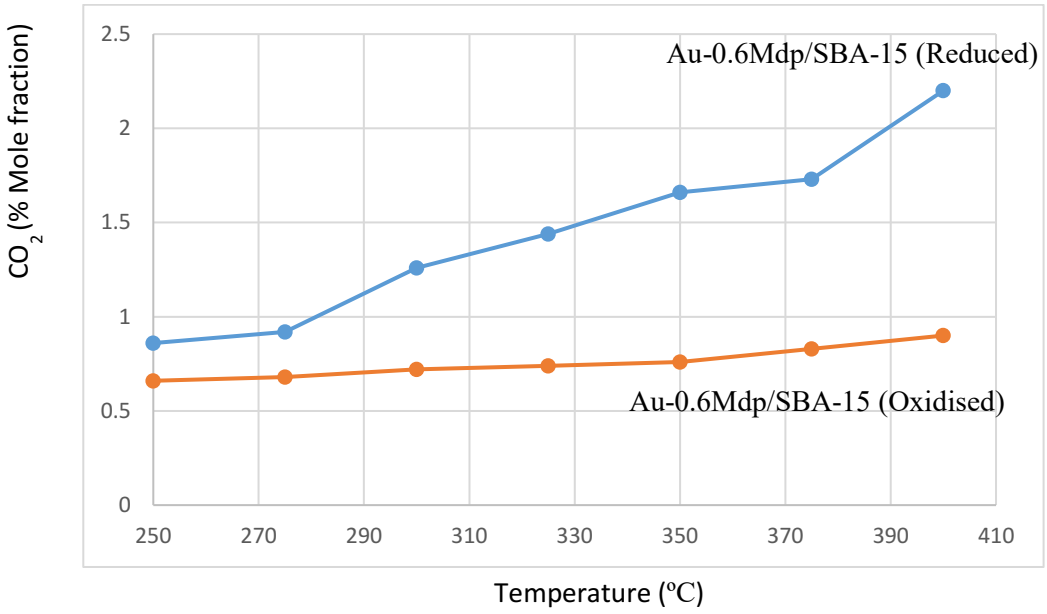

Figure 155. CO_2 response - comparison between the catalytic activity of reduced and as-synthesised Au-0.6Mdp/SBA-15 catalyst in propane oxidation

7.7.2. Catalyst life time test of the best Au/SBA-15 catalyst (reduced form) in propane oxidation

The stability of Au-0.6Mdp/SBA-15 catalyst was tested at 300 ºC for 25 hours in oxidation of propane with same GHSV (18, 450 h^{-1}). The result shown in Figure 82 reveal that the catalyst remained highly active and stable in the course of the reaction, maintaining 11 – 12 % propane conversion. The propane conversion result from SSR stability test is similar to the result obtained from TPRx measurements (Figure 156 - 11.4 % propane conversion at 300 ºC for 0.6Mdp/SBA-15 catalyst), which further validates TPRx experimental results.

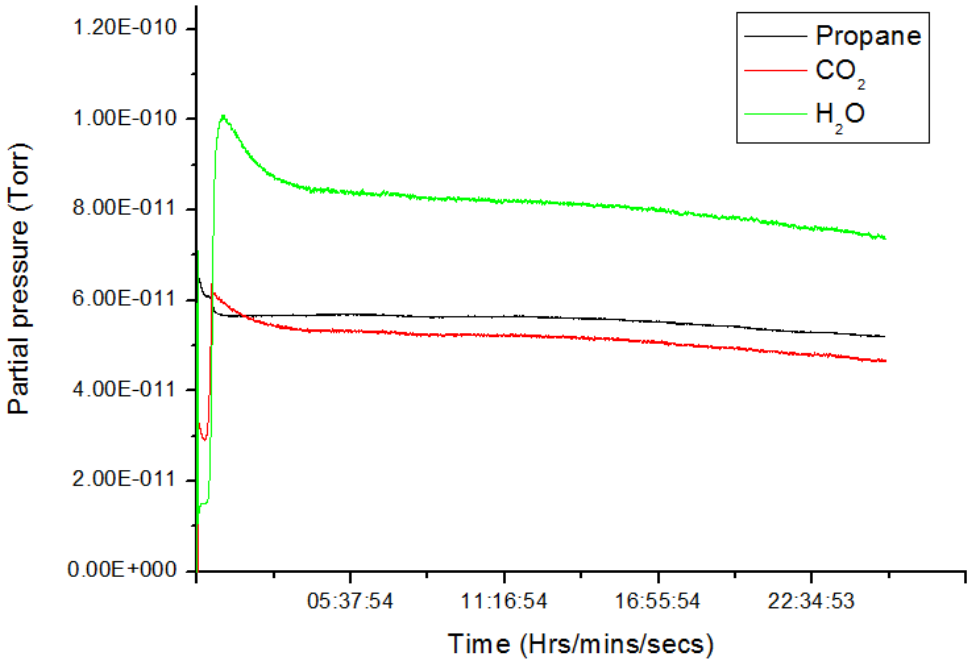

Figure 156. Catalyst life time test (Raw MS data) of Au-0.6Mdp/SBA-15 catalyst in propane oxidation at 300 ºC for 25 hours

7.8. BTEXB complete oxidation

In reality, VOCs exists not as individual compounds but as a mixture. A gas mixture, mostly aromatic hydrocarbons and an olefin (benzene, toluene, ethylbenzene, xylene and 1,3-

butadiene) specially mixed in one gas bottle was used as model for VOCs oxidation over the best Au/SBA-15 catalyst, i.e. Au-0.6Mdp/SBA-15 catalyst. The experimental procedure was explained in Chapter 3, section 3.3.2.1. The essence of this experiment is not to calculate conversion of each individual VOC in the mixture but to evaluate the catalytic performance of the as-synthesised and reduced forms of Au-0.6Mdp/SBA-15 catalyst in terms of CO_2 and H_2O formation.

Light off temperatures for both the reduced and as-synthesised Au-0.6Mdp/SBA-15 catalyst started around 250 ºC, and increased steadily up to 400 ºC (Figures 157 - 158)

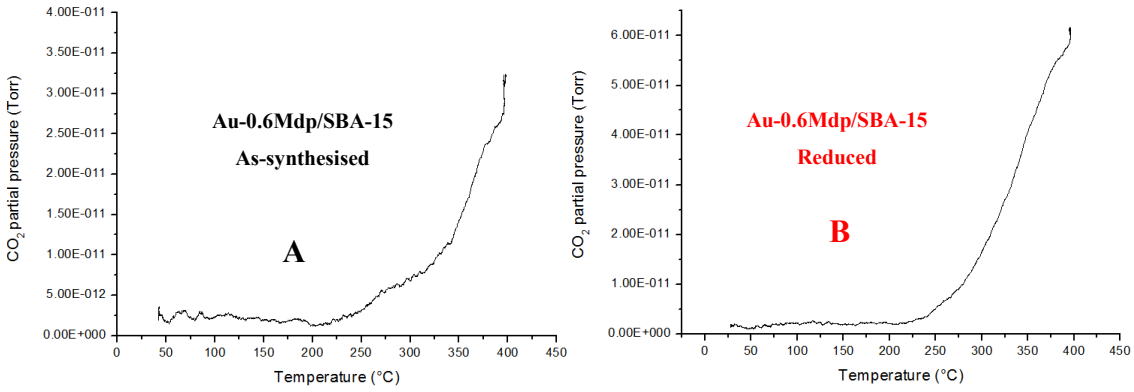

Figure 157. CO_2 response from TPRx of BTEXB over as-synthesised (A) and reduced (B) Au-0.6Mdp/SBA-15 catalyst

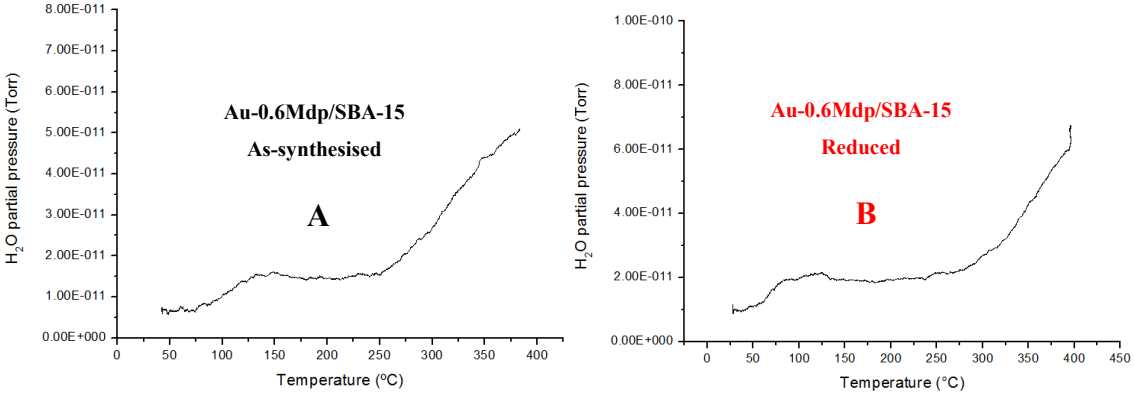

Figure 158. H_2O response from TPRx of BTEXB over as-synthesised (A) and reduced (B) Au-0.6Mdp/SBA-15 catalyst

As shown in Figures 157 - 158, the reduced form of Au-0.6Mdp/SBA-15 catalyst was more active than the as-synthesised form of the catalyst in complete oxidation of BTEXB mixture, having produced more CO_2 from 250 – 400 ºC. This indicates a higher BTEXB conversion with the reduced catalyst.

7.9. Dichloromethane complete oxidation

Chlorinated VOCs, such as dichloromethane, are very stable and difficult to oxidise completely at low temperature, with reported catalysts operating between 312 – 487 °C. Complete oxidation of the chlorinated VOCs produces hydrogen chloride or chlorine, which are poisons to most catalysts used in VOCs oxidation. The best Au-0.6Mdp/SBA-15 catalyst (as-synthesised and reduced forms) was tested in TPRx complete oxidation of dichloromethane, from room temperature to 400 °C. The experimental procedure was discussed in Chapter 3.

As seen in Figures 159A – 161A, there is complete oxidation of dichloromethane over as-synthesised Au-0.6Mdp/SBA-15 catalyst, with light off temperature starting at 290 °C and attaining 100 % conversion at 305 °C. This is confirmed by the corresponding formation CO_2 and H_2O. Detection and analysis of HCl/Cl_2 was not carried out due to none availability of appropriate analytical instruments such as electrolytic conductivity detector (ELCD).

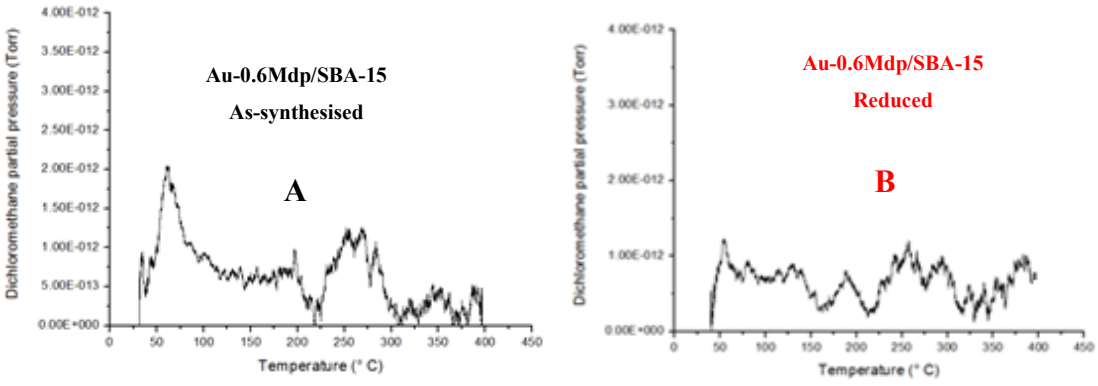

Figure 159. Dichloromethane complete oxidation over as-synthesised (A) and reduced (B) Au-0.6Mdp/SBA-15 catalyst

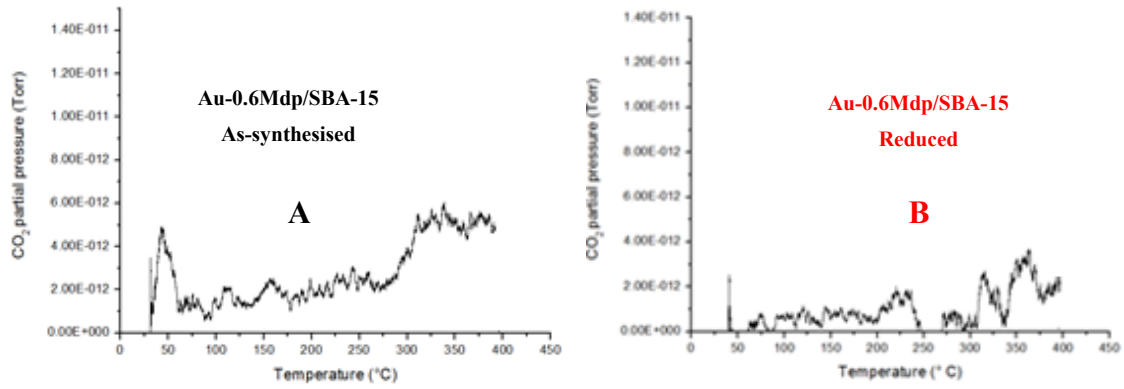

Figure 160. Dichloromethane complete oxidation (CO_2 response) over as-synthesised (A) and reduced (B) Au-0.6Mdp/SBA-15 catalyst

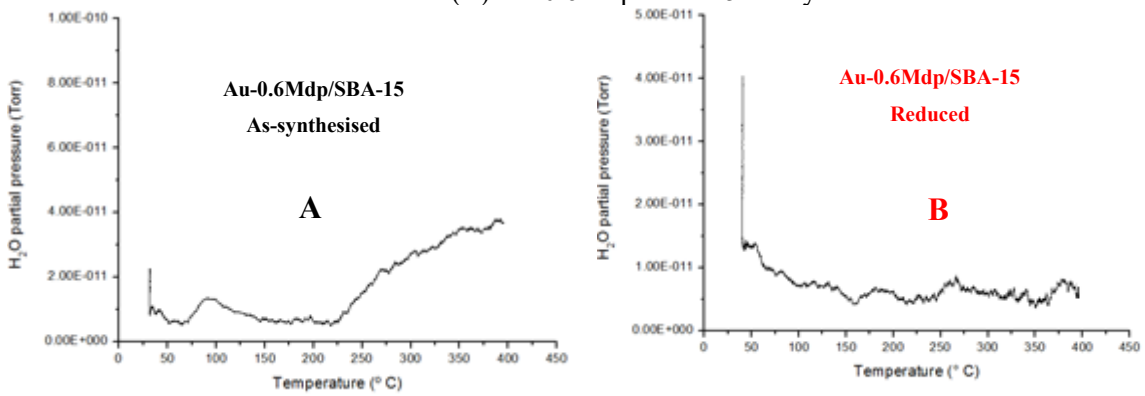

Figure 161. Dichloromethane complete oxidation (H_2O response) over as-synthesised (A) and reduced (B) Au-0.6Mdp/SBA-15 catalyst

The reduced form of Au-0.6Mdp/SBA-15 catalyst was inactive in oxidation of dichloromethane as observed from TPRx results shown in Figures 159B – 161B. The M-S partial pressures of dichloromethane, CO_2 and H_2O remained the same from initial reaction temperature to 400 °C. It is possible that the metallic gold in reduced Au/SBA-15 (Au^0) was strongly attached to chlorine to form stable gold chloride, thereby poising the catalyst for any possible oxidation of chlorinated VOCs. In conclusion therefore, it seems that only the as-synthesised form of Au/SBA-15 catalyst is suitable for the complete oxidation of chlorinated VOCs and not the reduced form. However, there is the need for further study and investigation into this matter.

7.10. Conclusions

An attempt was made in this research project to design and synthesise the best Au/SBA-15 catalyst, active for low temperature oxidation of VOCs. A novel Au/SBA-15 catalyst (Au-0.6Mdp/SBA-15 catalyst), with the highest ever reported surface area of 726 m^2/g, having well dispersed and firmly attached small gold nano-particles of 1.3 nm was developed. These excellent physical properties are responsible for its high catalytic performance in complete oxidation of VOCs at low temperatures. Along with this catalyst, five other Au/SBA-15 catalysts were synthesised and characterised. The following were found: Gold particles sizes greatly influenced the catalytic activates of the Au/SBA-15 catalysts, as the Au/SBA-15 catalysts with the smaller gold particles were more active than catalysts with bigger gold sizes. Size control of Au nanoparticles on SBA-15 mainly depend on the catalyst preparation method. One-pot synthesis of Au/SBA-15 catalyst with pre-determined amount of MPTMS produced the smallest gold nano-particles compared to the other synthetic methods, with the gold nano-particles highly dispersed and firmly attached to the SBA-15. The reason for the excellent result is due to the homogenous functionalisation of SBA-15 with MPTMS in one-pot synthesis, with minimal damage done to the SBA-15 meso-structure. The carefully selected procedure to produce SBA-15 with thicker pore walls prevented any significant damage to the SBA-15 meso-structure during functionalisation, calcination and gold loading, thereby preserving its high surface area. Thicker pore walls also improved catalyst structural stability, hydrothermal stability and catalyst resistance to gold sintering during the course of VOCs oxidation.

In terms of which oxidation state is most active (as-synthesised or hydrogen reduced), the following were observed:

1. Hydrogen reduced Au/SBA-15 catalysts were more active than their as-synthesised forms in complete oxidation of non-chlorinated VOCs such as acetone, propane and BTEXB.
2. There was a pronounced difference in the catalytic performance of the reduced and as-synthesised forms of Au/SBA-15 catalyst in complete oxidation of dichloromethane. Only the as-synthesised form of Au/SBA-15 catalyst was active. The reason for the inactivity of the reduced Au/SBA-15 catalyst could be that it was instantly poisoned and rendered inactive from the formation of stable gold chloride on the catalyst surface, as chlorine quickly reacted with Au^0. The as-synthesised catalyst was resistant to chlorine poisoning as it attained complete conversion of dichloromethane, starting at 290 ºC and attaining 100 % conversion at 305 ºC, which are the lowest temperatures ever reported for complete oxidation of dichloromethane.

Form the above observations, it is most probable that hydrogen reduction of cationic gold to metallic gold occurred at low temperature (below 50 ºC) as there was significant difference in the catalytic performances of the two forms of the Au/SBA-15 catalysts. However, further investigations and characterisations are required to better understand and explain the oxidation states of gold in Au/SBA-15 catalysts after hydrogen reduction and during VOC oxidation reactions.

The as-synthesised and reduced forms of the best Au/SBA-15 catalyst (Au-0.6Mdp/SBA-15 catalyst) were very stable over 25 hours test duration, maintaining high VOC conversion rates in complete oxidation of acetone at 270 ºC and 220 ºC respectively, and propane complete oxidation at 300 ºC for the reduced Au-0.6Mdp/SBA-15 catalyst.

A micro-reactor device was successfully designed and fabricated for the purpose of coating the best Au/SBA-15 catalyst in the channels [143] as an innovative idea in using less energy

to heat up the catalyst, and also use less expensive catalyst by the novel coating technique developed. The Au/SBA-15 catalyst (Au-0.6Mdp/SBA-15 catalyst) coated micro-reactor produced a much higher VOC (propane as model compound) conversion at lower temperatures compared to published catalysts as shown in Appendices.

Although gold is significantly more expensive than most metals used in catalysis, the amount of gold added in the synthesis of Au/SBA-15 catalyst is relatively low (0.08 g per 1.00g of SBA-15 support). The synthesis of Au/SBA-15 catalyst can also be improved upon by using lesser amount of gold. Also, the use of coated micro-reactor drastically reduces the amount of used Au/SBA-15 catalyst from 50 mg used in the conventional fixed bed reactor to 2.5 mg. Therefore, the cost of Au/SBA-15 coated micro-reactor is expected to be less significant compared to the high and stable catalytic conversion of VOCs it offers.

Appendices A - C compares the catalyst performance of the novel Au/SBA-15 catalyst to other published catalysts for VOC complete oxidation, and the results show that it is one of the most active, stable and versatile catalyst suitable for elimination of indoor VOCs at low temperatures.

7.11. Recommendations and further studies

The complete oxidation of propane was done using a very high propane concentration in air (24, 000 - 37, 000 ppm), over a small amount of Au/SBA-15 catalyst with high reactant flowrates, making it impossible to achieve 100 % propane conversions. It is therefore recommended that a much lower propane concentration (200 – 5000 ppm) be used to determine propane conversions using lower reactant flowrates in the conventional fixed bed and also in the catalyst coated micro-reactor. The study on the complete oxidation of VOCs mixture (BTEXB) over Au/SBA-15 catalyst can be improved upon, by first analysing the complete oxidation of individual VOCs and then comparing them in their mixture. Again, it was difficult to monitor the M-S partial pressure readings of individual VOCs in BTEXB

mixture. In the case of complete oxidation of dichloromethane, HCl/Cl_2 products were not monitored. It is therefore recommended that, in addition to the used of the quadrupole mass spectrometer for detection and analysis of reactants and products, other analytical techniques, such as online FT-IR, gas chromatograph equipped with an electrolytic conductivity detector (ELCD) (to detect chlorinated VOCs and products) be included [162]. Also, other detectors such as online gas chromatograph equipped with flame ionisation detector (GC-FID) with gas standards of individual BTEXB concentrations injected before BTEXB oxidation can be used to determine conversion of each compound, in addition to the use of thermal conductivity detector for sensing any presence of CO in the product streams [163].

There is also the need to study in detail, the effect of water vapour on VOC oxidation over Au/SBA-15 catalyst. This can be done by introducing small to large amounts of water vapour in the VOCs reactant gas streams to assess any inhibitory or promotional effects of water on the catalyst and in the catalytic performance of VOCs complete oxidation.

References

[1] H. Huang, Y. Xu, Q. Feng, D.Y.C. Leung, Low temperature catalytic oxidation of volatile organic compounds: a review, Catalysis Science & Technology, 5 (2015) 2649-2669.
[2] M. Haruta, T. Kobayashi, H. Sano, N. Yamada, Novel gold catalysts for the oxidation of carbon monoxide at a temperature far below 0. DEG. C, Chemistry Letters, (1987) 405-408.
[3] G.C. Bond, Gold: a relatively new catalyst, Catalysis Today, 72 (2002) 5-9.
[4] S. Scirè, L.F. Liotta, Supported gold catalysts for the total oxidation of volatile organic compounds, Applied Catalysis B: Environmental, 125 (2012) 222-246.
[5] M. Haruta, Size-and support-dependency in the catalysis of gold, Catalysis Today, 36 (1997) 153-166.
[6] M. Haruta, Gold as a novel catalyst in the 21st century: preparation, working mechanism and applications, Gold bulletin, 37 (2004) 27-36.
[7] G.C. Bond, C. Louis, D.T. Thompson, Catalysis by gold, Gold Bulletin, 39 (2006) 3.
[8] S. Minicò, S. Scirè, C. Crisafulli, R. Maggiore, S. Galvagno, Catalytic combustion of volatile organic compounds on gold/iron oxide catalysts, Applied Catalysis B: Environmental, 28 (2000) 245-251.
[9] J. Qi, J. Chen, G. Li, S. Li, Y. Gao, Z. Tang, Facile synthesis of core-shell Au@CeO2 nanocomposites with remarkably enhanced catalytic activity for CO oxidation, Energy & Environmental Science, 5 (2012) 8937-8941.
[10] P. Wu, P. Bai, Z. Lei, K.P. Loh, X.S. Zhao, Gold nanoparticles supported on functionalized mesoporous silica for selective oxidation of cyclohexane, Microporous and Mesoporous Materials, 141 (2011) 222-230.
[11] M.T. Bore, H.N. Pham, T.L. Ward, A.K. Datye, Role of pore curvature on the thermal stability of gold nanoparticles in mesoporous silica, Chemical Communications, (2004) 2620-2621.
[12] K. Zhu, J. Hu, R. Richards, Aerobic oxidation of cyclohexane by gold nanoparticles immobilized upon mesoporous silica, Catalysis letters, 100 (2005) 195-199.
[13] V.H. Grassian, Environmental catalysis, CRC press, 2005.
[14] M. Maroni, Bernd Seifert, and Thomas Lindvall, eds. Indoor air quality: a comprehensive reference book. Vol. 3. Elsevier, 1995.
[15] M. Shao, S. Lu, Y. Liu, X. Xie, C. Chang, S. Huang, Z. Chen, Volatile organic compounds measured in summer in Beijing and their role in ground-level ozone formation, Journal of Geophysical Research: Atmospheres, 114 (2009) n/a-n/a.
[16] Minnesota Department of Health. (2016). Volatile organic compounds (VOCs) in your home. [Online] Available at: www.health.state.mn.us/divs/eh/indoorair/voc/. [Accessed 22 August 2016].
[17] I.E. Sungkono, H. Kameyama, T. Koya, Iketani-6Development of catalytic combustion technology of VOC materials by anodic oxidation catalyst, Applied Surface Science, 121 (1997) 425-428.
[18] S. Zuo, R. Zhou, Al-pillared clays supported rare earths and palladium catalysts for deep oxidation of low concentration of benzene, Applied Surface Science, 253 (2006) 2508-2514.
[19] J. Li, C. Ma, X. Xu, J. Yu, Z. Hao, S. Qiao, Efficient Elimination of Trace Ethylene over Nano-Gold Catalyst under Ambient Conditions, Environmental Science & Technology, 42 (2008) 8947-8951.
[20] W.B. Li, J.X. Wang, H. Gong, Catalytic combustion of VOCs on non-noble metal catalysts, Catalysis Today, 148 (2009) 81-87.

[21] H.L. Tidahy, S. Siffert, F. Wyrwalski, J.F. Lamonier, A. Aboukaïs, Catalytic activity of copper and palladium based catalysts for toluene total oxidation, Catalysis Today, 119 (2007) 317-320.
[22] M. Taylor, E.N. Ndifor, T. Garcia, B. Solsona, A.F. Carley, S.H. Taylor, Deep oxidation of propane using palladium–titania catalysts modified by niobium, Applied Catalysis A: General, 350 (2008) 63-70.
[23] B. Solsona, T.E. Davies, T. Garcia, I. Vázquez, A. Dejoz, S.H. Taylor, Total oxidation of propane using nanocrystalline cobalt oxide and supported cobalt oxide catalysts, Applied Catalysis B: Environmental, 84 (2008) 176-184.
[24] B. Solsona, T. Garcia, E. Aylón, A.M. Dejoz, I. Vázquez, S. Agouram, T.E. Davies, S.H. Taylor, Promoting the activity and selectivity of high surface area Ni–Ce–O mixed oxides by gold deposition for VOC catalytic combustion, Chemical Engineering Journal, 175 (2011) 271-278.
[25] M.R. Morales, B.P. Barbero, L.E. Cadús, Total oxidation of ethanol and propane over Mn-Cu mixed oxide catalysts, Applied Catalysis B: Environmental, 67 (2006) 229-236.
[26] M.S. Kamal, S.A. Razzak, M.M. Hossain, Catalytic oxidation of volatile organic compounds (VOCs) – A review, Atmospheric Environment, 140 (2016) 117-134.
[27] G.F. Bennett, Air pollution: David H.F. Liu and Bela G. Liptak, Eds., Paul A. Bouis, Special Consultant, Lewis Publishers, Boca Raton, FL, 2000, US$59.95, 242 pp., 8 1/2 by 11-in. format. ISBN: 1-56670-513-4, Journal of Hazardous Materials, 77 (2000) 269-270.
[28] J. Okal, M. Zawadzki, W. Tylus, Microstructure characterization and propane oxidation over supported Ru nanoparticles synthesized by the microwave-polyol method, Applied Catalysis B: Environmental, 101 (2011) 548-559.
[29] M. Tomatis, H.-H. Xu, J. He, X.-D. Zhang, Recent Development of Catalysts for Removal of Volatile Organic Compounds in Flue Gas by Combustion: A Review, Journal of Chemistry, 2016 (2016) 15.
[30] C. Zhang, H. He, K.-i. Tanaka, Perfect catalytic oxidation of formaldehyde over a Pt/TiO2 catalyst at room temperature, Catalysis Communications, 6 (2005) 211-214.
[31] C. Zhang, H. He, A comparative study of TiO2 supported noble metal catalysts for the oxidation of formaldehyde at room temperature, Catalysis Today, 126 (2007) 345-350.
[32] C. Zhang, H. He, K.-i. Tanaka, Catalytic performance and mechanism of a Pt/TiO2 catalyst for the oxidation of formaldehyde at room temperature, Applied Catalysis B: Environmental, 65 (2006) 37-43.
[33] J. Peng, S. Wang, Performance and characterization of supported metal catalysts for complete oxidation of formaldehyde at low temperatures, Applied Catalysis B: Environmental, 73 (2007) 282-291.
[34] S. Ordóñez, L. Bello, H. Sastre, R. Rosal, F.V. Díez, Kinetics of the deep oxidation of benzene, toluene, n-hexane and their binary mixtures over a platinum on γ-alumina catalyst, Applied Catalysis B: Environmental, 38 (2002) 139-149.
[35] L.M. Gandía, M.A. Vicente, A. Gil, Complete oxidation of acetone over manganese oxide catalysts supported on alumina- and zirconia-pillared clays, Applied Catalysis B: Environmental, 38 (2002) 295-307.
[36] H. Huang, Y. Xu, Q. Feng, D.Y. Leung, Low temperature catalytic oxidation of volatile organic compounds: a review, Catalysis Science & Technology, 5 (2015) 2649-2669.
[37] Tomatis, Marco, et al. "Recent Development of Catalysts for Removal of Volatile Organic Compounds in Flue Gas by Combustion: A Review." Journal of Chemistry 2016 (2016).
[38] Q.H. Xia, K. Hidajat, S. Kawi, Adsorption and catalytic combustion of aromatics on platinum-supported MCM-41 materials, Catalysis Today, 68 (2001) 255-262.

[39] R.H. Harris, V.J. Boyd, G.J. Hutchings, S.H. Taylor, Water as a Promoter of the Complete Oxidation of Volatile Organic Compounds over Uranium Oxide Catalysts, Catalysis Letters, 78 (2002) 369-372.
[40] G. Zhao, Z. Zhao, J. Wu, D. Ye, Performance of a Novel Hydrophobic Mesoporous Material for High Temperature Catalytic Oxidation of Naphthalene, Journal of Spectroscopy, 2014 (2014) 7.
[41] F. Zhang, Y. Yan, H. Yang, Y. Meng, C. Yu, B. Tu, D. Zhao, Understanding Effect of Wall Structure on the Hydrothermal Stability of Mesostructured Silica SBA-15, The Journal of Physical Chemistry B, 109 (2005) 8723-8732.
[42] D. Zhao, Q. Huo, J. Feng, B.F. Chmelka, G.D. Stucky, Nonionic triblock and star diblock copolymer and oligomeric surfactant syntheses of highly ordered, hydrothermally stable, mesoporous silica structures, Journal of the American Chemical Society, 120 (1998) 6024-6036.
[43] P. Papaefthimiou, T. Ioannides, X.E. Verykios, Combustion of non-halogenated volatile organic compounds over group VIII metal catalysts, Applied Catalysis B: Environmental, 13 (1997) 175-184.
[44] E. Noordally, J.R. Richmond, S.F. Tahir, Destruction of volatile organic compounds by catalytic oxidation, Catalysis Today, 17 (1993) 359-366.
[45] P. Gélin, M. Primet, Complete oxidation of methane at low temperature over noble metal based catalysts: a review, Applied Catalysis B: Environmental, 39 (2002) 1-37.
[46] S. Huang, C. Zhang, H. He, Complete oxidation of o-xylene over Pd/Al2O3 catalyst at low temperature, Catalysis Today, 139 (2008) 15-23.
[47] G. Centi, Supported palladium catalysts in environmental catalytic technologies for gaseous emissions, Journal of Molecular Catalysis A: Chemical, 173 (2001) 287-312.
[48] Y. Wang, C. Zhang, F. Liu, H. He, Well-dispersed palladium supported on ordered mesoporous Co3O4 for catalytic oxidation of o-xylene, Applied Catalysis B: Environmental, 142–143 (2013) 72-79.
[49] K. Okumura, T. Kobayashi, H. Tanaka, M. Niwa, Toluene combustion over palladium supported on various metal oxide supports, Applied Catalysis B: Environmental, 44 (2003) 325-331.
[50] S.-K. Ihm, Y.-D. Jun, D.-C. Kim, K.-E. Jeong, Low-temperature deactivation and oxidation state of Pd/γ-Al2O3 catalysts for total oxidation of n-hexane, Catalysis Today, 93–95 (2004) 149-154.
[51] E.M. Cordi, J.L. Falconer, Oxidation of Volatile Organic Compounds on Al2O3, Pd/Al2O3, and PdO/Al2O3Catalysts, Journal of Catalysis, 162 (1996) 104-117.
[52] J. Bedia, J.M. Rosas, J. Rodríguez-Mirasol, T. Cordero, Pd supported on mesoporous activated carbons with high oxidation resistance as catalysts for toluene oxidation, Applied Catalysis B: Environmental, 94 (2010) 8-18.
[53] M. Li, D. Weng, X. Wu, J. Wan, B. Wang, Importance of re-oxidation of palladium by interaction with lanthana for propane combustion over Pd/Al2O3 catalyst, Catalysis Today, 201 (2013) 19-24.
[54] H.L. Tidahy, S. Siffert, J.F. Lamonier, R. Cousin, E.A. Zhilinskaya, A. Aboukaïs, B.L. Su, X. Canet, G. De Weireld, M. Frère, J.M. Giraudon, G. Leclercq, Influence of the exchanged cation in Pd/BEA and Pd/FAU zeolites for catalytic oxidation of VOCs, Applied Catalysis B: Environmental, 70 (2007) 377-383.
[55] H.L. Tidahy, S. Siffert, J.F. Lamonier, E.A. Zhilinskaya, A. Aboukaïs, Z.Y. Yuan, A. Vantomme, B.L. Su, X. Canet, G. De Weireld, M. Frère, T.B. N'Guyen, J.M. Giraudon, G. Leclercq, New Pd/hierarchical macro-mesoporous ZrO2, TiO2 and ZrO2-TiO2 catalysts for VOCs total oxidation, Applied Catalysis A: General, 310 (2006) 61-69.

[56] S.-W. Baek, J.-R. Kim, S.-K. Ihm, Design of dual functional adsorbent/catalyst system for the control of VOC's by using metal-loaded hydrophobic Y-zeolites, Catalysis Today, 93–95 (2004) 575-581.
[57] Z. Qu, S. Shen, D. Chen, Y. Wang, Highly active Ag/SBA-15 catalyst using post-grafting method for formaldehyde oxidation, Journal of Molecular Catalysis A: Chemical, 356 (2012) 171-177.
[58] D. Chen, Z. Qu, S. Shen, X. Li, Y. Shi, Y. Wang, Q. Fu, J. Wu, Comparative studies of silver based catalysts supported on different supports for the oxidation of formaldehyde, Catalysis Today, 175 (2011) 338-345.
[59] D. Delimaris, T. Ioannides, VOC oxidation over MnOx–CeO2 catalysts prepared by a combustion method, Applied Catalysis B: Environmental, 84 (2008) 303-312.
[60] S.C. Kim, The catalytic oxidation of aromatic hydrocarbons over supported metal oxide, Journal of Hazardous Materials, 91 (2002) 285-299.
[61] S. Wang, H. Ang, M.O. Tade, Volatile organic compounds in indoor environment and photocatalytic oxidation: state of the art, Environment international, 33 (2007) 694-705.
[62] V.H. Vu, J. Belkouch, A. Ould-Dris, B. Taouk, Removal of hazardous chlorinated VOCs over Mn–Cu mixed oxide based catalyst, Journal of Hazardous Materials, 169 (2009) 758-765.
[63] X. Liu, D. Wang, Y. Li, Synthesis and catalytic properties of bimetallic nanomaterials with various architectures, Nano Today, 7 (2012) 448-466.
[64] T. Barakat, J.C. Rooke, M. Franco, R. Cousin, J.-F. Lamonier, J.-M. Giraudon, B.-L. Su, S. Siffert, Pd- and/or Au-Loaded Nb- and V-Doped Macro-Mesoporous TiO2 Supports as Catalysts for the Total Oxidation of VOCs, European Journal of Inorganic Chemistry, 2012 (2012) 2812-2818.
[65] A. Bongiorno, U. Landman, Water-Enhanced Catalysis of CO Oxidation on Free and Supported Gold Nanoclusters, Physical Review Letters, 95 (2005) 106102.
[66] R.A. Ojifinni, N.S. Froemming, J. Gong, M. Pan, T.S. Kim, J.M. White, G. Henkelman, C.B. Mullins, Water-Enhanced Low-Temperature CO Oxidation and Isotope Effects on Atomic Oxygen-Covered Au(111), Journal of the American Chemical Society, 130 (2008) 6801-6812.
[67] K. Wong, Q. Zeng, A. Yu, Gold catalysts: A new insight into the molecular adsorption and CO oxidation, Chemical Engineering Journal, 155 (2009) 824-828.
[68] F. Bertinchamps, A. Attianese, M.M. Mestdagh, E.M. Gaigneaux, Catalysts for chlorinated VOCs abatement: Multiple effects of water on the activity of VOx based catalysts for the combustion of chlorobenzene, Catalysis Today, 112 (2006) 165-168.
[69] K. Poplawski, J. Lichtenberger, F.J. Keil, K. Schnitzlein, M.D. Amiridis, Catalytic oxidation of 1,2-dichlorobenzene over ABO3-type perovskites, Catalysis Today, 62 (2000) 329-336.
[70] H. Windawi, M. Wyatt, Catalytic Destruction of Halogenated Volatile Organic Compounds, Platinum Metals Review, 37 (1993) 186-193.
[71] M. Daté, M. Okumura, S. Tsubota, M. Haruta, Vital Role of Moisture in the Catalytic Activity of Supported Gold Nanoparticles, Angewandte Chemie International Edition, 43 (2004) 2129-2132.
[72] D. Zhao, J. Feng, Q. Huo, N. Melosh, G.H. Fredrickson, B.F. Chmelka, G.D. Stucky, Triblock Copolymer Syntheses of Mesoporous Silica with Periodic 50 to 300 Angstrom Pores, Science, 279 (1998) 548-552.
[73] A. Wolf, F. Schüth, A systematic study of the synthesis conditions for the preparation of highly active gold catalysts, Applied Catalysis A: General, 226 (2002) 1-13.

[74] W. Vogel, D.A.H. Cunningham, K. Tanaka, M. Haruta, Structural analysis of Au/Mg(OH)2 during deactivation by Debye function analysis, Catalysis Letters, 40 (1996) 175-181.
[75] M. Okumura, S. Nakamura, S. Tsubota, T. Nakamura, M. Azuma, M. Haruta, Chemical vapor deposition of gold on Al2O3, SiO2, and TiO2 for the oxidation of CO and of H2, Catalysis Letters, 51 (1998) 53-58.
[76] L. Zhou, J. Hu, S. Xie, H. Liu, Dispersion of Active Au Nanoparticles on Mesoporous SBA-15 Materials1, Chinese Journal of Chemical Engineering, 15 (2007) 507-511.
[77] Gutiérrez, Luis-Felipe, Safia Hamoudi, and Khaled Belkacemi. "Synthesis of gold catalysts supported on mesoporous silica materials: recent developments." Catalysts 1.1 (2011): 97-154.
[78] H. Zhu, Z. Ma, J.C. Clark, Z. Pan, S.H. Overbury, S. Dai, Low-temperature CO oxidation on Au/fumed SiO2-based catalysts prepared from Au(en)2Cl3 precursor, Applied Catalysis A: General, 326 (2007) 89-99.
[79] C.-m. Yang, M. Kalwei, F. Schüth, K.-j. Chao, Gold nanoparticles in SBA-15 showing catalytic activity in CO oxidation, Applied Catalysis A: General, 254 (2003) 289-296.
[80] Ma, Zhen, and Francisco Zaera. "Characterization of heterogeneous catalysts." Surface and Nanomolecular Catalysis (2006): 1-37.
[81] NPTEL, Chemical Engineering, Catalyst Science and Technology, Introduction & surface area analysis, Module 2: Heterogeneous catalysis, Lecture 10: Catalyst characterisation, (2004), Available at http://nptel.ac.in/courses/103103026/11 [Accessed 29 August 2016].
[82] Goldstein, Joseph, et al. Scanning electron microscopy and X-ray microanalysis: a text for biologists, materials scientists, and geologists. Springer Science & Business Media, 2012.
[83] A. Laskin, J.P. Cowin, Automated Single-Particle SEM/EDX Analysis of Submicrometer Particles down to 0.1 μm, Analytical Chemistry, 73 (2001) 1023-1029.
[84] Characterisation techniques chapter 2.2, [Online], Available at http://www.tdx.cat/bitstream/handle/10803/8595/13.pdf.txt?sequence=80. [Assessed 30 August 2016].
[85] Baerns, Manfred, ed. Basic principles in applied catalysis. Vol. 75. Springer Science & Business Media, 2013.
[86] Z.L. Wang, Transmission Electron Microscopy of Shape-Controlled Nanocrystals and Their Assemblies, The Journal of Physical Chemistry B, 104 (2000) 1153-1175.
[87] Ashcroft, Neil W., and N. David Mermin. "Solid state physics." (1976).
[88] A.W. Hull, A new method of chemical analysis, Journal of the American Chemical Society, 41 (1919) 1168-1175.
[89] B.E. Warren, Identification of crystalline substances by means of X-rays , Journal of the American Ceramic Society, 17 (1934) 73-77.
[90] Bragg, William Henry, and William Lawrence Bragg. "The reflection of X-rays by crystals." Proceedings of the Royal Society of London. Series A, Containing Papers of a Mathematical and Physical Character 88.605 (1913): 428-438.
[91] Moore, Duane Milton, and Robert C. Reynolds. X-ray Diffraction and the Identification and Analysis of Clay Minerals. Vol. 378. Oxford: Oxford university press, 1989.
[92] E.R. Crain, Crain's Petrophysical Handbook, 2000, [Online], Available at: www.spec2000.net/09-xrd.htm [Assessed 30 August 2016].
[93] A.L. Patterson, The Scherrer Formula for X-Ray Particle Size Determination, Physical Review, 56 (1939) 978-982.

[94] FT-IR spectroscopy (Fourier Transform Infrared), 2013, [Online]. Available at: http://chemistry.oregonstate.edu/courses/ch361-464/ch362/irinstrs.htm [Assessed 30 August 2016].
[95] National Science Foundation, How an FT-IR spectrometer operates, 2015, [Online], Available: http://chemwiki.ucdavis.edu/Core/Physical_Chemistry/Spectroscopy/Vibrational_Spectroscopy/Infrared_Spectroscopy/How_an_FTIR_Spectrometer_Operates.
[96] Griffiths, Peter R., and James A. De Haseth. Fourier transform infrared spectrometry. Vol. 171. John Wiley & Sons, 2007.
[97] P.B. Balbuena, K.E. Gubbins, Theoretical interpretation of adsorption behavior of simple fluids in slit pores, Langmuir, 9 (1993) 1801-1814.
[98] Brunauer, Stephen, Paul Hugh Emmett, and Edward Teller. "Adsorption of gases in multimolecular layers." Journal of the American chemical society60.2 (1938): 309-319.
[99] J.P. Thielemann, F. Girgsdies, R. Schlögl, C. Hess, Pore structure and surface area of silica SBA-15: influence of washing and scale-up, Beilstein Journal of Nanotechnology, 2 (2011) 110-118.
[100] Hiden Analytical CATLAB – PCS, A system for catalyst characterisation, kinetic and thermodynamic measurements, 2016 [Online], Avaialble at: www.hidenanalytical.com/products/for-catalysis-and-thermal-analysis/catlab-pcs/

[101] S.D. Robertson, B.D. McNicol, J.H. De Baas, S.C. Kloet, J.W. Jenkins, Determination of reducibility and identification of alloying in copper-nickel-on-silica catalysts by temperature-programmed reduction, Journal of Catalysis, 37 (1975) 424-431.
[102] A. Jones and B. D. McNicol, "Temperature Programmed Reduction for Solid Materials Characterization", CRC Press, Boca Raton, Florida, 1986.
[103] F. Arena, F. Frusteri, A. Parmaliana, N. Giordano, Temperature-programmed reaction: A powerful and reliable method for catalyst testing in the partial oxidation of methane to formaldehyde, Applied Catalysis A: General, 125 (1995) 39-59.
[104] Bhatia, Shyam, J. Beltramini, and D. D. Do. "Temperature programmed analysis and its applications in catalytic systems." Catalysis Today 7.3 (1990): 309-438.
[105] H. Xiong, H.N. Pham, A.K. Datye, Hydrothermally stable heterogeneous catalysts for conversion of biorenewables, Green Chemistry, 16 (2014) 4627-4643.
[106] Sing, Kenneth SW. "Reporting physisorption data for gas/solid systems with special reference to the determination of surface area and porosity (Recommendations 1984)." Pure and applied chemistry 57.4 (1985): 603-619.
[107] A. Corma, From Microporous to Mesoporous Molecular Sieve Materials and Their Use in Catalysis, Chemical Reviews, 97 (1997) 2373-2420.
[108] C. Perego, R. Millini, Porous materials in catalysis: challenges for mesoporous materials, Chemical Society Reviews, 42 (2013) 3956-3976.
[109] N. Kanellopoulous, Nanoporous Materials: Advanced Techniques for Characterization, Modeling, and Processing, in, Boca Raton, Fla. : London : CRC Press, London, 2011, pp. 578.
[110] H.C. Francesco Di Renzo, Roger Dutartre, A 28-year-old synthesis of micelle-templated mesoporous silica, Microporous Materials, 10 (1997) 283-286.
[111] S. Cabrera, J.E. Haskouri, J. Alamo, A. Beltrán, D. Beltrán, S. Mendioroz, M.D. Marcos, P. Amorós, Surfactant-Assisted Synthesis of Mesoporous Alumina Showing Continuously Adjustable Pore Sizes, Advanced Materials, 11 (1999) 379-381.
[112] J.S. Beck, J.C. Vartuli, W.J. Roth, M.E. Leonowicz, C.T. Kresge, K.D. Schmitt, C.T.W. Chu, D.H. Olson, E.W. Sheppard, A new family of mesoporous molecular sieves

prepared with liquid crystal templates, Journal of the American Chemical Society, 114 (1992) 10834-10843.
[113] E.M. Johansson, Controlling the Pore Size and Morphology of Mesoporous Silica, in: Linköping University, Department of Physics, Chemistry and Biology, Nanostructured Materials . Linköping University, The Institute of Technology., Linköping University, Linköping: Linköping University Electronic Press, 2010. 67 p, 2010, pp. 67.
[114] F. Hoffmann, M. Cornelius, J. Morell, M. Fröba, Silica-Based Mesoporous Organic–Inorganic Hybrid Materials, Angewandte Chemie International Edition, 45 (2006) 3216-3251.
[115] National Center for Biotechnology Information, 2005, [Online] PubChem Compound Database; CID=12682, Available at: https://pubchem.ncbi.nlm.nih.gov/compound/12682 [accessed 13 June, 2016].
[116] E.B. Jørgensen, S. Hvidt, W. Brown, K. Schillén, Effects of Salts on the Micellization and Gelation of a Triblock Copolymer Studied by Rheology and Light Scattering, Macromolecules, 30 (1997) 2355-2364.
[117] J.K. Armstrong, B.Z. Chowdhry, M.J. Snowden, S.A. Leharne, Effect of Sodium Chloride upon Micellization and Phase Separation Transitions in Aqueous Solutions of Triblock Copolymers: A High-Sensitivity Differential Scanning Calorimetry Study, Langmuir, 14 (1998) 2004-2010.
[118] N.J. Jain, V.K. Aswal, P.S. Goyal, P. Bahadur, Micellar Structure of an Ethylene Oxide−Propylene Oxide Block Copolymer: A Small-Angle Neutron Scattering Study, The Journal of Physical Chemistry B, 102 (1998) 8452-8458.
[119] T. Yamada, H. Zhou, K. Asai, I. Honma, Pore size controlled mesoporous silicate powder prepared by triblock copolymer templates, Materials Letters, 56 (2002) 93-96.
[120] F. Soxhlet, The gravimetric determination of milk fat, Digitalisierung Des Polytechnischen Journals, 232 (1879) 461 - 465.
[121] Q. Wei, H.-Q. Chen, Z.-R. Nie, Y.-L. Hao, Y.-L. Wang, Q.-Y. Li, J.-X. Zou, Preparation and characterization of vinyl-functionalized mesoporous SBA-15 silica by a direct synthesis method, Materials Letters, 61 (2007) 1469-1473.
[122] H. Cui, Y. Zhang, Z. Qiu, L. Zhao, Y. Zhu, Synthesis and characterization of cobalt-substituted SBA-15 and its high activity in epoxidation of styrene with molecular oxygen, Applied Catalysis B: Environmental, 101 (2010) 45-53.
[123] S.G. de Ávila, L.C.C. Silva, J.R. Matos, Optimisation of SBA-15 properties using Soxhlet solvent extraction for template removal, Microporous and Mesoporous Materials, 234 (2016) 277-286.
[124] B. Tian, X. Liu, C. Yu, F. Gao, Q. Luo, S. Xie, B. Tu, D. Zhao, Microwave assisted template removal of siliceous porous materials, Chemical Communications, (2002) 1186-1187.
[125] Y.K. Bae, O.H. Han, Removal of copolymer template from SBA-15 studied by 1H MAS NMR, Microporous and Mesoporous Materials, 106 (2007) 304-307.
[126] D. Margolese, J.A. Melero, S.C. Christiansen, B.F. Chmelka, G.D. Stucky, Direct Syntheses of Ordered SBA-15 Mesoporous Silica Containing Sulfonic Acid Groups, Chemistry of Materials, 12 (2000) 2448-2459.
[127] R.J.P. Corriu, A. Mehdi, C. Reye, C. Thieuleux, A. Frenkel, A. Gibaud, Preparation of ordered SBA-15 mesoporous silica containing chelating groups. Study of the complexation of Euiii inside the pore channels of the materials, New Journal of Chemistry, 28 (2004) 156-160.
[128] G.W.S. C. Jeffrey Brinker, Sol-Gel Science. The Physics and Chemistry of Sol-Gel Processing, Academic Press Limited, United Kingdom, 1990.

[129] D. Zhao, J. Sun, Q. Li, G.D. Stucky, Morphological control of highly ordered mesoporous silica SBA-15, Chemistry of Materials, 12 (2000) 275-279.
[130] A. Katiyar, S. Yadav, P.G. Smirniotis, N.G. Pinto, Synthesis of ordered large pore SBA-15 spherical particles for adsorption of biomolecules, Journal of Chromatography A, 1122 (2006) 13-20.
[131] Z. Jin, X. Wang, X. Cui, Synthesis and morphological investigation of ordered SBA-15-type mesoporous silica with an amphiphilic triblock copolymer template under various conditions, Colloids and Surfaces A: Physicochemical and Engineering Aspects, 316 (2008) 27-36.
[132] M. Mesa, L. Sierra, J.-L. Guth, Contribution to the study of the formation mechanism of mesoporous SBA-15 and SBA-16 type silica particles in aqueous acid solutions, Microporous and mesoporous materials, 112 (2008) 338-350.
[133] S. Kang, Y.B. Chae, J.-S. Yu, HCl as a key parameter in size-tunable synthesis of SBA-15 silica with rodlike morphology, Journal of nanoscience and nanotechnology, 9 (2009) 527-532.
[134] Q. Huo, D.I. Margolese, U. Ciesla, D.G. Demuth, P. Feng, T.E. Gier, P. Sieger, A. Firouzi, B.F. Chmelka, Organization of organic molecules with inorganic molecular species into nanocomposite biphase arrays, Chemistry of Materials, 6 (1994) 1176-1191.
[135] B.P. Block, J.C. Bailar, The Reaction of Gold(III) with Some Bidentate Coördinating Groups1, Journal of the American Chemical Society, 73 (1951) 4722-4725.
[136] Y. Jin, P. Wang, D. Yin, J. Liu, H. Qiu, N. Yu, Gold nanoparticles stabilized in a novel periodic mesoporous organosilica of SBA-15 for styrene epoxidation, Microporous and Mesoporous Materials, 111 (2008) 569-576.
[137] R.J.P. Corriu, A. Mehdi, C. Reye, Molecular chemistry and nanosciences: on the way to interactive materials, Journal of Materials Chemistry, 15 (2005) 4285-4294.
[138] Y. Ma, M. Chen, C. Song, X. Zheng, Catalytic Oxidation of Toluene, Acetone and Ethyl Acetate on a New Pt-Pd/Stainless Steel Wire Mesh Catalyst, Acta Physico-Chimica Sinica, 24 (2008) 1132-1136.
[139] C.A. McAuliffe, R.V. Parish, P.D. Randall, Gold(I) complexes of unidentate and bidentate phosphorus-, arsenic-, antimony-, and sulphur-donor ligands, Journal of the Chemical Society, Dalton Transactions, (1979) 1730-1735.
[140] M. Slany, M. Bardaji, M.-J. Casanove, A.-M. Caminade, J.-P. Majoral, B. Chaudret, Dendrimer Surface Chemistry. Facile Route to Polyphosphines and Their Gold Complexes, Journal of the American Chemical Society, 117 (1995) 9764-9765.
[141] T.Y. Suman, S.R. Radhika Rajasree, R. Ramkumar, C. Rajthilak, P. Perumal, The Green synthesis of gold nanoparticles using an aqueous root extract of Morinda citrifolia L, Spectrochimica Acta Part A: Molecular and Biomolecular Spectroscopy, 118 (2014) 11-16.
[142] Scherrer, P. "Determination of the size and internal structure of colloidal particles using X-rays." Math-Phys Klasse 2 (1918): 98-100.
[143] S. Odiba, Computational fluid dynamics for micro reactors used in environmental applications by COMSOL and HYSYS, in, Teesside University, 2016.
[144] Ehrfeld, W., V. Hessel, and H. Löwe. "Extending the knowledge base in microfabrication towards chemical engineering and fluid dynamic simulation." Proc. of the 4th Int. Conf. on Microreaction Technology, IMRET. Vol. 4. 2000.
[145] Ehrfeld, W., V. Hessel, and V. Haverkamp. "Microreactors, Ullmann's encyclopedia of industrial chemistry." (1999).
[146] K.F. Jensen, Microreaction engineering — is small better?, Chemical Engineering Science, 56 (2001) 293-303.
[147] C. Alépée, R. Maurer, L. Paratte, L. Vulpescu, P. Renaud, A. Renken, Fast Heating and Cooling for High Temperature Chemical Microreactors, in: W. Ehrfeld (Ed.)

Microreaction Technology: Industrial Prospects, Springer Berlin Heidelberg, 2000, pp. 514-525.
[148] L. Kiwi-Minsker, A. Renken, Microstructured reactors for catalytic reactions, Catalysis Today, 110 (2005) 2-14.
[149] H. Chen, L. Bednarova, R.S. Besser, W.Y. Lee, Surface-selective infiltration of thin-film catalyst into microchannel reactors, Applied Catalysis A: General, 286 (2005) 186-195.
[150] R. Grasselli, S. Oyama, A. Gaffney, J. Lyons, Gold as a low-temperature oxidation catalyst: factors controlling activity and selectivity, in: 3rd World Congress on Oxidation Catalysis: Proceedings of the 3rd World Congress on Oxidation Catalysis, San Diego, CA, USA, 21-26 September 1997, Elsevier Science Limited, 1997, pp. 123.
[151] G.J. Hutchings, Catalysis: A golden future, Gold Bulletin, 29 (1996) 123-130.
[152] T.V. Choudhary, S. Banerjee, V.R. Choudhary, Catalysts for combustion of methane and lower alkanes, Applied Catalysis A: General, 234 (2002) 1-23.
[153] L. Marchetti, L. Forni, Catalytic combustion of methane over perovskites, Applied Catalysis B: Environmental, 15 (1998) 179-187.
[154] R. Rota, F. Bonini, M. Morbidelli, S. Carrà, Experimental study and kinetic analysis of the oxidation of light hydrocarbon mixtures, Industrial & engineering chemistry research, 35 (1996) 2127-2136.
[155] E.C. Moretti, Reduce VOC and HAP emissions, Chemical Engineering Progress, 98 (2002) 30-40.
[156] N.A. Hodge, C.J. Kiely, R. Whyman, M.R.H. Siddiqui, G.J. Hutchings, Q.A. Pankhurst, F.E. Wagner, R.R. Rajaram, S.E. Golunski, Microstructural comparison of calcined and uncalcined gold/iron-oxide catalysts for low-temperature CO oxidation, Catalysis Today, 72 (2002) 133-144.
[157] M. Haruta, M. Daté, Advances in the catalysis of Au nanoparticles, Applied Catalysis A: General, 222 (2001) 427-437.
[158] J. Guzman, B.C. Gates, Simultaneous Presence of Cationic and Reduced Gold in Functioning MgO-Supported CO Oxidation Catalysts: Evidence from X-ray Absorption Spectroscopy, The Journal of Physical Chemistry B, 106 (2002) 7659-7665.
[159] A.C. Gluhoi, N. Bogdanchikova, B.E. Nieuwenhuys, The effect of different types of additives on the catalytic activity of Au/Al2O3 in propene total oxidation: transition metal oxides and ceria, Journal of Catalysis, 229 (2005) 154-162.
[160] F. Yinga, S. Wang, C.-T. Au, S.-Y. Lai, Effect of the oxidation state of gold on the complete oxidation of isobutane on Au/CeO2 catalysts, Gold Bulletin, 43 (2010) 241-251.
[161] G. Avgouropoulos, E. Oikonomopoulos, D. Kanistras, T. Ioannides, Complete oxidation of ethanol over alkali-promoted Pt/Al2O3 catalysts, Applied Catalysis B: Environmental, 65 (2006) 62-69.
[162] B. Chen, C. Bai, R. Cook, J. Wright, C. Wang, Proceedings of the 1st Global Conference of Young Chinese Scientist on Catalysis Science and TechnologyGold/cobalt oxide catalysts for oxidative destruction of dichloromethane, Catalysis Today, 30 (1996) 15-20.
[163] H.-J. Joung, J.-H. Kim, J.-S. Oh, D.-W. You, H.-O. Park, K.-W. Jung, Catalytic oxidation of VOCs over CNT-supported platinum nanoparticles, Applied Surface Science, 290 (2014) 267-273.
[164] Y. Xia, H. Dai, L. Zhang, J. Deng, H. He, C.T. Au, Ultrasound-assisted nanocasting fabrication and excellent catalytic performance of three-dimensionally ordered mesoporous chromia for the combustion of formaldehyde, acetone, and methanol, Applied Catalysis B: Environmental, 100 (2010) 229-237.

[165] Y. Xia, H. Dai, H. Jiang, L. Zhang, J. Deng, Y. Liu, Three-dimensionally ordered and wormhole-like mesoporous iron oxide catalysts highly active for the oxidation of acetone and methanol, Journal of Hazardous Materials, 186 (2011) 84-91.
[166] Guo, Hongmei, Bo Xue, and Min Chen. "Catalytic oxidation of VOCs over the structured bimetallic catalyst 0.1% Pt-0.75% CeO 2/SSWM." Sustainable Environment Research 25.3 (2015).
[167] N. Burgos, M.a. Paulis, M. Mirari Antxustegi, M. Montes, Deep oxidation of VOC mixtures with platinum supported on Al2O3/Al monoliths, Applied Catalysis B: Environmental, 38 (2002) 251-258.
[168] B. Solsona, E. Aylón, R. Murillo, A.M. Mastral, A. Monzonís, S. Agouram, T.E. Davies, S.H. Taylor, T. Garcia, Deep oxidation of pollutants using gold deposited on a high surface area cobalt oxide prepared by a nanocasting route, Journal of Hazardous Materials, 187 (2011) 544-552.
[169] B. Solsona, T. Garcia, S. Agouram, G.J. Hutchings, S.H. Taylor, The effect of gold addition on the catalytic performance of copper manganese oxide catalysts for the total oxidation of propane, Applied Catalysis B: Environmental, 101 (2011) 388-396.
[170] Ali, Arshid M., et al. "Effect of Au Precursor and Support on the Catalytic Activity of the Nano-Au-Catalysts for Propane Complete Oxidation." Journal of Nanomaterials 2015 (2015).
[171] Y. Yazawa, H. Yoshida, S.-i. Komai, T. Hattori, The additive effect on propane combustion over platinum catalyst: control of the oxidation-resistance of platinum by the electronegativity of additives, Applied Catalysis A: General, 233 (2002) 113-124.
[172] S. Pitkäaho, S. Ojala, T. Maunula, A. Savimäki, T. Kinnunen, R.L. Keiski, Oxidation of dichloromethane and perchloroethylene as single compounds and in mixtures, Applied Catalysis B: Environmental, 102 (2011) 395-403.
[173] J.I. Gutiérrez-Ortiz, R. López-Fonseca, U. Aurrekoetxea, J.R. González-Velasco, Low-temperature deep oxidation of dichloromethane and trichloroethylene by H-ZSM-5-supported manganese oxide catalysts, Journal of Catalysis, 218 (2003) 148-154.
[174] L. Wang, M. Sakurai, H. Kameyama, Catalytic oxidation of dichloromethane and toluene over platinum alumite catalyst, Journal of Hazardous Materials, 154 (2008) 390-395.
[175] L. Pinard, J. Mijoin, P. Ayrault, C. Canaff, P. Magnoux, On the mechanism of the catalytic destruction of dichloromethane over Pt zeolite catalysts, Applied Catalysis B: Environmental, 51 (2004) 1-8.
[176] L. Matějová, P. Topka, L. Kaluža, S. Pitkäaho, S. Ojala, J. Gaálová, R.L. Keiski, Total oxidation of dichloromethane and ethanol over ceria–zirconia mixed oxide supported platinum and gold catalysts, Applied Catalysis B: Environmental, 142–143 (2013) 54-64.

Appendices

Appendix A. Acetone complete oxidation - comparing the best Au/SBA-15 catalyst with other published catalysts

Table 8. List of catalysts including Au/SBA-15 used for complete oxidation of acetone

Catalyst	Acetone concentration (ppm)	Temperature at 100 % acetone conversion (°C)	References
Meso-Cr-400	500	140	[164]
Fe-CA-400	1000	210	[165]
Au/SBA-15	200	250	Iro's PhD thesis
Pt-Pd/SSWM	2500	260	[138]
$Cu_{0.50}Ce_{0.50}O_x$	500	270	[164]
Pt/CeO_2	2526	320	[166]
Mn/clay	600	336	[35]
Pt/Al_2O_3	225	340	[167]

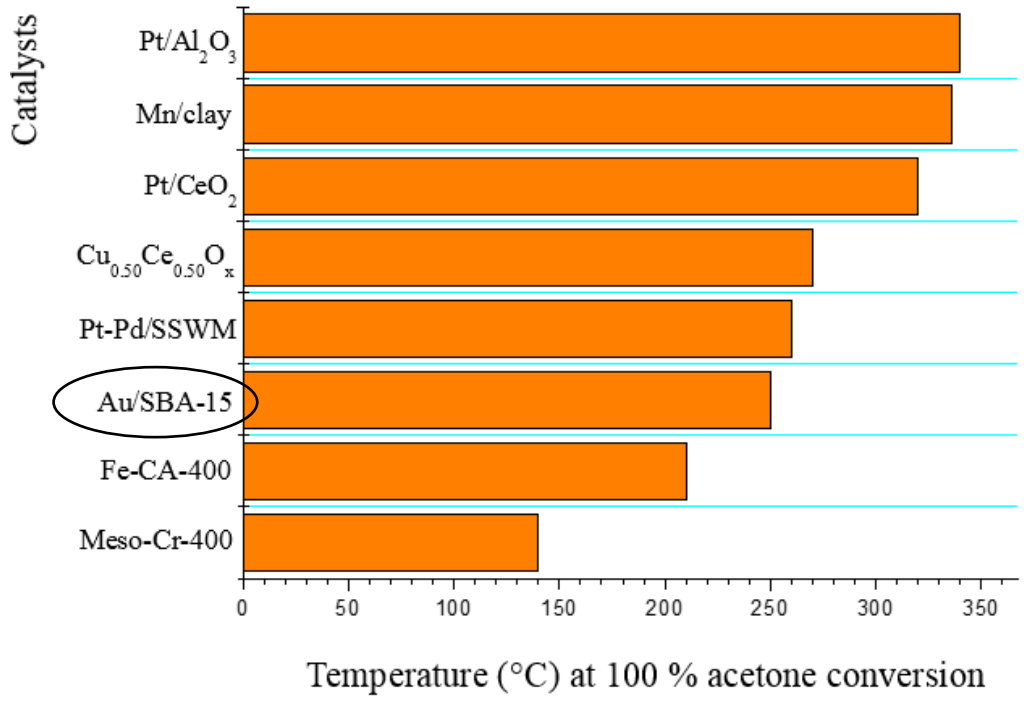

Figure 162. Comparison between Au/SBA-15 catalyst and other published catalysts in acetone complete oxidation

Appendix B. Propane complete oxidation - comparing the best Au/SBA-15 catalyst and Au/SBA-15 catalytic micro-reactor with other published catalysts

Table 9. A list of Au/SBA-15 catalyst, Au/SBA-15 catalyst coated micro-reactor and other published catalysts in propane complete oxidation

Catalyst	Propane concentration converted (ppm)	Temperature of converted propane (°C)	References
Au/SBA-15 coated micro-reactor	8140	160	Iro's Thesis, [143]
Au/CoOx	8000	215	[168]
Co_3O_4(CO – C30)	5000	250	[23]
3Au/$CuMnO_x$ - 300	5000	300	[169]
Au-SBA-15	5000	360	Iro's PhD Thesis
Au-Mn/TOS	5000	360	[170]
2.0%Pd3.0%Nb/TiO_2	5000	375	[22]
CuMnOx - 400	5000	400	[169]
Pd/Al_2O_3	1750	400	[53]
Au_{HAuCl4} -Ce	5000	450	[170]
Pt/Al_2O_3	2500	527	[171]

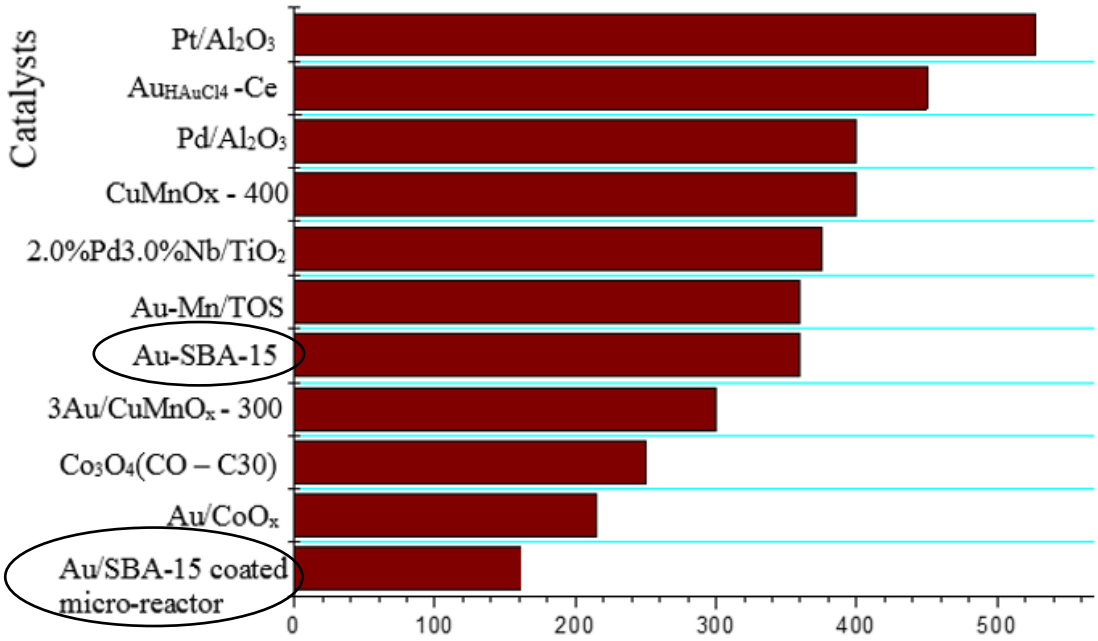

Figure 163. Comparing Au/SBA-15 catalyst, Au/SBA-15 catalyst coated micro-reactor and other published catalysts in propane complete oxidation

Appendix C. Dichloromethane (DCM) complete oxidation - comparing the best Au/SBA-15 catalyst with other published catalysts

Table 10. List of catalysts including Au/SBA-15 catalyst used for complete oxidation of DCM

Catalyst	DCM concentration (ppm)	Temperature at 100 % DCM conversion (°C)	References
Au/SBA-15	200	305	Iro's PhD thesis
Pt+V/Al	500	312	[172]
Mn/H-ZSM-5	1000	400	[173]
Pt/aluminate	100	402	[174]
Pt/HFAU	1000	460	[175]
0.2Pt/CeZr	1000	484	[176]
1.5Pt/CeZr	1000	485	[176]
0.3Au/CeZr	1000	487	[176]
CeZr	1000	497	[176]
2.8Au/CeZr	1000	500	[176]

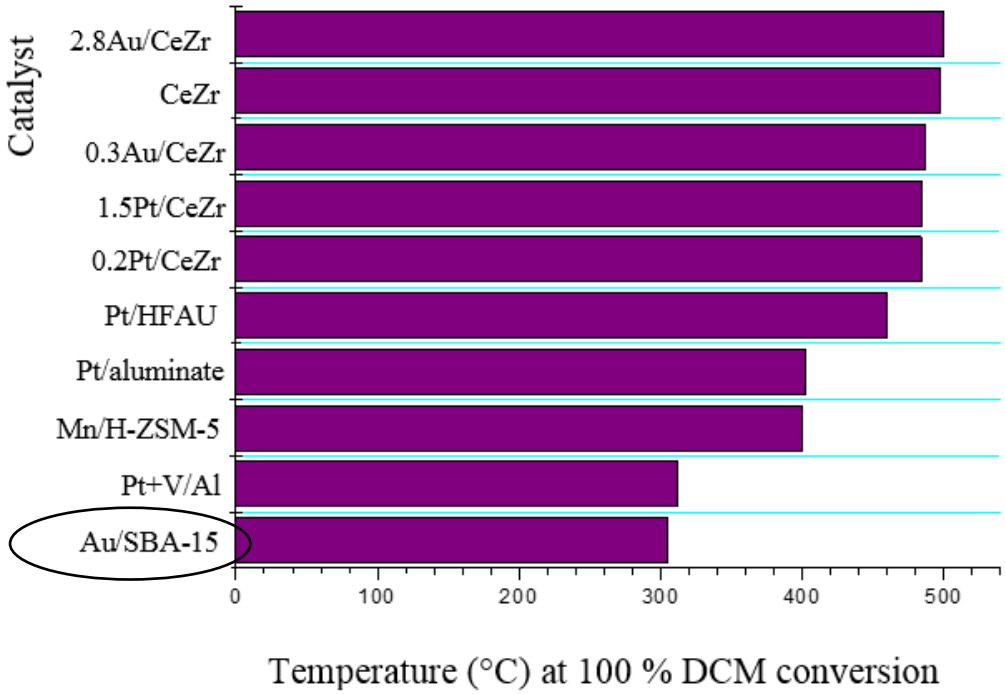

Figure 164. Comparison between Au/SBA-15 catalyst and other published catalysts in DCM complete oxidation